



**UiT** The Arctic University of Norway

Faculty of Health Sciences

## **ATG8s in the nucleus: Beyond the autophagy paradigm**

Athanasios Kournoutis

A dissertation for the degree of Philosophiae Doctor (PhD)

January 2024







# ATG8s in the nucleus: Beyond the autophagy paradigm

Athanasios Kournoutis

A dissertation for the degree of Philosophiae Doctor



UiT – The Arctic University of Norway

Faculty of Health Sciences

Department of Medical Biology

Autophagy Research Group

January 2024



# Acknowledgements

First and foremost, I would like to express my gratitude to my main supervisor, Terje Johansen, for his unwavering support, mentorship, and invaluable guidance throughout these years. His expertise and the opportunities he provided have been instrumental in shaping the trajectory of my work. I also extend my appreciation to my co-supervisor, Trond Lamark, whose enthusiasm and deep knowledge in our discussions have truly eased what was sometimes a challenging journey.

The technical assistance and guidance from Gry Evjen, Aud Øvervatn, and in the early days, Hanne Brenne, has been crucial to me, and I deeply appreciate their contributions. Apart from things work-related, I enjoyed their company very much, and I believe we had a great time and a lot of laughs!

As in every research group, people constantly come and go. In no particular order, I would like to thank Eva, Juncal, Pradip, Mutugi, Birendra, Yakubu, Anne, Olav Arne, and my most recent office co-holders Marcus and Jana. You have all been part of this PhD journey in one way or another and I am lucky to have met you. I would especially like to highlight those that I got to know a little better. Nikoline, Mireia, Hallvard and Anthimi, I consider myself quite lucky to have overlapped with you guys, your support and friendship in and out of the lab has been very important to me. I will never forget how you helped me navigate my mid-twenties!

I would also like to thank Yu Wang and Zhixun Dou for the collaboration, the hospitality and the great advice I received from them, both at UiT and at Harvard.

I also greatly appreciate the support from my family: my brothers, Giorgos and Alexandros, who ended up moving to Tromsø as well, giving a new, previously unthought of, perspective to our relationship; my parents, who never stopped calling me with a frequency that borders the fanatic, but at the same is understood and valued; my cousin Nikos in Oslo, who moved to Norway with me in in 2019 and, like me, is always available for a talking session.

Last but not least, my deepest gratitude and love I give to my partner Manu, who has supported me through good and bad moments, at a time when he had other family matters to attend to.

Athanasios Kournoutis  
January 2024

# Table of Contents

Abbreviations .....	I
Summary .....	III
List of papers.....	IV
1. Introduction .....	1
1.1 Protein degradation systems.....	1
1.2 Autophagy .....	2
1.2.1 Overview of the autophagic pathway.....	3
1.2.2 Selective autophagy and Sequestosome 1-like receptors.....	7
1.2.3 The ATG8 family of proteins.....	9
1.3 The cellular antioxidant defense .....	12
1.3.1 Reactive oxygen species (ROS) and oxidative stress .....	12
1.3.2 The mechanisms of antioxidant action.....	13
1.3.3 Transcription factors in the cellular antioxidant system .....	15
1.3.4 The NRF2-KEAP1 pathway .....	19
1.3.5 NRF2 target gene activation via p300/CBP .....	22
1.3.6 NRF2-activating compounds .....	23
1.3.7 Cytoprotective functions of NRF2 and its target genes .....	24
1.3.8 NRF2 in cancer .....	25
1.4 Senescence .....	26
1.4.1 The Senescence-associated secretory phenotype (SASP).....	27
1.4.2 Cytoplasmic Chromatin Fragments (CCFs).....	28
1.4.3 Chromatin Remodeling Complexes .....	29
1.4.4 Williams Syndrome Transcription Factor (WSTF).....	30
2. Aims of the study .....	33
3. Summary of papers.....	34
4. Discussion .....	36
4.1 Identification of NRF2 and WSTF as ATG8 interactors .....	37
4.2 The interactions between the ATG8s and NRF2 and WSTF .....	38
4.3 The role of LC3B in the transcriptional regulation of NRF2 target genes.....	42
4.4 LC3B as a transcriptional co-factor .....	44
4.5 Evolving selectivity in autophagy: NRF2 and NBR1 .....	45
4.6 Conclusions.....	46

5.	Methodological considerations.....	47
5.1	Cell lines as model systems.....	47
5.2	<i>In vitro</i> interaction studies.....	47
5.3	Luciferase assays.....	48
5.4	Transient and stable protein expression .....	48
5.5	Western blotting .....	49
5.6	Protein structure prediction using AlphaFold2 .....	50
6.	References .....	51

# Abbreviations

<b>53BP1</b>	p53-binding protein 1
<b>AML</b>	Acute myeloid leukemia
<b>AP1</b>	Activator Protein 1
<b>ARE</b>	Antioxidative response element
<b>ATF3,4</b>	Activating transcription factor 3 and 4
<b>ATG</b>	Autophagy-related gene
<b>BAZ</b>	Bromodomain adjacent to the zinc finger
<b>BRCA1,2</b>	Breast cancer susceptibility genes 1 and 2
<b>BRG1</b>	Brahma-related gene 1
<b>CALCOCO1</b>	Calcium-binding and coiled-coil domain-containing protein 1
<b>CBP</b>	CREB-binding protein
<b>CC</b>	coiled-coil
<b>CCF</b>	Cytoplasmic chromatin fragments
<b>CCL2</b>	Chemokine (C-C motif) ligand 2
<b>CNC</b>	Cap n' collar
<b>CREB</b>	cAMP response element-binding protein
<b>CRM1</b>	Chromosomal maintenance 1
<b>CUL3</b>	Cullin 3
<b>CXCL5</b>	C-X-C motif chemokine 5
<b>ERK</b>	Extracellular signal-regulated kinase
<b>ESCRT</b>	Endosomal sorting complex required for transport
<b>FAK</b>	Focal adhesion kinase
<b>FIP200</b>	Focal Adhesion Kinase Family Interacting Protein of 200 kDa
<b>FOX</b>	Forkhead box
<b>GABARAP</b>	Gamma-aminobutyric acid receptor-associated protein
<b>cGAS</b>	cyclic GMP-AMP synthase
<b>GCLC</b>	Glutamate-cysteine ligase catalytic subunit
<b>GCLM</b>	Glutamate-cysteine ligase regulatory subunit
<b>H2A</b>	Histone 2A
<b>HIF</b>	Hypoxia-inducible factor
<b>HO-1</b>	Heme oxygenase 1
<b>IL-6,-8,-10</b>	Interleukin 6, 8, 10
<b>ISWI</b>	Imitation switch complex
<b>KEAP1</b>	Kelch-like ECH-associated protein 1
<b>LAD</b>	Lamin-associated domains
<b>LAMP2A</b>	Lysosome-associated membrane protein 2A
<b>LDS</b>	LIR-docking site
<b>LIR</b>	LC3-interacting region
<b>LMX1B</b>	LIM homeobox transcription factor 1-beta
<b>MAP1LC3</b>	Microtubule-associated proteins 1A/1B light chain 3
<b>MAF</b>	Musculoaponeurotic fibrosarcoma oncogene
<b>MARE</b>	Maf responsive element
<b>MED16</b>	Mediator complex subunit 16
<b>MMP-1,-3</b>	Matrix metalloproteinase-1

<b>NBR1</b>	Neighbor of BRCA1 gene 1
<b>Neh</b>	NRF-ECH homology
<b>NFE2</b>	Nuclear factor, erythroid 2
<b>NFκB</b>	Nuclear factor kappa-light-chain-enhancer of activated B cells
<b>NRF2</b>	Nuclear factor, erythroid 2-related factor 2
<b>NUFIP1</b>	Nuclear FMR1 interacting protein 1
<b>PCNA</b>	Proliferating cell nuclear antigen
<b>PDGF-AA or -BB</b>	Platelet-derived growth factor, of two A or two B subunits
<b>PE</b>	phosphatidylethanolamine
<b>PHD</b>	Plant homeodomain
<b>PI3K</b>	Phosphoinositide 3-kinase
<b>PI3P</b>	Phosphatidylinositol 3-phosphate
<b>PML</b>	Promyelocytic leukemia protein
<b>PTEN</b>	Phosphatase and tensin homolog
<b>PVDF</b>	Polyvinylidene difluoride
<b>RB1CC1</b>	RB1-inducible coiled-coil protein 1
<b>Ref(2)p</b>	Refractory to sigma p
<b>ROS</b>	Reactive oxygen species
<b>SAR</b>	Selective autophagy receptor
<b>SASP</b>	Senescence-associated phenotype
<b>SFN</b>	Sulforaphane
<b>SIRT1</b>	Sirtuin 1
<b>SKN</b>	Protein skinhead-1
<b>SLR</b>	Sequestosome 1/p62-like receptor
<b>SNARE</b>	SNAP receptor
<b>SNAP</b>	Soluble N-ethylmaleimide-Sensitive factor attachment protein
<b>SQSTM1</b>	Sequestosome 1
<b>STING</b>	Stimulator of interferon genes
<b>SWI/SNF</b>	Switch/Sucrose Non-Fermentable
<b>tBHQ</b>	tert-Butylhydroquinone
<b>TNF</b>	Tumor necrosis factor
<b>TORC1,2</b>	Target of rapamycin complex 1, 2
<b>TRIM5</b>	Tripartite motif-containing protein 5
<b>TXNRD1</b>	Thioredoxin reductase 1
<b>UBA</b>	Ubiquitin associated domain
<b>UBD</b>	Ubiquitin binding domain
<b>ULK1</b>	Unc-51-like kinase 1
<b>VAMP8</b>	Vesicle-associated membrane protein 8
<b>VPS15</b>	Vacuolar protein sorting-associated protein 15, 34 and 37A
<b>WAC</b>	WSTF/Acf1/cbp146 (domain)
<b>WAKZ</b>	WSTF/Acf1/KIAA0314/ZK783.4) (motif)
<b>WD</b>	WD40 repeat
<b>WICH</b>	WIP- and CR16-homologous protein
<b>WIPI2</b>	WD repeat domain phosphoinositide-interacting protein 2
<b>WSTF</b>	Williams syndrome transcription factor
<b>ZIP</b>	Zipper, leucine (domain)

## Summary

Selective autophagy, is a cellular process that targets specific cellular components for lysosomal degradation, maintaining cellular homeostasis and determining cell fate under stress. The degradation process involves selective autophagy receptors and the ATG8 family of proteins, the latter consisting of small ubiquitin-like proteins. This thesis explores the interactions of ATG8s with nuclear components, a fairly unexplored aspect in autophagy research, and examines how these interactions may impact cellular processes previously unrelated to autophagy.

We address in this thesis the role of LC3B, a well-studied member of the ATG8 family, in the NRF2 – KEAP1 oxidative stress response pathway. We find that LC3B binds to the NRF2-ECH homology 5 domain (Neh5) of NRF2, a region important for its transcriptional activation, due to its interaction with p300/CBP and other co-factors, and that this interaction occurs in the nucleus. Binding of LC3B or other ATG8s to their interaction partners occur in most cases between the LC3 interacting region (LIR), a short sequence motif with a conserved core motif, and the LC3 docking site (LDS) in the ATG8s. We show that the mode of the NRF2 – LC3B interaction has attributes that fit the LIR – LDS model. Moreover, we demonstrate that NRF2 is not degraded by autophagy under oxidative stress. The lack of evidence for the autophagic degradation of NRF2, correlated with the localization of the interaction between NRF2 and LC3B in the nucleus, suggests that LC3B has a role in transcriptional regulation of NRF2 target genes. Consistent with this notion we showed that LC3B competes with p300/CBP for binding to an overlapping binding site in Neh5. Hence, LC3B can negatively regulate NRF2 target genes by competing for binding to NRF2 with p300/CBP.

Opposite from the role of LC3B in transcriptional repression, we report on a study which demonstrates that ATG8s can act as co-factors to the transcription factor LMX1B, stimulating transcription of autophagy genes and contributing to the maintenance of midbrain dopaminergic neurons.

Following previous studies that show that LC3B is mediating the autophagic degradation of nuclear components in senescence, we also explore the role that GABARAP plays in the same process. We find that GABARAP interacts with WSTF, a component of the nuclear ISWI chromatin remodeling complex, and drives its lysosomal degradation under senescence. The GABARAP-mediated degradation of WSTF has consequences in the transcriptional activation of genes of the senescence-associated secretory phenotype (SASP), with negative effects on inflammation.

We finally provide an overview of the ancestral selective autophagy receptor NBR1, which like NRF2 and WSTF, is an ATG8 interaction partner. Here, we delve into the evolution of NBR1 and discuss what is its molecular relationship with its more recent and well-studied homolog, p62.



# List of papers

## *Paper I*

### **Competitive binding between LC3B and p300/CBP to the NRF2 Neh5 domain regulates target gene transcriptional activation**

Athanasios Kournoutis, Birendra Kumar Shrestha, Hallvard Lauritz Olsvik, Yakubu Princely Abudu, Ashish Jain, Gry Evjen, Aud Øvervatn, Trond Lamark, Terje Johansen

*Manuscript*

## *Paper II*

### **Nuclear autophagy interactome unveils WSTF as a constitutive nuclear inhibitor of inflammation**

Yu Wang, Vinay V. Eapen, Athanasios Kournoutis, Angelique Onorati, Xianting Li, Xiaoting Zhou, Murat Cetinbas, Lu Wang, Jihe Liu, Corey Bretz, Zhuo Zhou, Shannan J. Ho Sui, Srinivas Vinod Saladi, Ruslan I. Sadreyev, Peter D. Adams, Robert E. Kingston, Zhenyu Yue, Terje Johansen, Zhixun Dou

(*bioRxiv* 2022.10.04.510822; <https://doi.org/10.1101/2022.10.04.510822>)

## *Paper III*

### **LC3B is a cofactor for LMX1B-mediated transcription of autophagy genes in dopaminergic neurons (Spotlight)**

Athanasios Kournoutis and Terje Johansen

(*Journal of Cell Biology*, 222(5), 2023; <https://doi.org/10.1083/JCB.202303008>)

## *Paper IV*

### **NBR1: The archetypal selective autophagy receptor**

Nikoline L. Rasmussen, Athanasios Kournoutis, Trond Lamark, Terje Johansen

(*Journal of Cell Biology*, 221(11), 2022; <https://doi.org/10.1083/JCB.202208092/213552>)

Other papers published during the PhD:

### **MORG1 limits mTORC1 signaling by inhibiting Rag GTPases**

Yakubu Princely Abudu, Athanasios Kournoutis, Hanne Britt Brenne, Trond Lamark, Terje Johansen

(*Molecular Cell*, 1097-2765, 2023; <https://doi.org/10.1016/j.molcel.2023.11.023>)



# 1. Introduction

## 1.1 Protein degradation systems

Proteins must maintain structural cohesion to function properly (Klaips et al., 2018). Stress conditions leave them at risk of misfolding and aggregation. As proteins become terminally misfolded, or are no longer functionally required, they must be degraded to avoid damaging effects that might arise from their presence.

There are two systems responsible for the degradation of intracellular material and cellular homeostasis in eukaryotic cells, the ubiquitin-proteasome system (UPS) and the autophagic pathway (Dikic, 2017). The ubiquitin-proteasome system (also known as ubiquitin proteasome pathway, UPP) selectively targets the degradation of intracellular proteins tagged with ubiquitin to a protein complex known as the proteasome. While the UPS is the designated degradation process for short-lived and soluble misfolded proteins, the cell also requires mechanisms that are able to perform degradation of components with a greater size. Autophagy (for the Greek word: *αυτόφαγος* (autóphagos) meaning self-eating) requires the formation of a double membrane structure containing the sequestered cytoplasmic material, called the autophagosome, which ultimately fuses with the lysosome to achieve degradation (Yu et al., 2018). The autophagic pathway can recognize and remove large cellular components, like aggregated proteins, organelles or macromolecular complexes. Both systems contribute to the cell's protein quality control and communicate with each other via different mechanisms in order to maintain cell homeostasis, playing important roles in physiological conditions and disease (Figure 1).

Both the ubiquitin-proteasome system and the autophagy process rely on the ubiquitin code for their function. Ubiquitin is a 76-amino acid protein that can be covalently linked to lysines (K) on other proteins through ubiquitination, by utilizing its C-terminal glycine (Komander & Rape, 2012). The process of ubiquitin attachment to a substrate involves an enzymatic cascade with E1, E2, and E3 ubiquitin enzymes. The term monoubiquitination refers to the addition of a single ubiquitin molecule to a substrate. Ubiquitin itself contains lysine residues, which allow the formation of polyubiquitin chains by consecutive attachment of other ubiquitin proteins. Polyubiquitin chains can be created using the internal ubiquitin lysines (K6, K11, K27, K29, K33, K48, K63) and the N-terminal methionine (M1). The diverse combinations of polyubiquitin types and lengths constitute the ubiquitin code.

Various ubiquitin modifications can be identified by specific proteins, leading to distinct outcomes. For example, K48-linked polyubiquitination primarily signals proteasomal degradation, whereas K63-linked polyubiquitination plays a role in the formation of protein complexes and can also designate substrates for degradation by autophagy, even though not exclusively.

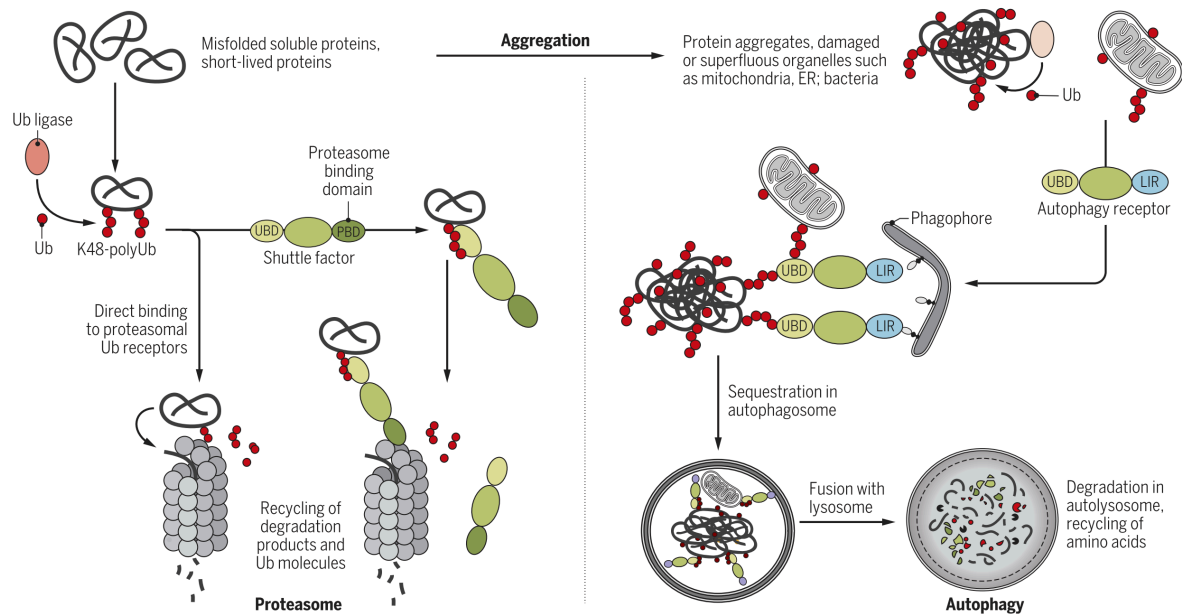


**Figure 1. Overview of the UPS and autophagy.** The UPS and selective autophagy represent distinct cellular mechanisms for maintaining protein homeostasis. (Left) The UPS relies on polyubiquitination of soluble proteins with Lys48 (K48)-linked polyubiquitin chains. These ubiquitinated substrates are recognized by proteasomal ubiquitin receptors or shuttle factors, before being deubiquitinated and degraded by proteases within the proteasome. (Right) Selective autophagy is capable of degrading diverse cytosolic materials, including aggregated proteins, organelles or bacteria. Recognition signals for autophagy include ubiquitin, lipid-based signals like galectins, or selective autophagy receptors by utilizing the ubiquitin binding domain (UBD) or the LC3 Interacting Region (LIR). The autophagic machinery engulfs the cargo and forms an autophagosome that fuses with the lysosome for degradation. Figure from (Pohl & Dikic, 2019).

## 1.2 Autophagy

Autophagy is an evolutionary conserved, lysosome-dependent degradation mechanism in eukaryotic cells that facilitates the organized breakdown and recycling of cellular components. The history of autophagy began with the discovery of the lysosome by Christian De Duve in 1955 (Duve, 2005; Duve et al., 1955). The lysosome is an acidic organelle that contains hydrolytic enzymes which can degrade proteins and protein complexes (Bonam et al., 2019). At the time of discovery it was difficult to imagine how the cells utilized the lysosome as a degradation medium, due to its acidic nature. The advancement of the electron microscopes led to the observation of double-membrane structures that engulf material and consecutively fuse with the lysosomes, delivering their contents for degradation (Arstila & Trump, 1968). The term autophagy was coined by de Duve at a conference in 1963 (Ohsumi, 2013).

Since its discovery there has been an overwhelming advancement in our understanding of the autophagic process and several types of autophagy have been uncovered. The engulfment of cytoplasmic material

within double-membrane structures, known as autophagosomes, and the consecutive fusion with the lysosomes is termed macroautophagy. Moreover, cytoplasmic material can also be taken up directly into the lysosomes by invagination of the lysosomal membrane, a process referred to as microautophagy (Galluzzi et al., 2017). The third type is called chaperone-mediated autophagy, and it involves the transfer of material into the lysosomes with the assistance of chaperone proteins and the lysosomal membrane protein LAMP2A (Kaushik & Cuervo, 2018) (Figure 2).

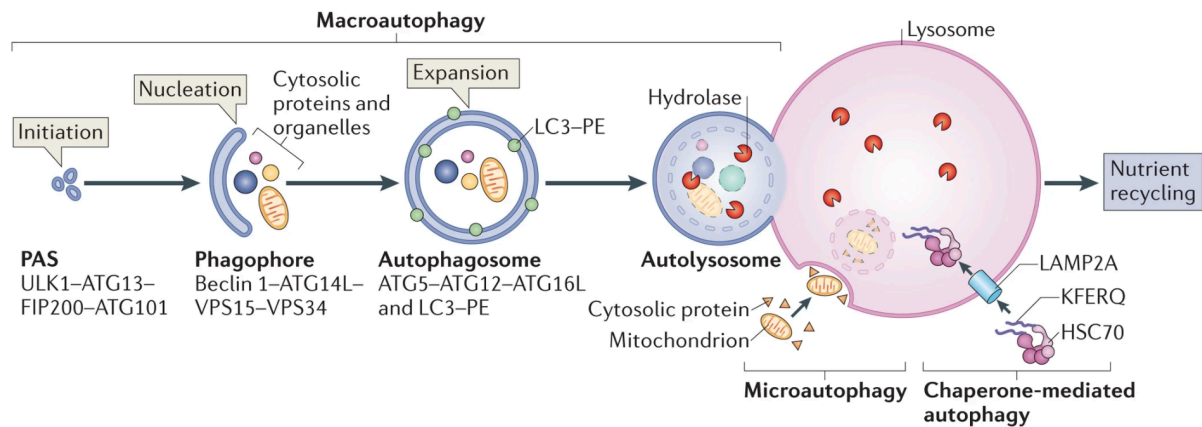


**Figure 2. Overview of the different types of autophagy**, showcasing how the autophagic cargo is degraded in the lysosome by macroautophagy, microautophagy and chaperone-mediated autophagy. Figure was modified from (Kaur & Debnath, 2015).

Even though autophagy was initially identified as a non-selective degradation pathway activated to safeguard the cell against starvation insult (Ohsumi, 2013), it is now evident that autophagy is triggered by a wide range of stressors and can be utilized accordingly for the degradation of specific substrates in a more targeted approach – a process now known as selective autophagy (Johansen & Lamark, 2011; Lamark & Johansen, 2021). Dysfunctions in autophagy have been associated with a range of human diseases, such as neurodegenerative disorders and cancer (Klionsky et al., 2021; Mizushima & Levine, 2020). Consequently, there has been an increasing interest in manipulating autophagy as a potential therapeutic approach for addressing these diseases.

### 1.2.1 Overview of the autophagic pathway

The process of macroautophagy involves a multistep process that begins with the initiation and nucleation of the double-membrane structure of the autophagosome, the sequestration of cargo and expansion and finally, the sealing and subsequent maturation and fusion with the lysosomes (Dikic & Elazar, 2018). These steps require the action of several proteins and protein complexes, including a

group of autophagy-related proteins (ATGs), which make up the core autophagic machinery (Mizushima et al., 2011). A number of these genes were discovered first in yeast through the pioneering work of Yoshinori Ohsumi, paving the way for understanding the process in higher eukaryotes (Ohsumi, 2013) (Figure 3).

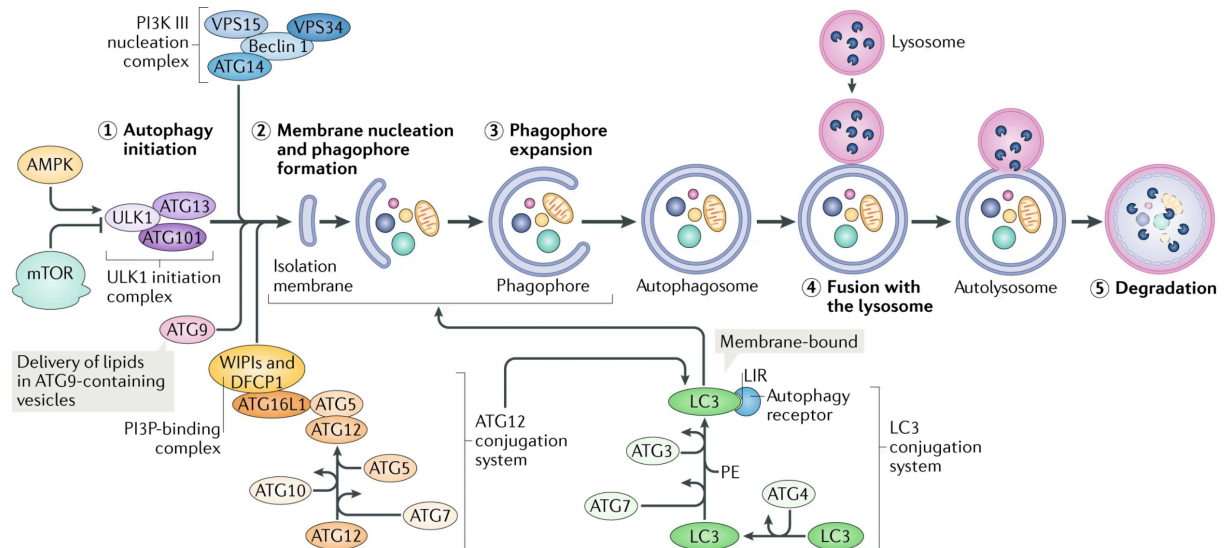


**Figure 3. Schematic representation depicting the processes and main regulatory machinery of autophagy.** For details, see main text. Figure was modified from (Hansen et al., 2018).

### 1.2.1.1 Initiation and nucleation

The complex which takes the role of initiation of autophagy is the Unc-51-like kinase 1 (ULK1) complex, consisting of the ULK1 kinase, ATG13, ATG101 and FAK family interacting protein of 200 kDa (FIP200, also known as retinoblastoma 1-inducible coiled-coil 1 (RB1CC1)) (Zachari & Ganley, 2017) (Figure 3). The central regulator of cellular metabolism and growth is the mechanistic target of rapamycin (mTOR), a serine-threonine kinase of the phosphatidylinositol-3-kinase (PI3K) related kinase family, that is present in two complexes, mTOR Complex 1 (mTORC1) and mTOR Complex 2 (mTORC2) (Brown et al., 1994; Jacinto et al., 2004; Loewith et al., 2002), with mTOR being the catalytic subunit common to both complexes.

Upon nutrient deprivation, the kinase activity of mTOR is inhibited, alleviating an inhibitory phosphorylation of the ULK1 complex by mTORC1 (Hosokawa et al., 2009; Jung et al., 2009). The ULK1 complex then is allowed to dissociate from mTOR, in order to phosphorylate targets that mediate other steps of autophagosome formation. The activated ULK1 complex marks the mammalian phagophore assembly site (mPAS) (Dikic & Elazar, 2018) or omegasome in mammals (Axe et al., 2008).

Beclin-1 is an important target of the ULK1 complex, being recruited by it to the phagophore nucleation site in order to form the phosphoinositide 3-kinase (PI3K) class III complex 1 (Russell et al., 2013). The class III PI3K complex 1, consisting of Beclin 1, VPS34, VPS15 and ATG14L, mediates the nucleation of the phagophore by generating phosphatidylinositol-3-phosphate (PI3P) from phosphatidylinositol (PtdIns) (Mizushima et al., 2011). The PI3P generated recruits PI3P-binding proteins to the forming phagophore. Among these are proteins of the WD-repeat protein interacting with phosphoinositides family (WIPI) 1-4 and the FYVE-containing protein 1 (DFCP1) (Axe et al., 2008; Proikas-Cezanne et al., 2015), which are needed for further expansion of the phagophore (Figure 3).

### **1.2.1.2 Elongation and sealing**

Among the WIPI proteins, WIPI2b is recognizing PI3P and recruits the ATG12-ATG5-ATG16L1 complex, which mediates the conjugation of ATG8 family proteins to phosphatidylethanolamine (PE) (Dooley et al., 2014; Polson et al., 2010). The ATG8 family of proteins are ubiquitin-like proteins that consist of 7 functional members in humans, divided in two subfamilies: the microtubule-associated protein light chain 1 (MAP1LC3) subfamily consisting of LC3A, LC3B, LC3B2 and LC3C; and the GABA type A receptor-associated protein (GABARAP) subfamily, consisting of GABARAP, GABARAPL1 and GABARAPL2 (Johansen & Lamark, 2019; Rogov et al., 2023; Shpilka et al., 2011). The ATG8s are expressed as precursors, which become cleaved to expose a C-terminal glycine that can conjugate to PE. After PE conjugation – termed also ATG8 lipidation – the ATG8 proteins can anchor to the growing phagophore, where they play important roles, ranging from the further elongation of the phagophore to the selection and recruitment of cargo (Johansen et al., 2017; Slobodkin & Elazar, 2013; Wesch et al., 2020). The roles of the ATG8 family of proteins, especially in the nucleus, will be elaborated further in a later section.

The incorporation of ATG8 family proteins into the phagophore through conjugation to PE, requires the activity of two ubiquitin-like conjugation systems; the ATG12 conjugation and the ATG8 modification (Ichimura et al., 2000; Tanida et al., 2004). After the expression of an ATG8 as a precursor, it is subsequently cleaved by the cysteine protease ATG4, exposing the C-terminal glycine. The ATG8 is then activated by the E1-like ATG7 and then transferred to the E2-like ATG3 enzyme. ATG12 is also being activated by ATG7, before being attached to the E2-like ATG10. ATG12 is then conjugated to ATG5, subsequently interacting with ATG16L1 to form the ATG12-ATG5-ATG16L1 complex (Mizushima et al., 1998; Tanida et al., 2004). Finally, the ATG8-ATG3 conjugate interacts with the ATG12-ATG5-ATG16L1 complex and ATG8 is lipidated through PE-conjugation. ATG4, the initial cysteine protease that cleaves pre-ATG8, plays also an important role in deconjugating ATG8 from PE, limiting the expansion of the phagophore and allowing the recycling of the ATG8s (Satoo et al., 2009).

In the same way as with the ATG8s, there is only one *Atg4* gene in yeast, whereas there are four Atg4 homologs in mammals (Atg4A, Atg4B, Atg4C, and Atg4D) (Betin et al., 2013; Mariño et al., 2003). The protease activity and binding efficiency to ATG8s varies significantly among Atg4 homologs. For instance, ATG4B demonstrates a processing efficiency of LC3B that is 1500-fold or more compared to other Atg4 homologs (Li et al., 2011). ATG4A exhibits a preference for GABARAP-L2 over LC3B, whereas ATG4B processes all Atg8 homologs (Li et al., 2011; Tanida et al., 2004), but also contains an LC3-Interacting Region (LIR) for efficient cleavage (Rasmussen et al., 2017). On the other hand, ATG4C and ATG4D display minimal protease activity towards any mammalian Atg8 homologs (Mariño et al., 2003). Interestingly, despite their vastly different catalytic efficiency, these four homologs exhibit similar binding affinity to Atg8 homologs (Li et al., 2011). Although not firmly established, it is possible that higher eukaryotes employ different homologs depending on cell type and specific contexts.

The main lipid source to be mobilized for the expansion of the phagophore membrane is believed to be the ER (Bento et al., 2016). Small vesicles that originate from the plasma membrane, recycling endosomes and the Golgi are also speculated to act as lipid sources (Nakatogawa, 2020). These vesicles can be positive for ATG9A, a lipid scramblase that can transfer phospholipids between the leaflets of a lipid bilayer (Maeda et al., 2020; Matoba et al., 2020). It has also been reported that ATG2, a lipid transferase that can move lipids between membranes, could also mediate phagophore expansion (Maeda et al., 2019; Osawa et al., 2019; Valverde et al., 2019). The widely accepted model suggests that ATG2 transfers lipids from the ER to ATG9A on the phagophore which then mediates the distribution of lipids between the lipid bilayers during phagophore formation (Ghanbarpour et al., 2021).

The autophagosome is considered to be complete when it is a closed double-membrane structure. The sealing of the phagophore has been suggested to be mediated by the endosomal sorting complex required for transport (ESCRT) proteins and the vacuolar protein sorting 37 homolog A (VPS37A) (Takahashi et al., 2019; Zhen et al., 2020).

### **1.2.1.3 Maturation and fusion with the lysosomes**

The fusion of the autophagosome with the lysosome, leads to the formation of an autolysosome. Inside that organelle, hydrolases degrade the autophagic cargo into building blocks. Autophagosomes, apart from fusing with lysosomes, can also fuse with endosomes to form amphisomes (Seglen et al., 1991), that also subsequently fuse with the lysosomes (Lőrincz & Juhász, 2020). Among the proteins and protein complexes that have been implicated in the autophagosome-lysosome fusion are the Rab GTPases and membrane tethering factors and soluble N-ethylmaleimide-sensitive factor attachment protein receptors (SNAREs). The interaction between the SNARE syntaxin 17 (Stx17), which sits on the membrane of sealed autophagosomes, and the synaptosomal-associated protein 29 (SNAP-29),



vesicle-associated membrane protein 8 (VAMP8) and the homotypic fusion and protein sorting (HOPS) complex, which sits on the lysosomes, mediates the autophagosome-lysosome fusion (Itakura et al., 2012; Jiang et al., 2014; Saleeb et al., 2019).

### 1.2.2 Selective autophagy and Sequestosome 1-like receptors

As previously mentioned, autophagy was initially considered to be a bulk process, where under nutrient deprivation, amino acids and other building blocks are made available by degradation of macromolecules and recycling the building blocks to maintain cellular homeostasis (Zaffagnini & Martens, 2016). While non-selective bulk autophagy is clearly being employed in yeast, a recent study has proposed that autophagy under nutrient deprivation in mammals is characterized by a prioritization of membrane protein cargo, specifically a targeted degradation of Golgi and the ER (Hickey et al., 2023). This model would suggest that autophagy was evolutionarily programmed to prioritize the recycling of lipids as well as proteins during nutrient stress in mammals. The different types of selective autophagy are usually named after the component that is being degraded; for example, mitophagy refers to the degradation of mitochondria; aggrephagy to the degradation of protein aggregates; xenophagy to the degradation of intracellular pathogens; pexophagy to the degradation of peroxisomes and ERphagy to the degradation of ER (Galluzzi et al., 2017) (Figure 4).

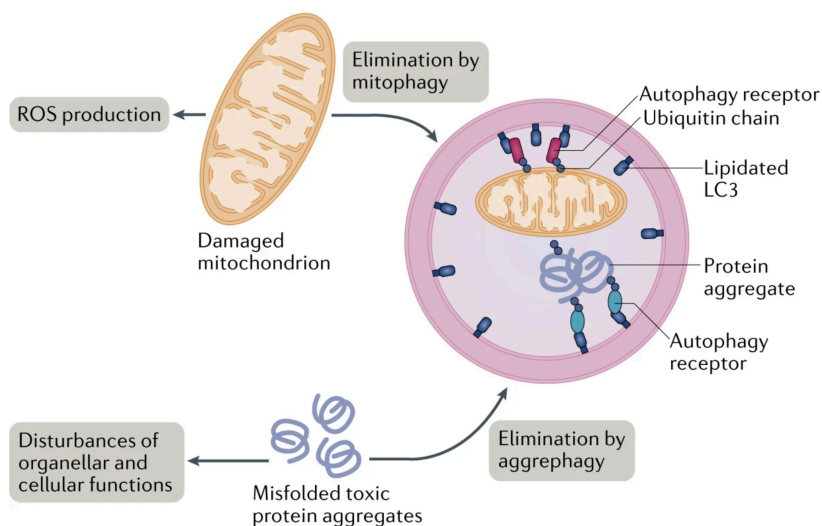


**Figure 4. Schematic representation of mitophagy and aggrephagy.** When mitochondria are damaged, they generate elevated levels of reactive oxygen species (ROS), which can endanger various cellular components such as proteins, lipids and DNA. Their elimination via selective autophagy is crucial in balancing oxidative stress. Harmful protein aggregates also need to be eliminated via selective autophagy, to avoid physiological implications. Figure modified from (Dikic & Elazar, 2018).

Mainly in a context other than nutrient starvation, selective autophagy, the targeted degradation of cargo, depends on a group of adaptor proteins termed selective autophagy receptors (SARs), which are responsible for targeting the specific cargo (Johansen & Lamark, 2019). The SARs achieve the targeting by binding to the cargo and interacting with members of the ATG8 family proteins, through their LC3-interacting regions (LIRs), the latter being lipidated and anchored in the membrane on the concave side of the developing autophagosome, allowing the cargo to be enclosed in the forming phagophore. (Birgisdottir et al., 2013; Lamark & Johansen, 2021). These receptors can be either soluble or membrane-bound (Johansen & Lamark, 2020a).

The most studied group of soluble SARs are the Sequestosome-1-like receptors (SLRs), which mediate cargo targeting through ubiquitin-binding domains (Lamark & Johansen, 2021). In addition, soluble SARs that involve cargo binding independently of ubiquitin-binding domains have also been identified, like the calcium-binding and coiled-coil domain-containing protein 1 (CALCOCO1), nuclear receptor coactivator 4 (NCO4) and tripartite motif-containing protein 5  $\alpha$  (TRIM5 $\alpha$ ) (Mancias et al., 2014; Mandell, Jain, et al., 2014; Nthiga et al., 2020).

#### **1.2.2.1 The sequestosome-1-receptors p62 and NBR1**

The sequence and functional similarity of all the SLRs are converging on the molecular characteristics of the first identified SAR: p62/SQSTM1 (Bjørkøy et al., 2005; Johansen & Lamark, 2011).

Specifically, p62 is central to the process of clearing polyubiquitinated aggregates (Pankiv et al., 2007; Zaffagnini & Martens, 2016). It contains among others, a C-terminal ubiquitin-binding domain (UBA), an N-terminal Phox and Bem1 (PB1)- domain which facilitates p62 oligomerization and formation of the structures referred as p62 bodies (Sun et al., 2018; Wurzer et al., 2015). These are dynamic liquid-liquid phase separated structures, considered to function as signaling and protein degradation platforms (Kageyama et al., 2021). Among others, p62 also plays a significant regulatory role in the antioxidative response, especially in the NRF2 – KEAP1 pathway, as will be explored in later sections.

The neighbor of BRCA1 gene 1 (NBR1) is another PB1 domain – containing protein which is a functional homolog of p62 (Lamark et al., 2003). Considering that plants lack the *p62* gene, but they do express an ancestral version of NBR1 with a PB1 domain capable of polymerization, it has been hypothesized that p62 is the result of a gene duplication of that ancestral gene (Svenning et al., 2011). The formation of p62 bodies is assisted by NBR1 and the history of the two genes has been closely linked as it will be explored in paper IV of this thesis.

## 1.2.3 The ATG8 family of proteins

### 1.2.3.1 LIR motif: Consensus sequence and functions

The existence of LIR motifs within the SARs sequences is central to the concept of selective autophagy, since they are responsible for the interaction with the ATG8s and consequently with the phagophore. The first LIR motif was identified in p62/SQSTM1 (Pankiv et al., 2007). The canonical LIR motif is described by the core sequence: [W/F/Y]<sub>0</sub>-X<sub>1</sub>-X<sub>2</sub>-[I/L/V]<sub>3</sub>, where X is any amino acid (Birgisdottir et al., 2013; Lamark & Johansen, 2021). The binding site on the ATG8 proteins responsible for the interaction with the LIR motif on the SAR, or other LIR-containing ATG8 interactors, is named LIR docking site (LDS) and consists of two hydrophobic pockets, HP1 and HP2. The aromatic residue (W/F/Y) at position 0 of the LIR docks into HP1 and the hydrophobic residue (I/L/V) at position 3 docks into HP2 (Noda et al., 2010) (Figure 5).

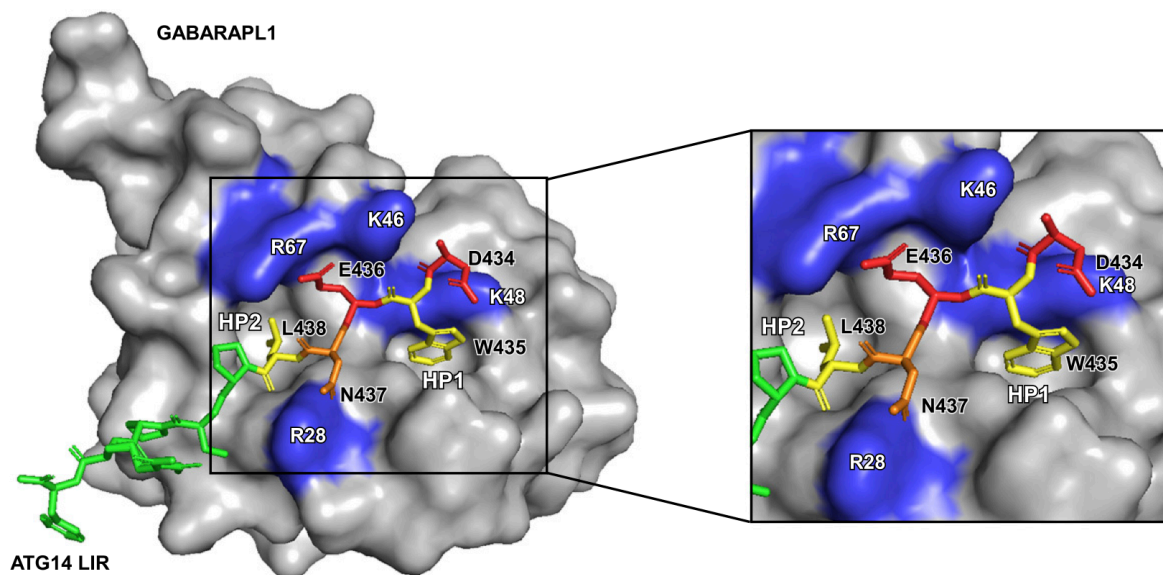


**Figure 5. Structural model depicting the LIR of ATG14 in the LDS of GABARAPL1.** The side chains of the aromatic tryptophane (W435) and the hydrophobic leucine (L438) in the ATG14 LIR dock into the pockets of the LDS of GABARAPL1 (highlighted in blue). Figure from (Johansen & Lamark, 2020).

The binding affinity and specificity of the interaction between the LIR motif and the ATG8 proteins is also affected by residues that flank the core LIR motif both N- and C- terminally. The generally basic surface of the LDS, for example, can explain the higher frequency of acidic residues, like aspartate (D) and glutamate (E), or residues that can be phosphorylated, like serine (S) and threonine (T), located N-terminally to the core LIR (Johansen & Lamark, 2020b). The residues in the positions X<sub>1</sub> and X<sub>2</sub>, while

theoretically they can be any amino acid, a selection arises because of the basic surface of the LDS against arginine (R) and lysine (K), in favor of acidic residues (Alemu et al., 2012). Amino acids like glycine (G) and proline (P) have a lower chance of being selected for these positions due to the structure interference they may impose on the LIR (Alemu et al., 2012; Johansen & Lamark, 2020b). Finally, the electrostatic interactions facilitated by residues that are flanking the core LIR motif are also very important in LIR – LDS interactions.

The ATG8 family of proteins is characterized by sequence homology and structural similarity. However, differences in the binding, even to the same LIR, exist. This specificity is mostly driven by the residues in the core LIR or in its flanking regions (Figure 6). The term GABARAP-interaction motifs (GIMs), for example, refer to LIRs that are preferentially binding to GABARAP over other ATG8s. The respective core consensus sequence is [W/F]<sub>0</sub>-[I/V]<sub>1</sub>-X<sub>2</sub>-V<sub>3</sub> (Rogov et al., 2017). In addition, some LIRs lack the aromatic [W/F/Y]<sub>0</sub> residue (Shrestha et al., 2020; Muhlinen et al., 2012). Others do not contain the hydrophobic [I/L/V]<sub>3</sub> residue. Hence, TRIM5 $\alpha$  possesses an interesting core LIR, DW<sup>196</sup>E, that interacts with both LC3 and the GABARAP subfamily members, but only the HP1 pocket is involved (Keown et al., 2018). This half-LIR corresponds to an  $\alpha$ -helical coiled coil region of TRIM5 $\alpha$  with W<sup>196</sup> extending into the HP1 hydrophobic pocket. This atypicality in the structural interface between TRIM5 $\alpha$  and the ATG8s, broadens the scope of LIRs to include  $\alpha$ -helical binding motifs, a concept very relevant to this thesis.

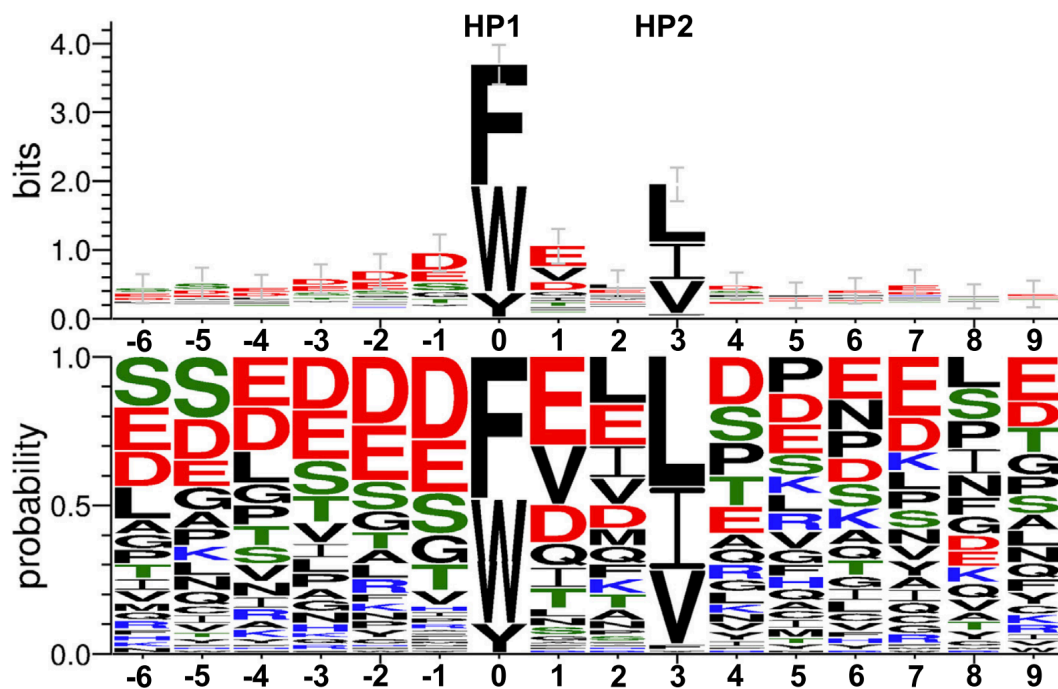


**Figure 6.** Sequence comparison generated by 100 known LIRs. Total stack height (upper diagram) corresponds to amino acid conservation at that position. The size of the lettering (lower diagram) indicates the probability of

finding a specific amino acid in the given position, relative to the aromatic residue at position 0 of the LIR. Figure adapted from (Johansen & Lamark, 2020).

### **1.2.3.2 Roles of ATG8s in the nucleus**

The functional significance of the ATG8s in the nucleus is largely unexplored, most studies focus on LC3B. While LC3 was for a long time believed to operate predominantly within the cytosol where the process of autophagy unfolds, there appeared to be a noticeable enrichment of LC3B in the nucleus compared to the cytoplasm in fluorescence images presented in several papers published before 2010 (Bampton et al., 2005; Ciechomska & Tolkovsky, 2007; Köchl et al., 2006; Kuma et al., 2007).

Up until then, no specific study of the nuclear pool of LC3B had been done, and the mechanisms governing the shuttling of LC3B between the cytoplasm and nucleus remained unidentified. In 2010, a study by Drake et al. explored the nucleocytoplasmic distribution of EGFP-LC3B. They showed that the rates of passive nuclear import and export of EGFP-LC3B are relatively slow and that when autophagy was induced by nutrient starvation, soluble EGFP-LC3B levels in the nucleus versus cytoplasm increased in the early stages. In this but also other studies (Drake et al., 2010; Kraft et al., 2014, 2016), they favored a model in which the diffusion of LC3B (tagged with Venus or EGFP) is slow (unusual for a protein of its size) because of its association with high molecular weight complexes in the nucleus, preventing its rapid equilibrium across the nuclear envelope under starvation and potentially other types of stress. In addition, Huang et al. demonstrated that nuclear LC3B is deacetylated and subsequently trafficked to the cytoplasm under starvation, postulating that the nuclear pool of LC3B is a source of autophagosome-targeted LC3B in starved cells (Huang et al., 2015).

A limited number of studies have focused also on the role of LC3B inside the nucleus. For example, it has been indicated that nuclear LC3B interacts with the promyelocytic leukemia (PML) protein (He et al., 2014), components of the extracellular signal-regulated kinases (ERK) pathway (Martinez-Lopez et al., 2013) and the ribosome receptor NUFIP1 (Shim et al., 2020). LC3B has also been identified in older studies as a fibronectin mRNA-binding protein enhancing fibronectin's translation (Ying et al., 2009; Zhou et al., 1997). In a more mechanistic approach, Dou et al. showed that LC3B directly interacts with lamin B1 in senescence, associates with transcriptionally inactive heterochromatin domains known as lamin-associated domains (LADs) and participates in the degradation of nuclear lamina in response to oncogenic insults (Dou et al., 2015). Sirtuin 1 (SIRT1), an important deacetylase whose levels have been shown to be low during ageing, was shown to be targeted to the lysosome by selective autophagy, involving direct nuclear capturing by LC3B (Xu et al., 2020). Recently, a study showed that the stability and transcriptional activity of the LIM homeodomain transcription factor (LMX1B) are in part regulated through LC3B, acting also as a transcriptional cofactor (Jiménez-Moreno et al., 2023).

Since the aforementioned studies suggest different functions of LC3B in the nucleus, ranging from degradation of nuclear proteins, like lamin B1 and SIRT1 to mRNA binding and presence in PML bodies, further research is needed in order to discover the exact roles of LC3B in the nucleus.

## 1.3 The cellular antioxidant defense

### 1.3.1 Reactive oxygen species (ROS) and oxidative stress

The term “oxidative stress” was first defined by Helmut Sies (Sies, 1985, 2015) as an imbalance between the production of oxidants and the biological systems’ antioxidant defense. When the cells are in such balance, they achieve a homeostatic redox status. In the event of an oxidative stress insult, an accumulation of reactive oxygen species (ROS) is being facilitated. Under homeostatic conditions, ROS are implicated in various physiological processes, such as cell survival, host defense, apoptosis, autophagy and cell differentiation (Forman & Zhang, 2021). Several signaling proteins and/or transcription factors, like NF- $\kappa$ B, MAPKs, PI3K and p53, execute their cellular functions in response to the homeostatic ROS generation (Budanov, 2014; Koundouros & Poulgiannis, 2018; Truong & Carroll, 2013; Wang et al., 2015).

The term ROS encompasses molecules derived from  $O_2$ , such as superoxide radicals ( $O_2^{\cdot-}$ ), hydrogen peroxide ( $H_2O_2$ ), hydroxyl radicals ( $\cdot OH$ ), and singlet oxygen ( $^1O_2$ ). The cellular (or endogenous) ROS are constantly produced in aerobic organisms as by-products from the mitochondrial oxidative metabolism and through the activity of oxidases. The exogenous ROS can be the result of xenobiotic compounds (like anticancer drugs) or external stressors, such as UV radiation, ionizing radiation, pollutants, heavy metals, that can significantly elevate ROS production (Figure 7).

The generation of ROS starts with the production of  $O_2^{\cdot-}$  as a consequence of electron leakage from the mitochondrial respiratory chain, particularly from ubiquinone ( $QH^{\cdot-}$ ) and the NADPH oxidases (Boveris et al., 1976; Lambeth, 2004). This  $O_2^{\cdot-}$  dismutates to  $H_2O_2$  either spontaneously or catalyzed by the superoxide dismutases (McCord & Fridovich, 1969). The rate of  $H_2O_2$  production determines whether redox signaling, oxidative stress or no oxidation will occur.  $H_2O_2$  is reduced enzymatically by different enzymes, like catalase or glutathione (GSH) peroxidases, to  $H_2O$  (Jones, 2008). In addition,  $H_2O_2$  can react rapidly with transition metals such as iron to produce  $\cdot OH$ , a reaction commonly referred to as the Fenton reaction (Koppenol, 1993).  $\cdot OH$  is a strong oxidant that will rapidly oxidize nearby molecules, like lipids with allylic hydrogens present in polyunsaturated fatty acids. The final oxidants to be considered are the hypohalous acids (HOX) that are catalyzed from  $H_2O_2$  by peroxidases (where  $X^-$  may be  $Cl^-$  or  $Br^-$ ) (Pattison et al., 2012).

Exposure to a changing environment causes cells to face circumstances that can affect their homeostatic redox status. ROS are counterbalanced by an antioxidant defense network, which functions to modulate ROS levels to allow their physiological roles whilst minimizing the oxidative damage they cause (Davies, 1986; Halliwell, 2023). Overwhelming the cellular antioxidant system through excessive ROS, or impairment of the antioxidant defense network, results in oxidative stress. Oxidative damage negatively affects the physiological function of macromolecules such as nucleic acids, proteins, and lipids. Excessive levels of ROS are constantly linked with several pathological conditions, such as ageing, diabetes, cancer, and neurodegenerative diseases (Pizzino et al., 2017).

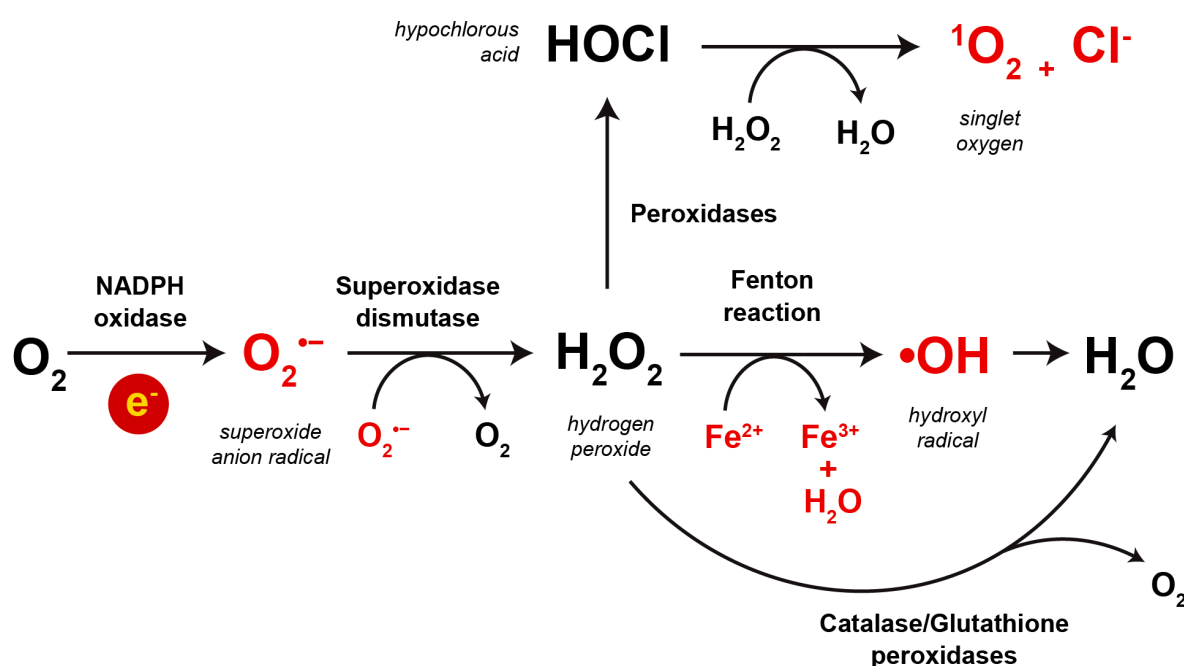


**Figure 7. Simplified representation of the generation of reactive oxygen species (ROS).** The majority of ROS, arise as byproducts of mitochondrial oxidative phosphorylation or as intermediates of oxidoreductase enzymes and metal-catalyzed oxidation. Due to the presence of two unpaired electrons in separate orbitals, oxygen is prone to radical formation. The sequential reduction of oxygen, involving the addition of electrons, results in the generation of various ROS, such as superoxide anion ( $O_2^{\cdot-}$ ), hydrogen peroxide ( $H_2O_2$ ), and hydroxyl radical ( $\cdot OH$ ). For more details, see main text.

### 1.3.2 The mechanisms of antioxidant action

As it was previously described, some ROS are free radicals (atoms or molecules containing one or more unpaired electrons), whereas others are non-radicals (all their electrons are paired together). Some ROS are generated accidentally (for example, by autoxidation reactions and leakage of electrons from electron transport chains) and others deliberately through signal transduction pathways, to support

essential processes such as defense against pathogens (Halliwell, 2023). To regulate the accumulation of ROS, biological systems are exploiting substances known as antioxidants.

An antioxidant is defined as a substance that reacts with ROS to regulate its reactions with other targets, thus influencing redox-dependent biological signaling pathways and/or oxidative damage (Murphy et al., 2022). Different antioxidants react with different ROS at variable rates, act in various cellular, subcellular and intra-organellar (especially in mitochondria) locations and protect molecular targets.

The primary defense includes enzymatic and non-enzymatic antioxidants that focus on the elimination of ROS. They encompass (Halliwell, 2023):

1. ROS-removing agents, such as the superoxide dismutase (SOD) enzymes, peroxiredoxins, glutathione peroxidases and catalases.
2. Proteins such as haptoglobin and transferrin, that bind or store putative pro-oxidants, like iron and copper ions, in non-redox forms, minimizing their availability.
3. Physical "quenchers" of ROS, such as some carotenoids, which scavenge several ROS and quench  $O_2^{\cdot-}$  by converting it back to  $O_2$  (Bohn et al., 2023; Han et al., 2012), glutathione (GSH), ubiquinol,  $\alpha$ -tocopherol, ascorbate (also known as vitamin C, (Padayatty & Levine, 2016)), albumin, mucus and plasmalogens.
4. Subcellular compartmentalization of pro-oxidant transition metal ions since the disruption of metal ion-restricting cellular structures (such as lysosomes) can accelerate oxidative damage.
5. Antioxidant effects stemming from lifestyle changes, like increasing exercise, avoiding obesity, control of blood glucose and cholesterol and following a high-quality diet (Halliwell, 2023).

These antioxidants can be produced in eukaryotic organisms or be obtained from dietary compounds of fruits and vegetable origin (like the vitamin C and E, carotenoids and sulforaphane) (Guerrero-Beltrán et al., 2012; Sies, 1997).

Organisms also employ various other strategies to minimize the production of ROS, which are also often characterized as antioxidants by the researchers that study them. For example, the mitochondrial uncoupling proteins (UCP1, UCP2, UCP3) regulate ROS production by preventing excessive protonmotive force, thus reducing electron leakage from the electron transport chain (Brand, 2016; Hirschenson et al., 2022). The organization of the mitochondrial electron carriers into complexes (I, II, III and IV) and supercomplexes also decreases electron leakage (Brand, 2016). In addition, the human vascular system has evolved to deliver an optimal amount of  $O_2$  to cells and tissues, avoiding both energy production impairment and oxidative damage and stem cells reside in hypoxic niches to minimize oxidative damage until needed (Harwell, 2007). Other strategies involve cells responding to increased ROS by modifying membrane lipids for increased resistance to peroxidation or replacing



ROS-sensitive enzymes with ROS-resistant ones (Cao et al., 2023; Liochev & Fridovich, 1993; Pedroso et al., 2009). These mechanisms collectively contribute to cellular protection against oxidative stress.

### 1.3.3 Transcription factors in the cellular antioxidant system

Oxidative insults can affect the transcriptional regulation of many genes. These either encode for antioxidant proteins and detoxifying enzymes that are participating in the antioxidant defense, or they are targets of other transcription factors that are directly disturbed by oxidants (Dharshini et al., 2020). For example, it has been well established that ROS can directly affect the conformation and activity of diverse sulfhydryl-containing proteins like transcriptional factors, by oxidation of their thiol functional groups, impacting protein-protein and protein-DNA interactions.

Among the transcription factors that can be regulated by H<sub>2</sub>O<sub>2</sub> and other ROS, is NF-κB and AP-1 (Meyer et al., 1993; Schreck et al., 1991). The mechanism of NF-κB activation involves its release in the cytoplasm from IκB (inhibitor of NF-κB). Upon exposure to oxidants, IκB gets phosphorylated and degraded by the proteasome and the released NF-κB translocates to the nucleus and transactivates its target genes. In the case of AP-1, its DNA-binding and transactivation ability are induced upon treatment with antioxidants, due to reduction of its cysteines', but are decreased when the same residues are oxidized (Nordberg & Arnér, 2001). Additionally, other important transcription factors are also directly or indirectly affected by the status of cellular ROS levels. These include p53, FOX (Forkhead Box O), HIF-1α (Hypoxia Inducible Factor-1) and, importantly, NRF2 (Dharshini et al., 2020).

#### 1.3.3.1 Cap 'n' collar transcription factors

Cap'n'collar (Cnc) proteins are a family of basic leucine zipper (bZIP) transcription factors (Sykiotis & Bohmann, 2010). They are found across a variety of organisms such as worms, insects, fish, birds and mammals but are not present in plants and fungi. These proteins are characterized by a conserved 43-amino acid Cap 'n' collar (Cnc) domain located on the N-terminal side of the DNA binding domain. Members of the Cnc family play key roles in development, while others are vital for maintaining homeostasis amid environmental insults, like oxidative stress (Sekine & Motohashi, 2021; Sykiotis & Bohmann, 2010).

The Cnc transcription factor family encompasses the *Caenorhabditis elegans* SKN-1 (Skinhead family member-1) (Blackwell et al., 2015), the *Drosophila melanogaster* Cnc (Pitoniak & Bohmann, 2015) and four vertebrate counterparts—the p45 NF-E2 (Ney et al., 1993), the NFE2-related factors NRF1 (Chan et al., 1993), NRF2 (Moi et al., 1994), and NRF3 (Kobayashi et al., 1999). In *D. melanogaster* and vertebrates, Cnc proteins contain a bZIP motif which is rich in basic residues, required

for DNA-binding, followed by six heptad repeats of hydrophobic residues, creating a leucine zipper utilized for homo- and heterodimerization (Landschulz et al., 1988). SKN-1 in *C. elegans* lack a leucine zipper region and it binds to DNA as a monomer (An & Blackwell, 2003). The p45 NF-E2 has been reported to play a role in platelet development transducing signals via an AP-1-like DNA binding motif but lacks the N-terminal hydrophobic and transactivation domains present in other Cnc's in vertebrates (Andrews, 1998; Shivdasani, 1996) (Figure 8).

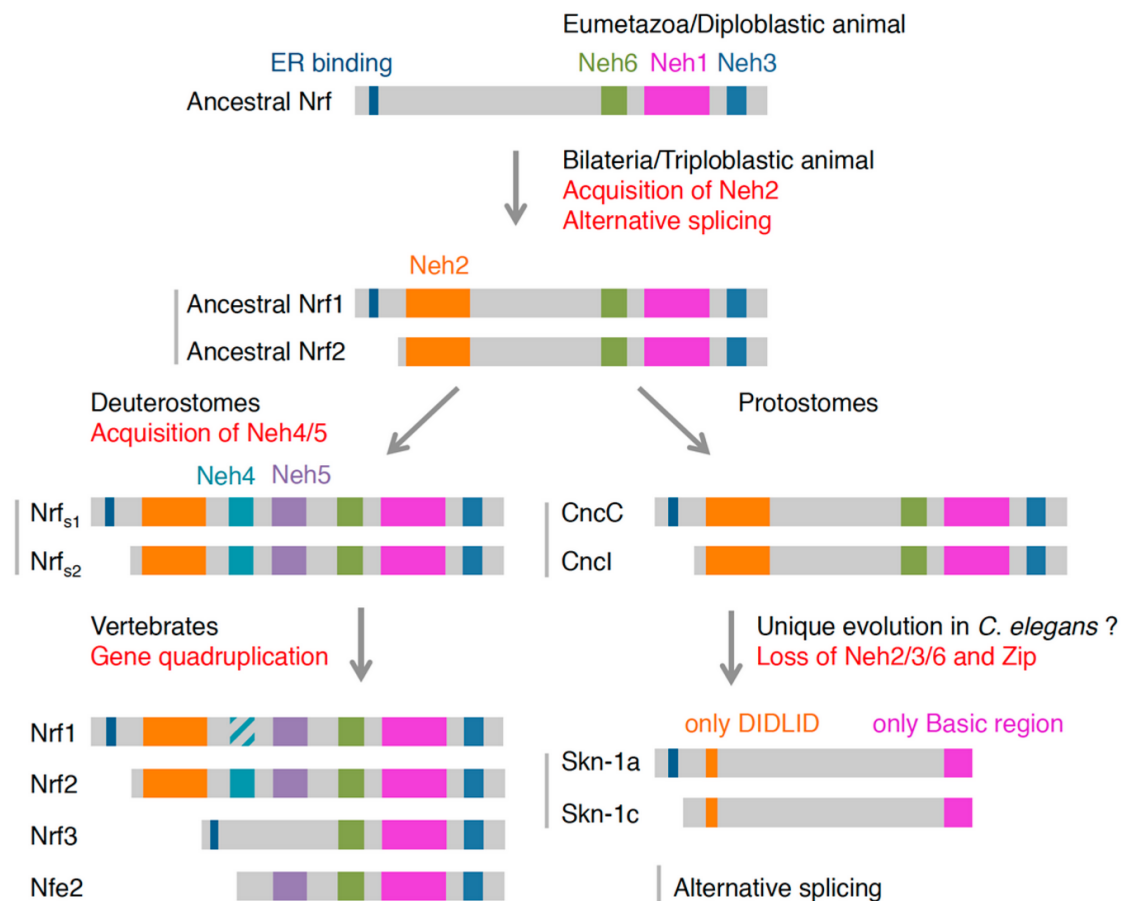


**Figure 8. The putative evolutionary path of the NRF/Cnc transcription factors.** Gray bars and subscripts (s1 and s2) denote putative products of alternative splicing. Figure from (Fuse et al., 2017).

The NRF1, NRF2 and NRF3 transcription factors have a Cnc-bZIP domain for DNA binding on the promoter of their target genes (Toki et al., 1997). They have distinct but partly overlapping expression patterns and function as stress-activated transcription factors. They are also reported to trigger the transcription of cytoprotective genes by interacting with antioxidant response elements (AREs) present in their cis regulatory regions (Sykietis & Bohmann, 2010). NRF2 and CncC have emerged as the main regulators of the cellular antioxidant defense system in vertebrates and *D. melanogaster*, respectively.

### 1.3.3.2 Antioxidant Response Elements

The transcriptional regulatory elements known as antioxidant response elements (ARE) or electrophile response elements (EpRE) are conserved sequence motifs in the cis regulatory regions of antioxidant defense genes (Raghunath et al., 2018). AREs are recognized as crucial regulators of cellular redox balance and protection against oxidative stress.

The ARE motif was first identified as a xenobiotic response element (XRE), a  $\beta$ -NF responsive element in the 5'-flanking region of rat *GSTY2* (glutathione transferase  $\alpha$  2) gene (Telakowski-Hopkins et al., 1988). Later, while studying the *NQO1* (NAD(P)H: quinone oxidoreductase 1) and *GSTY2* genes, XRE was renamed to ARE with the consensus 5' – RGTGACnnnGC – 3' (n = A, C, G or T) due to its responsiveness to H<sub>2</sub>O<sub>2</sub> and phenolic antioxidant stress (Rushmore et al., 1991). Some years after its establishment, essential nucleotides outside the previously identified core sequence were shown to be required for inducible expression and the suggested ARE consensus sequence was extended to 5' – TMAnnRTGAYnnnGCRwww – 3' (M = A or C, R = A or G, Y = C or T, w = A or T, core sequence underlined) (Wasserman & Fahl, 1997). To converge ARE sequences found in previous studies, a computational analysis was performed (Wang et al., 2007), where experimentally identified ARE sequences from the NCBI literature database were used to identify ARE sequences in the human genome (Figure 9).

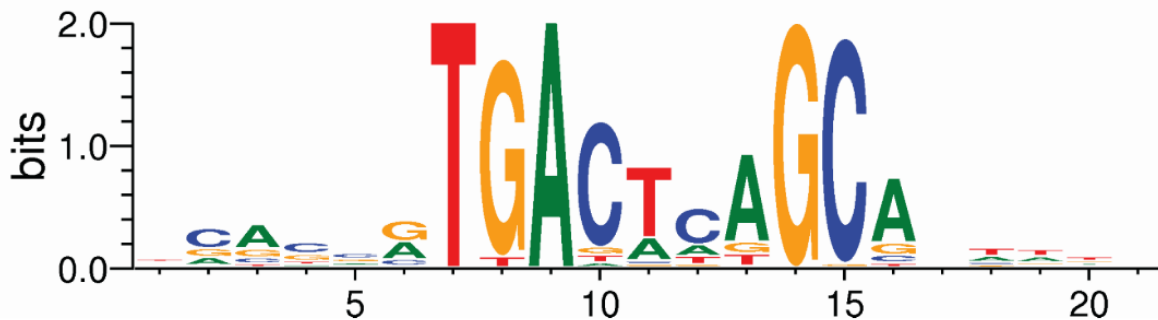


**Figure 9. The ARE consensus based on 57 functional AREs tested by experimental methods.** The ARE consensus sequence logo, showing contributions of individual nucleotides and their respective positions. The overall height of each stack indicates the sequence conservation at that position (measured in bits), and the height of each nucleotide within the stack corresponds to its occurrence at that position. Figure adapted from (Wang et al., 2007).

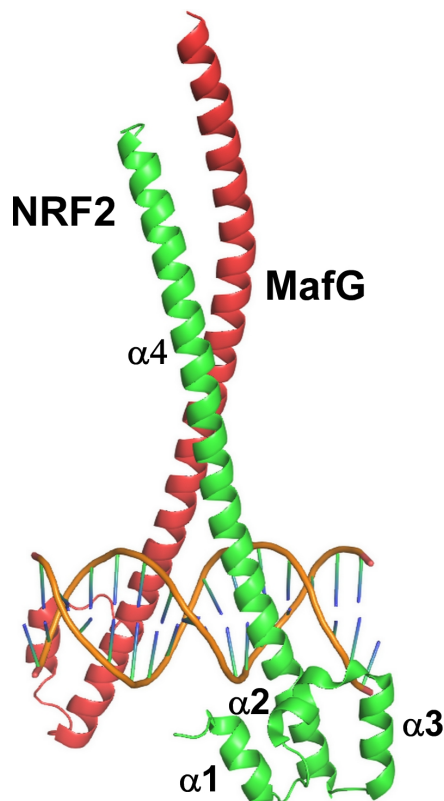
### 1.3.3.3 Small musculoaponeurotic fibrosarcoma proteins (sMAFs)

The Cnc family of transcription factors require the small Maf proteins as dimerization partners in the nucleus, in order to bind to the AREs (Itoh et al., 1997). The Maf proteins were named after the initial

member of the family known as the avian musculoaponeurotic fibrosarcoma (*vMAF*) viral oncogene, which encodes a leucine zipper motif sharing similarities with other bZIP proteins (Nishizawa et al., 1989). They are divided into large and small Mafs but only the small Mafs are relevant for the Cnc transcriptional activity. Notably, Fujiwara and colleagues initially identified two small Maf proteins, MafK and MafF, with an approximate molecular weight of 18 kDa (Fujiwara et al., 1993). Then another related gene, *MAFG*, displayed significant homology with MafK and MafF (Kataoka et al., 1995). MafK, MafF, and MafG constitute the small Maf (sMaf) protein group (Katsuoka & Yamamoto, 2016) (Figure 10).

The sMafs create heterodimers with members of the Cnc family of transcription factors, which can recognize AREs. Depending on whether the Cnc subunit possesses a transactivation domain, these heterodimers function as either transcriptional activators or repressors (Raghunath et al., 2018).

In addition, sMaf proteins have the ability to form homodimers that selectively bind to sequences called Maf-responsive elements (MAREs), acting as transcriptional repressors (Katsuoka & Yamamoto, 2016). The consensus sequences of AREs and MAREs exhibit similarities, and both Cnc–sMaf heterodimers and sMaf homodimers often bind to these elements, albeit with slightly different binding affinities. Competitive binding occurs between Cnc–sMaf heterodimers, sMaf homodimers, and other bZIP proteins on regulatory DNA elements (Motohashi et al., 2000; Roychoudhuri et al., 2016; Yang et al., 2010). The relative abundances and affinities of these dimers for the elements play a crucial role in determining whether their target genes undergo transcription.



sMafs possess two important domains: a basic DNA-binding region and leucine zipper domain that mediates their dimerization (Katsuoka & Yamamoto, 2016). Through structural and computational analyses, a recent study uncovered distinctive characteristics inherent in the interaction between NRF2 and the sMaf proteins (Sengoku et al., 2022). Notably, the authors showed that the affinity to DNA was significantly elevated in the NRF2-MafG-DNA complex (Figure 10), owing mainly to the CNC motif of NRF2, than with other canonical bZIP family members, such as AP-1 proteins.

**Figure 10. Overall structure of the NRF2-MafG-CsMBE complex.** The DNA binding domain of NRF2, which contains three  $\alpha$  helices ( $\alpha 1$ - $\alpha 3$ ) followed by a large one ( $\alpha 4$ ), is also known as the CNC motif and mediates the interaction with MafG and the DNA. NRF2 and MafG each contact a half-site of the CNC-sMAF binding element (CsMBE). (PDB ID: 7X5F) (Sengoku et al., 2022)

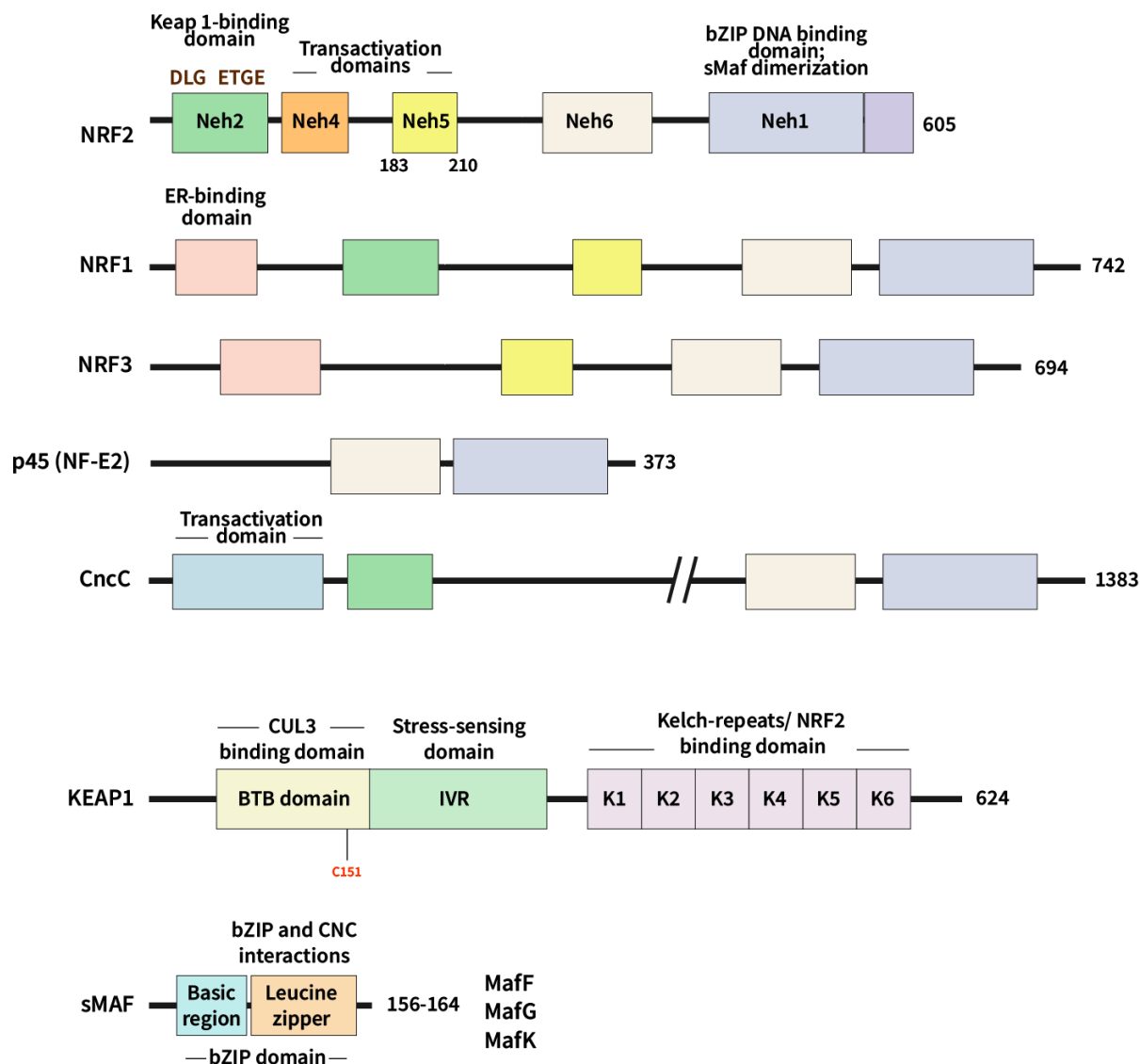


**Figure 11. Schematic representation of Cnc transcription factors, KEAP1 and small MAF.** NRF2: for details on the functions of the NRF2 regions, see main text. KEAP1: The Broad Complex, Tramtrack, and Bric-a-Brac (BTB) domain is responsible for binding with CUL3 and homodimerization and contains the C151 residue which is part of the response to NRF2-activating compounds. The Intervening Region (IVR) contains redox-sensitive cysteines and Kelch-repeats domain binds to NRF2 through the DLG and ETGE motifs in the Neh2 domain. sMAF: The general domain architecture of MafF, MafG and MafK contains a bZIP domain for its interaction with members of the CNC transcription factor family, which include NRF2.

### 1.3.4 The NRF2-KEAP1 pathway

As mentioned, NRF2 is a transcription factor that is vital for the antioxidative response. It was identified as an interactor of the NF-E2 element of the hemoglobin subunit beta (*HBB*) gene promoter (Moi et al., 1994). It is ubiquitously expressed in all tissues but not required for development of mice into adulthood (Chan et al., 1996). NRF2 is activated by several different oxidative insults such as ROS,

electrophiles, xenobiotics, UV radiation and heavy metals, and it induces the expression of antioxidant response genes (Hayes & Dinkova-Kostova, 2014; Tonelli et al., 2018).

NRF2 is comprised of seven NRF2-ECH homology domains (Neh1–7), each serving distinct functions (Tonelli et al., 2018) (Figure 11). The **Neh1** domain encompasses the CNC-bZIP region, which plays a vital role in DNA binding and its interaction with NRF2 dimerization partners, specifically the sMaf proteins. The **Neh2** domain contains two highly conserved amino acid sequences, known as the DLG and ETGE motifs. They facilitate the interaction with NRF2's negative regulator, Kelch-like ECH-associated protein 1 (KEAP1). The C-terminal **Neh3** domain possesses transactivation activity and collaborates with the **Neh4** and **Neh5** domains to activate the transcription of NRF2 target genes. The **Neh6** domain, characterized by its serine-rich region, plays a role in negatively regulating NRF2's stability, independently of KEAP1. The **Neh7** domain is involved in repressing NRF2's transcriptional activity through a physical association between NRF2 and the retinoid X receptor  $\alpha$  (RXR $\alpha$ ).

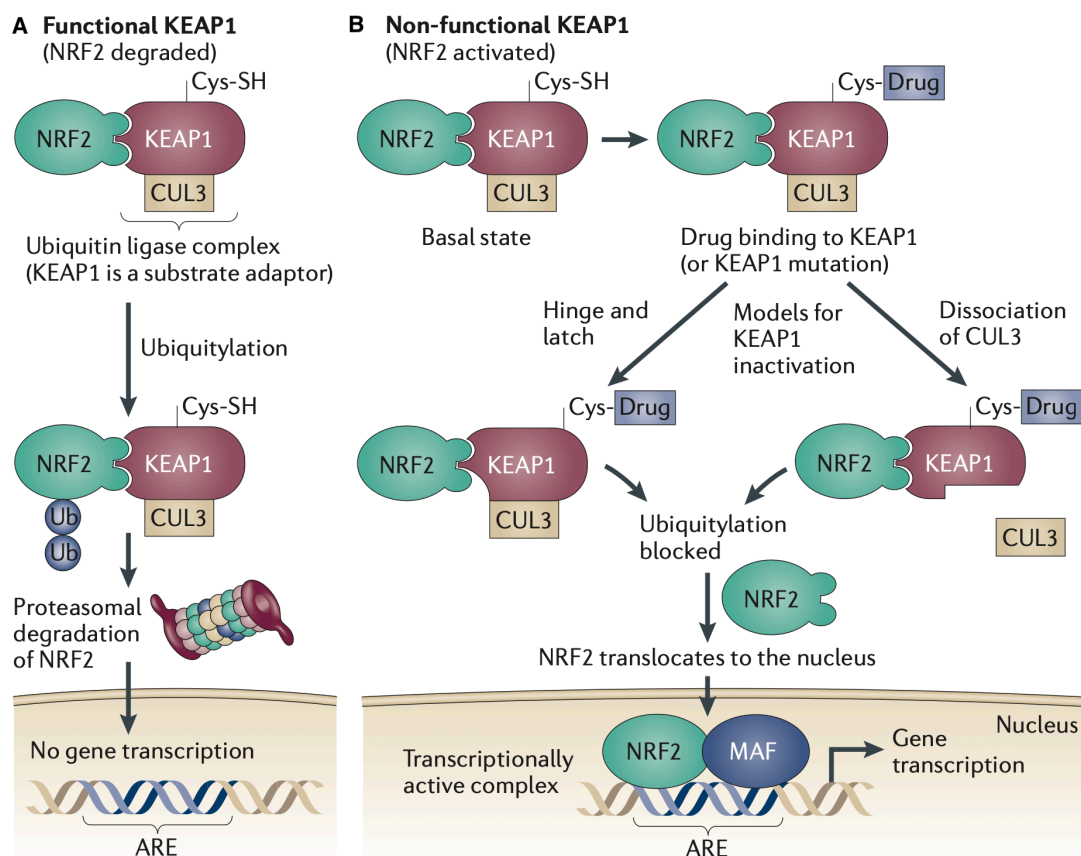


**Figure 12. Overview of the NRF2-KEAP1 pathway.** (A) Under basal conditions, NRF2 is polyubiquitinated by the KEAP1-CUL3 complex. CUL3 is a ubiquitin ligase and KEAP1 a substrate adaptor. This polyubiquitination results in NRF2 being degraded in the proteasome. (B) The ubiquitylation is blocked due to KEAP1 being rendered non-functional by a drug or electrophile, and NRF2 is not degraded by the proteasome. The newly translated NRF2 translocates then to the nucleus, where it becomes transcriptionally active by the MAF proteins or other co-factors, upregulating the transcription of antioxidative genes. Figure from (Sporn & Liby, 2012).

The NRF2 levels are intricately regulated by the UPS, through its interaction with KEAP1, which serves as a redox-sensitive adaptor for the E3 ubiquitin ligase (Itoh et al., 2003; McMahon et al., 2003) (Figure 12). In basal cellular conditions, KEAP1 forms a complex with the Neh2 domain of NRF2. Two molecules of KEAP1 bind one molecule of NRF2, at the DLG and ETGE motifs, respectively, through its Kelch-repeat domain (Baird & Yamamoto, 2020; Cuadrado et al., 2019) (Figure 13). Within this complex, KEAP1 acts as an essential adaptor for the CUL3 E3 ubiquitin ligase, which is responsible for maintaining NRF2's low levels by facilitating its constant ubiquitylation and degradation (Kobayashi et al., 2006). NRF2 typically has a short half-life of around 10–30 minutes in unperturbed conditions (Nguyen et al., 2003; Stewart et al., 2003).

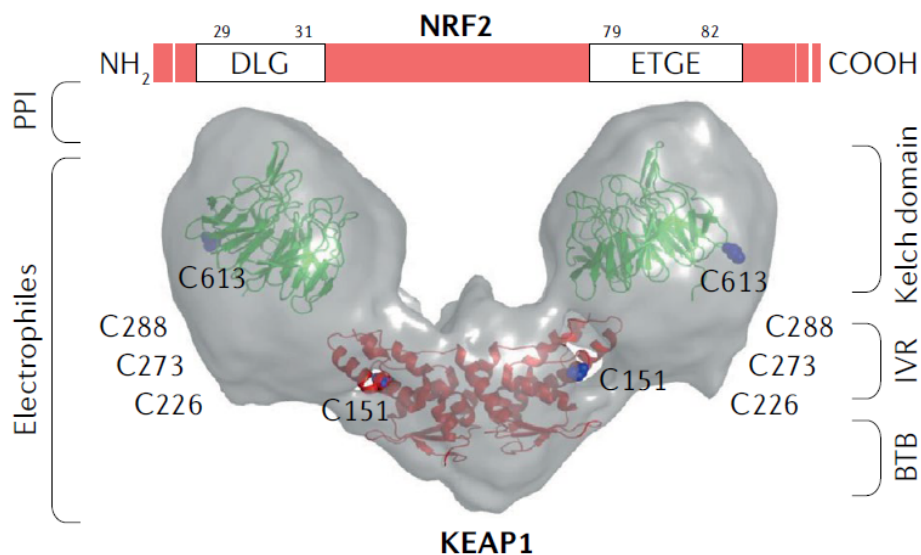


**Figure 13. Regulation of NRF2 by KEAP1.** Representation of a KEAP1 dimer, highlighting the BTB domain (red ribbons; Protein Data Bank identifier: 5NLB) and Kelch-repeat domains (green ribbons; PDB ID: 1ZGK). The reactive cysteines C151 and C613 are represented as blue spheres. The KEAP1 homodimer interacts with the transcription factor NRF2, at two motifs with varying affinities (29-DLG-31 and 79-ETGE-82), leading to ubiquitylation and proteasomal degradation of NRF2. Disruption of this interaction can be achieved through strategies such as the use of electrophiles that modify sulfhydryl groups of cysteines (e.g., C151, C273, and C288) in KEAP1 and protein–protein interaction inhibitors that affect the docking of NRF2 to KEAP1. Figure from (Cuadrado et al., 2019).

However, when the cells experience oxidative stress, KEAP1 undergoes oxidation at specific cysteine residues, rendering it inactive (Takaya et al., 2012). This event leads to the stabilization of NRF2 via a Hinge-Latch mechanism (Tong et al., 2007). The Hinge-Latch model explain that under a relevant oxidative insult, NRF2 remains associated with KEAP1, and the newly translated pool is the one that translocate to the nucleus (Horie et al., 2021). After its nuclear translocation, NRF2 forms heterodimers



with members of the sMaf protein family. The NRF2-sMaf complex exhibits sequence-specific binding to the AREs found in the promoter region of NRF2's target genes. Further research has broadened the scope of genes regulated by the ARE gene battery, encompassing those associated with drug detoxification, antioxidant responses, NADPH regeneration, and metabolic regulation.

### 1.3.5 NRF2 target gene activation via p300/CBP

NRF2 orchestrates the initiation of transcription through the recruitment of co-activators and components of the transcription machinery, with p300/CBP histone acetyltransferases and sMafs being detected in the ARE-binding complex (Fahl, 2001). One of the earliest co-activators identified to interact with NRF2 is the CREB binding protein (CBP) with two NRF2 domains, Neh4 and Neh5, acting synergistically to bind to CBP (Kato et al., 2001). It was later also shown that the Neh5 domain is crucial for the inducible expression of NRF2 target genes with specific residues in the same domain being differentially utilized for the activation of different genes (Zhang et al., 2007). Regarding the importance of CBP, it has also been demonstrated that displacement of CBP from the CBP-NRF2 complex leads to repression of NRF2-induced transcription (Brown et al., 2008).

The mechanism by which p300/CBP directly binds to NRF2 and acetylates the C-terminal Neh1 domain under arsenite-induced oxidative stress, in order to augment the promoter-specific DNA binding ability of NRF2 (Sun et al., 2009), revealed a big piece of the puzzle regarding NRF2 target gene activation. This concept was expanded by another study where the Neh3 domain was revealed to be acetylated as well, being functionally relevant, especially in terms of the HO-1 gene activation (Kawai et al., 2011). In addition, it was found that SIRT1 can deacetylate NRF2, resulting in a decrease in NRF2-dependent gene transcription and a redistribution of NRF2 in favor of re-localization to the cytoplasm. Regarding the nucleocytoplasmic shuttling of NRF2, it has also been shown that sustained interaction between Nrf2 and the sMafs prevented nuclear exit of NRF2 (Li et al., 2008). The authors suggested that this interaction masks the nuclear export signals in NRF2, preventing it from interacting with the CRM1/exportin 1 nuclear export receptor. The precise mechanism by which NRF2 and CBP collaborate to activate the ARE gene battery, as well as the interactions that are regulating this apparatus, remain to be fully understood (Figure 14).

Consequently, this affects the transcription of genes such as *NQO1*, *TXNRD1* and *GCLM*. In conjunction with histone-modifying enzymes, NRF2 also interacts with MED16 of the Mediator, a multi-subunit protein complex responsible for conveying activation signals from a DNA-bound transcription factor to RNA polymerase II (Pol II) (Sekine et al., 2016) or Brahma-related gene 1 (BRG1), the central ATPase subunit of the SWI/SNF chromatin-remodeling complex (Zhang et al., 2006), with the Neh5 domain to be relevant in these interactions.



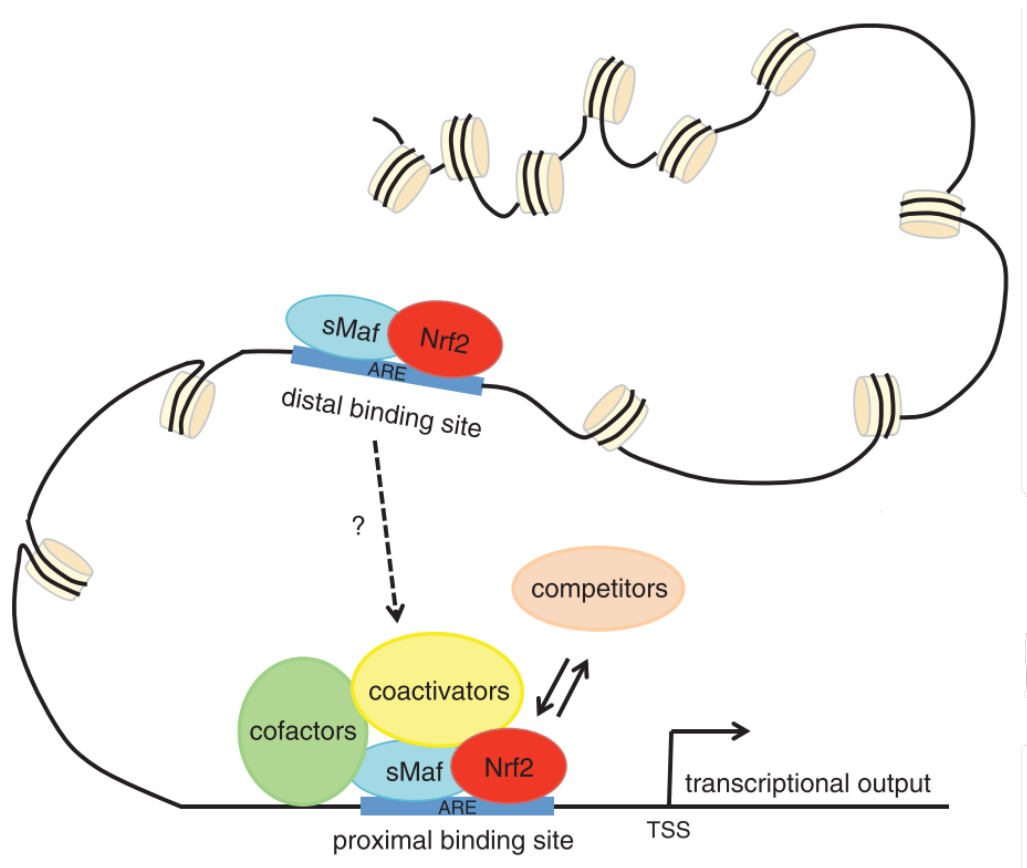


**Figure 14. The NRF2 transcription complex in the nucleus.** NRF2 occupies a central position within an intricate regulatory network. The control of gene expression depends on factors such as cellular context, the inducing agent, recognition of the ARE, interactions with binding partners, cofactors, and competitors, cross-influences with other signaling pathways, and even the epigenetic configurations of the target gene promoters. Figure adapted from (Tonelli et al., 2018).

### 1.3.6 NRF2-activating compounds

The induction of NRF2 is mediated by several substances, like phenol antioxidants, electrophilic compounds and/or heavy metals (Hayes & Dinkova-Kostova, 2014). One of the best characterized class of NRF2 activators are the KEAP1 Cys<sup>151</sup>-targeting compounds, with sulforaphane (SFN) and tert-butylhydroquinone (tBHQ) being the most prominent (Robledinos-Antón et al., 2019). SFN is a naturally occurring isothiocyanate originating from cruciferous vegetables, such as broccoli. It activates NRF2 without disrupting the KEAP1-Neh2 interaction (Horie et al., 2021). In addition, tBHQ, a phenol oxidant, utilizes the same Cys<sup>151</sup> residue of KEAP1 to activate NRF2.

### 1.3.7 Cytoprotective functions of NRF2 and its target genes

As it was previously discussed, the upregulation of NRF2 target genes containing upstream AREs is important for retaining the homeostatic redox status under oxidative insults and imbalances. These gene products perform cellular functions (among others drug metabolism, ROS scavenging and glutathione homeostasis) that are part of the antioxidant defense system (Zhang, 2021). Extensive studies on antioxidant enzyme induction focus on regulatory mechanisms, disease implications, and potential therapeutic inducers. While various redox-sensitive transcription factors are involved, NRF2, through the induction of antioxidant genes including *GCLC*, *GCLM*, *HO1*, *NQO1*, *TXNRD1*, *p62*, has the broadest impact. The induction of drug metabolism and transport via ARE gene products most likely originated as a detoxification strategy against endogenous oxidants, evolving to adapt to exogenous (or environmental) toxicants. NRF2 governs the metabolic fate of various pro-oxidants and electrophiles by controlling both basal and induced expression of drug-metabolizing enzymes and transporters (Hayes et al., 2014).

Among these, **NAD(P)H:quinone oxidoreductase 1 (NQO1)** is a central reductase, which catalyzes the two-electron reduction of quinones (reactive molecules that cause DNA damage), using either NADH or NADPH as the hydride donor, reducing the chance of ROS intermediates generation (Dinkova-Kostova & Talalay, 2010). The ARE sequence in the *NQO1* promoter has been mapped and reported to be responsible for its expression in response xenobiotics (Nioi et al., 2003).

The genes coding for the two subunits of a **glutamate cysteine ligase (Gcl)**, **GCLC** (catalytic subunit) and **GCLM** (modifier subunit) are responsible for the synthesis of  $\gamma$ -glutamyl-cysteinyl-glycine (GSH), a tripeptide important for redox status maintenance. GSH detoxifies xenobiotics and scavenges free radicals by functioning as a cofactor of the glutathione peroxidase (GPx), a  $H_2O_2$  metabolizing enzyme. In addition, it serves as a **glutathione S-transferase (GST)**-assisting electron donor, reducing disulfide bonds. Both the promoters of *GCLC* and *GCLM* contain ARE motifs (Dickinson et al., 2004; Erickson et al., 2002).

The **GST** gene battery products play also an important role in detoxifying xenobiotic electrophiles, conjugating them with glutathione. The different isoforms of *GST* contain ARE-motifs in their promoters and are sensitive to NRF2-activating agents (Chanas et al., 2002).

**Heme oxygenase 1 (HMOX1, commonly HO-1)**, is an enzyme that mediates the catabolism of heme to biliverdin which consecutively catalyzes to bilirubin by the biliverdin reductase (Otterbein et al., 2003). The expression of *HO-1* is mediated by the ARE-motif in its upstream regulatory region (Alam et al., 1999).

**Thioredoxin reductase 1 (TXNRD1)** is an enzyme belonging to the mammalian thioredoxin reductases (TrxRs), which is a family of selenium-containing pyridine nucleotide-disulphide oxidoreductases with mechanistic and sequence identity (J. Huang & Zhong, 2012). TrxRs catalyzes the NADPH-dependent reduction of the redox protein thioredoxin (Trx), as well as of other endogenous and exogenous compounds, having a central role in the protection against oxidative stress.

The expression of the selective autophagy receptor p62 was also shown to be induced by NRF2, through the direct binding of NRF2 to a conserved ARE in its promoter/enhancer. The p62 protein itself is able to augment its expression via that same element forming a positive feedback loop (Jain et al., 2010, 2015). The role of p62 is even more extensive in the NRF2-KEAP1 pathway, as it can bind to KEAP1 and mediate its degradation by autophagy, leading to the stabilization of NRF2 and the increase in its target gene expression (Jain et al., 2010).

### **1.3.8 NRF2 in cancer**

Since NRF2 is considered to be a master regulator of the antioxidative response, there is a debate that revolves around the dual nature of NRF2, questioning whether it acts as a tumor suppressor or, conversely, whether it promotes oncogenesis. This dilemma raises the crucial issue of targeting NRF2 in anticancer therapeutic strategies. As it was so far described, NRF2 under physiological conditions, maintains the cellular redox homeostasis and also exerts anti-inflammatory functions (Chowdhry et al., 2010; I. T. Lee et al., 2009; Rushworth et al., 2008), and other anticancer activities which inhibit tumorigenesis (Chen et al., 2009; Dickinson et al., 2009; Gorrini et al., 2013), supporting cell survival.

Clinically, the excessive expression of NRF2 is associated with poor prognosis (Solis et al., 2010). Various mechanisms have been identified to explain the constitutive activation of the NRF2 signaling pathway in different cancers. These include: (a) enhanced Nrf2 transcription facilitated by oncogenic Myc, K - Ras, and B - Raf mutations via mitogen - activated protein kinases (MAPKs) (Denicola et al., 2011), (b) somatic mutations or loss of exons in the KEAP1, NRF2, or CUL3 genes which disrupt the interaction between NRF2 and KEAP1, affecting the stability of NRF2 (Goldstein et al., 2016; Kim et al., 2010; Ooi et al., 2013; Yoo et al., 2012), (c) epigenetic methylation of the KEAP1 gene promoter, which have been shown to reduce KEAP1 expression levels (Hanada et al., 2012), (d) mutations in the tumor suppressor gene PTEN and epigenetic changes amplifying Nrf2 levels (Mitsuishi et al., 2012), or (e) interference with the interaction between NRF2 and KEAP1 by KEAP1 - competing proteins such as the partner and localizer of BRCA2 (PALB2), dipeptidyl peptidase 3 (DPP3), Wilms tumor gene on X chromosome (WTX), p21, and the selective autophagy receptor p62 (Hast et al., 2013; Komatsu et al., 2010; Ma et al., 2012).

Different mechanisms and correlations have been described by which persistent activation of NRF2 can potentially lead to cancer cell growth and proliferation (Reddy et al., 2008; Singh et al., 2013; Wu et al., 2011), suppression of cancer cell apoptosis (Niture & Jaiswal, 2012; Rushworth & MacEwan, 2008), promotion of cancer stem cell renewal (Blanpain et al., 2011; Murakami et al., 2014; Zhu et al., 2014), promotion of anti-inflammation processes (Iizuka et al., 2005; Kobayashi et al., 2016; Thimmulappa et al., 2006), induction of angiogenesis (Kim et al., 2011; Meng et al., 2010; Shibuya et al., 2010) or the enhancement of chemoresistance and radioresistance of cancer cells (Jayakumar et al., 2014; Moeller et al., 2004; Singh et al., 2010; Wang et al., 2008; Zhan et al., 2012). This has prompted the development of NRF2 inhibitors, as proof of concept specifically for cancer treatment (Bollong et al., 2015; Singh et al., 2016; Tsuchida et al., 2017). However, reviews in the field argue that the pathological context is important and NRF2 is double-edged sword when it comes to tackling cancer diseases (Wu et al., 2019).

In addition, studies that advocate for the continued pharmacological development of drugs enhancing NRF2 activity and their proponents, argue that such drugs could not only prevent cancer but also address various diseases where oxidative and inflammatory stress play pivotal roles in pathogenesis (Sporn & Liby, 2012). Numerous drugs that activate NRF2, alongside other targets, are currently undergoing clinical trials for diverse indications (Robledinos-Antón et al., 2019b). Examples include sulforaphane for neuroprotection in oxidative stress conditions (Egea et al., 2015), dimethyl fumarate for multiple sclerosis treatment (Li et al., 2017; Smith et al., 2017) and bardoxolone methyl for diabetic nephropathy (Lynch et al., 2019).

The aforementioned studies have sparked considerable interest, but the role of NRF2 in carcinogenesis and cancer development remains actively disputed and unresolved (Hayes et al., 2020). Beyond the academic discourse, the ongoing clinical use of NRF2 activators underscores the urgent need to assess the long-term safety of administering these drugs .

## **1.4 Senescence**

Cellular senescence is a process in which cells irreversibly halt their division and experience notable phenotypic changes, including significant alterations in chromatin and their secretome, along with activation of tumor-suppressor mechanisms (Van Deursen, 2014). The term “senescence” was initially coined by Hayflick and Moorhead to describe the irreversible growth cessation observed in human diploid cell strains, following extensive serial passaging in a cultured environment (Hayflick & Moorhead, 1961). Subsequently, this specific form of senescence, known as replicative senescence, was associated with the process of telomere shortening, which can lead to chromosomal instability and foster tumorigenesis. This connection reinforced the theory suggesting that senescence serves as a protective measure against the unchecked proliferation of damaged cells.

Cellular senescence serves beneficial biological functions in regulating embryonic development, wound healing, fibrosis resolution, and tumor suppression (Huang et al., 2022). In contrast, prolonged senescence can lead to adverse consequences, including tumor development, immune deficiency and chronic inflammation. There is a growing interest in cellular senescence and interventions that modulate senescence due to observations suggesting its involvement not only in aging but also in the pathogenesis of chronic diseases such as osteoporosis, metabolic syndrome, type 2 diabetes mellitus, cancer, reproductive aging, atherosclerosis, neurodegeneration, glaucoma, and chronic kidney disease (Micco et al., 2020).

#### **1.4.1 The Senescence-associated secretory phenotype (SASP)**

The senescence-associated secretory phenotype (SASP) is a characteristic phenotype that represents a crucial aspect of senescent cells, involving the release of various cytokines, chemokines, growth factors, into the extracellular environment (Basisty et al., 2020; Huang et al., 2022). SASP is mediated through the release of extracellular vesicles, containing cargoes such as proteins, lipids, and nucleic acids, that play a role in inter-cellular communication under senescence (Terlecki-Zaniewicz et al., 2018). Through the secretion of these SASP factors, senescence can influence pathways in nearby cells, tissues, and even distant locations. Senescent cells can be induced by different stress stimuli that may exhibit distinct SASP components (Özcan et al., 2016).

The regulation of the SASP involves intricate mechanisms which depend on DNA damage response (DDR) and non-DDR pathways (Huang et al., 2022). The transcription factors NF- $\kappa$ B and the CCAAT/enhancer-binding protein- $\beta$  (C/EBP $\beta$ ) cooperatively activate SASP gene promoters (Salotti & Johnson, 2019). NF- $\kappa$ B-independent pathways also exist, as seen in cytoplasmic DNA accumulation, which triggers the cGAS-STING cytoplasmic DNA sensors, inducing interferon- $\beta$  and promoting SASP gene activation (Takahashi et al., 2018). Downregulation of the lamin B receptor, crucial for heterochromatin organization, is essential for cytoplasmic DNA generation (En et al., 2020). Infections, such as exposure to lipopolysaccharide and the SARS-CoV-2 S antigen, are associated with increased release of pro-inflammatory, pro-fibrotic, and pro-apoptotic SASP factors by senescent cells (Tripathi et al., 2021).

SASP factors exhibit dual roles, manifesting both beneficial and detrimental effects. Among the positive effects, CXCL5 plays a role in embryonic development (Kawagoe et al., 2020), PDGF-AA aids in tissue repair (Demaria et al., 2014), IL-6 supports cellular reprogramming (Mosteiro et al., 2018), MMP1 and MMP33 aid in fibrosis resolution (Jun & Lau, 2010), and CCL2 exhibits anti-tumorigenic properties (Iannello et al., 2013). Additionally, SASP factors play a role in attracting immune cells for the elimination of pre-malignant senescent cells (Kang et al., 2011). This mechanism, known as senescence

surveillance, significantly contributes to the anti-tumorigenic characteristics of senescent cells (Kang et al., 2011). In contrast, negative effects include the roles of IL-8, IL-10, and TNF in promoting inflammation (Alimbetov et al., 2016), PDGF-BB's involvement in fibrogenesis (Rana et al., 2020), and the tumorigenic potential of MMP1 and MMP3 (Liu & Hornsby, 2007). Certain SASP cytokines, such as IL-6, IL-8, and CCL2, additionally foster vascular smooth muscle cell calcification and impair insulin sensitivity (Barinda et al., 2020; Zuccolo et al., 2020).

### 1.4.2 Cytoplasmic Chromatin Fragments (CCFs)

Cells in a senescent state exhibit structures in the cytoplasm resembling chromatinized micronuclei (Suzuki et al., 2002) (Figure 15). However, contrary to actual micronuclei, a considerable number of these structures materialize independently of the cell cycle progression. They seem to originate from an evidently intact nucleus through a process resembling chromatin blebbing into the cytoplasm, and they carry unique molecular markers (Miller et al., 2021). These cytoplasmic DNA forms were defined as cytoplasmic chromatin fragments (CCF), to distinguish them from micronuclei or other cytoplasmic

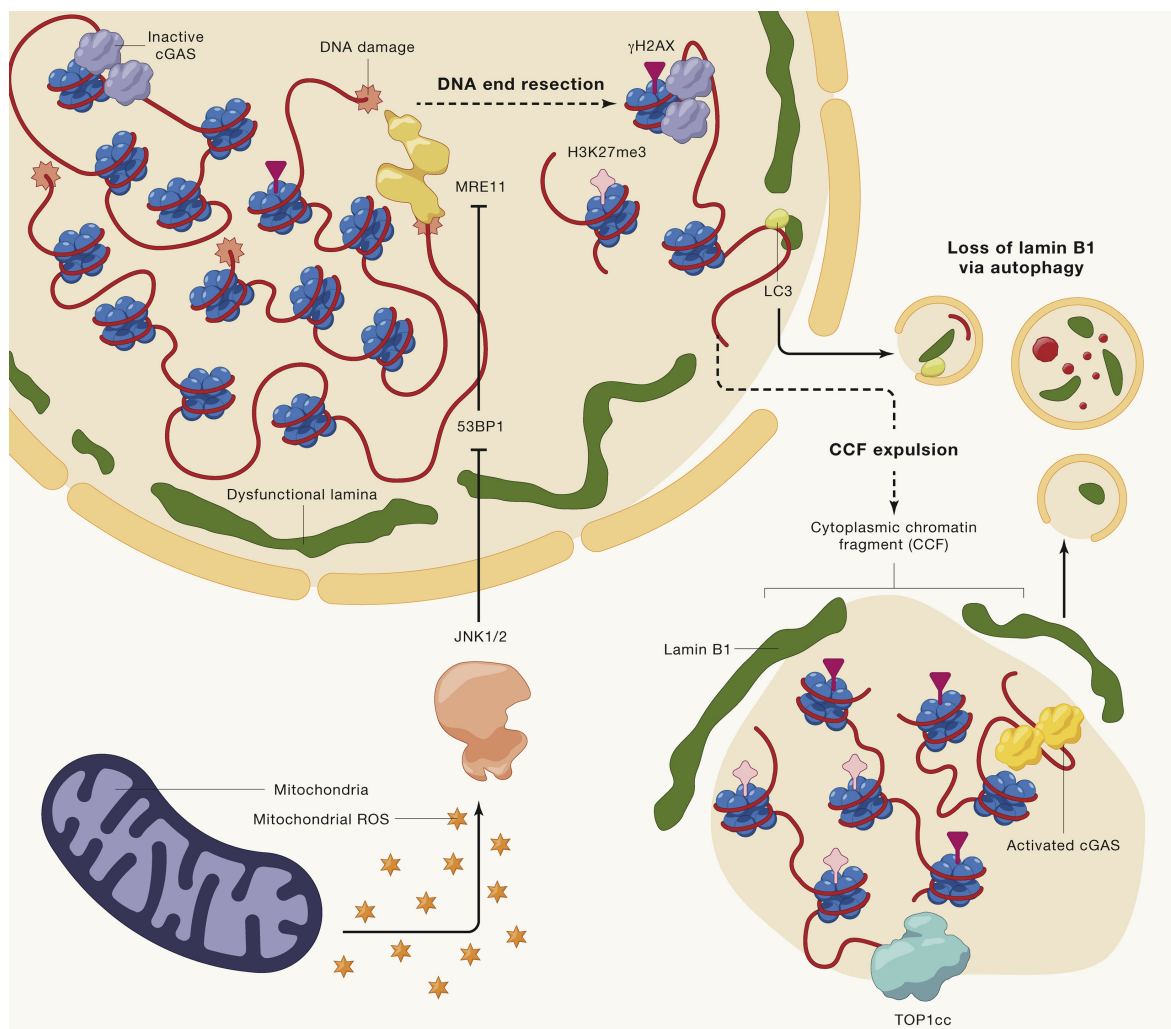


**Figure 15. Formation of cytoplasmic chromatin fragments (CCFs).** The formation of CCFs involves multiple mechanisms, including the loss of lamin B1, potentially triggered by nuclear autophagy and other processes, leading to compromised nuclear membrane integrity. Mitochondria contribute to CCF formation by generating mitochondrial reactive oxygen species (mtROS), activating the JNK1/2 signaling pathway. In the nucleus, the protein 53BP1 suppresses CCF formation, potentially by inhibiting MRE11-dependent resection of double-strand DNA breaks. CCFs are characterized by various markers, such as the DNA damage marker  $\gamma$ H2AX, the heterochromatin marker H3K27me3, the topoisomerase 1 cleavage complex (TOP1cc) that enhances DNA binding to cGAS, and the nuclear lamina protein lamin B1. Figure from (Miller et al., 2021).

DNA species. CCFs exhibit a range of chromatin alterations, which include the presence of heterochromatin-associated H3K27me3 and a relative lack of euchromatin-associated H3K9Ac, indicating their formation from heterochromatin, even though the exact genome locus of origin is yet to be determined (Adams et al., 2013). The emergence of CCFs is linked with the breakdown of the nuclear membrane integrity in senescent cells (Dou et al., 2015).

### 1.4.3 Chromatin Remodeling Complexes

The eukaryotic genome is highly compacted inside the nucleus of every cell. The foundation of this condensed DNA structure is the nucleosome. Comprising 147 base pairs of DNA coiled around a histone octamer, each histone octamer consists of two copies each of histones H2A, H2B, H3, and H4 (Luger et al., 1997). The compaction state of the DNA is dynamic, leading to varied folding levels in chromatin regions during the cell cycle, transcription, and repair processes (Klemm et al., 2019). Heterochromatin, characterized by lower transcriptional activity compared to euchromatin, is closely linked to prolonged gene silencing (Lee et al., 2020). The formation of heterochromatin establishes a physical barrier between DNA and the transcription machinery, suppressing gene expression. The molecular motors responsible for nucleosome positioning and displacement, are known as ATP-dependent chromatin remodelers. These nuclear complexes exploit the energy from ATP hydrolysis for assembly, repositioning, or eviction of nucleosomes, thereby exposing (or covering) specific sections of DNA that are necessary for transcription, replication, or repair (Magaña-Acosta & Valadez-Graham, 2020).

The chromatin remodeling complexes are classified into subfamilies based on the specific ATPase the complex utilizes. The imitation switch complexes ISWI and ISW/SNF are two of the most extensively studied subfamilies of ATP-dependent remodelers (Goodwin & Picketts, 2018; Toto et al., 2014) (Figure 16). The SWI/SNF complexes have both activation and repression functions and tend to be larger complexes, containing up to 15 subunits, while the ISWI complexes generally contain fewer subunits, often 2–4, and are commonly involved in remodeling chromatin to repress gene activity (Aydin et al., 2014; Goodwin & Picketts, 2018; Li et al., 2021).

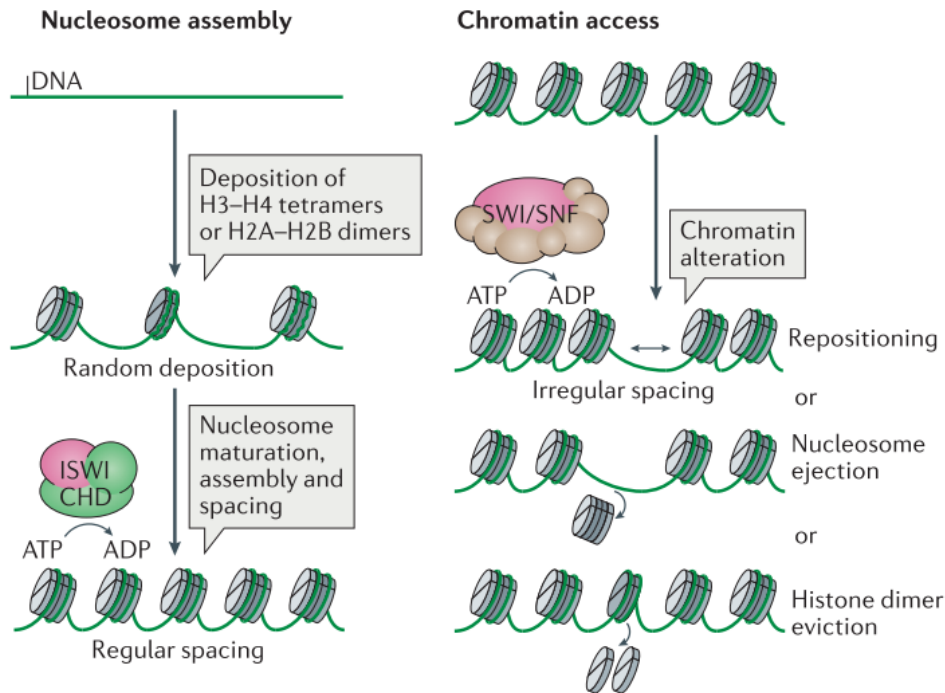


**Figure 16. Functions of the ISWI and SWI/SNF chromatin remodelers.** (Left) The ATPase subunit is depicted in pink; the imitation switch (ISWI) subunit and the switch/sucrose non-fermentable (SWI/SNF) subunit are depicted in green and brown respectively. (Left) The ISWI complex participates in the nucleosome assembly through the maturation, assembly and spacing of nucleosomes. (Right) The SWI/SNF chromatin remodelers alter the chromatin by repositioning or ejecting nucleosomes or by histone dimer eviction. It is noted that the illustration above is a simplification and that the same remodelers can promote different actions depending on context. Figure from (Clapier et al., 2017).

#### 1.4.4 Williams Syndrome Transcription Factor (WSTF)

The bromodomain adjacent to the zinc finger domain 1B (BAZ1B) or Williams syndrome transcription factor (WSTF) belongs to the BAZ/WAL protein family and is characterized by the presence of six specific motifs arranged sequentially, starting from the N-terminus (Jones et al., 2000): a WW domain-containing adapter protein with a coiled-coil (WAC) motif that spans 107 residues, distinguishing it from other BAZ proteins (Ito et al., 1999); a DNA-binding homeobox-containing proteins and Different Transcription and chromatin remodeling factors (DDT) domain (Doerks et al., 2001); a bromodomain adjacent to the zinc finger domain 1 (BAZ1), facilitating WSTF interaction with ISWI; BAZ2; a WAKZ motif (Ito et al., 1999; Jones et al., 2000; Quong et al., 1993); a PHD finger and a bromodomain (Jones et al., 2000) (Figure 17).



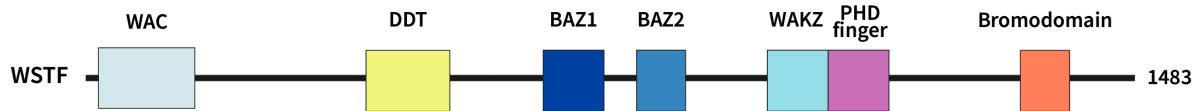


**Figure 17. Schematic representation of WSTF/BAZ1B.** The WAC domain is presumed to play a role in DNA binding and associating with the PHD finger and Bromodomain (Ito et al., 1999). It encompasses residues 21–120. DDT, representing DNA-binding homeobox-containing proteins and various transcription and chromatin remodeling factors, shares a domain spanning nearly 60 residues. This domain is exclusively linked to nuclear domains, including the PHD finger, Bromodomain, and DNA-binding homeodomain (Doerks et al., 2001), covering residues 604–668. DDT is followed by two BAZ motifs (Jones et al., 2000). The C-terminally positioned domains include the WAKZ and PHD zinc finger (residues 1184 to 1234) and bromodomain (residues 1356–1426).

It is a known subunit of two ATP-dependent chromatin remodelers: (a) the WSTF-ISWI chromatin remodeling complex (WICH) and the (b) B-WICH (Barnett & Krebs, 2010; Bozhenok et al., 2002; Lu et al., 1998). It is universally expressed, with the highest transcript levels to be detected in the adult brain, heart, ovaries, placenta and skeletal muscle tissues (Sharif et al., 2021).

The WICH complex is constituted by WSTF and the human sucrose nonfermenting protein 2 homolog (SNF2H, encoded by the *SMARCA5* gene) and extends across vertebrate phyla (Aydin et al., 2014; Bartholomew, 2014). In each mammalian chromatin remodeling complex, either SNF2L or SNF2H, both members of the SNF2 family, is present (Aydin et al., 2014). SNF2 serves as the ATPase subunit in human chromatin remodeling complexes. WSTF interacts with SNF2H via its DDT domain, while SNF2H is bound to DNA via its SANT domain (Sharif et al., 2021). Through participating in WICH, WSTF is hypothesized to play a role in facilitating heterochromatin replication or its assembly post-replication (Bozhenok et al., 2002; Culver-Cochran & Chadwick, 2012), but also in contributing to opposite roles, such as the maintenance of an open chromatin structure by interacting with the proliferating cell nuclear antigen (PCNA) (Poot et al., 2004).

Other findings report the participation of WSTF in RNA Pol-I and Pol-III transcription, through a distinctive variant of B-WICH complex (Cavellán et al., 2006; Percipalle et al., 2006). B-WICH, a unique 3-MDa assembly, becomes evident during active transcription and encompasses six extra proteins that engage with the fundamental elements of the WICH complex (WSTF/SNF2H) and have distinct functions. Notably, one of the components, Cockayne syndrome protein B (CSB) is involved in transcription-coupled repair, base excision repair, and neurogenesis (Bradsher et al., 2002; Ciaffardini et al., 2014; Selby & Sancar, 1997). Nuclear RNA helicase II (DDX21) plays a crucial role in ribosomal RNA transcription and processing (Calo et al., 2014). Other subunits include splicing factor 3B subunit 1 (SF3b1), essential for pre-mRNA splicing (Cretu et al., 2016), and Myb-binding protein 1a

(MYBBP1a), linking ribosome biogenesis to cell cycle regulation (Yamauchi et al., 2008). Additionally, the complex includes DEK (a ubiquitous chromatin protein named after the initials of the acute myeloid leukemia (AML) patient it was discovered in), associated with various human diseases and functioning as a proto-oncogene senescence inhibitor and transcriptional target of HPV E7 proteins (Waldmann et al., 2004; Wise-Draper et al., 2005). Nuclear myosin 1 (NM1 or MYO1C) is a crucial component of the B-WICH complex, characterized as a splice isoform of myosin 1b, and known to colocalize with RNA Pol-II within the nucleus (Percipalle et al., 2006; Pestic-Dragovich et al., 2000). NM1 plays a vital role in stabilizing the B-WICH complex, as well as in facilitating the correct repositioning of nucleosomes, a process mediated by SNF2H (Almuzzaini et al., 2015).

WSTF plays a crucial role in multiple chromatin remodeling processes by serving as a subunit in two widely recognized chromatin remodeling complexes, namely WICH and B-WICH (Sharif et al., 2021; Toto et al., 2014). These complexes are responsible for coordinating diverse molecular functions, such as the generation of newly formed heterochromatin after DNA replication (Bozhenok et al., 2002; Culver-Cochran & Chadwick, 2013), enabling the activity of RNA polymerases I, II, and III through the creation of open chromatin and accessible DNA (Almuzzaini et al., 2015; Cavellán et al., 2006; Sadeghifar et al., 2015), overseeing the DNA damage repair response by inducing specific protein modifications on H2AX nucleosomes (Xiao et al., 2008), or contributing to the cell's determination between survival and apoptosis, as well as developmental processes (Barnett et al., 2012; Lalli et al., 2016; Zanella et al., 2019). As part of the ISWI-including chromatin remodeling complexes, its function can be either repression or activation of gene expression.

## 2. Aims of the study

The ATG8 family proteins are involved at different stages of the autophagic pathway. Specifically, they act in cargo selection and sequestration, autophagosome formation and membrane expansion, autophagosome maturation and fusion with lysosomes, among others. These processes are contained in the cytoplasm, where the autophagic machinery is located. However, a small number of publications have described the dynamics of LC3B, an autophagy marker and member of the ATG8s, in the nucleus, or its interaction with nuclear substrates, i.e. the nuclear lamina protein lamin B1, reporting on its autophagic degradation. An overarching hypothesis in this work is that ATG8s can function as transcriptional regulators in the nucleus. To this end, the following aims were put forward for this study:

- i. Identify nuclear ATG8 interactors that have the capacity to bind to ATG8s in the nucleus and/or cytoplasm.
- ii. Explore whether these interactions are based on the previously described LIR-LDS model or if they are atypical, possibly suggesting a new expanded mode of interaction that is specific for nuclear interactions.
- iii. Investigate the functional significance of the mechanisms by which ATG8s affect the activity of these nuclear interactors and whether these are autophagy-dependent or -independent.

### 3. Summary of papers

#### *Paper I*

#### **Competitive binding between LC3B and p300/CBP to the NRF2 Neh5 domain regulates target gene transcriptional activation**

Athanasios Kournoutis, Birendra Kumar Shrestha, Hallvard Lauritz Olsvik, Yakubu Princely Abudu, Ashish Jain, Gry Evjen, Aud Øvervatn, Trond Lamark and Terje Johansen

#### *Manuscript*

In this study we established LC3B as a nuclear interactor of NRF2. We performed an interaction mapping and uncovered that the Neh5 region of NRF2 is responsible for the binding to LC3B through a LIR-LDS interaction. Earlier studies have shown that p300/CBP binds to Neh5 to acetylate lysine residues in the two C terminal domains, Neh1 and Neh3. Here, we found that LC3B can compete with p300/CBP for binding to NRF2 in a highly conserved region of Neh5. We demonstrated that the subcellular location of the interaction between NRF2 and LC3B was the nucleus. We verified the functionality of this interaction by examining the expression of NRF2 target genes under oxidative stress and overexpression of LC3B. The accumulation of LC3B inside the cell, and importantly in the nucleus, became apparent after prolonged oxidative stress, suggesting that the interaction between LC3B and NRF2 is acting as a brake to the antioxidative response transcription program driven by NRF2, with LC3B taking on the role of a negative transcriptional regulator.

#### *Paper II*

#### **Nuclear autophagy interactome unveils WSTF as a constitutive nuclear inhibitor of inflammation**

Yu Wang, Vinay V. Eapen, Athanasios Kournoutis, Angelique Onorati, Xianting Li, Xiaoting Zhou, Murat Cetinbas, Lu Wang, Jihe Liu, Corey Bretz, Zhuo Zhou, Shannan J. Ho Sui, Srinivas Vinod Saladi, Ruslan I. Sadreyev, Peter D. Adams, Robert E. Kingston, Zhenyu Yue, Terje Johansen, Zhixun Dou  
(*bioRxiv* 2022.10.04.510822; <https://doi.org/10.1101/2022.10.04.510822>)

In this study, we identified and investigated the role of WSTF as a novel nuclear substrate of autophagy. We showed that the autophagic degradation of WSTF is facilitated by its interaction with GABARAP. This degradation induced senescence-associated inflammation, by enhancing chromatin accessibility over inflammatory genes, and affected the immune surveillance of activated oncogenes in mice. The mapping and *in silico* modeling of the interaction between WSTF and GABARAP indicated that the 10 amino acids long region of WSTF that is required for binding to GABARAP is predicted to be  $\alpha$  helical. WSTF is shown to be degraded in the cytoplasm by autophagy mediated by GABARAP during

senescence. This is the first study that demonstrates GABARAP to have a role in the degradation of a nuclear component.

### *Paper III*

#### **LC3B is a cofactor for LMX1B-mediated transcription of autophagy genes in dopaminergic neurons (Spotlight)**

Athanasios Kournoutis and Terje Johansen

(*Journal of Cell Biology*, 222(5), 2023; <https://doi.org/10.1083/JCB.202303008>)

In this mini-review, we report on a study that was published by Jiménez-Moreno et al. and explores a concept similar to paper I. Specifically, LC3B binds here to the LIM homeodomain of LMX1B, a transcription factor that has been published to control the expression of dopaminergic neuronal regulatory and autophagy gene pathways. This LIR-like interaction allows LC3B to act as a co-factor for the LMX1B-transcription of autophagy genes, ensuring the survival of midbrain dopaminergic neurons. The difference to the concept we report on in paper I is that there, we demonstrate that LC3B acts as a negative transcriptional regulator of NRF2, while for LMX1B it acts as a positive regulator. We discuss the contribution of the study to our understanding of transcriptional regulation of autophagy genes by LC3B.

### *Paper IV*

#### **NBR1: The archetypal selective autophagy receptor**

Nikoline L. Rasmussen, Athanasios Kournoutis, Trond Lamark, Terje Johansen

(*Journal of Cell Biology*, 221(11), 2022; <https://doi.org/10.1083/JCB.202208092/213552>)

In this review, we draw parallels between the selective autophagy receptor NBR1 and its more evolutionarily recent cousin p62/SQSTM1. While the number of studies focusing on p62 vastly outnumbers those focused on NBR1, evolutionary analyses suggest that NBR1 is the archetypal autophagy receptor. We discuss the NBR1 homologs in yeast, specifically Atg19 and Atg34, as well as the roles of NBR1 in the regulation of p62 bodies, aggrephagy and pexophagy. We also highlight studies that have demonstrated an important role for NBR1 in pathogens and pathogen components clearance in plants, the same not being true in mammals. We also draw attention to roles of NBR1 associated with disease, specifically cancer development and metastasis. We attempt in this review not only to bring NBR1 to the forefront, but also to emphasize how central the evolutionary context is to the functionality of a protein, a concept that is relevant both to paper I and paper II.

## 4. Discussion

During the past years, the field of autophagy has expanded greatly, with knowledge being produced that attempts to unravel the complexity of the pathway and how autophagy can affect health and disease. In this thesis, we set out to study the functionality of the interactions between ATG8s, critical components of the autophagic machinery, and nuclear proteins or components. We find that this functionality can be either autophagy-dependent or -independent, according to context and can have consequences that affect important physiological processes.

In paper I, we set out to elucidate the direct role of LC3B in the transcriptional regulation of the target genes of NRF2, a notion which originated conceptually from two reports published by our group. Both reports focused on the involvement of p62/SQSTM1 in the NRF2-driven gene transcription (Jain et al., 2010, 2015). In the earlier report (Jain et al., 2010), it was demonstrated that *p62* is a target gene of NRF2, and that when it is translated, it can bind directly to KEAP1, via a motif named KEAP1-interacting region (KIR), leading KEAP1 to the lysosome for degradation resulting in stabilization of NRF2. This raised questions regarding the role of autophagy and, by proximity, the role of ATG8s in the NRF2 pathway. The latter report (Jain et al., 2015) explored Ref(2)P, the *Drosophila melanogaster* p62 homolog, which neither has a functional KIR motif nor does it interact with DmKeap1 (Jain et al., 2015). It was also shown that DmAtg8a, the homolog of LC3B in *D. melanogaster*, directly interacts with DmKEAP1, even though the authors did not show that this interaction was required for its degradation through autophagy. This emergence of a more direct interaction of DmAtg8a with CncC stabilization laid the grounds for us to ask whether LC3B directly interacts with NRF2, in *D. melanogaster* or in mammals, which we confirmed. In the same paper, we find no evidence of autophagic degradation of NRF2. Instead, our data support a role for LC3B in the nucleus and the transcriptional regulation of NRF2 target genes.

In paper II, we examine the degradation of WSTF by autophagy, which is a different fate in terms of the ATG8 interaction than the concepts demonstrated in paper I and reported on in paper III. Here, the novelty lies in that this is the first study to our knowledge, where GABARAP is exhibited to be responsible for the degradation of a nuclear component in senescence. Even though the function of the ATG8 protein is different here, we spotted similarities in the mode of WSTF's interaction with GABARAP and NRF2's interaction with LC3B, which will be discussed further in this section.

Lastly, the emergence of proteins that contain LIRs and how they evolved in terms of functional diversification and specialization is relevant in the discussion regarding ATG8 interaction partners and can shed light in the functionality of the ATG8 interaction itself in these instances. This concept is reviewed in paper IV, where we focus on NBR1 as the archetypal selective autophagy receptor. It is relevant to consider that the majority of LIR-containing proteins are cytoplasmic and the ATG8s participating in interactions with them are lipidated/conjugated to the phagophore (Lamark & Johansen,

2021). Of these proteins, those that sit on the outer side of the phagophore, are usually adaptors responsible for the recruitment and transport of proteins relevant for the autophagic machinery and the autophagosome biogenesis, while at the inner, concave membrane face of the phagophore selective autophagy receptors recruit cargo destined for degradation (Johansen & Lamark, 2020b; Lamark & Johansen, 2021). However, the nuclear ATG8s are probably not lipidated and whether they are cleaved by ATG4 is also unexplored (Rasmussen et al., 2017), leaving the question as to how they functionally evolved to acquire roles in the nucleus. Their degradation route is also unclear. The nuclear proteasome has not been excluded as a possibility (Franić et al., 2021). We are also not aware of how their nuclear levels are regulated. Is it a balance between continuous and regulated nucleocytoplasmic shuttling? Is the nuclear pool of LC3B protected from degradation via the association with heterochromatic lamin-associated domains (LADs)?

## 4.1 Identification of NRF2 and WSTF as ATG8 interactors

In paper I, we demonstrated using *in vitro* and *in vivo* assays, that NRF2 is a very strong interactor of the ATG8 family of proteins. We consequently asked whether this is also the case for NRF1 and CncC, a mammalian and the *D. melanogaster* homologs, respectively. Indeed, their binding to Atg8s was of comparable levels with NRF2 demonstrating the evolutionary conservation of this interaction. Specifically, in the assay using the mammalian ATG8 proteins, we observed that the binding of NRF2 with GABARAP and GABARAPL1 was stronger than with the other ATG8s. It is clear that most ATG8 interactors bind best to GABARAP and GABARAPL1 (Alemu et al., 2012; Bhujabal et al., 2017; Birgisdottir et al., 2019; Genau et al., 2015; Ichimura et al., 2014; Rogov et al., 2017). A recent study, using x-ray crystallography and mutational analyses, demonstrated that the residues within a core LIR and its flanking C-terminal region, combined with specific residues in the LDS on the respective ATG8, are the ones determining specificity between members of the ATG8 family (Wirth et al., 2019). This difference in specificity could potentially be a matter of ATG8 redundancy of the interaction between NRF2 and the ATG8s. Or it could be that ATG8s are characterized by different modes of action when they interact with NRF2.

Due to the strong ATG8 interaction, we examined whether NRF2 could be degraded through the lysosomal route and autophagy. This was considered due to the already well described functions of the ATG8s in the autophagic machinery and their role in selective autophagy (Johansen & Lamark, 2020b; Lamark & Johansen, 2021), involving recruitment of LIR-containing proteins to the phagophore. Another indication was previous reports demonstrating that the inner nuclear membrane protein lamin B1 and the NAD-dependent deacetylase SIRT1, both acting in the nucleus, are autophagy substrates under senescence (Dou et al., 2015; Xu et al., 2020). Here, we observed that there was no degradation of NRF2 upon Bafilomycin A1 treatment (an inhibitor of the lysosomal vacuolar-type H<sup>+</sup>-ATPase (V-

ATPase, which neutralizes the lysosomes and inhibits the autophagy flux) when coupled with DL-sulforaphane (SFN) treatment, which stabilizes NRF2 through KEAP1 degradation (Cullinan et al., 2004). As a positive control in the same experiment, we used the proteasomal inhibitor MG132 in combination with SFN, which causes total proteasomal inhibition. Functionally, this result forced us to postulate that the role of ATG8s in their direct interaction with NRF2 is not coupled to any autophagy-dependent degradation pathway for NRF2, but rather could have a role in regulating the transcriptional activity of NRF2. The role of LC3B in its indirect role in the NRF2 – KEAP1 pathway, specifically in the selective degradation of the p62 – KEAP1 complex in mammals and Keap1 in *D. melanogaster*, had already been explored by others, including our group (Copple et al., 2010; Jain et al., 2010, 2015; Kageyama et al., 2018).

The emergence of WSTF as an autophagic substrate in senescence was uncovered in an interactome analysis which focused on nuclear and chromatin interactions of members of the ATG8 family of proteins, and is one of the main findings of paper II. While unbiased proteomic studies of the interactions of ATG8s with other proteins have been conducted before (Behrends et al., 2010a; Le Guerroué et al., 2017; Wild et al., 2014), the nuclear ATG8 interactome demonstrated in the paper, is a systematic resource for identifying and studying nuclear proteins whose interaction with the ATG8s is functionally important for the senescent phenotype. NRF2 was not found in this specific nuclear ATG8 interactome, possibly because it doesn't have a role in senescence, in which the interactome analysis was focused on. But mainly, we show here that the degradation of WSTF depends on its interaction with GABARAP, and the autophagic degradation of WSTF promotes chromatin accessibility of inflammatory genes and upregulates the SASP program. Paper II is also novel because previous reports have only indicated that the ISWI complex and WSTF, are playing roles in neuronal development (Barnett et al., 2012b; Percipalle et al., 2006; Zanella et al., 2019), but not in senescence and inflammation, uncovering a new way in how SASP can be regulated. It also adds to the two already mentioned reports in the literature that demonstrate that lamin B1 and the SIRT1, both acting in the nucleus, are autophagy substrates under senescence (Dou et al., 2015; Xu et al., 2020).

## **4.2 The interactions between the ATG8s and NRF2 and WSTF**

The assessment that NRF2 is not an autophagic substrate degraded under oxidative stress, which we made in paper I, prompted us to ask two questions. First, whether the interaction is based on the well-established LIR – LDS model (Birgisdottir et al., 2013; Johansen & Lamark, 2020b; Rogov et al., 2023), as is the case with most ATG8 binding partners, autophagic substrates or receptors. Second, whether the spatio-temporal relationship between NRF2 and LC3B was unfolding in the nucleus or in the cytoplasm.

We addressed the first question in paper I, by performing interaction mapping by GST pulldown assays aided by in vitro mutagenesis, peptide array, and structure modeling of the interaction between NRF2



and the ATG8s, most specifically LC3B with some studies done with GABARAP. We concluded that the region responsible for binding to LC3B is specifically the Neh5 domain of NRF2 (amino acid residues 178 to 208), while for GABARAP the same domain is partially redundant, as it was demonstrated in a GST pulldown assay where we tested NRF2 with a deletion ( $\Delta$ 178-208) encompassing Neh5 for binding both to LC3B and GABARAP. We decided not to proceed with further experiments using GABARAP to address it, since we considered LC3B as the most likely interaction partner in the nucleus. The focus on LC3B also simplified our approach since it only required the Neh5 domain for binding. In the Neh5 domain, the tryptophan and leucine residues W188 and L191, as well as their proximal residues, fit the aromatic and hydrophobic residues in positions one and four of the core LIR motif consensus (Birgisdottir et al., 2013; Rogov et al., 2023). One could speculate then that by mutating these residues into alanines, there would be a reduction in the binding affinity of NRF2 with LC3B. We verified that NRF2 W188A/L191A has indeed a significant decrease in the binding with LC3B, making us speculate that the interaction is indeed fitting the LIR – LDS model. However, by testing alanine substitutions of phenylalanine in position 52 (F52) and leucine in position 53 (L53) on the LC3B sequence corresponding to the LDS (Behrends et al., 2010; Pankiv et al., 2007), we noticed that the interaction between NRF2 and LC3B was not affected. This either meant that F52 and L53 are not important for this particular interaction or that the binding interface doesn't fit the LIR – LDS model, leaving the HP1 and HP2 hydrophobic pockets without being properly occupied and/or off-core LIR residues to be stabilizing the NRF2 – LC3B interaction.

To obtain a more nuanced perspective of the binding, we performed *in silico* NRF2-LC3B complex predictions using the ColabFold tool, which utilizes the AlphaFold2 prediction model (Mirdita et al., 2022; Pettersen et al., 2021), and we initially concluded that the Neh5 domain is helical, and not an extended  $\beta$  sheet, which is usually the case for most studied LIRs (Rogov et al., 2023). The only other LIR which has been characterized to be  $\alpha$  helical is that of TRIM5 $\alpha$  (Keown et al., 2018; Mandell et al., 2014), whose LIR is projected on its coiled coil region, protruding into the hydrophobic pocket HP1 of LC3B. Even though the binding affinity between TRIM5 $\alpha$  and LC3B is not strong (Keown et al., 2018), it can form a dimer due to its coiled coil domain and can bind two ATG8 molecules, increasing its binding affinity. In that particular model, we also observed that the HP1 and HP2 were not engaged in the binding interface, which we considered highly unusual. In contrast with NRF2, AlphaFold2 predictions of the binding of NRF1 and NFE2 (p45) to LC3B, showed that the aromatic and hydrophobic residues of the respective evolutionarily conserved domains docked within the hydrophobic pockets HP1 and HP2 of LC3B in a parallel  $\beta$ -strand configuration, as expected in a typical LIR – LDS interaction (Rogov et al., 2023). By utilizing AlphaFold2 and the SWISS MODEL (Guex et al., 2009; Kiefer et al., 2009), we used the structure of the NFE2 – LC3B complex as a template to guide the positioning of a peptide incorporating the putative NRF2 LIR to LC3B. In this final model, we observed that the docking of W188 and L191 to HP1 and HP2 respectively was successful.

Then, in addition to the F52 and L53 alanine substitutions, we also tested whether other residues on LC3B, namely the arginines R10 and R11 in the N terminal arm, which have been deemed important for the binding to lamin B1 upon its nuclear exodus and autophagic degradation (Dou et al., 2015), as well as the arginines R69 and R70, which belong to a surface exposed  $\alpha$  helical triple arginine motif shown to be important for the association of LC3B with large complexes in the nucleus (Kraft et al., 2014, 2016). It is also key to mention that the electropositive residues R10 and R11 are distinctive features specific to the LC3 subfamily. These residues establish crucial electrostatic interactions with acidic residues found at positions N terminal to the core LIR motif (Ichimura et al., 2008; Noda et al., 2008; Olsvik et al., 2015). For instance, in the FYCO1 LIR, an electrostatic interaction is maintained between R10 in LC3B and D1277 at the -3 position of the FYCO1 LIR, stabilizing the interaction (Olsvik et al., 2015). Similarly, the p62 LIR is stabilized through interactions involving R10 and R11 in LC3B with D337 and D338 at the -3 to -2 positions in the p62 LIR (Ichimura et al., 2008). Regarding the R70, there are LIR motifs, like the FYCO1 LIR, which feature a negatively charged residue at the +7 position (Cheng et al., 2016; Olsvik et al., 2015) which facilitates the establishment of an electrostatic interaction with R70 in LC3B (or R67 in GABARAP). Specifically, in the AlphaFold2 prediction of the NRF2 – LC3B complex, we saw that a number of residues flanking the core LIR, are indeed engaged in electrostatic interactions with the R10/R11 and R69/R70 residues on LC3B. We verified this experimentally through alanine substitutions of these arginines, demonstrating that they indeed have a strong effect in reducing the binding affinity of LC3B to NRF2, especially when a combinatory LC3B R10A/R70A was used.

Consequently, we tested other alanine substitutions in the Neh5 domain in a search for important residues that could shed light in how the binding interface is materializing, like in aspartic acids (D) in the positions 176, 178 and 183 or the glutamic acids (E) between W188 and L191 on the sequence. The D183A and E189A/E190A did lead to significant reductions in the binding of NRF2 to LC3B. We deem the interaction between NRF2 and LC3B to be canonical, but an extended mutational analysis coupled with in vitro interaction assays or x-ray crystallography need to be employed, in order to make that statement with confidence. In addition, we cannot exclude the possibility that the NRF2 LIR is helical, as the initial AlphaFold2 prediction showed.

We answered the latter question, whether the spatiotemporal relationship between NRF2 and LC3B was unfolding in the nucleus or in the cytoplasm, using endogenous staining but also by performing a bimolecular fluorescence complementation assay (Hu et al., 2002; Kerppola, 2006; Shaner et al., 2013), where we tagged NRF2 at its N terminus with the 10 N-terminal  $\beta$  strands of the  $\beta$  barrel of NeonGreen and fused the 11<sup>th</sup>  $\beta$  strand to the N terminus of LC3B. The complementation of the two splits of NeonGreen inside the cell produces fluorescence with an excitation peak at 506 nm, similar to the green fluorescent protein (GFP), which peaks at 588 nm (Hu et al., 2002; Shaner et al., 2013). We saw the interaction to be localized inside the nucleus in a diffused state, possibly due to the transfection-induced

overexpression. To our knowledge, this is the first time the interaction between LC3B, and a transcription factor is spatially detected in such a manner, in the nucleus. As a positive control we used MafG tagged with the N terminal 0  $\beta$  strands of NeonGreen, instead of NRF2. This interaction was also verified to occur in the nucleus. It has been reported that LC3B passively diffuses into the nucleus and that its rudimentary partial detention there is mediated by its association with high-molecular weight, slowly diffusing complexes (Drake et al., 2010; Kraft et al., 2014, 2016). It is possible that these high-molecular complexes are transcriptional complexes, in this case the NRF2 – sMaf heterodimer associated with the histone acetyltransferase p300/CBP, the Mediator complex, the SWI/SNF remodeling complex and/or other co-activators or transcription factors (He et al., 2001; Hirotsu et al., 2012; Itoh et al., 1997; Kawai et al., 2011; Sekine et al., 2016; Sun et al., 2009). We also showed in paper I, that the endogenous interaction between NRF2 and LC3B is occurring under prolonged oxidative stress, specifically after 8 hours of treatment with SFN, which also coincides with the accumulation of LC3B in the nucleus. This could be explained either by the possibility that the promoter of *LC3B* contains an ARE sequence, in the same manner that p62 does (Jain et al., 2010), thus oxidative stress would drive an NRF2-mediated upregulation of LC3B transcription and translation with LC3B stabilizing under prolonged stress, or by another LC3B-stabilizing mechanism like obstruction of its autophagic degradation. We do observe here using a western blot analysis that p62 is indeed stabilized after 4 or 8 hours of SFN treatment, which led us to postulate that same mechanism could be employed with LC3B. It is also worth noting that a pool of LC3B might be stabilizing, through its engagement with p62 (Pankiv et al., 2007).

The interaction between WSTF with GABARAP, which we demonstrate in paper II, is shown to be based on an  $\alpha$  helical LIR motif, as it was predicted using ColabFold/Chimera X (Bertoline et al., 2023; Mirdita et al., 2022; Pettersen et al., 2021). While the WSTF LIR is seemingly atypical, in the sense that our in silico prediction shows it to be helical, it is possible that a different binding interface is taking place, like an extended  $\beta$  sheet configuration. Further experiments that can increase the confidence in the model, like x-ray crystallography of the LIR peptide, would shed light on the WSTF – GABARAP and assist in theorizing a more specific mode of interaction. It is also important to note that the interaction between NRF2 and GABARAP would also be an interesting one to explore, since the possibility of a different binding mode is highly likely.

While there are molecular determinants between LC3B, GABARAP and the other ATG8s that can lead to differences in their binding affinities to LIR-containing proteins (Wirth et al., 2019), it is possible that there is no specific feature which could potentially differentiate the binding between nuclear and cytoplasmic proteins to ATG8s. For example, we can't be confident that the helicality of the LIR, which was our initial hypothesis after the initial prediction of the NRF2 LIR and the WSTF LIR, can be the defining factor for the selectivity of ATG8s to nuclear proteins and components. By producing AlphaFold2 predictions for NRF1 and NFE2 (p45) in paper I, this notion was confirmed.

### 4.3 The role of LC3B in the transcriptional regulation of NRF2 target genes

It has been reported that the mutation of 18 lysines to arginines in the Neh1 domain, where it was shown that p300 is acetylating NRF2, compromised the ability of NRF2 to bind to DNA and consequently the transcription of the *NQO1*, *TXNRD1* and *GCLM* genes but not that of *HO1* (Sun et al., 2009). That is relevant because in paper I, we observed a significant downregulation of the *HO1* gene in different experimental settings compared with other NRF2 target genes, under prolonged oxidative stress coupled with overexpression of LC3B. In another paper, however, it was shown that the p300-mediated acetylation in the Neh3 was relevant for the *HO1* gene (Kawai et al., 2011). The *HO1* downregulation could be the result of a displacement of a different NRF2 co-factor by LC3B, like the activating transcription factor 4 (ATF4), since the NRF2-ATF4 has been shown to be a potent inducer of *HO1* specifically (He et al., 2001; Rössler & Thiel, 2017). Whether the Neh5 domain is important for the ATF4-NRF2 dimer interaction, is unknown.

In collaboration with histone-modifying enzymes, it also has been shown that NRF2 operates by recruiting the Mediator, a protein complex with multiple subunits that facilitates the transmission of regulatory signals from a DNA-bound transcription factor to the RNA polymerase II (Pol II) (Allen & Taatjes, 2015; Sekine et al., 2016). The composition of the Mediator subunits is dynamic, allowing for the addition or removal of subunits, thereby impacting its biological function (Allen & Taatjes, 2015). NRF2 has been shown to establish a direct interaction with the MED16 subunit of the Mediator complex through its Neh1, Neh4 and Neh5 domains (Sekine et al., 2016). The authors show that MED16 acts as an intermediary, bridging the interaction between NRF2 and the Mediator complex. They also find that depletion of MED16 specifically hampers the transcription of several NRF2 target genes without impacting cell proliferation. Apart from the histone modifying enzymes p300 and CBP and the Mediator complex, it has also been reported that NRF2 recruits ATP-dependent nucleosome remodeling complexes (Zhang et al., 2006). Here the authors showed that BRG1, the central ATPase subunit of the SWI/SNF chromatin-remodeling complex, interacts with NRF2 and enhances its transcriptional activity, also through the Neh4 and Neh5 domains. The interesting finding is that, while NRF2 recruits BRG1 to both to the *HO-1* and *NQO1* regulatory regions, BRG1 knockdown selectively decreased the recruitment of RNA Pol II to the *HO-1* promoter and not to the *NQO1* promoter (Zhang et al., 2006). The authors explain that this is because *HO-1*, but not the other NRF2 target genes, contains a sequence of TG repeats that can lead to Z-DNA formation with BRG1 assistance. The significant activation reduction we observe in the *HO-1* gene in paper I after LC3B overexpression, for example, could also be partly because of a putative competition between LC3B and BRG1 on the Neh5 domain of NRF2, that would result in a reduction in BRG1 recruitment to NRF2 and a subsequent target gene activation reduction.

Taking the above into consideration, our results in paper I that demonstrate differences in the levels of downregulation of the target genes of NRF2 after LC3B overexpression, we postulate that there might be a competition between LC3B and another single protein or subunit of a transcriptional complex that is different from p300/CBP, like MED16, the subunit of the Mediator, or BRG1, the ATPase subunit of the SWI/SNF chromatin-remodeling complex. It is crucial to note that all of the aforementioned proteins/subunits do interact with NRF2 and affect its transcriptional activity through the Neh5 domain, among others, and that that is the region where we demonstrate a strong interaction between LC3B and NRF2. To take this further, we hypothesize that LC3B affects multiple nodes of the transcriptional network which has NRF2 at its center.

It is also true that the differences in NRF2 target gene downregulation, can be explained by what has been demonstrated in previous studies in integrated analyses of NRF2 binding and transcription profiles, specifically that not all the genes in the vicinity of bound NRF2 are transcriptionally regulated as a result of NRF2 binding (Chorley et al., 2012; Hirotsu et al., 2012; Malhotra et al., 2010). It is possible that these genes require the recruitment of specific co-factors for a complete activation that are different from the ones involved in the experiments in paper I, a hypothesis we can't exclude when discussing the LC3B-mediated effect on the transcriptional activity of NRF2. This is also indicated in the fact that in a motif analysis of NRF2 binding sites, consensus motifs for other transcription factors, such as Fos, Mafk, Lhx3 and MEF2A, were also identified (Malhotra et al., 2010). In addition, other CNC transcription factors and/or members of the AP1 complex, such as Jun, Fos and ATF3, have been reported to recognize ARE-like sequences when tested using electrophoretic mobility shift assays (Alam et al., 2003), with NRF2 also having been reported to form heterodimers specifically with ATF4 (He et al., 2001), an interaction that is important for the expression of HO-1. This suggests that other transcription factors acting on ARE-like sequences might be concealing the measurable effect that LC3B has in the target gene expression of NRF2.

In addition to the above, in order to mimic oxidative stress in paper I we used SFN, which we know acts on the cysteine code of KEAP1 and changes its conformation, disrupting its interaction with NRF2 and eventually inducing the latter's stabilization (Horie et al., 2021), it is possible that other chemical inducers of NRF2 stabilization used in the literature, like sodium arsenite (As(III)) (Córdova et al., 2014; Sun et al., 2009) or *tert*-butylhydroquinone (tBHQ) (Lau et al., 2013) can have a different impact on different target genes of NRF2. It is also important to note, that while this might be the case, there is agreement in the field that NRF2 regulates a common set of genes, such as *Nqo1*, *Gclc*, *Gclm* and *Txnrd1*, irrespective of the type of stimulus and the cellular context (Barve et al., 2008; Córdova et al., 2014; Kobayashi et al., 2016; Lau et al., 2013; Mitsuishi et al., 2012; Woods et al., 2009; Wu et al., 2011b), and that that is a program conserved from *Drosophila* to humans (Lacher et al., 2015).

Whether different chemical inducers would lead to different LC3B-mediated effects on the transcription of NRF2 target genes would require further experiments and remains to be determined.

To conclude this section, in order to fully understand the effect we see LC3B has on the NRF2-mediated gene transactivation, a holistic approach needs to be considered, that includes the notion of cooperation and/or competition of NRF2 with other transcriptional factors and co-factors, the possibility that default NRF2 target genes can be activated by transcriptional factors without NRF2 participation, as well as the variability produced by the different chemical agents we use to mimic oxidative stress and induce NRF2 stabilization. Our conclusion is that an increase in nuclear LC3B appears to have a significant effect on the transcriptional activity of NRF2 target genes, and definitely on *HO1*, but further experiments need to be performed in order to improve the accuracy of our model.

#### **4.4 LC3B as a transcriptional co-factor**

In paper III, we discuss an article that is highly relevant with the content of paper I, reporting on the role of LC3B as a co-factor of the LMX1B transcription factor (Jiménez-Moreno et al., 2023). The authors show that LMX1B is responsible for the upregulation of autophagy genes through the FLAT elements in the promoters of these genes, by engaging in interactions with members of the ATG8 family of proteins. Opposite to what we observed with NRF2 in paper I, the use of the LC3B F52A and L53A mutants in in vitro binding assays significantly reduced the binding to LMX1B, possibly conforming to the tyrosine-type group of identified LIR-containing proteins, such as NBR1 and ATG4B (Kirkin et al., 2009; Satoo et al., 2009). However, the core LIR alanine substitutions of the aromatic residues (Birgisdottir et al., 2013; Rogov et al., 2023). However, alanine substitutions of the key tyrosine and leucine residues (Y309A/L312A) within the proposed LMX1B LIR did not impact the binding to the ATG8s, possibly due to off-core LIR interactions (Johansen & Lamark, 2020; Rogov et al., 2023). An expanded truncation the LMX1B putative LIR ( $\Delta$ 308-317) did have an effect, having no effect in stimulating expression from FLAT element reporters or protecting against rotenone-induced cell death in midbrain dopaminergic neurons. Due to the lack of an extended mutational analysis of the LMX1B LIR-like interaction with LC3B, we cannot draw parallels with the NRF2 – LC3B predicted complex which we demonstrate in paper I.

Nevertheless, it is important to note that Jiménez-Moreno et al. clearly demonstrated evidence showcasing the ability of ATG8s to function as transcriptional cofactors within mammalian cells. Questions arise then as to how does LC3B function to enhance transcription? Does it serve as an adaptor that binds to recruit transcriptional cofactors, or competes with transcriptional repressors? While in paper I, our conclusion is that LC3B displaces p300, or possibly other transcriptional co-factors, from nuclear NRF2, hence negatively affecting its target gene expression, in this case, the opposite seems to be the case. Notably, the role of ATG8s as a transcriptional repressor is not entirely new, as it has been

previously shown in a *Drosophila* model that another transcription factor that interacts with ATG8 through the LDS, called Sequoia, can repress autophagy gene transcription (Jacomin et al., 2020). The mechanism hasn't been described in detail, but the authors clearly show that DmAtg8a leads to autophagy gene transcriptional suppression in nutrient-replete conditions. It is evidently anticipated that new roles for ATG8 family members within the nucleus will be unveiled, identifying new roles of additional transcription factors influenced by ATG8 binding, as is the case in paper I.

## 4.5 Evolving selectivity in autophagy: NRF2 and NBR1

In paper IV, our review of the autophagy receptor NBR1 sheds light on the origin of selective autophagy. We put forward the hypothesis suggested by phylogenetic, structural and biochemical analyses that NBR1 is the ancestral selective autophagy receptor and the origin of selective autophagy. A gene duplication during the development of early multicellular organisms (metazoans), between the Precambrian and Cambrian eras around 500 million years ago, likely gave rise to p62 (Svenning et al., 2011). Most non-metazoans contain only NBR1, while generally, metazoans contain both NBR1 and p62. As a selective autophagy receptor, NBR1 interacts with ATG8s, the latter in turn being lipidated and sitting on the phagophore (Johansen & Lamark, 2020).

While NRF2 emerged very early in evolutionary time, having evolved from an early eukaryotic peptide which contained a bZIP/CNC domain sequence during the last stage of the Great Oxygenation Event (GOE), there is a lack of nuclear NRF2-like response to oxidative stress in plants (Shao et al., 2008), and an absence of detectable homology to the NRF2 – KEAP1 pathway in plant genomes (Gacesa et al., 2015). The earliest evolutionary homolog of NRF2 with a similar function in the antioxidative response to mammals, that has been empirically studied, is SKN-1 in *C. elegans* (An et al., 2005; Choe et al., 2012). SKN-1 lacks the regulatory KEAP1 interaction which is present in *D. melanogaster* (Gacesa et al., 2016; Sykiotis & Bohmann, 2008), through which it has been demonstrated that dmAtg8 regulates NRF2 stability (Jain et al., 2015). The lack of a KEAP1-like regulatory mechanism in *C. elegans*, possibly indicates that SKN-1 and/or earlier metazoan ancestors interacted directly with an ancestral Atg8, since it is also already known that the two conjugation systems with ATG8 and ATG12 are conserved in most eukaryotic clades (Zhang et al., 2022). It is also possible that the KEAP1-like regulation of NRF2 existed before the *C. elegans* split and it was lost later in evolution, after the split of the *C. elegans* evolutionary line. In order to validate this hypothesis, SKN-1 would also have to be tested for an interaction with the two Atg8 homologs in *C. elegans*, namely LGG-1 and LGG-2 (Wu et al., 2015). Either SKN-1 is an autophagic substrate and like NBR1, can be directly degraded by autophagy, which as we showed in paper I it doesn't occur in mammals, or a similar regulation of transcription is taking place, like the one we investigated in paper I. Both would be interesting to explore in future studies.

## 4.6 Conclusions

The elucidation of the nuclear roles of the ATG8 family of proteins, affecting autophagy or autophagy-independent processes, will have a big impact in the field and can prove valuable when it comes to targeting these processes in clinical treatment regimens for cancer and/or neurodegenerative diseases. Here we show that LC3B, the most prominent member of the ATG8 proteins, competes with p300 for binding to NRF2 under prolonged oxidative stress, negatively regulating the transcriptional program of NRF2 and by proxy, the NRF2-mediated antioxidative response. We propose that the purpose of this competition is for LC3B to act as a brake of this antioxidative response, in order to avoid complications that may rise from a prolonged oxidative stimulus. In addition, we contribute to the mapping of the interaction between WSTF, a subunit of a chromatin remodeling complex with roles in senescence-associated inflammation, and GABARAP. This binding is crucial for the autophagic degradation of WSTF and the promotion of chromatin accessibility over inflammatory genes to allow their expression. These observations highlight the need to expand the knowledge in the field of ATG8 signaling in the nucleus, uncovering the roles in different gene regulatory programs.



## 5. Methodological considerations

### 5.1 Cell lines as model systems

Selecting appropriate cell lines is a critical consideration for cell-based studies. In this thesis, numerous cell biological findings were based on HeLa cells, a widely used model in biomedical research established in 1951 from a cervical adenocarcinoma patient, Henrietta Lacks (Lucey et al., 2009). HeLa cells have been extensively employed globally and come with various tools, including established knockout clones, which were beneficial for our study, like the ATG8 KO HeLa cells made in our lab.

However, the widespread use of HeLa cells has led to genetic divergence, attributed to their inherent genetic instability as a cancer cell line (Frattini et al., 2015). Multi-omics analyses have revealed significant heterogeneity among HeLa cells from different laboratories, and the accumulation of genetic alterations over passaging time can impact reproducibility (Liu et al., 2019). To enhance robustness, it is advisable to replicate experiments in different HeLa variants and other cell lines. Because of the above, U2OS cells, a human osteosarcoma cell line, were also utilized in paper I, yielding similar results to HeLa cells.

The primary human IMR90 and BJ fibroblasts, isolated from lung and skin tissue respectively, were used for the senescence experiments, due to their finite lifespan, and they have been previously used in similar studies (Dou et al., 2015; Xu et al., 2020).

### 5.2 *In vitro* interaction studies

In this work, *in vitro* GST pulldown assays were employed as part of a process to profile the binding of NRF2 and its homologs, as well as WSTF, with the ATG8 proteins. The advantage this method provides is its cell-free nature, enabling detailed biochemical examinations of direct protein interactions and affinity assessments. However, the absence of cellular components raises the possibility of bringing together proteins that may not encounter each other in a physiological context. For example, proteins found in different cellular compartments may interact *in vitro* but not *in vivo*. Post-translational modifications crucial for cellular interactions may be absent *in vitro*, and protein folding may differ.

It is also possible that these interactions can't be pinpointed *in vivo* because of the technical issues, like the lack of antibodies that recognize the regions where the interactions don't take place, leading to false negative results. The *in vitro* translation system used in our studies has been reported to involve ubiquitination of proteins. This also introduces the potential for false negative or positive results. To address these limitations, it is recommended to complement *in vitro* GST pulldown studies with other assays assessing interactions in a cellular context, such as immunofluorescent microscopy for

colocalization, proximity labeling like bimolecular complementation assays and/or co-immunoprecipitation. Another drawback of co-immunoprecipitations, beyond the putative lack of the right antibodies, is that it cannot distinguish between direct and indirect interactions through complexes or that the cell lysis may expose proteins normally confined to distinct subcellular compartments.

In the case of our observed interaction of ATG8 proteins with NRF2 and WSTF, multiple validation methods were employed, including co-localization studies, bimolecular fluorescent complementation assays, co-immunoprecipitations and subcellular fractionations. For the interactions between LC3B and NRF2 mutants, confirmation has been limited to *in vitro* studies, with others reporting similar findings from large-scale screens. Regarding the competition assays, we want to note that only the three proteins we studied in paper I, namely NRF2, LC3B and p300, were used, which opens up the question whether other regulatory proteins or co-factors contribute to this interaction, which were not present in the assay but are present in the cells. This is observations lead to the conclusion that further experiments are needed to expand the validation of these interactions in a cellular context.

### **5.3 Luciferase assays**

In order to examine the binding capacity of NRF2 to the ARE promoter, we performed luciferase assays using the promoter of *nqo1*. While there are small differences in the ARE sequences between the promoters of the target genes of NRF2, there has been no comparative experimental study, to our knowledge, that attempts to explore these differences. Hence, the changes we saw in the NRF2 target gene activation in paper I, could be either because of differences in the ARE sequences but also because of other parameters, such as the contribution of co-factors, as these were discussed in section 4 of this thesis. Lastly, due to the co-expression of plasmids and for reasons that will be explained in the next paragraph, luciferase assays can be unstable between repeats. This is the reason we decided to use RT-qPCR to measure the target gene mRNA levels, and in combination, produce conclusions.

### **5.4 Transient and stable protein expression**

To investigate the LC3B-NRF2 and the impact of mutations to NRF2 target gene expression, we employed both stable and transient protein expression methods. Transient transfection offers a quick and simple approach, but its downside lies in the temporary nature of expression and challenges in regulating protein levels, often resulting in overexpression compared to endogenous levels.

However, in the case of paper I, NRF2 levels under basal conditions are low, almost undetectable, which makes it easier to measure a phenotype by RT-qPCR after overexpression of different mutants. In the same paper, RT-qPCR experiments with both transient overexpression and stable expression (HA-

tagged) of LC3B led to similar results. NeonGreen-tagged 1-10  $\beta$ -strands NRF2 and -11 LC3B, expressed through transient transfection, cells displaying very high levels of both proteins, seemed to generate strong green signal in the nucleus. It's important to acknowledge that overexpression of these two proteins might contribute to a forced interaction in the nucleus, of which the affinity is much stronger or localized in different nuclear components, than what actually happens under non-external expression conditions. Furthermore, transient transfection involves introducing DNA as a plasmid, which might inadvertently trigger changes that can resemble oxidative stress. Given NRF2's role in responding to oxidative insults stimuli, this kind of stress could impact our study.

## 5.5 Western blotting

Western blotting was utilized to assess protein levels in diverse cellular conditions and treatments. This widely adopted technique involves the separation of proteins through sodium dodecyl sulfate-polyacrylamide gel electrophoresis (SDS-PAGE) and subsequent transfer to a nitrocellulose or polyvinylidene fluoride (PVDF) membrane. Primary antibodies against the target protein, followed by secondary antibodies containing a probe (e.g., horseradish peroxidase or a fluorophore), are used for protein detection (Mahmood & Yang, 2012). The multistep process introduces various opportunities for variations or errors, encompassing sample preparation, electrophoresis, buffers, transfer systems, immunolabeling, and detection, potentially complicating result comparisons across labs, researchers, and experiments.

Despite its limitations, western blotting is frequently employed to quantify protein levels and attain statistically significant results. Due to the numerous variables affecting outcomes, it is generally considered a semi-quantitative method, allowing for relative comparisons within a membrane but lacking absolute protein quantity values (Mahmood & Yang, 2012). Relative protein levels are normalized against housekeeping genes, yet discrepancies in the dynamic range of housekeeping genes compared to the protein of interest can impact normalization accuracy (Pillai-Kastoori et al., 2020).

In our lab, two detection systems are employed: chemiluminescent and near-infrared detection. Chemiluminescent detection relies on an enzymatic reaction between a substrate and horseradish peroxidase, where the reaction rate and signal are substrate and enzyme concentration-dependent, introducing non-linearity (Pillai-Kastoori et al., 2020). Uneven substrate distribution and strong signals from highly expressed proteins may affect signal quality. Near-infrared detection, relying on direct fluorophore detection without substrate addition, allows simultaneous detection of two proteins with different emission spectra, reducing variabilities associated with chemiluminescent detection and enhancing reliability.

In our studies, near-infrared detection was the standard for achieving quantifiable results, with chemiluminescent detection used when certain antibodies proved incompatible or when the signal was too weak. To enhance confidence in quantification, at least three individual experiments were conducted and quantified for each western blot, unless stated otherwise. However, the obtained values provide only an approximation of changes in protein levels, considering potential sources of variation and error discussed here that could impact result interpretation.

## **5.6 Protein structure prediction using AlphaFold2**

The structural predictions for the interactions between NRF2, NRF1, p45 and LC3B in paper I were made using the ColabFold tool, which utilizes the AlphaFold2 deep learning model (Bertoline et al., 2023; Mirdita et al., 2022; Pettersen et al., 2021). While AlphaFold2 is a powerful tool for protein structure prediction, there are certain limitations and challenges associated with its use. Specifically, the system is trained on a large dataset of known protein structures, such as those found in the Protein Data Bank (PDB), using a deep learning architecture that includes attention mechanisms and convolutional neural networks. If there have no similar structure complex solved, of the protein complex which we want to predict, which is determined by the aminoacidic sequence and among others, the evolutionary conservation of the specific regions that participate in the binding, the accuracy of the prediction can be compromised. On top of that argument, different regions within a protein structure may be structurally disordered or long loops, which, when coupled with the dynamic nature of proteins and the conformational changes that they can undergo, predictions of structural complexes can be challenging. Solving the structure with experimental techniques, like nuclear magnetic resonance (NMR) or cryo-electron microscopy could provide complementary information that is crucial for determining the binding interface. In our studies, we approached the interaction mapping between NRF2 and LC3B using a mutational analysis and in vitro studies of their direct interaction.

## 6. References

- Adams, P. D., Ivanov, A., Pawlikowski, J., Manoharan, I., Tuyn, J. Van, Nelson, D. M., Singh Rai, T., Shah, P. P., Hewitt, G., Korolchuk, V. I., Passos, J. F., Wu, H., & Berger, S. L. (2013). Lysosome-mediated processing of chromatin in senescence. *Journal of Cell Biology*, *202*(1), 129–143. <https://doi.org/10.1083/jcb.201212110>
- Alam, J., Killeen, E., Gong, P., Naquin, R., Hu, B., Stewart, D., Ingelfinger, J. R., & Nath, K. A. (2003). Heme activates the heme oxygenase-1 gene in renal epithelial cells by stabilizing Nrf2. *American Journal of Physiology - Renal Physiology*, *284*(4 53-4). <https://doi.org/10.1152/AJPRENAL.00376.2002/ASSET/IMAGES/LARGE/H20431088008.JPG>
- Alam, J., Stewart, D., Touchard, C., Boinapally, S., Choi, A. M. K., & Cook, J. L. (1999). Nrf2, a Cap'n'Collar Transcription Factor, Regulates Induction of the Heme Oxygenase-1 Gene. *Journal of Biological Chemistry*, *274*(37), 26071–26078. <https://doi.org/10.1074/JBC.274.37.26071>
- Alemu, E. A., Lamark, T., Torgersen, K. M., Birgisdottir, A. B., Larsen, K. B., Jain, A., Olsvik, H., Øvervatn, A., Kirkin, V., & Johansen, T. (2012). ATG8 Family Proteins Act as Scaffolds for Assembly of the ULK Complex: Sequence Requirements for LC3-Interacting Region (LIR) Motifs. *Journal of Biological Chemistry*, *287*(47), 39275–39290. <https://doi.org/10.1074/JBC.M112.378109>
- Alimbetov, D., Davis, T., Brook, A. J. C., Cox, L. S., Faragher, R. G. A., Nurgozhin, T., Zhumadilov, Z., & Kipling, D. (2016). Suppression of the senescence-associated secretory phenotype (SASP) in human fibroblasts using small molecule inhibitors of p38 MAP kinase and MK2. *Biogerontology*, *17*(2), 305–315. <https://doi.org/10.1007/S10522-015-9610-Z/FIGURES/3>
- Allen, B. L., & Taatjes, D. J. (2015). The Mediator complex: a central integrator of transcription. *Nature Reviews Molecular Cell Biology*, *16*(3), 155–166. <https://doi.org/10.1038/nrm3951>
- Almuzzaini, B., Sarshad, A. A., Farrants, A. K. Ö., & Percipalle, P. (2015a). Nuclear myosin 1 contributes to a chromatin landscape compatible with RNA polymerase II transcription activation. *BMC Biology*, *13*(1), 1–15. <https://doi.org/10.1186/S12915-015-0147-Z/FIGURES/7>
- An, J. H., & Blackwell, T. K. (2003). SKN-1 links C. elegans mesendodermal specification to a conserved oxidative stress response. *Genes & Development*, *17*(15), 1882–1893. <https://doi.org/10.1101/GAD.1107803>
- An, J. H., Vranas, K., Lucke, M., Inoue, H., Hisamoto, N., Matsumoto, K., & Blackwell, T. K. (2005). Regulation of the Caenorhabditis elegans oxidative stress defense protein SKN-1 by glycogen synthase kinase-3. *Proceedings of the National Academy of Sciences of the United States of America*, *102*(45), 16275–16280. [https://doi.org/10.1073/PNAS.0508105102/SUPPL\\_FILE/INDEX.HTML](https://doi.org/10.1073/PNAS.0508105102/SUPPL_FILE/INDEX.HTML)
- Andrews, N. C. (1998). The NF-E2 transcription factor. *International Journal of Biochemistry and Cell Biology*, *30*(4), 429–432. [https://doi.org/10.1016/S1357-2725\(97\)00135-0](https://doi.org/10.1016/S1357-2725(97)00135-0)

- Arstila, A. U., & Trump, B. F. (1968). Studies on cellular autophagocytosis. The formation of autophagic vacuoles in the liver after glucagon administration. *The American Journal of Pathology*, *53*(5), 687. <https://www.ncbi.nlm.nih.gov/pmc/articles/PMC2013521/>
- Axe, E. L., Walker, S. A., Manifava, M., Chandra, P., Roderick, H. L., Habermann, A., Griffiths, G., & Ktistakis, N. T. (2008). Autophagosome formation from membrane compartments enriched in phosphatidylinositol 3-phosphate and dynamically connected to the endoplasmic reticulum. *Journal of Cell Biology*, *182*(4), 685–701. <https://doi.org/10.1083/JCB.200803137/VIDEO-7>
- Aydin, Ö. Z., Vermeulen, W., & Lans, H. (2014). ISWI chromatin remodeling complexes in the DNA damage response. *Cell Cycle*, *13*(19), 3016–3025. <https://doi.org/10.4161/15384101.2014.956551>
- Baird, L., & Yamamoto, M. (2020). The Molecular Mechanisms Regulating the KEAP1-NRF2 Pathway. *Molecular and Cellular Biology*, *40*(13), 23.
- Bampton, E. T. W., Goemans, C. G., Niranjana, D., Mizushima, N., & Tolkovsky, A. M. (2005). The dynamics of autophagy visualized in live cells: from autophagosome formation to fusion with endo/lysosomes. *Autophagy*, *1*(1), 23–36. <https://doi.org/10.4161/AUTO.1.1.1495>
- Barinda, A. J., Ikeda, K., Nugroho, D. B., Wardhana, D. A., Sasaki, N., Honda, S., Urata, R., Matoba, S., Hirata, K. ichi, & Emoto, N. (2020). Endothelial progeria induces adipose tissue senescence and impairs insulin sensitivity through senescence associated secretory phenotype. *Nature Communications*, *11*(1), 1–13. <https://doi.org/10.1038/s41467-020-14387-w>
- Barnett, C., & Krebs, J. E. (2010). WSTF does it all: a multifunctional protein in transcription, repair, and replication. *https://Doi.Org/10.1139/O10-114*, *89*(1), 12–23. <https://doi.org/10.1139/O10-114>
- Barnett, C., Yazgan, O., Kuo, H. C., Malakar, S., Thomas, T., Fitzgerald, A., Harbour, W., Henry, J. J., & Krebs, J. E. (2012a). Williams Syndrome Transcription Factor is critical for neural crest cell function in *Xenopus laevis*. *Mechanisms of Development*, *129*(9–12), 324–338. <https://doi.org/10.1016/J.MOD.2012.06.001>
- Bartholomew, B. (2014). ISWI chromatin remodeling: one primary actor or a coordinated effort? *Current Opinion in Structural Biology*, *24*(1), 150–155. <https://doi.org/10.1016/J.SBI.2014.01.010>
- Barve, A., Tin, O. K., Nair, S., Lin, W., Yu, S., Jain, M. R., Chan, J. Y., & Kong, A. N. (2008). Pharmacokinetics, Pharmacodynamics and Drug Metabolism: Pharmacogenomic Profile of Soy Isoflavone Concentrate in the Prostate of Nrf2 Deficient and Wild-Type Mice. *Journal of Pharmaceutical Sciences*, *97*(10), 4528–4545. <https://doi.org/10.1002/JPS.21311>
- Basisty, N., Kale, A., Jeon, O. H., Kuehnemann, C., Payne, T., Rao, C., Holtz, A., Shah, S., Sharma, V., Ferrucci, L., Campisi, J., & Schilling, B. (2020). A proteomic atlas of senescence-associated secretomes for aging biomarker development. *PLOS Biology*, *18*(1), e3000599. <https://doi.org/10.1371/JOURNAL.PBIO.3000599>

- Behrends, C., Sowa, M. E., Gygi, S. P., & Harper, J. W. (2010). Network organization of the human autophagy system. *Nature*, *466*(7302), 68–76. <https://doi.org/10.1038/nature09204>
- Bento, C. F., Renna, M., Ghislat, G., Puri, C., Ashkenazi, A., Vicinanza, M., Menzies, F. M., & Rubinsztein, D. C. (2016). Mammalian Autophagy: How Does It Work? *Annual Review of Biochemistry*, *85*, 685–713. <https://doi.org/10.1146/ANNUREV-BIOCHEM-060815-014556>
- Bertoline, L. M. F., Lima, A. N., Krieger, J. E., & Teixeira, S. K. (2023). Before and after AlphaFold2: An overview of protein structure prediction. *Frontiers in Bioinformatics*, *3*, 1120370. <https://doi.org/10.3389/FBINF.2023.1120370/BIBTEX>
- Betin, V. M. S., Singleton, B. K., Parsons, S. F., Anstee, D. J., & Lane, J. D. (2013). Autophagy facilitates organelle clearance during differentiation of human erythroblasts. *Autophagy*, *9*(6), 881–893. <https://doi.org/10.4161/AUTO.24172>
- Bhujabal, Z., Birgisdottir, Á. B., Sjøttem, E., Brenne, H. B., Øvervatn, A., Habisov, S., Kirkin, V., Lamark, T., & Johansen, T. (2017). FKBP8 recruits LC3A to mediate Parkin-independent mitophagy. *EMBO Reports*, *18*(6), 947–961. [https://doi.org/10.15252/EMBR.201643147/SUPPL\\_FILE/EMBR201643147-SUP-0003-SDATAFIG4.JPG](https://doi.org/10.15252/EMBR.201643147/SUPPL_FILE/EMBR201643147-SUP-0003-SDATAFIG4.JPG)
- Birgisdottir, Á. B., Lamark, T., & Johansen, T. (2013). The LIR motif - crucial for selective autophagy. In *Journal of Cell Science* (Vol. 126, Issue 15, pp. 3237–3247). J Cell Sci. <https://doi.org/10.1242/jcs.126128>
- Birgisdottir, Á. B., Mouilleron, S., Bhujabal, Z., Wirth, M., Sjøttem, E., Evjen, G., Zhang, W., Lee, R., O'Reilly, N., Tooze, S. A., Lamark, T., & Johansen, T. (2019). Members of the autophagy class III phosphatidylinositol 3-kinase complex I interact with GABARAP and GABARAPL1 via LIR motifs. *Autophagy*, *15*(8), 1333–1355. <https://doi.org/10.1080/15548627.2019.1581009>
- Bjørkøy, G., Lamark, T., Brech, A., Outzen, H., Perander, M., Øvervatn, A., Stenmark, H., & Johansen, T. (2005). p62/SQSTM1 forms protein aggregates degraded by autophagy and has a protective effect on huntingtin-induced cell death. *Journal of Cell Biology*, *171*(4), 603–614. <https://doi.org/10.1083/JCB.200507002/VIDEO-3>
- Blackwell, T. K., Steinbaugh, M. J., Hourihan, J. M., Ewald, C. Y., & Isik, M. (2015). SKN-1/Nrf, stress responses, and aging in *Caenorhabditis elegans*. *Free Radical Biology and Medicine*, *88*(Part B), 290–301. <https://doi.org/10.1016/J.FREERADBIOMED.2015.06.008>
- Blanpain, C., Mohrin, M., Sotiropoulou, P. A., & Passegué, E. (2011). DNA-damage response in tissue-specific and cancer stem cells. *Cell Stem Cell*, *8*(1), 16–29. <https://doi.org/10.1016/J.STEM.2010.12.012>
- Bohn, T., De Lera, A. R., Landrier, J. F., & Rühl, R. (2023). Carotenoid metabolites, their tissue and blood concentrations in humans and further bioactivity via retinoid receptor-mediated signalling. *Nutrition Research Reviews*, *36*(2), 498–511. <https://doi.org/10.1017/S095442242200021X>

- Bollong, M. J., Yun, H., Sherwood, L., Woods, A. K., Lairson, L. L., & Schultz, P. G. (2015). A Small Molecule Inhibits Deregulated NRF2 Transcriptional Activity in Cancer. *ACS Chemical Biology*, *10*(10), 2193–2198. [https://doi.org/10.1021/ACSCHEMBIO.5B00448/ASSET/IMAGES/LARGE/CB-2015-00448M\\_0005.JPEG](https://doi.org/10.1021/ACSCHEMBIO.5B00448/ASSET/IMAGES/LARGE/CB-2015-00448M_0005.JPEG)
- Bonam, S. R., Wang, F., & Muller, S. (2019). Lysosomes as a therapeutic target. *Nature Reviews Drug Discovery*, *18*(12), 923–948. <https://doi.org/10.1038/s41573-019-0036-1>
- Boveris, A., Cadenas, E., & Stoppani, A. O. M. (1976). Role of ubiquinone in the mitochondrial generation of hydrogen peroxide. *Biochemical Journal*, *156*(2), 435. <https://doi.org/10.1042/BJ1560435>
- Bozhenok, L., Wade, P. A., & Varga-Weisz, P. (2002). WSTF–ISWI chromatin remodeling complex targets heterochromatic replication foci. *The EMBO Journal*, *21*(9), 2231–2241. <https://doi.org/10.1093/EMBOJ/21.9.2231>
- Bradsher, J., Auriol, J., De Santis, L. P., Iben, S., Vonesch, J. L., Grummt, I., & Egly, J. M. (2002). CSB Is a Component of RNA Pol I Transcription. *Molecular Cell*, *10*(4), 819–829. [https://doi.org/10.1016/S1097-2765\(02\)00678-0](https://doi.org/10.1016/S1097-2765(02)00678-0)
- Brand, M. D. (2016). Mitochondrial generation of superoxide and hydrogen peroxide as the source of mitochondrial redox signaling. *Free Radical Biology and Medicine*, *100*, 14–31. <https://doi.org/10.1016/J.FREERADBIOMED.2016.04.001>
- Brown, E. J., Albers, M. W., Bum Shin, T., Ichikawa, K., Keith, C. T., Lane, W. S., & Schreiber, S. L. (1994). A mammalian protein targeted by G1-arresting rapamycin–receptor complex. *Nature*, *369*(6483), 756–758. <https://doi.org/10.1038/369756a0>
- Brown, S. L., Sekhar, K. R., Rachakonda, G., Sasi, S., & Freeman, M. L. (2008). Activating transcription factor 3 is a novel repressor of the nuclear factor erythroid-derived 2-related factor 2 (Nrf2)-regulated stress pathway. *Cancer Research*, *68*(2), 364–368. <https://doi.org/10.1158/0008-5472.CAN-07-2170>
- Budanov, A. V. (2014). The role of tumor suppressor p53 in the antioxidant defense and metabolism. *Sub-Cellular Biochemistry*, *85*, 337. [https://doi.org/10.1007/978-94-017-9211-0\\_18](https://doi.org/10.1007/978-94-017-9211-0_18)
- Calo, E., Flynn, R. A., Martin, L., Spitale, R. C., Chang, H. Y., & Wysocka, J. (2014). RNA helicase DDX21 coordinates transcription and ribosomal RNA processing. *Nature*, *518*(7538), 249–253. <https://doi.org/10.1038/nature13923>
- Cao, J. L., He, W. X., Zou, Y. N., & Wu, Q. S. (2023). An endophytic fungus, *Piriformospora indica*, enhances drought tolerance of trifoliolate orange by modulating the antioxidant defense system and composition of fatty acids. *Tree Physiology*, *43*(3), 452–466. <https://doi.org/10.1093/TREEPHYS/TPAC126>



- Cavellán, E., Asp, P., Percipalle, P., & Farrants, A. K. Ö. (2006a). The WSTF-SNF2h Chromatin Remodeling Complex Interacts with Several Nuclear Proteins in Transcription. *Journal of Biological Chemistry*, *281*(24), 16264–16271. <https://doi.org/10.1074/JBC.M600233200>
- Cavellán, E., Asp, P., Percipalle, P., & Farrants, A. K. Ö. (2006b). The WSTF-SNF2h Chromatin Remodeling Complex Interacts with Several Nuclear Proteins in Transcription. *Journal of Biological Chemistry*, *281*(24), 16264–16271. <https://doi.org/10.1074/JBC.M600233200>
- Chan, J. Y., Han, X. L., & Yuet Wai Kan. (1993). Cloning of Nrf1, an NF-E2-related transcription factor, by genetic selection in yeast. *Proceedings of the National Academy of Sciences of the United States of America*, *90*(23), 11371–11375. <https://doi.org/10.1073/PNAS.90.23.11371>
- Chan, K., Lu, R., Chang, J. C., & Kan, Y. W. (1996). NRF2, a member of the NFE2 family of transcription factors, is not essential for murine erythropoiesis, growth, and development. *Proceedings of the National Academy of Sciences of the United States of America*, *93*(24), 13943–13948. <https://doi.org/10.1073/PNAS.93.24.13943>
- Chanas, S. A., Jiang, Q., McMahon, M., McWalter, G. K., McLellan, L. I., Elcombe, C. R., Henderson, C. J., Wolf, C. R., Moffat, G. J., Itoh, K., Yamamoto, M., & Hayes, J. D. (2002). Loss of the Nrf2 transcription factor causes a marked reduction in constitutive and inducible expression of the glutathione S-transferase *Gsta1*, *Gsta2*, *Gstm1*, *Gstm2*, *Gstm3* and *Gstm4* genes in the livers of male and female mice. *Biochemical Journal*, *365*(2), 405–416. <https://doi.org/10.1042/BJ20020320>
- Chen, W., Sun, Z., Wang, X. J., Jiang, T., Huang, Z., Fang, D., & Zhang, D. D. (2009). Direct interaction between Nrf2 and p21(Cip1/WAF1) upregulates the Nrf2-mediated antioxidant response. *Molecular Cell*, *34*(6), 663–673. <https://doi.org/10.1016/J.MOLCEL.2009.04.029>
- Cheng, X., Wang, Y., Gong, Y., Li, F., Guo, Y., Hu, S., Liu, J., & Pan, L. (2016). Structural basis of FYCO1 and MAP1LC3A interaction reveals a novel binding mode for Atg8-family proteins. *Autophagy*, *12*(8), 1330–1339. <https://doi.org/10.1080/15548627.2016.1185590>
- Choe, K. P., Leung, C. K., & Miyamoto, M. M. (2012). Unique structure and regulation of the nematode detoxification gene regulator, SKN-1: implications to understanding and controlling drug resistance. *Drug Metabolism Reviews*, *44*(3), 209–223. <https://doi.org/10.3109/03602532.2012.684799>
- Chorley, B. N., Campbell, M. R., Wang, X., Karaca, M., Sambandan, D., Bangura, F., Xue, P., Pi, J., Kleeberger, S. R., & Bell, D. A. (2012). Identification of novel NRF2-regulated genes by ChIP-Seq: influence on retinoid X receptor alpha. *Nucleic Acids Research*, *40*(15), 7416–7429. <https://doi.org/10.1093/NAR/GKS409>
- Chowdhry, S., Nazmy, M. H., Meakin, P. J., Dinkova-Kostova, A. T., Walsh, S. V., Tsujita, T., Dillon, J. F., Ashford, M. L. J., & Hayes, J. D. (2010). Loss of Nrf2 markedly exacerbates nonalcoholic steatohepatitis. *Free Radical Biology & Medicine*, *48*(2), 357–371. <https://doi.org/10.1016/J.FREERADBIOMED.2009.11.007>

- Ciaffardini, F., Nicolai, S., Caputo, M., Canu, G., Paccosi, E., Costantino, M., Frontini, M., Balajee, A. S., & Proietti-De-Santis, L. (2014). The cockayne syndrome B protein is essential for neuronal differentiation and neurogenesis. *Cell Death & Disease*, *5*(5), e1268–e1268. <https://doi.org/10.1038/cddis.2014.228>
- Ciechomska, I. A., & Tolkovsky, A. M. (2007). Non-autophagic GFP-LC3 puncta induced by saponin and other detergents. *Autophagy*, *3*(6), 586–590. <https://doi.org/10.4161/AUTO.4843>
- Clapier, C. R., Iwasa, J., Cairns, B. R., & Peterson, C. L. (2017). Mechanisms of action and regulation of ATP-dependent chromatin-remodelling complexes. *Nature Reviews Molecular Cell Biology*, *18*(7), 407–422. <https://doi.org/10.1038/nrm.2017.26>
- Copple, I. M., Lister, A., Obeng, A. D., Kitteringham, N. R., Jenkins, R. E., Layfield, R., Foster, B. J., Goldring, C. E., & Park, B. K. (2010). Physical and functional interaction of sequestosome 1 with Keap1 regulates the Keap1-Nrf2 cell defense pathway. *Journal of Biological Chemistry*, *285*(22), 16782–16788. <https://doi.org/10.1074/jbc.M109.096545>
- Córdova, E. J., Martínez-Hernández, A., Uribe-Figueroa, L., Centeno, F., Morales-Marín, M., Koneru, H., Coleman, M. A., & Orozco, L. (2014). The NRF2-KEAP1 Pathway Is an Early Responsive Gene Network in Arsenic Exposed Lymphoblastoid Cells. *PLOS ONE*, *9*(2), e88069. <https://doi.org/10.1371/JOURNAL.PONE.0088069>
- Cretu, C., Schmitzová, J., Ponce-Salvatierra, A., Dybkov, O., De Laurentiis, E. I., Sharma, K., Will, C. L., Urlaub, H., Lüthmann, R., & Pena, V. (2016). Molecular Architecture of SF3b and Structural Consequences of Its Cancer-Related Mutations. *Molecular Cell*, *64*(2), 307–319. <https://doi.org/10.1016/J.MOLCEL.2016.08.036>
- Cuadrado, A., Rojo, A. I., Wells, G., Hayes, J. D., Cousin, S. P., Rumsey, W. L., Attucks, O. C., Franklin, S., Levonen, A. L., Kensler, T. W., & Dinkova-Kostova, A. T. (2019). Therapeutic targeting of the NRF2 and KEAP1 partnership in chronic diseases. *Nature Reviews Drug Discovery*, *18*(4), 295–317. <https://doi.org/10.1038/s41573-018-0008-x>
- Cullinan, S. B., Gordan, J. D., Jin, J., Harper, J. W., & Diehl, J. A. (2004). The Keap1-BTB protein is an adaptor that bridges Nrf2 to a Cul3-based E3 ligase: oxidative stress sensing by a Cul3-Keap1 ligase. *Molecular and Cellular Biology*, *24*(19), 8477–8486. <https://doi.org/10.1128/MCB.24.19.8477-8486.2004>
- Culver-Cochran, A. E., & Chadwick, B. P. (2012). The WSTF-ISWI Chromatin Remodeling Complex Transiently Associates with the Human Inactive X Chromosome during Late S-Phase Prior to BRCA1 and  $\gamma$ -H2AX. *PLOS ONE*, *7*(11), e50023. <https://doi.org/10.1371/JOURNAL.PONE.0050023>
- Culver-Cochran, A. E., & Chadwick, B. P. (2013). Loss of WSTF results in spontaneous fluctuations of heterochromatin formation and resolution, combined with substantial changes to gene expression. *BMC Genomics*, *14*(1), 1–18. <https://doi.org/10.1186/1471-2164-14-740/FIGURES/8>

- Davies, K. J. A. (1986). Intracellular proteolytic systems may function as secondary antioxidant defenses: an hypothesis. *Journal of Free Radicals in Biology & Medicine*, 2(3), 155–173. [https://doi.org/10.1016/S0748-5514\(86\)80066-6](https://doi.org/10.1016/S0748-5514(86)80066-6)
- Deursen, J. M. (2014). The role of senescent cells in ageing. In *Nature* (Vol. 509, Issue 7501, pp. 439–446). Nature Publishing Group. <https://doi.org/10.1038/nature13193>
- Duve, C. (2005). The lysosome turns fifty. *Nature Cell Biology*, 7(9), 847–849. <https://doi.org/10.1038/ncb0905-847>
- Duve, C., Pressman, B. C., Gianetto, R., Wattiaux, R., & Appelmas, F. (1955). Intracellular distribution patterns of enzymes in rat-liver tissue. *Biochemical Journal*, 60(4), 604–617. <https://doi.org/10.1042/BJ0600604>
- Demaria, M., Ohtani, N., Youssef, S. A., Rodier, F., Toussaint, W., Mitchell, J. R., Laberge, R. M., Vijg, J., VanSteeg, H., Dollé, M. E. T., Hoeijmakers, J. H. J., deBruin, A., Hara, E., & Campisi, J. (2014). An Essential Role for Senescent Cells in Optimal Wound Healing through Secretion of PDGF-AA. *Developmental Cell*, 31(6), 722–733. <https://doi.org/10.1016/J.DEVCEL.2014.11.012>
- Denicola, G. M., Karreth, F. A., Humpton, T. J., Gopinathan, A., Wei, C., Frese, K., Mangal, D., Yu, K. H., Yeo, C. J., Calhoun, E. S., Scrimieri, F., Winter, J. M., Hruban, R. H., Iacobuzio-Donahue, C., Kern, S. E., Blair, I. A., & Tuveson, D. A. (2011). Oncogene-induced Nrf2 transcription promotes ROS detoxification and tumorigenesis. *Nature*, 475(7354), 106–109. <https://doi.org/10.1038/nature10189>
- Dharshini, L. C. P., Vishnupriya, S., Sakthivel, K. M., & Rasmi, R. R. (2020). Oxidative stress responsive transcription factors in cellular signalling transduction mechanisms. *Cellular Signalling*, 72, 109670. <https://doi.org/10.1016/j.cellsig.2020.109670>
- Dickinson, D. A., Levonen, A. L., Moellering, D. R., Arnold, E. K., Zhang, H., Darley-Usmar, V. M., & Forman, H. J. (2004). Human glutamate cysteine ligase gene regulation through the electrophile response element. *Free Radical Biology and Medicine*, 37(8), 1152–1159. <https://doi.org/10.1016/J.FREERADBIOMED.2004.06.011>
- Dickinson, S. E., Melton, T. F., Olson, E. R., Zhang, J., Saboda, K., & Bowden, G. T. (2009). Inhibition of activator protein-1 by sulforaphane involves interaction with cysteine in the cFos DNA-binding domain: implications for chemoprevention of UVB-induced skin cancer. *Cancer Research*, 69(17), 7103–7110. <https://doi.org/10.1158/0008-5472.CAN-09-0770>
- Dikic, I. (2017). Proteasomal and Autophagic Degradation Systems. *Annual Review of Biochemistry*, 86, 193–224. <https://doi.org/10.1146/ANNUREV-BIOCHEM-061516-044908>
- Dikic, I., & Elazar, Z. (2018). Mechanism and medical implications of mammalian autophagy. *Nature Reviews Molecular Cell Biology* 2018 19:6, 19(6), 349–364. <https://doi.org/10.1038/s41580-018-0003-4>

- Dinkova-Kostova, A. T., & Talalay, P. (2010). NAD(P)H:quinone acceptor oxidoreductase 1 (NQO1), a multifunctional antioxidant enzyme and exceptionally versatile cytoprotector. *Archives of Biochemistry and Biophysics*, *501*(1), 116–123. <https://doi.org/10.1016/J.ABB.2010.03.019>
- Doerks, T., Copley, R., & Bork, P. (2001). DDT - A novel domain in different transcription and chromosome remodeling factors. *Trends in Biochemical Sciences*, *26*(3), 145–146. [https://doi.org/10.1016/S0968-0004\(00\)01769-2](https://doi.org/10.1016/S0968-0004(00)01769-2)
- Dooley, H. C., Razi, M., Polson, H. E. J., Girardin, S. E., Wilson, M. I., & Tooze, S. A. (2014). WIPI2 Links LC3 Conjugation with PI3P, Autophagosome Formation, and Pathogen Clearance by Recruiting Atg12–5–16L1. *Molecular Cell*, *55*(2), 238–252. <https://doi.org/10.1016/J.MOLCEL.2014.05.021>
- Dou, Z., Xu, C., Donahue, G., Shimi, T., Pan, J. A., Zhu, J., Ivanov, A., Capell, B. C., Drake, A. M., Shah, P. P., Catanzaro, J. M., Ricketts, M. D., Lamark, T., Adam, S. A., Marmorstein, R., Zong, W. X., Johansen, T., Goldman, R. D., Adams, P. D., & Berger, S. L. (2015). Autophagy mediates degradation of nuclear lamina. *Nature*, *527*(7576), 105–109. <https://doi.org/10.1038/nature15548>
- Drake, K. R., Kang, M., & Kenworthy, A. K. (2010). Nucleocytoplasmic distribution and dynamics of the autophagosome marker EGFP-LC3. *PLOS ONE*, *5*(3), e9806. <https://doi.org/10.1371/journal.pone.0009806>
- Egea, J., Buendía, I., Parada, E., Navarro, E., Rada, P., Cuadrado, A., López, M. G., García, A. G., & León, R. (2015). Melatonin–sulforaphane hybrid ITH12674 induces neuroprotection in oxidative stress conditions by a ‘drug–prodrug’ mechanism of action. *British Journal of Pharmacology*, *172*(7), 1807–1821. <https://doi.org/10.1111/BPH.13025>
- En, A., Takauji, Y., Ayusawa, D., & Fujii, M. (2020). The role of lamin B receptor in the regulation of senescence-associated secretory phenotype (SASP). *Experimental Cell Research*, *390*(1), 111927. <https://doi.org/10.1016/J.YEXCR.2020.111927>
- Erickson, A. M., Nevarea, Z., Gipp, J. J., & Timothy Mulcahy, R. (2002). Identification of a Variant Antioxidant Response Element in the Promoter of the Human Glutamate–Cysteine Ligase Modifier Subunit Gene. *Journal of Biological Chemistry*, *277*(34), 30730–30737. <https://doi.org/10.1074/JBC.M205225200>
- Forman, H. J., & Zhang, H. (2021). Targeting oxidative stress in disease: promise and limitations of antioxidant therapy. *Nature Reviews Drug Discovery*, *20*(9), 689–709. <https://doi.org/10.1038/s41573-021-00233-1>
- Franić, D., Zubčić, K., & Boban, M. (2021). Nuclear Ubiquitin-Proteasome Pathways in Proteostasis Maintenance. *Biomolecules*, *11*(1), 54. <https://doi.org/10.3390/BIOM11010054>
- Frattini, A., Fabbri, M., Valli, R., De Paoli, E., Montalbano, G., Gribaldo, L., Pasquali, F., & Maserati, E. (2015). High variability of genomic instability and gene expression profiling in different HeLa clones. *Scientific Reports*, *5*. <https://doi.org/10.1038/SREP15377>

- Fujiwara K T, Kataoka K, & Nishizawa M. (1993). Two new members of the maf oncogene family, mafK and mafF, encode nuclear b-Zip proteins lacking putative trans-activator domain. *Oncogene*, 2371(80), 8–9. <https://pubmed.ncbi.nlm.nih.gov/8361754/>
- Fuse, Y., Kobayashi, M., Saso, L., Dux, L., Wegrzyn, G., & Csont, T. (2017). Conservation of the Keap1-Nrf2 System: An Evolutionary Journey through Stressful Space and Time. *Molecules*, 22(3), 436. <https://doi.org/10.3390/MOLECULES22030436>
- Gacesa, R., Dunlap, W. C., Barlow, D. J., Laskowski, R. A., & Long, P. F. (2016). Rising levels of atmospheric oxygen and evolution of Nrf2. *Scientific Reports*, 6(1), 1–5. <https://doi.org/10.1038/srep27740>
- Gacesa, R., Dunlap, W. C., & Long, P. F. (2015). Bioinformatics analyses provide insight into distant homology of the Keap1–Nrf2 pathway. *Free Radical Biology and Medicine*, 88(Part B), 373–380. <https://doi.org/10.1016/J.FREERADBIOMED.2015.06.015>
- Galluzzi, L., Baehrecke, E. H., Ballabio, A., Boya, P., Pedro, J. M. B.-S., Cecconi, F., Choi, A. M., Chu, C. T., Codogno, P., Colombo, M. I., Cuervo, A. M., Debnath, J., Deretic, V., Dikic, I., Eskelinen, E.-L., Fimia, G. M., Fulda, S., Gewirtz, D. A., Green, D. R., ... Kroemer, G. (2017). Molecular definitions of autophagy and related processes. *The EMBO Journal*, 36(13), 1811–1836. <https://doi.org/10.15252/EMBJ.201796697>
- Genau, H. M., Huber, J., Baschieri, F., Akutsu, M., Dötsch, V., Farhan, H., Rogov, V., & Behrends, C. (2015). CUL3-KBTBD6/KBTBD7 Ubiquitin Ligase Cooperates with GABARAP Proteins to Spatially Restrict TIAM1-RAC1 Signaling. *Molecular Cell*, 57(6), 995–1010. <https://doi.org/10.1016/j.molcel.2014.12.040>
- Ghanbarpour, A., Valverde, D. P., Melia, T. J., & Reinisch, K. M. (2021). A model for a partnership of lipid transfer proteins and scramblases in membrane expansion and organelle biogenesis. *Proceedings of the National Academy of Sciences of the United States of America*, 118(16), e2101562118. <https://doi.org/10.1073/pnas.2101562118>
- Goldstein, L. D., Lee, J., Gnad, F., Klijn, C., Schaub, A., Reeder, J., Daemen, A., Bakalarski, C. E., Holcomb, T., Shames, D. S., Hartmaier, R. J., Chmielecki, J., Seshagiri, S., Gentleman, R., & Stokoe, D. (2016). Recurrent Loss of NFE2L2 Exon 2 Is a Mechanism for Nrf2 Pathway Activation in Human Cancers. *Cell Reports*, 16(10), 2605–2617. <https://doi.org/10.1016/J.CELREP.2016.08.010>
- Goodwin, L. R., & Picketts, D. J. (2018). The role of ISWI chromatin remodeling complexes in brain development and neurodevelopmental disorders. *Molecular and Cellular Neuroscience*, 87, 55–64. <https://doi.org/10.1016/J.MCN.2017.10.008>
- Gorrini, C., Baniasadi, P. S., Harris, I. S., Silvester, J., Inoue, S., Snow, B., Joshi, P. A., Wakeham, A., Molyneux, S. D., Martin, B., Bouwman, P., Cescon, D. W., Elia, A. J., Winterton-Perks, Z., Cruickshank, J., Brenner, D., Tseng, A., Musgrave, M., Berman, H. K., ... Gauthier, M. L. (2013). BRCA1 interacts with Nrf2 to regulate antioxidant signaling and cell survival. *The Journal of Experimental Medicine*, 210(8), 1529–1544. <https://doi.org/10.1084/JEM.20121337>

- Guerrero-Beltrán, C. E., Calderón-Oliver, M., Pedraza-Chaverri, J., & Chirino, Y. I. (2012). Protective effect of sulforaphane against oxidative stress: recent advances. *Experimental and Toxicologic Pathology*, *64*(5), 503–508. <https://doi.org/10.1016/J.ETP.2010.11.005>
- Gueux, N., Peitsch, M. C., & Schwede, T. (2009). Automated comparative protein structure modeling with SWISS-MODEL and Swiss-PdbViewer: A historical perspective. *Electrophoresis*, *30*(S1), S162–S173. <https://doi.org/10.1002/ELPS.200900140>
- Halliwel, B. (2023). Understanding mechanisms of antioxidant action in health and disease. *Nature Reviews Molecular Cell Biology*, 1–21. <https://doi.org/10.1038/s41580-023-00645-4>
- Han, R. M., Zhang, J. P., & Skibsted, L. H. (2012). Reaction Dynamics of Flavonoids and Carotenoids as Antioxidants. *Molecules*, *17*(2), 2140–2160. <https://doi.org/10.3390/MOLECULES17022140>
- Hanada, N., Takahata, T., Zhou, Q., Ye, X., Sun, R., Itoh, J., Ishiguro, A., Kijima, H., Mimura, J., Itoh, K., Fukuda, S., & Saijo, Y. (2012). Methylation of the KEAP1 gene promoter region in human colorectal cancer. *BMC Cancer*, *12*. <https://doi.org/10.1186/1471-2407-12-66>
- Harwell, B. (2007). Biochemistry of oxidative stress. *Biochemical Society Transactions*, *35*(5), 1147–1150. <https://doi.org/10.1042/BST0351147>
- Hast, B. E., Goldfarb, D., Mulvaney, K. M., Hast, M. A., Siesser, P. F., Yan, F., Hayes, D. N., & Major, M. B. (2013). Proteomic analysis of ubiquitin ligase KEAP1 reveals associated proteins that inhibit NRF2 ubiquitination. *Cancer Research*, *73*(7), 2199–2210. <https://doi.org/10.1158/0008-5472.CAN-12-4400>
- Hayes, J. D., & Dinkova-Kostova, A. T. (2014). The Nrf2 regulatory network provides an interface between redox and intermediary metabolism. *Trends in Biochemical Sciences*, *39*(4), 199–218. <https://doi.org/10.1016/J.TIBS.2014.02.002>
- Hayes, J. D., Dinkova-Kostova, A. T., & Tew, K. D. (2020). Oxidative Stress in Cancer. *Cancer Cell*, *38*(2), 167–197. <https://doi.org/10.1016/J.CCELL.2020.06.001>
- Hayflick, L., & Moorhead, P. S. (1961). The serial cultivation of human diploid cell strains. *Experimental Cell Research*, *25*(3), 585–621. [https://doi.org/10.1016/0014-4827\(61\)90192-6](https://doi.org/10.1016/0014-4827(61)90192-6)
- He, C. H., Gong, P., Hu, B., Stewart, D., Choi, M. E., Choi, A. M. K., & Alam, J. (2001). Identification of Activating Transcription Factor 4 (ATF4) as an Nrf2-interacting Protein. *Journal of Biological Chemistry*, *276*(24), 20858–20865. <https://doi.org/10.1074/jbc.m101198200>
- He, W., Hu, C. X., Hou, J. K., Fan, L., Xu, Y. W., Liu, M. H., Yan, S. Y., Chen, G. Q., & Huang, Y. (2014). Microtubule-Associated Protein 1 Light Chain 3 Interacts with and Contributes to Growth Inhibiting Effect of PML. *PLOS ONE*, *9*(11), e113089. <https://doi.org/10.1371/JOURNAL.PONE.0113089>

- Hickey, K. L., Swarup, S., Smith, I. R., Paoli, J. C., Miguel Whelan, E., Paulo, J. A., & Harper, J. W. (2023). Proteome census upon nutrient stress reveals Golgiphagy membrane receptors. *Nature*, *623*(7985), 167–174. <https://doi.org/10.1038/s41586-023-06657-6>
- Hirotsu, Y., Katsuoka, F., Funayama, R., Nagashima, T., Nishida, Y., Nakayama, K., Douglas Engel, J., & Yamamoto, M. (2012). Nrf2–MafG heterodimers contribute globally to antioxidant and metabolic networks. *Nucleic Acids Research*, *40*(20), 10228–10239. <https://doi.org/10.1093/NAR/GKS827>
- Hirschenson, J., Melgar-Bermudez, E., & Mailloux, R. J. (2022). The Uncoupling Proteins: A Systematic Review on the Mechanism Used in the Prevention of Oxidative Stress. *Antioxidants*, *11*(2), 322. <https://doi.org/10.3390/ANTIOX11020322>
- Horie, Y., Suzuki, T., Inoue, J., Iso, T., Wells, G., Moore, T. W., Mizushima, T., Dinkova-Kostova, A. T., Kasai, T., Kamei, T., Koshihara, S., & Yamamoto, M. (2021). Molecular basis for the disruption of Keap1–Nrf2 interaction via Hinge & Latch mechanism. *Communications Biology*, *4*(1), 1–11. <https://doi.org/10.1038/s42003-021-02100-6>
- Hosokawa, N., Hara, T., Kaizuka, T., Kishi, C., Takamura, A., Miura, Y., Iemura, S. I., Natsume, T., Takehana, K., Yamada, N., Guan, J. L., Oshiro, N., & Mizushima, N. (2009). Nutrient-dependent mTORC1 association with the ULK1–Atg13–FIP200 complex required for autophagy. *Molecular Biology of the Cell*, *20*(7), 1981–1991. <https://doi.org/10.1091/MBE08-12-1248>
- Hu, C. D., Chinenov, Y., & Kerppola, T. K. (2002). Visualization of Interactions among bZIP and Rel Family Proteins in Living Cells Using Bimolecular Fluorescence Complementation. *Molecular Cell*, *9*(4), 789–798. [https://doi.org/10.1016/S1097-2765\(02\)00496-3](https://doi.org/10.1016/S1097-2765(02)00496-3)
- Huang, J., & Zhong, L. (2012). Thioredoxin reductase. In *Advanced Topics in Science and Technology in China* (Vol. 346, Issue Pt 1, pp. 41–64). Portland Press Ltd. [https://doi.org/10.1007/978-3-642-22236-8\\_3](https://doi.org/10.1007/978-3-642-22236-8_3)
- Huang, R., Xu, Y., Wan, W., Shou, X., Qian, J., You, Z., Liu, B., Chang, C., Zhou, T., Lippincott-Schwartz, J., & Liu, W. (2015). Deacetylation of nuclear LC3 drives autophagy initiation under starvation. *Molecular Cell*, *57*(3), 456–466. <https://doi.org/10.1016/j.molcel.2014.12.013>
- Huang, W., Hickson, L. T. J., Eirin, A., Kirkland, J. L., & Lerman, L. O. (2022). Cellular senescence: the good, the bad and the unknown. *Nature Reviews Nephrology*, *18*(10), 611–627. <https://doi.org/10.1038/s41581-022-00601-z>
- Iannello, A., Thompson, T. W., Ardolino, M., Lowe, S. W., & Raulet, D. H. (2013). p53-dependent chemokine production by senescent tumor cells supports NKG2D-dependent tumor elimination by natural killer cells. *Journal of Experimental Medicine*, *210*(10), 2057–2069. <https://doi.org/10.1084/JEM.20130783>
- Ichimura, Y., Kirisako, T., Takao, T., Satomi, Y., Shimonishi, Y., Ishihara, N., Mizushima, N., Tanida, I., Kominami, E., Ohsumi, M., Noda, T., & Ohsumi, Y. (2000). A ubiquitin-like system mediates protein lipidation. *Nature*, *408*(6811), 488–492. <https://doi.org/10.1038/35044114>

- Ichimura, Y., Kumanomidou, T., Sou, Y. S., Mizushima, T., Ezaki, J., Ueno, T., Kominami, E., Yamane, T., Tanaka, K., & Komatsu, M. (2008). Structural basis for sorting mechanism of p62 in selective autophagy. *Journal of Biological Chemistry*, 283(33), 22847–22857. <https://doi.org/10.1074/jbc.M802182200>
- Ichimura, Y., Takagi, K., Yang, Y., Pankiv, S., Kanegae, Y., Kageyama, S., Suzuki, M., Saito, I., Mizushima, T., Komatsu, M., & Simonsen, A. (2014). Structural determinants in GABARAP required for the selective binding and recruitment of ALFY to LC3B-positive structures. *EMBO Reports*, 15(5), 557–565. [https://doi.org/10.1002/EMBR.201338003/SUPPL\\_FILE/EMBR201338003-SOURCEDATA-FIG4E.PDF](https://doi.org/10.1002/EMBR.201338003/SUPPL_FILE/EMBR201338003-SOURCEDATA-FIG4E.PDF)
- Iizuka, T., Ishii, Y., Itoh, K., Kiwamoto, T., Kimura, T., Matsuno, Y., Morishima, Y., Hegab, A. E., Homma, S., Nomura, A., Sakamoto, T., Shimura, M., Yoshida, A., Yamamoto, M., & Sekizawa, K. (2005). Nrf2-deficient mice are highly susceptible to cigarette smoke-induced emphysema. *Genes to Cells*, 10(12), 1113–1125. <https://doi.org/10.1111/J.1365-2443.2005.00905.X>
- Itakura, E., Kishi-Itakura, C., & Mizushima, N. (2012). The Hairpin-type Tail-Anchored SNARE Syntaxin 17 Targets to Autophagosomes for Fusion with Endosomes/Lysosomes. *Cell*, 151(6), 1256–1269. <https://doi.org/10.1016/J.CELL.2012.11.001>
- Ito, T., Levenstein, M. E., Fyodorov, D. V., Kutach, A. K., Kobayashi, R., & Kadonaga, J. T. (1999). ACF consists of two subunits, Acfl and ISWI, that function cooperatively in the ATP-dependent catalysis of chromatin assembly. *Genes & Development*, 13(12), 1529–1539. <https://doi.org/10.1101/GAD.13.12.1529>
- Itoh, K., Chiba, T., Takahashi, S., Ishii, T., Igarashi, K., Katoh, Y., Oyake, T., Hayashi, N., Satoh, K., Hatayama, I., Yamamoto, M., & Nabeshima, Y. (1997). An Nrf2/small Maf heterodimer mediates the induction of phase II detoxifying enzyme genes through antioxidant response elements. *Biochemical and Biophysical Research Communications*, 236(2), 313–322. <https://doi.org/10.1006/bbrc.1997.6943>
- Itoh, K., Wakabayashi, N., Katoh, Y., Ishii, T., O'Connor, T., & Yamamoto, M. (2003). Keap1 regulates both cytoplasmic-nuclear shuttling and degradation of Nrf2 in response to electrophiles. *Genes to Cells*, 8(4), 379–391. <https://doi.org/10.1046/J.1365-2443.2003.00640.X>
- Jacinto, E., Loewith, R., Schmidt, A., Lin, S., Ruegg, M. A., Hall, A., & Hall, M. N. (2004). Mammalian TOR complex 2 controls the actin cytoskeleton and is rapamycin insensitive. *Nature Cell Biology*, 6(11), 1122–1128. <https://doi.org/10.1038/ncb1183>
- Jacomín, A. C., Petridi, S., Di Monaco, M., Bhujabal, Z., Jain, A., Mulakkal, N. C., Palara, A., Powell, E. L., Chung, B., Zampronio, C., Jones, A., Cameron, A., Johansen, T., & Nezis, I. P. (2020). Regulation of Expression of Autophagy Genes by Atg8a-Interacting Partners Sequoia, YL-1, and Sir2 in Drosophila. *Cell Reports*, 31(8). <https://doi.org/10.1016/j.celrep.2020.107695>
- Jain, A., Lamark, T., Sjøttem, E., Larsen, K. B., Awuh, J. A., Øvervatn, A., McMahon, M., Hayes, J. D., & Johansen, T. (2010). p62/SQSTM1 is a target gene for transcription factor NRF2 and creates a positive feedback loop by inducing antioxidant response element-driven gene



- transcription. *Journal of Biological Chemistry*, 285(29), 22576–22591.  
<https://doi.org/10.1074/jbc.M110.118976>
- Jain, A., Rusten, T. E., Katheder, N., Elvenes, J., Bruun, J. A., Sjøttem, E., Lamark, T., & Johansen, T. (2015a). p62/Sequestosome-1, Autophagy-related Gene 8, and Autophagy in *Drosophila* Are Regulated by Nuclear Factor Erythroid 2-related Factor 2 (NRF2), Independent of Transcription Factor TFEB. *Journal of Biological Chemistry*, 290(24), 14945–14962.  
<https://doi.org/10.1074/JBC.M115.656116>
- Jain, A., Rusten, T. E., Katheder, N., Elvenes, J., Bruun, J. A., Sjøttem, E., Lamark, T., & Johansen, T. (2015b). p62/sequestosome-1, autophagy-related gene 8, and autophagy in *Drosophila* are regulated by nuclear factor erythroid 2-related factor 2(NRF2), independent of transcription factor TFEB. *Journal of Biological Chemistry*, 290(24), 14945–14962.  
<https://doi.org/10.1074/jbc.M115.656116>
- Jayakumar, S., Kunwar, A., Sandur, S. K., Pandey, B. N., & Chaubey, R. C. (2014). Differential response of DU145 and PC3 prostate cancer cells to ionizing radiation: role of reactive oxygen species, GSH and Nrf2 in radiosensitivity. *Biochimica et Biophysica Acta*, 1840(1), 485–494.  
<https://doi.org/10.1016/J.BBAGEN.2013.10.006>
- Jiang, P., Nishimura, T., Sakamaki, Y., Itakura, E., Hatta, T., Natsume, T., & Mizushima, N. (2014). The HOPS complex mediates autophagosome-lysosome fusion through interaction with syntaxin 17. *Molecular Biology of the Cell*, 25(8), 1327–1337. <https://doi.org/10.1091/MBC.E13-08-0447>
- Jiménez-Moreno, N., Kollareddy, M., Stathakos, P., Moss, J. J., Antón, Z., Shoemark, D. K., Sessions, R. B., Witzgall, R., Caldwell, M., & Lane, J. D. (2023). ATG8-dependent LMX1B-autophagy crosstalk shapes human midbrain dopaminergic neuronal resilience. *Journal of Cell Biology*, 222(5). <https://doi.org/10.1083/jcb.201910133>
- Johansen, T., Birgisdottir, B., Huber, J., Kniss, A., Dötsch, V., Kirkin, V., & Rogov, V. V. (2017). Methods for Studying Interactions Between Atg8/LC3/GABARAP and LIR-Containing Proteins. *Methods in Enzymology*, 587, 143–169. <https://doi.org/10.1016/BS.MIE.2016.10.023>
- Johansen, T., & Lamark, T. (2011). Selective autophagy mediated by autophagic adapter proteins. *Autophagy*, 7(3), 279–296. <https://doi.org/10.4161/AUTO.7.3.14487>
- Johansen, T., & Lamark, T. (2019). Selective Autophagy: ATG8 Family Proteins, LIR Motifs and Cargo Receptors. *Journal of Molecular Biology*, 432(xxxx), 80–103.  
<https://doi.org/10.1016/j.jmb.2019.07.016>
- Johansen, T., & Lamark, T. (2020). Selective Autophagy: ATG8 Family Proteins, LIR Motifs and Cargo Receptors. *Journal of Molecular Biology*, 432(1), 80–103.  
<https://doi.org/10.1016/J.JMB.2019.07.016>
- Jones, D. P. (2008). Radical-free biology of oxidative stress. *American Journal of Physiology - Cell Physiology*, 295(4), C849. <https://doi.org/10.1152/AJPCELL.00283.2008>

- Jones, M. H., Hamana, N., Nezu, J. I., & Shimane, M. (2000). A Novel Family of Bromodomain Genes. *Genomics*, *63*(1), 40–45. <https://doi.org/10.1006/GENO.1999.6071>
- Jun, J. II, & Lau, L. F. (2010). The matricellular protein CCN1 induces fibroblast senescence and restricts fibrosis in cutaneous wound healing. *Nature Cell Biology*, *12*(7), 676–685. <https://doi.org/10.1038/ncb2070>
- Jung, C. H., Jun, C. B., Ro, S. H., Kim, Y. M., Otto, N. M., Cao, J., Kundu, M., & Kim, D. H. (2009). ULK-Atg13-FIP200 complexes mediate mTOR signaling to the autophagy machinery. *Molecular Biology of the Cell*, *20*(7), 1992–2003. <https://doi.org/10.1091/MBC.E08-12-1249/ASSET/IMAGES/LARGE/ZMK0070990150007.JPEG>
- Kageyama, S., Gudmundsson, S. R., Sou, Y. S., Ichimura, Y., Tamura, N., Kazuno, S., Ueno, T., Miura, Y., Noshiro, D., Abe, M., Mizushima, T., Miura, N., Okuda, S., Motohashi, H., Lee, J. A., Sakimura, K., Ohe, T., Noda, N. N., Waguri, S., ... Komatsu, M. (2021). p62/SQSTM1-droplet serves as a platform for autophagosome formation and anti-oxidative stress response. *Nature Communications* *2021 12:1*, *12*(1), 1–16. <https://doi.org/10.1038/s41467-020-20185-1>
- Kageyama, S., Saito, T., Obata, M., Koide, R., Ichimura, Y., & Komatsu, M. (2018). Negative Regulation of the Keap1-Nrf2 Pathway by a p62/Sqstm1 Splicing Variant. *Molecular and Cellular Biology*, *38*(7). <https://doi.org/10.1128/MCB.00642-17>
- Kang, T. W., Yevsa, T., Woller, N., Hoenicke, L., Wuestefeld, T., Dauch, D., Hohmeyer, A., Gereke, M., Rudalska, R., Potapova, A., Iken, M., Vucur, M., Weiss, S., Heikenwalder, M., Khan, S., Gil, J., Bruder, D., Manns, M., Schirmacher, P., ... Zender, L. (2011). Senescence surveillance of pre-malignant hepatocytes limits liver cancer development. *Nature*, *479*(7374), 547–551. <https://doi.org/10.1038/nature10599>
- Kataoka, K., Igarashi, K., Itoh, K., Fujiwara, K. T., Noda, M., Yamamoto, M., & Nishizawa, M. (1995). Small Maf Proteins Heterodimerize with Fos and May Act as Competitive Repressors of the NF-E2 Transcription Factor. *Molecular and Cellular Biology*, *15*(4), 2180–2190. <https://doi.org/10.1128/MCB.15.4.2180>
- Katoh, Y., Itoh, K., Yoshida, E., Miyagishi, M., Fukamizu, A., & Yamamoto, M. (2001). Two domains of Nrf2 cooperatively bind CBP, a CREB binding protein, and synergistically activate transcription. *Genes to Cells*, *6*(10), 857–868. <https://doi.org/10.1046/j.1365-2443.2001.00469.x>
- Katsuoka, F., & Yamamoto, M. (2016). Small Maf proteins (MafF, MafG, MafK): History, structure and function. *Gene*, *586*(2), 197–205. <https://doi.org/10.1016/J.GENE.2016.03.058>
- Kaushik, S., & Cuervo, A. M. (2018). The coming of age of chaperone-mediated autophagy. *Nature Reviews Molecular Cell Biology*, *19*(6), 365–381. <https://doi.org/10.1038/s41580-018-0001-6>
- Kawagoe, Y., Kawashima, I., Sato, Y., Okamoto, N., Matsubara, K., & Kawamura, K. (2020). CXCL5-CXCR2 signaling is a senescence-associated secretory phenotype in preimplantation embryos. *Aging Cell*, *19*(10), e13240. <https://doi.org/10.1111/ACEL.13240>

- Kawai, Y., Garduño, L. K., Theodore, M., Yang, J., & Arinze, I. J. (2011). Acetylation-deacetylation of the transcription factor Nrf2 (nuclear factor erythroid 2-related factor 2) regulates its transcriptional activity and nucleocytoplasmic localization. *Journal of Biological Chemistry*, 286(9), 7629–7640. <https://doi.org/10.1074/jbc.M110.208173>
- Keown, J. R., Black, M. M., Ferron, A., Yap, M., Barnett, M. J., Grant Pearce, F., Stoye, J. P., & Goldstone, D. C. (2018). A helical LC3-interacting region mediates the interaction between the retroviral restriction factor Trim5 $\alpha$  and mammalian autophagy-related ATG8 proteins. *Journal of Biological Chemistry*, 293(47), 18378–18386. <https://doi.org/10.1074/JBC.RA118.004202>
- Kerppola, T. K. (2006). Design and implementation of bimolecular fluorescence complementation (BiFC) assays for the visualization of protein interactions in living cells. *Nature Protocols*, 1(3), 1278–1286. <https://doi.org/10.1038/nprot.2006.201>
- Kiefer, F., Arnold, K., Künzli, M., Bordoli, L., & Schwede, T. (2009). The SWISS-MODEL Repository and associated resources. *Nucleic Acids Research*, 37(suppl\_1), D387–D392. <https://doi.org/10.1093/NAR/GKN750>
- Kim, T. H., Hur, E. G., Kang, S. J., Kim, J. A., Thapa, D., Mie Lee, Y., Ku, S. K., Jung, Y., & Kwak, M. K. (2011). NRF2 blockade suppresses colon tumor angiogenesis by inhibiting hypoxia-induced activation of HIF-1 $\alpha$ . *Cancer Research*, 71(6), 2260–2275. <https://doi.org/10.1158/0008-5472.CAN-10-3007>
- Kim, Y. R., Oh, J. E., Kim, M. S., Kang, M. R., Park, S. W., Han, J. Y., Eom, H. S., Yoo, N. J., & Lee, S. H. (2010). Oncogenic NRF2 mutations in squamous cell carcinomas of oesophagus and skin. *Journal of Pathology*, 220(4), 446–451. <https://doi.org/10.1002/PATH.2653>
- Kirkin, V., Lamark, T., Sou, Y. S., Bjørkøy, G., Nunn, J. L., Bruun, J. A., Shvets, E., McEwan, D. G., Clausen, T. H., Wild, P., Bilusic, I., Theurillat, J. P., Øvervatn, A., Ishii, T., Elazar, Z., Komatsu, M., Dikic, I., & Johansen, T. (2009). A Role for NBR1 in Autophagosomal Degradation of Ubiquitinated Substrates. *Molecular Cell*, 33(4), 505–516. <https://doi.org/10.1016/j.molcel.2009.01.020>
- Klaips, C. L., Jayaraj, G. G., & Hartl, F. U. (2018). Pathways of cellular proteostasis in aging and disease. *Journal of Cell Biology*, 217(1), 51–63. <https://doi.org/10.1083/JCB.201709072>
- Klemm, S. L., Shipony, Z., & Greenleaf, W. J. (2019). Chromatin accessibility and the regulatory epigenome. *Nature Reviews Genetics*, 20(4), 207–220. <https://doi.org/10.1038/s41576-018-0089-8>
- Klionsky, D. J., Petroni, G., Amaravadi, R. K., Baehrecke, E. H., Ballabio, A., Boya, P., Pedro, J. M. B.-S., Cadwell, K., Cecconi, F., Choi, A. M. K., Choi, M. E., Chu, C. T., Codogno, P., Colombo, M. I., Cuervo, A. M., Deretic, V., Dikic, I., Elazar, Z., Eskelinen, E.-L., ... Pietrocola, F. (2021). Autophagy in major human diseases. *The EMBO Journal*, 40(19), e108863. <https://doi.org/10.15252/EMBJ.2021108863>
- Kobayashi, A., Ito, E., Toki, T., Kogame, K., Takahashi, S., Igarashi, K., Hayashi, N., & Yamamoto, M. (1999). Molecular Cloning and Functional Characterization of a New Cap'n' Collar Family

- Transcription Factor Nrf3. *Journal of Biological Chemistry*, 274(10), 6443–6452.  
<https://doi.org/10.1074/JBC.274.10.6443>
- Kobayashi, A., Kang, M.-I., Watai, Y., Tong, K. I., Shibata, T., Uchida, K., & Yamamoto, M. (2006). Oxidative and Electrophilic Stresses Activate Nrf2 through Inhibition of Ubiquitination Activity of Keap1. *Molecular and Cellular Biology*, 26(1), 221–229.  
<https://doi.org/10.1128/mcb.26.1.221-229.2006>
- Kobayashi, E. H., Suzuki, T., Funayama, R., Nagashima, T., Hayashi, M., Sekine, H., Tanaka, N., Moriguchi, T., Motohashi, H., Nakayama, K., & Yamamoto, M. (2016). Nrf2 suppresses macrophage inflammatory response by blocking proinflammatory cytokine transcription. *Nature Communications*, 7. <https://doi.org/10.1038/NCOMMS11624>
- Köchli, R., Hu, X. W., Chan, E. Y. W., & Tooze, S. A. (2006). Microtubules facilitate autophagosome formation and fusion of autophagosomes with endosomes. *Traffic*, 7(2), 129–145.  
<https://doi.org/10.1111/J.1600-0854.2005.00368.X>
- Komander, D., & Rape, M. (2012). The Ubiquitin Code. *Annual Review of Biochemistry*, 81, 203–229.  
<https://doi.org/10.1146/ANNUREV-BIOCHEM-060310-170328>
- Komatsu, M., Kurokawa, H., Waguri, S., Taguchi, K., Kobayashi, A., Ichimura, Y., Sou, Y. S., Ueno, I., Sakamoto, A., Tong, K. I., Kim, M., Nishito, Y., Iemura, S. I., Natsume, T., Ueno, T., Kominami, E., Motohashi, H., Tanaka, K., & Yamamoto, M. (2010). The selective autophagy substrate p62 activates the stress responsive transcription factor Nrf2 through inactivation of Keap1. *Nature Cell Biology*, 12(3), 213–223. <https://doi.org/10.1038/NCB2021>
- Koppenol, W. H. (1993). The centennial of the Fenton reaction. *Free Radical Biology and Medicine*, 15(6), 645–651. [https://doi.org/10.1016/0891-5849\(93\)90168-T](https://doi.org/10.1016/0891-5849(93)90168-T)
- Koundouros, N., & Pouligiannis, G. (2018). Phosphoinositide 3-Kinase/Akt Signaling and Redox Metabolism in Cancer. *Frontiers in Oncology*, 8(MAY), 160.  
<https://doi.org/10.3389/FONC.2018.00160>
- Kraft, L. J., Manral, P., Dowler, J., & Kenworthy, A. K. (2016). Nuclear LC3 Associates with Slowly Diffusing Complexes that Survey the Nucleolus. *Traffic*, 17(4), 369–399.  
<https://doi.org/10.1111/tra.12372>
- Kraft, L. J., Nguyen, T. A., Vogel, S. S., & Kenworthy, A. K. (2014). Size, stoichiometry, and organization of soluble LC3-associated complexes. *Autophagy*, 10(5), 861–877.  
<https://doi.org/10.4161/auto.28175>
- Kuma, A., Matsui, M., & Mizushima, N. (2007). LC3, an autophagosome marker, can be incorporated into protein aggregates independent of autophagy: caution in the interpretation of LC3 localization. *Autophagy*, 3(4), 323–328. <https://doi.org/10.4161/AUTO.4012>
- Lacher, S. E., Lee, J. S., Wang, X., Campbell, M. R., Bell, D. A., & Slattery, M. (2015). Beyond antioxidant genes in the ancient Nrf2 regulatory network. *Free Radical Biology and Medicine*, 88(Part B), 452–465. <https://doi.org/10.1016/J.FREERADBIOMED.2015.06.044>

- Lalli, M. A., Jang, J., Park, J. H. C., Wang, Y., Guzman, E., Zhou, H., Audouard, M., Bridges, D., Tovar, K. R., Papuc, S. M., Tutulan-Cunita, A. C., Huang, Y., Budisteanu, M., Arghir, A., & Kosik, K. S. (2016). Haploinsufficiency of BAZ1B contributes to Williams syndrome through transcriptional dysregulation of neurodevelopmental pathways. *Human Molecular Genetics*, *25*(7), 1294–1306. <https://doi.org/10.1093/HMG/DDW010>
- Lamark, T., & Johansen, T. (2021). Mechanisms of Selective Autophagy. *Annual Review of Cell and Developmental Biology*, *37*, 143–169. <https://doi.org/10.1146/ANNUREV-CELLBIO-120219-035530>
- Lamark, T., Perander, M., Outzen, H., Kristiansen, K., Øvervatn, A., Michaelsen, E., Bjørkoy, G., & Johansen, T. (2003). Interaction Codes within the Family of Mammalian Phox and Bem1p Domain-containing Proteins. *Journal of Biological Chemistry*, *278*(36), 34568–34581. <https://doi.org/10.1074/JBC.M303221200>
- Lambeth, J. D. (2004). NOX enzymes and the biology of reactive oxygen. *Nature Reviews Immunology*, *4*(3), 181–189. <https://doi.org/10.1038/NRI1312>
- Landschulz, W. H., Johnson, P. F., & McKnight, S. L. (1988). The Leucine Zipper: A Hypothetical Structure Common to a New Class of DNA Binding Proteins. *Science*, *240*(4860), 1759–1764. <https://doi.org/10.1126/SCIENCE.3289117>
- Lau, A., Zheng, Y., Tao, S., Wang, H., Whitman, S. A., White, E., & Zhang, D. D. (2013). Arsenic Inhibits Autophagic Flux, Activating the Nrf2-Keap1 Pathway in a p62-Dependent Manner. *Molecular and Cellular Biology*, *33*(12), 2436–2446. <https://doi.org/10.1128/MCB.01748-12>
- Le Guerroué, F., Eck, F., Jung, J., Starzetz, T., Mittelbronn, M., Kaulich, M., & Behrends, C. (2017). Autophagosomal Content Profiling Reveals an LC3C-Dependent Piecemeal Mitophagy Pathway. *Molecular Cell*, *68*(4), 786–796.e6. <https://doi.org/10.1016/J.MOLCEL.2017.10.029>
- Lee, I. T., Luo, S. F., Lee, C. W., Wang, S. W., Lin, C. C., Chang, C. C., Chen, Y. L., Chau, L. Y., & Yang, C. M. (2009). Overexpression of HO-1 Protects against TNF- $\alpha$ -Mediated Airway Inflammation by Down-Regulation of TNFR1-Dependent Oxidative Stress. *The American Journal of Pathology*, *175*(2), 519–532. <https://doi.org/10.2353/AJPATH.2009.090016>
- Lee, J. H., Kim, E. W., Croteau, D. L., & Bohr, V. A. (2020). Heterochromatin: an epigenetic point of view in aging. *Experimental & Molecular Medicine*, *52*(9), 1466–1474. <https://doi.org/10.1038/s12276-020-00497-4>
- Li, M., Hou, Y., Wang, J., Chen, X., Shao, Z. M., & Yin, X. M. (2011). Kinetics comparisons of mammalian Atg4 homologues indicate selective preferences toward diverse Atg8 substrates. *Journal of Biological Chemistry*, *286*(9), 7327–7338. <https://doi.org/10.1074/jbc.M110.199059>
- Li, R., Rezk, A., Ghadiri, M., Luessi, F., Zipp, F., Li, H., Giacomini, P. S., Antel, J., & Bar-Or, A. (2017). Dimethyl Fumarate Treatment Mediates an Anti-Inflammatory Shift in B Cell Subsets of Patients with Multiple Sclerosis. *The Journal of Immunology*, *198*(2), 691–698. <https://doi.org/10.4049/JIMMUNOL.1601649>

- Li, W., Yu, S., Liu, T., Kim, J. H., Blank, V., Li, H., & Kong, A. N. T. (2008). Heterodimerization with small Maf proteins enhances nuclear retention of Nrf2 via masking the NESzip motif. *Biochimica et Biophysica Acta (BBA) - Molecular Cell Research*, 1783(10), 1847–1856. <https://doi.org/10.1016/J.BBAMCR.2008.05.024>
- Li, Y., Gong, H., Wang, P., Zhu, Y., Peng, H., Cui, Y., Li, H., Liu, J., & Wang, Z. (2021). The emerging role of ISWI chromatin remodeling complexes in cancer. *Journal of Experimental & Clinical Cancer Research*, 40(1), 1–27. <https://doi.org/10.1186/S13046-021-02151-X>
- Liochev, S. I., & Fridovich, I. (1993). Modulation of the Fumarases of Escherichia coli in Response to Oxidative Stress. *Archives of Biochemistry and Biophysics*, 301(2), 379–384. <https://doi.org/10.1006/ABBI.1993.1159>
- Liu, D., & Hornsby, P. J. (2007). Senescent Human Fibroblasts Increase the Early Growth of Xenograft Tumors via Matrix Metalloproteinase Secretion. *Cancer Research*, 67(7), 3117–3126. <https://doi.org/10.1158/0008-5472.CAN-06-3452>
- Liu, Y., Mi, Y., Mueller, T., Kreibich, S., Williams, E. G., Van Drogen, A., Borel, C., Frank, M., Germain, P. L., Bludau, I., Mehnert, M., Seifert, M., Emmenlauer, M., Sorg, I., Bezrukov, F., Bena, F. S., Zhou, H., Dehio, C., Testa, G., ... Aebersold, R. (2019). Multi-omic measurements of heterogeneity in HeLa cells across laboratories. *Nature Biotechnology*, 37(3), 314–322. <https://doi.org/10.1038/s41587-019-0037-y>
- Loewith, R., Jacinto, E., Wullschleger, S., Lorberg, A., Crespo, J. L., Bonenfant, D., Oppliger, W., Jenoe, P., & Hall, M. N. (2002). Two TOR complexes, only one of which is rapamycin sensitive, have distinct roles in cell growth control. *Molecular Cell*, 10(3), 457–468. [https://doi.org/10.1016/S1097-2765\(02\)00636-6](https://doi.org/10.1016/S1097-2765(02)00636-6)
- Lőrincz, P., & Juhász, G. (2020). Autophagosome-Lysosome Fusion. *Journal of Molecular Biology*, 432(8), 2462–2482. <https://doi.org/10.1016/J.JMB.2019.10.028>
- Lu, X., Meng, X., Morris, C. A., & Keating, M. T. (1998). A Novel Human Gene, WSTF, Is Deleted in Williams Syndrome. *Genomics*, 54(2), 241–249. <https://doi.org/10.1006/GENO.1998.5578>
- Lucey, B. P., Nelson-Rees, W. A., & Hutchins, G. M. (2009). Henrietta Lacks, HeLa cells, and cell culture contamination. *Archives of Pathology and Laboratory Medicine*, 133(9), 1463–1467. <https://doi.org/10.5858/133.9.1463>
- Luger, K., Mäder, A. W., Richmond, R. K., Sargent, D. F., & Richmond, T. J. (1997). Crystal structure of the nucleosome core particle at 2.8 Å resolution. *Nature*, 389(6648), 251–260. <https://doi.org/10.1038/38444>
- Lynch, D. R., Farmer, J., Hauser, L., Blair, I. A., Wang, Q. Q., Mesaros, C., Snyder, N., Boesch, S., Chin, M., Delatycki, M. B., Giunti, P., Goldsberry, A., Hoyle, C., McBride, M. G., Nachbauer, W., O’Grady, M., Perlman, S., Subramony, S. H., Wilmot, G. R., ... Meyer, C. (2019). Safety, pharmacodynamics, and potential benefit of omaveloxolone in Friedreich ataxia. *Annals of Clinical and Translational Neurology*, 6(1), 15–26. <https://doi.org/10.1002/ACN3.660>

- Ma, J., Cai, H., Wu, T., Sobhian, B., Huo, Y., Alcivar, A., Mehta, M., Cheung, K. L., Ganesan, S., Kong, A.-N. T., Zhang, D. D., & Xia, B. (2012). PALB2 interacts with KEAP1 to promote NRF2 nuclear accumulation and function. *Molecular and Cellular Biology*, *32*(8), 1506–1517. <https://doi.org/10.1128/MCB.06271-11>
- Maeda, S., Otomo, C., & Otomo, T. (2019). The autophagic membrane tether ATG2A transfers lipids between membranes. *ELife*, *8*. <https://doi.org/10.7554/ELIFE.45777>
- Maeda, S., Yamamoto, H., Kinch, L. N., Garza, C. M., Takahashi, S., Otomo, C., Grishin, N. V., Forli, S., Mizushima, N., & Otomo, T. (2020). Structure, lipid scrambling activity and role in autophagosome formation of ATG9A. *Nature Structural & Molecular Biology*, *27*(12), 1194–1201. <https://doi.org/10.1038/s41594-020-00520-2>
- Magaña-Acosta, M., & Valadez-Graham, V. (2020). Chromatin Remodelers in the 3D Nuclear Compartment. *Frontiers in Genetics*, *11*, 600615. <https://doi.org/10.3389/FGENE.2020.600615/BIBTEX>
- Mahmood, T., & Yang, P. C. (2012). Western blot: technique, theory, and trouble shooting. *North American Journal of Medical Sciences*, *4*(9), 429–434. <https://doi.org/10.4103/1947-2714.100998>
- Malhotra, D., Portales-Casamar, E., Singh, A., Srivastava, S., Arenillas, D., Happel, C., Shyr, C., Wakabayashi, N., Kensler, T. W., Wasserman, W. W., & Biswal, S. (2010). Global mapping of binding sites for Nrf2 identifies novel targets in cell survival response through ChIP-Seq profiling and network analysis. *Nucleic Acids Research*, *38*(17), 5718–5734. <https://doi.org/10.1093/NAR/GKQ212>
- Mancias, J. D., Wang, X., Gygi, S. P., Harper, J. W., & Kimmelman, A. C. (2014). Quantitative proteomics identifies NCOA4 as the cargo receptor mediating ferritinophagy. *Nature*, *509*(7498), 105–109. <https://doi.org/10.1038/nature13148>
- Mandell, M. A., Jain, A., Arko-Mensah, J., Chauhan, S., Kimura, T., Dinkins, C., Silvestri, G., Münch, J., Kirchhoff, F., Simonsen, A., Wei, Y., Levine, B., Johansen, T., & Deretic, V. (2014). TRIM Proteins Regulate Autophagy and Can Target Autophagic Substrates by Direct Recognition. *Developmental Cell*, *30*(4), 394–409. <https://doi.org/10.1016/J.DEVCEL.2014.06.013>
- Mandell, M. A., Kimura, T., Jain, A., Johansen, T., & Deretic, V. (2014). TRIM proteins regulate autophagy: TRIM5 is a selective autophagy receptor mediating HIV-1 restriction. *Autophagy*, *10*(12), 2387–2388. <https://doi.org/10.4161/15548627.2014.984278>
- Mariño, G., Uría, J. A., Puente, X. S., Quesada, V., Bordallo, J., & López-Otín, C. (2003). Human autophagins, a family of cysteine proteinases potentially implicated in cell degradation by autophagy. *Journal of Biological Chemistry*, *278*(6), 3671–3678. <https://doi.org/10.1074/jbc.M208247200>

- Martinez-Lopez, N., Athonvarangkul, D., Mishall, P., Sahu, S., & Singh, R. (2013). Autophagy proteins regulate ERK phosphorylation. *Nature Communications*, 4(1), 1–14. <https://doi.org/10.1038/ncomms3799>
- Matoba, K., Kotani, T., Tsutsumi, A., Tsuji, T., Mori, T., Noshiro, D., Sugita, Y., Nomura, N., Iwata, S., Ohsumi, Y., Fujimoto, T., Nakatogawa, H., Kikkawa, M., & Noda, N. N. (2020). Atg9 is a lipid scramblase that mediates autophagosomal membrane expansion. *Nature Structural & Molecular Biology*, 27(12), 1185–1193. <https://doi.org/10.1038/s41594-020-00518-w>
- McCord, J. M., & Fridovich, I. (1969). Superoxide Dismutase: An enzymic function for erythrocyte (hemocuprein). *Journal of Biological Chemistry*, 244(22), 6049–6055. [https://doi.org/10.1016/S0021-9258\(18\)63504-5](https://doi.org/10.1016/S0021-9258(18)63504-5)
- McMahon, M., Itoh, K., Yamamoto, M., & Hayes, J. D. (2003). Keap1-dependent Proteasomal Degradation of Transcription Factor Nrf2 Contributes to the Negative Regulation of Antioxidant Response Element-driven Gene Expression. *Journal of Biological Chemistry*, 278(24), 21592–21600. <https://doi.org/10.1074/JBC.M300931200>
- Meng, D., Wang, X., Chang, Q., Hitron, A., Zhang, Z., Xu, M., Chen, G., Luo, J., Jiang, B., Fang, J., & Shi, X. (2010). Arsenic promotes angiogenesis in vitro via a heme oxygenase-1-dependent mechanism. *Toxicology and Applied Pharmacology*, 244(3), 291–299. <https://doi.org/10.1016/J.TAAP.2010.01.004>
- Meyer, M., Schreck, R., & Baeuerle, P. A. (1993). H<sub>2</sub>O<sub>2</sub> and antioxidants have opposite effects on activation of NF-kappa B and AP-1 in intact cells: AP-1 as secondary antioxidant-responsive factor. *The EMBO Journal*, 12(5), 2005–2015. <https://doi.org/10.1002/J.1460-2075.1993.TB05850.X>
- Micco, R., Krizhanovsky, V., Baker, D., & d’Adda di Fagagna, F. (2020). Cellular senescence in ageing: from mechanisms to therapeutic opportunities. *Nature Reviews Molecular Cell Biology*, 22(2), 75–95. <https://doi.org/10.1038/s41580-020-00314-w>
- Miller, K. N., Victorelli, S. G., Salmonowicz, H., Dasgupta, N., Liu, T., Passos, J. F., & Adams, P. D. (2021). Cytoplasmic DNA: sources, sensing, and role in aging and disease. *Cell*, 184(22), 5506–5526. <https://doi.org/10.1016/J.CELL.2021.09.034>
- Mirdita, M., Schütze, K., Moriwaki, Y., Heo, L., Ovchinnikov, S., & Steinegger, M. (2022). *ColabFold: making protein folding accessible to all*. 19(6), 679–682. <https://doi.org/10.1038/s41592-022-01488-1>
- Mitsuishi, Y., Taguchi, K., Kawatani, Y., Shibata, T., Nukiwa, T., Aburatani, H., Yamamoto, M., & Motohashi, H. (2012a). Nrf2 redirects glucose and glutamine into anabolic pathways in metabolic reprogramming. *Cancer Cell*, 22(1), 66–79. <https://doi.org/10.1016/J.CCR.2012.05.016>
- Mitsuishi, Y., Taguchi, K., Kawatani, Y., Shibata, T., Nukiwa, T., Aburatani, H., Yamamoto, M., & Motohashi, H. (2012b). Nrf2 Redirects Glucose and Glutamine into Anabolic Pathways in



- Metabolic Reprogramming. *Cancer Cell*, 22(1), 66–79.  
<https://doi.org/10.1016/J.CCR.2012.05.016>
- Mizushima, N., & Levine, B. (2020). Autophagy in Human Diseases. *New England Journal of Medicine*, 383(16), 1564–1576.  
[https://doi.org/10.1056/NEJMRA2022774/SUPPL\\_FILE/NEJMRA2022774\\_DISCLOSURES.PDF](https://doi.org/10.1056/NEJMRA2022774/SUPPL_FILE/NEJMRA2022774_DISCLOSURES.PDF)
- Mizushima, N., Noda, T., Yoshimori, T., Tanaka, Y., Ishii, T., George, M. D., Klionsky, D. J., Ohsumi, M., & Ohsumi, Y. (1998). A protein conjugation system essential for autophagy. *Nature*, 395(6700), 395–398. <https://doi.org/10.1038/26506>
- Mizushima, N., Yoshimori, T., & Ohsumi, Y. (2011). The Role of Atg Proteins in Autophagosome Formation. *Annual Review of Cell and Developmental Biology*, 27, 107–132.  
<https://doi.org/10.1146/ANNUREV-CELLBIO-092910-154005>
- Moeller, B. J., Cao, Y., Li, C. Y., & Dewhirst, M. W. (2004). Radiation activates HIF-1 to regulate vascular radiosensitivity in tumors: Role of reoxygenation, free radicals, and stress granules. *Cancer Cell*, 5(5), 429–441. [https://doi.org/10.1016/S1535-6108\(04\)00115-1](https://doi.org/10.1016/S1535-6108(04)00115-1)
- Moi, P., Chan, K., Asunis, I., Cao, A., & Kan, Y. W. (1994). Isolation of NF-E2-related factor 2 (Nrf2), a NF-E2-like basic leucine zipper transcriptional activator that binds to the tandem NF-E2/AP1 repeat of the beta-globin locus control region. *Proceedings of the National Academy of Sciences of the United States of America*, 91(21), 9926–9930.  
<https://doi.org/10.1073/PNAS.91.21.9926>
- Mosteiro, L., Pantoja, C., de Martino, A., & Serrano, M. (2018). Senescence promotes in vivo reprogramming through p16INK4a and IL-6. *Aging Cell*, 17(2), e12711.  
<https://doi.org/10.1111/ACEL.12711>
- Motohashi, H., Katsuoka, F., Shavit, J. A., Engel, J. D., & Yamamoto, M. (2000). Positive or negative MARE-dependent transcriptional regulation is determined by the abundance of small Maf proteins. *Cell*, 103(6), 865–876. [https://doi.org/10.1016/S0092-8674\(00\)00190-2](https://doi.org/10.1016/S0092-8674(00)00190-2)
- Muhlinen, N., Akutsu, M., Ravenhill, B. J., Foeglein, Á., Bloor, S., Rutherford, T. J., Freund, S. M. V., Komander, D., & Randow, F. (2012). LC3C, bound selectively by a noncanonical LIR motif in NDP52, is required for antibacterial autophagy. *Molecular Cell*, 48(3), 329–342.  
<https://doi.org/10.1016/J.MOLCEL.2012.08.024>
- Murakami, S., Shimizu, R., Romeo, P. H., Yamamoto, M., & Motohashi, H. (2014). Keap1-Nrf2 system regulates cell fate determination of hematopoietic stem cells. *Genes to Cells*, 19(3), 239–253. <https://doi.org/10.1111/GTC.12126>
- Murphy, M. P., Bayir, H., Belousov, V., Chang, C. J., Davies, K. J. A., Davies, M. J., Dick, T. P., Finkel, T., Forman, H. J., Janssen-Heininger, Y., Gems, D., Kagan, V. E., Kalyanaraman, B., Larsson, N. G., Milne, G. L., Nyström, T., Poulsen, H. E., Radi, R., Van Remmen, H., ... Halliwell, B. (2022). Guidelines for measuring reactive oxygen species and oxidative damage in

- cells and in vivo. *Nature Metabolism*, 4(6), 651–662. <https://doi.org/10.1038/s42255-022-00591-z>
- Nakatogawa, H. (2020). Mechanisms governing autophagosome biogenesis. *Nature Reviews Molecular Cell Biology*, 21(8), 439–458. <https://doi.org/10.1038/s41580-020-0241-0>
- Ney, P. A., Andrews, N. C., Jane, S. M., Safer, B., Purucker, M. E., Weremowicz, S., Morton, C. C., Goff, S. C., Orkin, S. H., & Nienhuis, A. W. (1993). Purification of the human NF-E2 complex: cDNA cloning of the hematopoietic cell-specific subunit and evidence for an associated partner. *Molecular and Cellular Biology*, 13(9), 5604–5612. <https://doi.org/10.1128/MCB.13.9.5604-5612.1993>
- Nguyen, T., Sherratt, P. J., Huang, H. C., Yang, C. S., & Pickett, C. B. (2003). Increased Protein Stability as a Mechanism That Enhances Nrf2-mediated Transcriptional Activation of the Antioxidant Response Element: Degradation of NRF2 by the 26S proteasome. *Journal of Biological Chemistry*, 278(7), 4536–4541. <https://doi.org/10.1074/JBC.M207293200>
- Nioi, P., McMahon, M., Itoh, K., Yamamoto, M., & Hayes, J. D. (2003). Identification of a novel Nrf2-regulated antioxidant response element (ARE) in the mouse NAD(P)H:quinone oxidoreductase 1 gene: reassessment of the ARE consensus sequence. *Biochemical Journal*, 374(Pt 2), 337. <https://doi.org/10.1042/BJ20030754>
- Nishizawa, M., Kataoka, K., Goto, N., Fujiwara, K. T., & Kawai, S. (1989). v-maf, a viral oncogene that encodes a “leucine zipper” motif. *Proceedings of the National Academy of Sciences of the United States of America*, 86(20), 7711–7715. <https://doi.org/10.1073/PNAS.86.20.7711>
- Niture, S. K., & Jaiswal, A. K. (2012). Nrf2 protein up-regulates antiapoptotic protein Bcl-2 and prevents cellular apoptosis. *Journal of Biological Chemistry*, 287(13), 9873–9886. <https://doi.org/10.1074/JBC.M111.312694>
- Noda, N. N., Kumeta, H., Nakatogawa, H., Satoo, K., Adachi, W., Ishii, J., Fujioka, Y., Ohsumi, Y., & Inagaki, F. (2008). Structural basis of target recognition by Atg8/LC3 during selective autophagy. *Genes to Cells*, 13(12), 1211–1218. <https://doi.org/10.1111/J.1365-2443.2008.01238.X>
- Noda, N. N., Ohsumi, Y., & Inagaki, F. (2010). Atg8-family interacting motif crucial for selective autophagy. *FEBS Letters*, 584(7), 1379–1385. <https://doi.org/10.1016/J.FEBSLET.2010.01.018>
- Nordberg, J., & Arnér, E. S. J. (2001). Reactive oxygen species, antioxidants, and the mammalian thioredoxin system. *Free Radical Biology and Medicine*, 31(11), 1287–1312. [https://doi.org/10.1016/S0891-5849\(01\)00724-9](https://doi.org/10.1016/S0891-5849(01)00724-9)
- Nthiga, T. M., Shrestha, B. K., Sjøttem, E., Bruun, J.-A., Larsen, K. B., Bhujabal, Z., Lamark, T., & Johansen, T. (2020). CALCOCO1 acts with VAMP-associated proteins to mediate ER-phagy. *The EMBO Journal*, 39(15), e103649. <https://doi.org/10.15252/EMBJ.2019103649>
- Ohsumi, Y. (2013). Historical landmarks of autophagy research. *Cell Research 2014 24:1*, 24(1), 9–23. <https://doi.org/10.1038/cr.2013.169>

- Olsvik, H. L., Lamark, T., Takagi, K., Larsen, K. B., Evjen, G., Øvervatn, A., Mizushima, T., & Johansen, X. T. (2015). FYCO1 contains a C-terminally extended, LC3A/B-preferring LC3-interacting region (LIR) motif required for efficient maturation of autophagosomes during basal autophagy. *Journal of Biological Chemistry*, *290*(49), 29361–29374. <https://doi.org/10.1074/jbc.M115.686915>
- Ooi, A., Dykema, K., Ansari, A., Petillo, D., Snider, J., Kahnoski, R., Anema, J., Craig, D., Carpten, J., Teh, B. T., & Furge, K. A. (2013). CUL3 and NRF2 mutations confer an NRF2 activation phenotype in a sporadic form of papillary renal cell carcinoma. *Cancer Research*, *73*(7), 2044–2051. <https://doi.org/10.1158/0008-5472.CAN-12-3227>
- Osawa, T., Kotani, T., Kawaoka, T., Hirata, E., Suzuki, K., Nakatogawa, H., Ohsumi, Y., & Noda, N. (2019). Atg2 mediates direct lipid transfer between membranes for autophagosome formation. *Nature Structural & Molecular Biology*, *26*(4), 281–288. <https://doi.org/10.1038/s41594-019-0203-4>
- Otterbein, L. E., Soares, M. P., Yamashita, K., & Bach, F. H. (2003). Heme oxygenase-1: unleashing the protective properties of heme. *Trends in Immunology*, *24*(8), 449–455. [https://doi.org/10.1016/S1471-4906\(03\)00181-9](https://doi.org/10.1016/S1471-4906(03)00181-9)
- Özcan, S., Alessio, N., Acar, M. B., Mert, E., Omerli, F., Peluso, G., & Galderisi, U. (2016). Unbiased analysis of senescence associated secretory phenotype (SASP) to identify common components following different genotoxic stresses. *Aging*, *8*(7), 1316–1329. <https://doi.org/10.18632/AGING.100971>
- Padayatty, S. J., & Levine, M. (2016). Vitamin C: the known and the unknown and Goldilocks. *Oral Diseases*, *22*(6), 463–493. <https://doi.org/10.1111/ODI.12446>
- Pankiv, S., Clausen, T. H., Lamark, T., Brech, A., Bruun, J. A., Outzen, H., Øvervatn, A., Bjørkøy, G., & Johansen, T. (2007). p62/SQSTM1 Binds Directly to Atg8/LC3 to Facilitate Degradation of Ubiquitinated Protein Aggregates by Autophagy. *Journal of Biological Chemistry*, *282*(33), 24131–24145. <https://doi.org/10.1074/JBC.M702824200>
- Pattison, D. I., Davies, M. J., & Hawkins, C. L. (2012). Reactions and reactivity of myeloperoxidase-derived oxidants: differential biological effects of hypochlorous and hypothiocyanous acids. *Free Radical Research*, *46*(8), 975–995. <https://doi.org/10.3109/10715762.2012.667566>
- Pedroso, N., Matias, A. C., Cyrne, L., Antunes, F., Borges, C., Malhó, R., de Almeida, R. F. M., Herrero, E., & Marinho, H. S. (2009). Modulation of plasma membrane lipid profile and microdomains by H<sub>2</sub>O<sub>2</sub> in *Saccharomyces cerevisiae*. *Free Radical Biology and Medicine*, *46*(2), 289–298. <https://doi.org/10.1016/J.FREERADBIOMED.2008.10.039>
- Percipalle, P., Fomproix, N., Cavellán, E., Voit, R., Reimer, G., Krüger, T., Thyberg, J., Scheer, U., Grummt, I., & Östlund Farrants, A. K. (2006a). The chromatin remodelling complex WSTF-SNF2h interacts with nuclear myosin 1 and has a role in RNA polymerase I transcription. *EMBO Reports*, *7*(5), 525–530. [https://doi.org/10.1038/SJ.EMBOR.7400657/SUPPL\\_FILE/EMBR7400657-SUP-0001.PDF](https://doi.org/10.1038/SJ.EMBOR.7400657/SUPPL_FILE/EMBR7400657-SUP-0001.PDF)

- Percipalle, P., Fomproix, N., Cavellán, E., Voit, R., Reimer, G., Krüger, T., Thyberg, J., Scheer, U., Grummt, I., & Östlund Farrants, A. K. (2006b). The chromatin remodelling complex WSTF-SNF2h interacts with nuclear myosin I and has a role in RNA polymerase I transcription. *EMBO Reports*, 7(5), 525–530.  
[https://doi.org/10.1038/SJ.EMBOR.7400657/SUPPL\\_FILE/EMBR7400657-SUP-0001.PDF](https://doi.org/10.1038/SJ.EMBOR.7400657/SUPPL_FILE/EMBR7400657-SUP-0001.PDF)
- Pestic-Dragovich, L., Stojiljkovic, L., Philimonenko, A. A., Nowak, G., Ke, Y., Settlage, R. E., Shabanowitz, J., Hunt, D. F., Hozak, P., & De Lanerolle, P. (2000). A myosin I isoform in the nucleus. *Science*, 290(5490), 337–340.  
[https://doi.org/10.1126/SCIENCE.290.5490.337/SUPPL\\_FILE/1054468S1\\_THUMB.GIF](https://doi.org/10.1126/SCIENCE.290.5490.337/SUPPL_FILE/1054468S1_THUMB.GIF)
- Pettersen, E. F., Goddard, T. D., Huang, C. C., Meng, E. C., Couch, G. S., Croll, T. I., Morris, J. H., & Ferrin, T. E. (2021). UCSF ChimeraX: Structure visualization for researchers, educators, and developers. *Protein Science*, 30(1), 70–82. <https://doi.org/10.1002/pro.3943>
- Pillai-Kastoori, L., Schutz-Geschwender, A. R., & Harford, J. A. (2020). A systematic approach to quantitative Western blot analysis. *Analytical Biochemistry*, 593, 113608.  
<https://doi.org/10.1016/J.AB.2020.113608>
- Pitoniak, A., & Bohmann, D. (2015). Mechanisms and Functions of Nrf2 Signaling in Drosophila. *Free Radical Biology and Medicine*, 88(Pt B), 302.  
<https://doi.org/10.1016/J.FREERADBIOMED.2015.06.020>
- Pizzino, G., Irrera, N., Cucinotta, M., Pallio, G., Mannino, F., Arcoraci, V., Squadrito, F., Altavilla, D., & Bitto, A. (2017). Oxidative Stress: Harms and Benefits for Human Health. *Oxidative Medicine and Cellular Longevity*, 2017. <https://doi.org/10.1155/2017/8416763>
- Pohl, C., & Dikic, I. (2019). Cellular quality control by the ubiquitin-proteasome system and autophagy. *Science*, 366(6467), 818–822.  
[https://doi.org/10.1126/SCIENCE.AAX3769/ASSET/E8FDA115-2BC6-4041-9C89-85627086ED0C/ASSETS/GRAPHIC/366\\_818\\_F3.JPEG](https://doi.org/10.1126/SCIENCE.AAX3769/ASSET/E8FDA115-2BC6-4041-9C89-85627086ED0C/ASSETS/GRAPHIC/366_818_F3.JPEG)
- Polson, H. E. J., De Lartigue, J., Rigden, D. J., Reedijk, M., Urbé, S., Clague, M. J., & Tooze, S. A. (2010). Mammalian Atg18 (WIPI2) localizes to omegasome-anchored phagophores and positively regulates LC3 lipidation. *Autophagy*, 6(4), 506–522.  
<https://doi.org/10.4161/AUTO.6.4.11863>
- Poot, R. A., Bozhenok, L., van den Berg, D. L. C., Steffensen, S., Ferreira, F., Grimaldi, M., Gilbert, N., Ferreira, J., & Varga-Weisz, P. D. (2004). The Williams syndrome transcription factor interacts with PCNA to target chromatin remodelling by ISWI to replication foci. *Nature Cell Biology*, 6(12), 1236–1244. <https://doi.org/10.1038/ncb1196>
- Proikas-Cezanne, T., Takacs, Z., Dönnies, P., & Kohlbacher, O. (2015). WIPI proteins: Essential PtdIns3P effectors at the nascent autophagosome. *Journal of Cell Science*, 128(2), 207–217.  
<https://doi.org/10.1242/JCS.146258/259897/AM/WIPI-PROTEINS-ESSENTIAL-PTDINS3P-EFFECTORS-AT-THE>

- Quong, M. W., Massari, M. E., Zwart, R., & Murre, C. (1993). A New Transcriptional-Activation Motif Restricted to a Class of Helix-Loop-Helix Proteins Is Functionally Conserved in Both Yeast and Mammalian Cells. *Molecular and Cellular Biology*, *13*(2), 792–800. <https://doi.org/10.1128/MCB.13.2.792-800.1993>
- Raghunath, A., Sundarraj, K., Nagarajan, R., Arfuso, F., Bian, J., Kumar, A. P., Sethi, G., & Perumal, E. (2018). Antioxidant response elements: Discovery, classes, regulation and potential applications. *Redox Biology*, *17*, 297–314. <https://doi.org/10.1016/J.REDOX.2018.05.002>
- Rana, T., Jiang, C., Liu, G., Miyata, T., Antony, V., Thannickal, V. J., & Liu, R. M. (2020). PAI-1 regulation of TGF- $\beta$ 1-induced alveolar Type II cell senescence, SASP secretion, and SASP-mediated activation of alveolar macrophages. *American Journal of Respiratory Cell and Molecular Biology*, *62*(3), 319–330. [https://doi.org/10.1165/RCMB.2019-0071OC/SUPPL\\_FILE/DISCLOSURES.PDF](https://doi.org/10.1165/RCMB.2019-0071OC/SUPPL_FILE/DISCLOSURES.PDF)
- Rasmussen, M. S., Mouilleron, S., Kumar Shrestha, B., Wirth, M., Lee, R., Bowitz Larsen, K., Abudu Princely, Y., O'Reilly, N., Sjøttem, E., Tooze, S. A., Lamark, T., & Johansen, T. (2017). ATG4B contains a C-terminal LIR motif important for binding and efficient cleavage of mammalian orthologs of yeast Atg8. *Autophagy*, *13*(5), 834–853. <https://doi.org/10.1080/15548627.2017.1287651>
- Rawet Slobodkin, M., & Elazar, Z. (2013). The Atg8 family: Multifunctional ubiquitin-like key regulators of autophagy. *Essays in Biochemistry*, *55*(1), 51–64. <https://doi.org/10.1042/BSE0550051>
- Reddy, N. M., Kleeberger, S. R., Bream, J. H., Fallon, P. G., Kensler, T. W., Yamamoto, M., & Reddy, S. P. (2008). Genetic disruption of the Nrf2 compromises cell-cycle progression by impairing GSH-induced redox signaling. *Oncogene*, *27*(44), 5821–5832. <https://doi.org/10.1038/onc.2008.188>
- Robledinos-Antón, N., Fernández-Ginés, R., Manda, G., & Cuadrado, A. (2019a). Activators and Inhibitors of NRF2: A Review of Their Potential for Clinical Development. *Oxidative Medicine and Cellular Longevity*, *2019*. <https://doi.org/10.1155/2019/9372182>
- Rogov, V. V., Nezis, I. P., Tsapras, P., Zhang, H., Dagdas, Y., Noda, N. N., Nakatogawa, H., Wirth, M., Mouilleron, S., McEwan, D. G., Behrends, C., Deretic, V., Elazar, Z., Tooze, S. A., Dikic, I., Lamark, T., & Johansen, T. (2023). Atg8 family proteins, LIR/AIM motifs and other interaction modes. *Autophagy Reports*, *2*(1). <https://doi.org/10.1080/27694127.2023.2188523>
- Rogov, V. V., Stolz, A., Ravichandran, A. C., Rios-Szwed, D. O., Suzuki, H., Kniss, A., Löhr, F., Wakatsuki, S., Dötsch, V., Dikic, I., Dobson, R. C., & McEwan, D. G. (2017). Structural and functional analysis of the GABARAP interaction motif (GIM). *EMBO Reports*, *18*(8), 1382–1396. [https://doi.org/10.15252/EMBR.201643587/SUPPL\\_FILE/EMBR201643587-SUP-0005-SDATAFIG5.PDF](https://doi.org/10.15252/EMBR.201643587/SUPPL_FILE/EMBR201643587-SUP-0005-SDATAFIG5.PDF)

- Rössler, O. G., & Thiel, G. (2017). Specificity of Stress-Responsive Transcription Factors Nrf2, ATF4, and AP-1. *Journal of Cellular Biochemistry*, *118*(1), 127–140. <https://doi.org/10.1002/JCB.25619>
- Roychoudhuri, R., Clever, D., Li, P., Wakabayashi, Y., Quinn, K. M., Klebanoff, C. A., Ji, Y., Sukumar, M., Eil, R. L., Yu, Z., Spolski, R., Palmer, D. C., Pan, J. H., Patel, S. J., Macallan, D. C., Fabozzi, G., Shih, H. Y., Kanno, Y., Muto, A., ... Restifo, N. P. (2016). BACH2 regulates CD8+ T cell differentiation by controlling access of AP-1 factors to enhancers. *Nature Immunology*, *17*(7), 851–860. <https://doi.org/10.1038/ni.3441>
- Rushmore, T. H., Morton, M. R., & Pickett, C. B. (1991). The antioxidant responsive element: Activation by oxidative stress and identification of the DNA consensus sequence required for functional activity. *Journal of Biological Chemistry*, *266*(18), 11632–11639. [https://doi.org/10.1016/s0021-9258\(18\)99004-6](https://doi.org/10.1016/s0021-9258(18)99004-6)
- Rushworth, S. A., & MacEwan, D. J. (2008). HO-1 underlies resistance of AML cells to TNF-induced apoptosis. *Blood*, *111*(7), 3793–3801. <https://doi.org/10.1182/BLOOD-2007-07-104042>
- Rushworth, S. A., MacEwan, D. J., & O'Connell, M. A. (2008). Lipopolysaccharide-induced expression of NAD(P)H:quinone oxidoreductase 1 and heme oxygenase-1 protects against excessive inflammatory responses in human monocytes. *Journal of Immunology*, *181*(10), 6730–6737. <https://doi.org/10.4049/JIMMUNOL.181.10.6730>
- Russell, R. C., Tian, Y., Yuan, H., Park, H. W., Chang, Y. Y., Kim, J., Kim, H., Neufeld, T. P., Dillin, A., & Guan, K. L. (2013). ULK1 induces autophagy by phosphorylating Beclin-1 and activating VPS34 lipid kinase. *Nature Cell Biology*, *15*(7), 741–750. <https://doi.org/10.1038/ncb2757>
- Sadeghifar, F., Böhm, S., Vintermist, A., & Östlund Farrants, A. K. (2015). The B-WICH chromatin-remodelling complex regulates RNA polymerase III transcription by promoting Max-dependent c-Myc binding. *Nucleic Acids Research*, *43*(9), 4477–4490. <https://doi.org/10.1093/NAR/GKV312>
- Saleeb, R. S., Kavanagh, D. M., Dun, A. R., Dalgarno, P. A., & Duncan, R. R. (2019). A VPS33A-binding motif on syntaxin 17 controls autophagy completion in mammalian cells. *Journal of Biological Chemistry*, *294*(11), 4188–4201. <https://doi.org/10.1074/JBC.RA118.005947>
- Salotti, J., & Johnson, P. F. (2019). Regulation of senescence and the SASP by the transcription factor C/EBP $\beta$ . *Experimental Gerontology*, *128*, 110752. <https://doi.org/10.1016/J.EXGER.2019.110752>
- Satoo, K., Noda, N. N., Kumeta, H., Fujioka, Y., Mizushima, N., Ohsumi, Y., & Inagaki, F. (2009). The structure of Atg4B-LC3 complex reveals the mechanism of LC3 processing and delipidation during autophagy. *The EMBO Journal*, *28*(9), 1341–1350. <https://doi.org/10.1038/EMBOJ.2009.80>
- Schreck, R., Rieber, P., & Baeuerle, P. A. (1991). Reactive oxygen intermediates as apparently widely used messengers in the activation of the NF-kappa B transcription factor and HIV-1. *The EMBO Journal*, *10*(8), 2247. <https://doi.org/10.1002/J.1460-2075.1991.TB07761.X>

- Seglen, P. O., Gordon, P. B., Holen, I., & Høyvik, H. (1991). Hepatocytic autophagy. *Biomed Biochim Acta*, *50*(4–6), 373–381.
- Sekine, H., & Motohashi, H. (2021). Roles of CNC Transcription Factors NRF1 and NRF2 in Cancer. *Cancers*, *13*(3), 1–14. <https://doi.org/10.3390/CANCERS13030541>
- Sekine, H., Okazaki, K., Ota, N., Shima, H., Katoh, Y., Suzuki, N., Igarashi, K., Ito, M., Motohashi, H., & Yamamoto, M. (2016). The Mediator Subunit MED16 Transduces NRF2-Activating Signals into Antioxidant Gene Expression. *Molecular and Cellular Biology*, *36*(3), 407–420. <https://doi.org/10.1128/MCB.00785-15>
- Selby, C. P., & Sancar, A. (1997). Cockayne syndrome group B protein enhances elongation by RNA polymerase II. *Proceedings of the National Academy of Sciences of the United States of America*, *94*(21), 11205–11209. <https://doi.org/10.1073/PNAS.94.21.11205/ASSET/4D303477-E49C-4431-A918-0B31DCF77A6B/ASSETS/GRAPHIC/PQ2172698004.JPEG>
- Sengoku, T., Shiina, M., Suzuki, K., Hamada, K., Sato, K., Uchiyama, A., Kobayashi, S., Oguni, A., Itaya, H., Kasahara, K., Moriwaki, H., Watanabe, C., Honma, T., Okada, C., Baba, S., Ohta, T., Motohashi, H., Yamamoto, M., & Ogata, K. (2022). Structural basis of transcription regulation by CNC family transcription factor, Nrf2. *Nucleic Acids Research*, *50*(21), 12543–12557. <https://doi.org/10.1093/NAR/GKAC1102>
- Shaner, N. C., Lambert, G. G., Chamma, A., Ni, Y., Cranfill, P. J., Baird, M. A., Sell, B. R., Allen, J. R., Day, R. N., Israelsson, M., Davidson, M. W., & Wang, J. (2013). A bright monomeric green fluorescent protein derived from Branchiostoma lanceolatum. *Nature Methods*, *10*(5), 407–409. <https://doi.org/10.1038/nmeth.2413>
- Shao, H. bo, Chu, L. ye, Shao, M. an, Jaleel, C. A., & Hong-mei, M. (2008). Higher plant antioxidants and redox signaling under environmental stresses. *Comptes Rendus Biologies*, *331*(6), 433–441. <https://doi.org/10.1016/J.CRVI.2008.03.011>
- Sharif, S. B., Zamani, N., & Chadwick, B. P. (2021). BAZ1B the Protean Protein. *Genes*, *12*(10), 1541. <https://doi.org/10.3390/GENES12101541>
- Shibuya, A., Onda, K., Kawahara, H., Uchiyama, Y., Nakayama, H., Omi, T., Nagaoka, M., Matsui, H., & Hirano, T. (2010). Sofalcone, a gastric mucosa protective agent, increases vascular endothelial growth factor via the Nrf2-heme-oxygenase-1 dependent pathway in gastric epithelial cells. *Biochemical and Biophysical Research Communications*, *398*(3), 581–584. <https://doi.org/10.1016/J.BBRC.2010.06.124>
- Shim, M. S., Nettesheim, A., Hirt, J., & Liton, P. B. (2020). The autophagic protein LC3 translocates to the nucleus and localizes in the nucleolus associated to NUFIP1 in response to cyclic mechanical stress. *Autophagy*, *16*(7), 1248–1261. <https://doi.org/10.1080/15548627.2019.1662584>
- Shivdasani, R. A. (1996). The role of transcription factor NF-E2 in megakaryocyte maturation and platelet production. *Stem Cells*, *14 Suppl 1*(SUPPL. 1), 112–115. <https://doi.org/10.1002/STEM.5530140714>

- Shpilka, T., Weidberg, H., Pietrokovski, S., & Elazar, Z. (2011). Atg8: An autophagy-related ubiquitin-like protein family. *Genome Biology*, *12*(7), 1–11. <https://doi.org/10.1186/GB-2011-12-7-226/FIGURES/4>
- Shrestha, B. K., Skytte Rasmussen, M., Abudu, Y. P., Bruun, J.-A., Larsen, K. B., Alemu, E. A., Sjøttem, E., Lamark, T., & Johansen, T. (2020). NIMA-related kinase 9–mediated phosphorylation of the microtubule-associated LC3B protein at Thr-50 suppresses selective autophagy of p62/sequestosome 1. *Journal of Biological Chemistry*, *295*(5), 1240–1260. [https://doi.org/10.1016/S0021-9258\(17\)49883-8](https://doi.org/10.1016/S0021-9258(17)49883-8)
- Sies, H. (1985). Oxidative Stress: Introductory Remarks. *Academic Press*, 1–8. <https://doi.org/10.1016/B978-0-12-642760-8.50005-3>
- Sies, H. (1997). Oxidative stress: oxidants and antioxidants. *Experimental Physiology*, *82*(2), 291–295. <https://doi.org/10.1113/EXPPHYSIOL.1997.SP004024>
- Sies, H. (2015). Oxidative stress: a concept in redox biology and medicine. *Redox Biology*, *4*, 180–183. <https://doi.org/10.1016/J.REDOX.2015.01.002>
- Singh, A., Bodas, M., Wakabayashi, N., Bunz, F., & Biswal, S. (2010). Gain of Nrf2 function in non-small-cell lung cancer cells confers radioresistance. *Antioxidants & Redox Signaling*, *13*(11), 1627–1637. <https://doi.org/10.1089/ARS.2010.3219>
- Singh, A., Happel, C., Manna, S. K., Acquah-Mensah, G., Carrerero, J., Kumar, S., Nasipuri, P., Krausz, K. W., Wakabayashi, N., Dewi, R., Boros, L. G., Gonzalez, F. J., Gabrielson, E., Wong, K. K., Girnun, G., & Biswal, S. (2013). Transcription factor NRF2 regulates miR-1 and miR-206 to drive tumorigenesis. *Journal of Clinical Investigation*, *123*(7), 2921–2934. <https://doi.org/10.1172/JCI66353>
- Singh, A., Venkannagari, S., Oh, K. H., Zhang, Y. Q., Rohde, J. M., Liu, L., Nimmagadda, S., Sudini, K., Brimacombe, K. R., Gajghate, S., Ma, J., Wang, A., Xu, X., Shahane, S. A., Xia, M., Woo, J., Mensah, G. A., Wang, Z., Ferrer, M., ... Biswal, S. (2016). Small molecule inhibitor of NRF2 selectively intervenes therapeutic resistance in KEAP1-deficient NSCLC tumors. *ACS Chemical Biology*, *11*(11), 3214–3225. [https://doi.org/10.1021/ACSCHEMPIO.6B00651/ASSET/IMAGES/LARGE/CB-2016-006512\\_0008.JPEG](https://doi.org/10.1021/ACSCHEMPIO.6B00651/ASSET/IMAGES/LARGE/CB-2016-006512_0008.JPEG)
- Smith, M. D., Martin, K. A., Calabresi, P. A., & Bhargava, P. (2017). Dimethyl fumarate alters B-cell memory and cytokine production in MS patients. *Annals of Clinical and Translational Neurology*, *4*(5), 351–355. <https://doi.org/10.1002/ACN3.411>
- Solis, L. M., Behrens, C., Dong, W., Suraokar, M., Ozburn, N. C., Moran, C. A., Corvalan, A. H., Biswal, S., Swisher, S. G., Bekele, B. N., Minna, J. D., Stewart, D. J., & Wistuba, I. I. (2010). Nrf2 and Keap1 abnormalities in non-small cell lung carcinoma and association with clinicopathologic features. *Clinical Cancer Research*, *16*(14), 3743–3753. <https://doi.org/10.1158/1078-0432.CCR-09-3352/83887/AM/NRF2-AND-KEAP1-ABNORMALITIES-IN-NON-SMALL-CELL>



- Sporn, M. B., & Liby, K. T. (2012). NRF2 and cancer: The good, the bad and the importance of context. In *Nature Reviews Cancer* (Vol. 12, Issue 8, pp. 564–571). <https://doi.org/10.1038/nrc3278>
- Stewart, D., Killeen, E., Naquin, R., Alam, S., & Alam, J. (2003). Degradation of Transcription Factor Nrf2 via the Ubiquitin-Proteasome Pathway and Stabilization by Cadmium. *Journal of Biological Chemistry*, 278(4), 2396–2402. <https://doi.org/10.1074/JBC.M209195200>
- Sun, D., Wu, R., Zheng, J., Li, P., & Yu, L. (2018). Polyubiquitin chain-induced p62 phase separation drives autophagic cargo segregation. *Cell Research*, 28(4), 405–415. <https://doi.org/10.1038/s41422-018-0017-7>
- Sun, Z., Chin, Y. E., & Zhang, D. D. (2009). Acetylation of Nrf2 by p300/CBP Augments Promoter-Specific DNA Binding of Nrf2 during the Antioxidant Response. *Molecular and Cellular Biology*, 29(10), 2658–2672. <https://doi.org/10.1128/mcb.01639-08>
- Suzuki, T., Fujii, M., & Ayusawa, D. (2002). Demethylation of classical satellite 2 and 3 DNA with chromosomal instability in senescent human fibroblasts. *Experimental Gerontology*, 37(8–9), 1005–1014. [https://doi.org/10.1016/S0531-5565\(02\)00061-X](https://doi.org/10.1016/S0531-5565(02)00061-X)
- Svenning, S., Lamark, T., Krause, K., & Johansen, T. (2011). Plant NBR1 is a selective autophagy substrate and a functional hybrid of the mammalian autophagic adapters NBR1 and p62/SQSTM1. *Autophagy*, 7(9), 993–1010. <https://doi.org/10.4161/AUTO.7.9.16389>
- Sykiotis, G. P., & Bohmann, D. (2008). Keap1/Nrf2 Signaling Regulates Oxidative Stress Tolerance and Lifespan in *Drosophila*. *Developmental Cell*, 14(1), 76–85. <https://doi.org/10.1016/J.DEVCEL.2007.12.002>
- Sykiotis, G. P., & Bohmann, D. (2010). Stress-activated cap'n'collar transcription factors in aging and human disease. *Science Signaling*, 3(112). <https://doi.org/10.1126/SCISIGNAL.3112RE3/ASSET/CB4F158E-6B94-49E4-A138-628D984FD248/ASSETS/GRAPHIC/3112RE3-F3.JPEG>
- Takahashi, A., Loo, T. M., Okada, R., Kamachi, F., Watanabe, Y., Wakita, M., Watanabe, S., Kawamoto, S., Miyata, K., Barber, G. N., Ohtani, N., & Hara, E. (2018). Downregulation of cytoplasmic DNases is implicated in cytoplasmic DNA accumulation and SASP in senescent cells. *Nature Communications*, 9(1), 1–12. <https://doi.org/10.1038/s41467-018-03555-8>
- Takahashi, Y., Liang, X., Hattori, T., Tang, Z., He, H., Chen, H., Liu, X., Abraham, T., Imamura-Kawawasa, Y., Buchkovich, N. J., Young, M. M., & Wang, H. G. (2019). VPS37A directs ESCRT recruitment for phagophore closure. *Journal of Cell Biology*, 218(10), 3336–3354. <https://doi.org/10.1083/JCB.201902170>
- Takaya, K., Suzuki, T., Motohashi, H., Onodera, K., Satomi, S., Kensler, T. W., & Yamamoto, M. (2012). Validation of the multiple sensor mechanism of the Keap1-Nrf2 system. *Free Radical Biology and Medicine*, 53(4), 817–827. <https://doi.org/10.1016/j.freeradbiomed.2012.06.023>

- Tanida, I., Sou, Y. S., Ezaki, J., Minematsu-Ikeguchi, N., Ueno, T., & Kominami, E. (2004). HsAtg4B/HsApg4B/autophagin-1 cleaves the carboxyl termini of three human Atg8 homologues and delipidates microtubule-associated protein light chain 3- and GABAA receptor-associated protein-phospholipid conjugates. *Journal of Biological Chemistry*, *279*(35), 36268–36276. <https://doi.org/10.1074/jbc.M401461200>
- Tanida, I., Ueno, T., & Kominami, E. (2004). LC3 conjugation system in mammalian autophagy. *International Journal of Biochemistry and Cell Biology*, *36*(12), 2503–2518. <https://doi.org/10.1016/j.biocel.2004.05.009>
- Telakowski-Hopkins, C. A., King, R. G., & Pickett, C. B. (1988). Glutathione S-transferase Ya subunit gene: identification of regulatory elements required for basal level and inducible expression. *Proceedings of the National Academy of Sciences of the United States of America*, *85*(4), 1000–1004. <https://doi.org/10.1073/PNAS.85.4.1000>
- Terlecki-Zaniewicz, L., Lämmermann, I., Latreille, J., Bobbili, M. R., Pils, V., Schosserer, M., Weinmüller, R., Dellago, H., Skalicky, S., Pum, D., Almaraz, J. C. H., Scheideler, M., Morizot, F., Hackl, M., Gruber, F., & Grillari, J. (2018). Small extracellular vesicles and their miRNA cargo are anti-apoptotic members of the senescence-associated secretory phenotype. *Aging*, *10*(5), 1103–1132. <https://doi.org/10.18632/AGING.101452>
- Thimmulappa, R. K., Lee, H., Rangasamy, T., Reddy, S. P., Yamamoto, M., Kensler, T. W., & Biswal, S. (2006). Nrf2 is a critical regulator of the innate immune response and survival during experimental sepsis. *Journal of Clinical Investigation*, *116*(4), 984–995. <https://doi.org/10.1172/JCI25790>
- Toki, T., Itoh, J., Kitazawa, J., Arai, K., Hatakeyama, K., Akasaka, J. I., Igarashi, K., Nomura, N., Yokoyama, M., Yamamoto, M., & Ito, E. (1997). Human small Maf proteins form heterodimers with CNC family transcription factors and recognize the NF-E2 motif. *Oncogene*, *14*(16), 1901–1910. <https://doi.org/10.1038/sj.onc.1201024>
- Tonelli, C., Chio, I. I. C., & Tuveson, D. A. (2018). Transcriptional Regulation by Nrf2. *Antioxidants & Redox Signaling*, *29*(17), 1727–1745. <https://doi.org/10.1089/ars.2017.7342>
- Tong, K. I., Padmanabhan, B., Kobayashi, A., Shang, C., Hirotsu, Y., Yokoyama, S., & Yamamoto, M. (2007). Different electrostatic potentials define ETGE and DLG motifs as hinge and latch in oxidative stress response. *Molecular and Cellular Biology*, *27*(21), 7511–7521. <https://doi.org/10.1128/MCB.00753-07>
- Toto, M., D'Angelo, G., & Corona, D. F. V. (2014). Regulation of ISWI chromatin remodelling activity. *Chromosoma*, *123*(1–2), 91–102. <https://doi.org/10.1007/S00412-013-0447-4/FIGURES/3>
- Tripathi, U., Nchioua, R., Prata, L. G. P. L., Zhu, Y., Gerdes, E. O. W., Giorgadze, N., Pirtskhalava, T., Parker, E., Xue, A., Espindola-Netto, J. M., Stenger, S., Robbins, P. D., Niedernhofer, L. J., Dickinson, S. L., Allison, D. B., Kirchhoff, F., Sparrer, K. M. J., Tchkonja, T., & Kirkland, J. L. (2021). SARS-CoV-2 causes senescence in human cells and exacerbates the senescence-

- associated secretory phenotype through TLR-3. *Aging*, *13*(18), 21838–21854.  
<https://doi.org/10.18632/AGING.203560>
- Truong, T. H., & Carroll, K. S. (2013). Redox Regulation of Protein Kinases. *Critical Reviews in Biochemistry and Molecular Biology*, *48*(4), 332. <https://doi.org/10.3109/10409238.2013.790873>
- Tsuchida, K., Tsujita, T., Hayashi, M., Ojima, A., Keleku-Lukwete, N., Katsuoka, F., Otsuki, A., Kikuchi, H., Oshima, Y., Suzuki, M., & Yamamoto, M. (2017). Halofuginone enhances the chemo-sensitivity of cancer cells by suppressing NRF2 accumulation. *Free Radical Biology and Medicine*, *103*, 236–247. <https://doi.org/10.1016/J.FREERADBIOMED.2016.12.041>
- Valverde, D. P., Yu, S., Boggavarapu, V., Kumar, N., Lees, J. A., Walz, T., Reinisch, K. M., & Melia, T. J. (2019). ATG2 transports lipids to promote autophagosome biogenesis. *Journal of Cell Biology*, *218*(6), 1787–1798. <https://doi.org/10.1083/JCB.201811139>
- Deursen, J. M. (2014). The role of senescent cells in ageing. In *Nature* (Vol. 509, Issue 7501, pp. 439–446). Nature Publishing Group. <https://doi.org/10.1038/nature13193>
- Waldmann, T., Scholten, I., Kappes, F., Hu, H. G., & Knippers, R. (2004). The DEK protein—an abundant and ubiquitous constituent of mammalian chromatin. *Gene*, *343*(1), 1–9.  
<https://doi.org/10.1016/J.GENE.2004.08.029>
- Wang, W., Nag, S. A., & Zhang, R. (2015). Targeting the NFκB Signaling Pathways for Breast Cancer Prevention and Therapy. *Current Medicinal Chemistry*, *22*(2), 264.  
<https://doi.org/10.2174/0929867321666141106124315>
- Wang, X. J., Sun, Z., Villeneuve, N. F., Zhang, S., Zhao, F., Li, Y., Chen, W., Yi, X., Zheng, W., Wondrak, G. T., Wong, P. K., & Zhang, D. D. (2008). Nrf2 enhances resistance of cancer cells to chemotherapeutic drugs, the dark side of Nrf2. *Carcinogenesis*, *29*(6), 1235–1243.  
<https://doi.org/10.1093/CARCIN/BGN095>
- Wang, X., Tomso, D. J., Chorley, B. N., Cho, H. Y., Cheung, V. G., Kleeberger, S. R., & Bell, D. A. (2007). Identification of polymorphic antioxidant response elements in the human genome. *Human Molecular Genetics*, *16*(10), 1188–1200. <https://doi.org/10.1093/HMG/DDM066>
- Wasserman, W. W., & Fahl, W. E. (1997). Functional antioxidant responsive elements. *Proceedings of the National Academy of Sciences of the United States of America*, *94*(10), 5361–5366.  
<https://doi.org/10.1073/PNAS.94.10.5361/ASSET/AA8CEDCB-D5CF-4D33-B575-B84E15268830/ASSETS/GRAPHIC/PQ0970738006.JPEG>
- Wesch, N., Kirkin, V., & Rogov, V. V. (2020). Atg8-Family Proteins-Structural Features and Molecular Interactions in Autophagy and Beyond. In *Cells* (Vol. 9, Issue 9, pp. 1–25).  
<https://doi.org/10.3390/cells9092008>
- Wild, P., McEwan, D. G., & Dikic, I. (2014). The LC3 interactome at a glance. *Journal of Cell Science*, *127*(1), 3–9. <https://doi.org/10.1242/JCS.140426/259864/AM/THE-LC3-INTERACTOME-AT-A-GLANCE>

- Wirth, M., Zhang, W., Razi, M., Nyoni, L., Joshi, D., O'Reilly, N., Johansen, T., Tooze, S. A., & Mouilleron, S. (2019). Molecular determinants regulating selective binding of autophagy adaptors and receptors to ATG8 proteins. *Nature Communications*, *10*(1). <https://doi.org/10.1038/s41467-019-10059-6>
- Wise-Draper, T. M., Allen, H. V., Thobe, M. N., Jones, E. E., Habash, K. B., Münger, K., & Wells, S. I. (2005). The Human DEK Proto-Oncogene Is a Senescence Inhibitor and an Upregulated Target of High-Risk Human Papillomavirus E7. *Journal of Virology*, *79*(22), 14309–14317. <https://doi.org/10.1128/JVI.79.22.14309-14317.2005/ASSET/CAB70972-E367-4760-BFC9-8DCF5C2B7722/ASSETS/GRAPHIC/ZJV0220570460005.JPEG>
- Woods, C. G., Fu, J., Xue, P., Hou, Y., Pluta, L. J., Yang, L., Zhang, Q., Thomas, R. S., Andersen, M. E., & Pi, J. (2009). Dose-dependent transitions in Nrf2-mediated adaptive response and related stress responses to hypochlorous acid in mouse macrophages. *Toxicology and Applied Pharmacology*, *238*(1), 27–36. <https://doi.org/10.1016/J.TAAP.2009.04.007>
- Wu, F., Watanabe, Y., Guo, X. Y., Qi, X., Wang, P., Zhao, H. Y., Wang, Z., Fujioka, Y., Zhang, H., Ren, J. Q., Fang, T. C., Shen, Y. X., Feng, W., Hu, J. J., Noda, N. N., & Zhang, H. (2015). Structural Basis of the Differential Function of the Two *C. elegans* Atg8 Homologs, LGG-1 and LGG-2, in Autophagy. *Molecular Cell*, *60*(6), 914–929. <https://doi.org/10.1016/J.MOLCEL.2015.11.019>
- Wu, K. C., Cui, J. Y., & Klaassen, C. D. (2011). Beneficial role of Nrf2 in regulating NADPH generation and consumption. *Toxicological Sciences*, *123*(2), 590–600. <https://doi.org/10.1093/TOXSCI/KFR183>
- Wu, S., Lu, H., & Bai, Y. (2019). Nrf2 in cancers: A double-edged sword. *Cancer Medicine*, *8*(5), 2252–2267. <https://doi.org/10.1002/CAM4.2101>
- Wurzer, B., Zaffagnini, G., Fracchiolla, D., Turco, E., Abert, C., Romanov, J., & Martens, S. (2015). Oligomerization of p62 allows for selection of ubiquitinated cargo and isolation membrane during selective autophagy. *ELife*, *4*(September 2015). <https://doi.org/10.7554/ELIFE.08941>
- Xiao, A., Li, H., Shechter, D., Ahn, S. H., Fabrizio, L. A., Erdjument-Bromage, H., Ishibe-Murakami, S., Wang, B., Tempst, P., Hofmann, K., Patel, D. J., Elledge, S. J., & Allis, C. D. (2008). WSTF regulates the H2A.X DNA damage response via a novel tyrosine kinase activity. *Nature*, *457*(7225), 57–62. <https://doi.org/10.1038/nature07668>
- Xu, C., Wang, L., Fozouni, P., Evjen, G., Chandra, V., Jiang, J., Lu, C., Nicastri, M., Bretz, C., Winkler, J. D., Amaravadi, R., Garcia, B. A., Adams, P. D., Ott, M., Tong, W., Johansen, T., Dou, Z., & Berger, S. L. (2020). SIRT1 is downregulated by autophagy in senescence and ageing. In *Nature Cell Biology* (Vol. 22, Issue 10, pp. 1170–1179). Nature Research. <https://doi.org/10.1038/s41556-020-00579-5>
- Yamauchi, T., Keough, R. A., Gonda, T. J., & Ishii, S. (2008). Ribosomal stress induces processing of Mybbp1a and its translocation from the nucleolus to the nucleoplasm. *Genes to Cells*, *13*(1), 27–39. <https://doi.org/10.1111/J.1365-2443.2007.01148.X>

- Yang, H., Ko, K., Xia, M., Li, T. W. H., Oh, P., Li, J., & Lu, S. C. (2010). Induction of avian musculoaponeurotic fibrosarcoma proteins by toxic bile acid inhibits expression of glutathione synthetic enzymes and contributes to cholestatic liver injury in mice. *Hepatology*, *51*(4), 1291–1301. <https://doi.org/10.1002/HEP.23471>
- Yau, R., & Rape, M. (2016). The increasing complexity of the ubiquitin code. *Nature Cell Biology*, *18*(6), 579–586. <https://doi.org/10.1038/ncb3358>
- Ying, L., Lau, A., Alvira, C. M., West, R., Cann, G. M., Zhou, B., Kinnear, C., Jan, E., Sarnow, P., Van de Rijn, M., & Rabinovitch, M. (2009). LC3-mediated fibronectin mRNA translation induces fibrosarcoma growth by increasing connective tissue growth factor. *Journal of Cell Science*, *122*(9), 1441–1451. <https://doi.org/10.1242/JCS.025957>
- Yoo, N. J., Kim, H. R., Kim, Y. R., An, C. H., & Lee, S. H. (2012). Somatic mutations of the KEAP1 gene in common solid cancers. *Histopathology*, *60*(6), 943–952. <https://doi.org/10.1111/J.1365-2559.2012.04178.X>
- Yu, L., Chen, Y., & Tooze, S. A. (2018). Autophagy pathway: Cellular and molecular mechanisms. *Autophagy*, *14*(2), 207–215. <https://doi.org/10.1080/15548627.2017.1378838>
- Zachari, M., & Ganley, I. G. (2017). The mammalian ULK1 complex and autophagy initiation. *Essays in Biochemistry*, *61*(6), 585. <https://doi.org/10.1042/EBC20170021>
- Zaffagnini, G., & Martens, S. (2016). Mechanisms of Selective Autophagy. *Journal of Molecular Biology*, *428*(9), 1714–1724. <https://doi.org/10.1016/J.JMB.2016.02.004>
- Zanella, M., Vitriolo, A., Andirko, A., Martins, P. T., Sturm, S., O'Rourke, T., Laugsch, M., Malerba, N., Skaros, A., Trattaro, S., Germain, P. L., Mihailovic, M., Merla, G., Rada-Iglesias, A., Boeckx, C., & Testa, G. (2019a). Dosage analysis of the 7q11.23 Williams region identifies BAZ1B as a major human gene patterning the modern human face and underlying self-domestication. *Science Advances*, *5*(12). [https://doi.org/10.1126/SCIADV.AAW7908/SUPPL\\_FILE/AAW7908\\_TABLE\\_S2A\\_TO\\_S2N.XLS](https://doi.org/10.1126/SCIADV.AAW7908/SUPPL_FILE/AAW7908_TABLE_S2A_TO_S2N.XLS)
- Zanella, M., Vitriolo, A., Andirko, A., Martins, P. T., Sturm, S., O'Rourke, T., Laugsch, M., Malerba, N., Skaros, A., Trattaro, S., Germain, P. L., Mihailovic, M., Merla, G., Rada-Iglesias, A., Boeckx, C., & Testa, G. (2019b). Dosage analysis of the 7q11.23 Williams region identifies BAZ1B as a major human gene patterning the modern human face and underlying self-domestication. *Science Advances*, *5*(12). [https://doi.org/10.1126/SCIADV.AAW7908/SUPPL\\_FILE/AAW7908\\_TABLE\\_S2A\\_TO\\_S2N.XLS](https://doi.org/10.1126/SCIADV.AAW7908/SUPPL_FILE/AAW7908_TABLE_S2A_TO_S2N.XLS)
- Zhan, L., Zhang, H., Zhang, Q., Woods, C. G., Chen, Y., Xue, P., Dong, J., Tokar, E. J., Xu, Y., Hou, Y., Fu, J., Yarborough, K., Wang, A., Qu, W., Waalkes, M. P., Andersen, M. E., & Pi, J. (2012). Regulatory role of KEAP1 and NRF2 in PPAR $\gamma$  expression and chemoresistance in human non-small-cell lung carcinoma cells. *Free Radical Biology & Medicine*, *53*(4), 758–768. <https://doi.org/10.1016/J.FREERADBIOMED.2012.05.041>

- Zhang, J., Hosoya, T., Maruyama, A., Nishikawa, K., Maher, J. M., Ohta, T., Motohashi, H., Fukamizu, A., Shibahara, S., Itoh, K., & Yamamoto, M. (2007). Nrf2 Neh5 domain is differentially utilized in the transactivation of cytoprotective genes. *Biochemical Journal*, *404*(3), 459–466. <https://doi.org/10.1042/BJ20061611>
- Zhang, J., Ohta, T., Maruyama, A., Hosoya, T., Nishikawa, K., Maher, J. M., Shibahara, S., Itoh, K., & Yamamoto, M. (2006). BRG1 Interacts with Nrf2 To Selectively Mediate HO-1 Induction in Response to Oxidative Stress. *Molecular and Cellular Biology*, *26*(21), 7942–7952. <https://doi.org/10.1128/mcb.00700-06>
- Zhang, S., Yazaki, E., Sakamoto, H., Yamamoto, H., & Mizushima, N. (2022). Evolutionary diversification of the autophagy-related ubiquitin-like conjugation systems. *Autophagy*, *18*(12), 2969–2984. <https://doi.org/10.1080/15548627.2022.2059168>
- Zhen, Y., Spangenberg, H., Munson, M. J., Brech, A., Schink, K. O., Tan, K. W., Sørensen, V., Wenzel, E. M., Radulovic, M., Engedal, N., Simonsen, A., Raiborg, C., & Stenmark, H. (2020). ESCRT-mediated phagophore sealing during mitophagy. *Autophagy*, *16*(5), 826–841. <https://doi.org/10.1080/15548627.2019.1639301>
- Zhou, B., Boudreau, N., Coulber, C., Hammarback, J., & Rabinovitch, M. (1997). Microtubule-associated protein 1 light chain 3 is a fibronectin mRNA-binding protein linked to mRNA translation in lamb vascular smooth muscle cells. *The Journal of Clinical Investigation*, *100*(12), 3070–3082. <https://doi.org/10.1172/JCI119862>
- Zhu, J., Wang, H., Ji, X., Zhu, L., Sun, Q., Cong, Z., Zhou, Y., Liu, H., & Zhou, M. (2014). Differential Nrf2 expression between glioma stem cells and non-stem-like cells in glioblastoma. *Oncology Letters*, *7*(3), 693–698. <https://doi.org/10.3892/OL.2013.1760>
- Zhu, M., & Fahl, W. E. (2001). Functional Characterization of Transcription Regulators That Interact with the Electrophile Response Element. *Biochemical and Biophysical Research Communications*, *289*(1), 212–219. <https://doi.org/10.1006/BBRC.2001.5944>
- Zuccolo, E., Badi, I., Scavello, F., Gambuzza, I., Mancinelli, L., Macrì, F., Tedesco, C. C., Veglia, F., Bonfigli, A. R., Olivieri, F., & Raucci, A. (2020). The microRNA-34a-Induced Senescence-Associated Secretory Phenotype (SASP) Favors Vascular Smooth Muscle Cells Calcification. *International Journal of Molecular Sciences*, *21*(12), 4454. <https://doi.org/10.3390/IJMS21124454>

All the images that have been used, contain the reference from the source that they have been copied from and they have permission, wherever it was needed, through the Copyright Clearance Center ®.

# PAPER I

**Competitive binding between LC3B and p300/CBP to the NRF2 Neh5 domain regulates target gene transcriptional activation**

Athanasios Kournoutis, Birendra Kumar Shrestha, Hallvard Lauritz Olsvik, Yakubu Princely Abudu, Ashish Jain, Gry Evjen, Aud Øvervatn, Trond Lamark and Terje Johansen\*

*Autophagy Research Group, Department of Medical Biology, UiT – The Arctic University of Norway, 9037 Tromsø, Norway*

\*Corresponding author: tel: +47 77644720, email: [terje.johansen@uit.no](mailto:terje.johansen@uit.no)

Keywords: Autophagy, NRF2, LC3B, p300, ATG8, oxidative stress



## **ABSTRACT**

The transcription factor NRF2 serves as a master regulator orchestrating the anti-oxidative response, significantly contributing to cellular defense mechanisms against oxidative stress. NRF2 undergoes transcriptional activation upon translocation to the nucleus, a process that is facilitated by its interaction with the acetyltransferase p300/CBP. This interaction occurs on the Neh5 (Nrf2-ECH homology 5) domain of NRF2, followed by acetylation events on Neh1 and Neh3, and results in enhancing NRF2's affinity to its target gene promoters. In this study, we explore the involvement of LC3B, a member of the ATG8 family of autophagy proteins, in the p300/CBP-driven transcriptional activation of NRF2. Our findings reveal that NRF2 strongly interacts with LC3B and the other ATG8s, but its stability remains unaffected by LC3B. LC3B binds to the Neh5 domain of NRF2, the same domain responsible for its interaction with p300/CBP. We show that LC3B competes with p300/CBP for binding to Neh5. LC3B interacts with NRF2 in the nucleus and acts as a negative regulator of NRF2, functioning as a brake to the NRF2-driven antioxidative stress response within the nucleus by inhibiting its activation by p300/CBP.

## INTRODUCTION

Oxidative stress, defined as the negative effect of oxidants in different physiological functions, is well-established as an important factor in acute toxicity caused by different environmental stressors (Sies, 1985, 1997). Dysfunctional oxidative stress regulation is widely implicated in the pathogenesis of cancer, neurodegenerative disorders, and various diseases associated with aging (Chen et al., 2008; Forman & Zhang, 2021; Pizzino et al., 2017). The transcription factor NRF2 (nuclear factor erythroid 2-related factor 2) serves as a crucial regulator of the oxidative stress response. It activates the transcription of antioxidant response genes by binding to the antioxidant response elements (AREs) on their promoters (Katsuoka et al., 2005; Nioi et al., 2003; Tonelli et al., 2018).

The regulation of NRF2 protein levels is intricately managed by the ubiquitin-proteasome system (UPS), through its interaction with KEAP1 (Itoh et al., 2003; McMahon et al., 2003). Under basal conditions, KEAP1, acting as a redox-sensitive adaptor, regulates NRF2's degradation by forming a complex with CUL3 and RBX1 to form a functional E3 ubiquitin ligase, via the Neh2 domain of NRF2 (Cullinan et al., 2004; Kobayashi et al., 2004; Zhang et al., 2004). This complex involves two KEAP1 molecules binding through their Kelch-repeat domain, to the DLG and ETGE motifs of one NRF2 molecule. In this context, KEAP1 serves as a crucial adaptor for the CUL3 – RBX1 E3 ubiquitin ligase complex, responsible for maintaining low levels of NRF2, by facilitating constant ubiquitylation and degradation. Hence, NRF2 has a short half-life of approximately 10–30 minutes under normal, unperturbed conditions (Nguyen et al., 2003). However, during oxidative stress, specific cysteine residues on KEAP1 undergo oxidation, rendering it inactive (Takaya et al., 2012). This inactivation leads to NRF2 stabilization through a Hinge-Latch mechanism (Horie et al., 2021). This model explains that under oxidative stress, NRF2 remains stably associated with KEAP1, and the newly translated pool of NRF2 translocates to the nucleus and activates its antioxidant program. The activation of ARE-containing gene promoters by NRF2 is generally leading to the induction of the expression of antioxidant proteins, which allow cells to respond to oxidative stress (Raghunath et al., 2018). NRF2 achieves this by recruiting co-activators like p300/CBP histone acetyltransferases and the small musculoaponeurotic fibrosarcoma proteins (sMAFs) to form the ARE-binding complex. It was initially suggested that two NRF2 domains, Nrf2-ECH homology 4 and 5 (Neh4 and Neh5) cooperate to bind to CBP (Kato et al., 2001) and that displacement of CBP from the CBP-NRF2 complex leads to repression of NRF2-induced transcription (Brown et al., 2008). However, the crucial domain for NRF2's target gene expression is Neh5, and specific residues in this domain affect the activation of different target genes (J. Zhang et al., 2007). Under oxidative stress conditions, p300/CBP directly binds to NRF2, acetylating the C-terminal Neh1 domain to enhance the binding of NRF2 to the promoter of its target genes (Sun et al., 2009). Among the genes tested, were *HO-1*, *GCLM*, *TXNRD1* and *NQO1*, with *HO-1* having the weakest Neh1-acetylation dependent activation. Interestingly, it was shown in

the same study that mutations of the Neh1 lysine sites didn't affect NRF2 stability. Then, Kawai and colleagues, complemented the findings by Sun et al. by revealing that acetylation of the Neh3 domain by p300/CBP is especially relevant for the *HO-1* gene activation as well, on top of NRF2's other target genes (Kawai et al., 2011), and that SIRT1 can deacetylate NRF2, reducing NRF2-dependent gene transcription.

Macroautophagy (hereafter referred to as autophagy), is an evolutionarily conserved lysosomal degradation pathway that plays a crucial role in preserving macromolecular and organellar homeostasis (Klionsky et al., 2021). The members of the ATG8 family of proteins are crucial components of the autophagic pathway, functioning as membrane scaffolds for other ATG proteins, and facilitating the formation and fusion of autophagosomes with lysosomes (Johansen & Lamark, 2020). They also participate in selective autophagy, a form of selective autophagic degradation of cellular components. Selective autophagy receptors directly bind to the ATG8s through a 10–15 amino acid-long LC3 interacting region (LIR) motif (Birgisdottir et al., 2013; Johansen & Lamark, 2020). This motif, characterized by a core sequence [W/F/Y]<sub>0</sub>-X<sub>1</sub>-X<sub>2</sub>-[I/L/V]<sub>3</sub>, involves the aromatic residue in position 0 docking into hydrophobic pocket 1 (HP1) and the hydrophobic residue in position 3 docking into hydrophobic pocket 2 (HP2) of the LIR docking site (LDS) on the ATG8 protein.

The functions of ATG8 proteins extend beyond autophagy, among others in the nucleus, where a few studies have explored the role LC3B. Nuclear LC3B has been observed to interact with various proteins, including promyelocytic leukemia (PML), components of the extracellular signal-regulated kinases (ERK) pathway, and the ribosome receptor Nuclear FMR1 Interacting Protein 1 (NUFIP1) (He et al., 2014; Martinez-Lopez et al., 2013; Shim et al., 2020). LC3B was also found to directly interact with lamin B1 during senescence, associating with transcriptionally inactive heterochromatin domains (lamin-associated domains, LADs) and contributing to the degradation of the nuclear lamina in response to oncogenic insults (Dou et al., 2015). Sirtuin 1 (SIRT1), a key nuclear deacetylase linked to aging, was shown to undergo lysosomal degradation through selective autophagy, involving direct targeting in the nucleus by LC3B (L. Wang et al., 2021). Recently, their role as transcriptional co-factors for the LMX1B-mediated transcription of autophagy genes in dopaminergic neurons (Jiménez-Moreno et al., 2023; Kournoutis & Johansen, 2023) was described.

Here we show that LC3B competes with p300 for the binding to the Neh5 domain of NRF2, acting as a transcriptional repressor in the nucleus. As it has previously been reported, p300 interacts with NRF2 on its Neh5 domain and acetylates its Neh1 and Neh3 domains, resulting in an increase in NRF2's DNA binding capacity and subsequent target gene expression (Kawai et al., 2011; Sun et al., 2009). Through the NRF2 – LC3B – p300 competition, we hypothesize that LC3B acts as a break to the persistent NRF2 target gene activation, regulating the antioxidant response driven by NRF2.

## MATERIALS AND METHODS

**Antibodies and reagents.** The following primary antibodies were used: rabbit monoclonal anti-NRF2 (Abcam, ab62352, WB: 1:1000), rabbit anti-lamin B1 (Abcam, ab16048, WB: 1:1000, IF: 1:1000), rabbit polyclonal anti-LC3B (Novus, NB100-2220, WB: 1:1000, IF: 1:750), rabbit polyclonal anti-LC3B (Sigma, L7543, WB: 1:1000, IF: 1:750), mouse monoclonal anti-LC3B (Nanotools, 0231-100/lc3-5F10, IF: 1:750), rabbit polyclonal anti-FYCO1 (Sigma, HPA035526, WB: 1:1000), mouse anti-p62 (BD Biosciences, #610833, WB: 1:1000), mouse monoclonal anti-Myc (Cell Signaling, 9B11, WB: 1:1000), mouse anti-tubulin  $\beta$  (Sigma, T4026, WB: 1:2000), rabbit anti-actin (Sigma, A2066, WB: 1:3000). The following secondary antibodies were used for WB: IRDye 800CW goat anti-rabbit IgG (LI-COR, 926-32211), IRDye 680LT goat anti-mouse IgG (LI-COR, 926-68020), IRDye 680LT donkey anti-guinea pig IgG (LI-COR 926-68030), HRP-conjugated goat anti-rabbit IgG (BD Pharmingen<sup>TM</sup>, 554021). The following secondary antibodies were used for immunofluorescent labeling: Alexa Fluor<sup>®</sup> 555-conjugated goat anti-rabbit IgG (Life Technologies, A-21428), Alexa Fluor<sup>®</sup> 488-conjugated goat anti-mouse IgG (Life Technologies, A-11029). Reagents used were DL-Sulforaphane (SFN) (Thermo Fisher Scientific, ICN19378125), Bafilomycin A1 (Sigma, B1793), MG132 (Sigma, C2759), dimethyl sulfoxide (DMSO) (Honeywell, #472301).

**Plasmids.** The plasmids used are listed in **Table 1**. The truncation constructs were done using InFusion cloning technology (Takara Bio). Cloning into pDest-vectors was done using the Gateway cloning system (Invitrogen). QuickChange site-directed mutagenesis kit (Stratagene) was used to create desired point mutations, which were verified by DNA sequencing (BigDye Sequencing kits, Applied Biosystems). Oligonucleotides for mutagenesis and truncations are listed in **Table 2**. All plasmid constructs were verified by sequencing (BigDye, Applied Biosystems) and/or restrictive digestion.

**Cell culture and transfection.** U2OS, HEK293T, HeLa FlpIn T-Rex (Invitrogen, R714-07) were cultured in Dulbecco's Modified Eagle's Medium (DMEM) (Sigma, D6046 or Sigma, D5796) supplemented with 10% heat-inactivated fetal bovine serum (Biocrom, S0615) and 1% streptomycin-penicillin (Sigma, P4333). Sub-confluent (70-80%) cells were transfected using TransIT-LT1 (Mirus, MIR2300) or Metafectene Pro (Biontex Laboratories GmbH), following the manufacturer's instructions.

**Recombinant protein production and GST pulldown assay.** GST or GST-tagged proteins were expressed in *Escherichia coli* strain SoluBL21 (Genlantis, #C700200). Expression of recombinant protein was induced by treating bacterial cultures with isopropyl  $\beta$ -D-1-thiogalactopyranoside (IPTG;

50  $\mu$ M) for 4h at room temperature. GST or GST fusion proteins were purified and immobilized on Glutathione-Sepharose 4 Fast Flow beads (GE Healthcare, 17-5132-01). Myc- or V1-tagged proteins were translated in vitro using the TNT T7 reticulocyte Lysate system (Promega, #14610) in the presence of  $^{35}$ S-methionine. The translated protein was pre-incubated with 10  $\mu$ l Glutathione-Sepharose beads and 100  $\mu$ l of NETN buffer (50 mM Tris pH 8.0; 150 mM NaCl; 1 mM EDTA; 0,5% Nonidet P-40) with cOmplete Mini EDTA-free protease inhibitor mixture tablet (1 tablet/10 ml) (Roche Applied Science, 11836170001) for 30 min at 4°C to reduce unspecific binding. The pre-incubated lysate was then incubated with the immobilized GST fusion protein on a rotator for 1 hour at 4°C. The beads were washed five times with NETN buffer, boiled with 2x SDS gel loading buffer (125 mM Tris pH 7.5; 4% SDS; 0.04% bromphenol blue; 8% sucrose; 100 mM dithiothreitol) and subjected to SDS-PAGE. Gels were stained with Coomassie Brilliant Blue R-250 Dye (Thermo Fisher Scientific, #20278) to visualize GST fusion proteins and then vacuum dried. Signals from  $^{35}$ S-labeled proteins were detected by a Fujifilm bioimaging analyzer BAS-5000 (Fujifilm).

**Immunoprecipitation.** Cell lysis was carried out using immunoprecipitation buffer (20 mM Tris (pH 7.5), 137 mM NaCl, 1 mM MgCl<sub>2</sub>, 1 mM CaCl<sub>2</sub> and 1% NP-40) supplemented with a cOmplete Mini EDTA-free protease inhibitor mixture tablet (1 tablet/10 ml) (Roche Applied Science, 11836170001) along with benzonase (Millipore, 70746) (2 units/ml). The addition of benzonase is crucial for the release of chromatin-bound proteins into the supernatant, with MgCl<sub>2</sub> playing a pivotal role in facilitating its activity. Subsequently, the lysates were subjected to rotation at 4 °C for 30–60 minutes. After a centrifugation at 16000 g for 5 min at 4 °C, the supernatant was then incubated overnight at 4 °C with antibody-conjugated protein A Dynabeads (Life Technologies, 10001D). The immunoprecipitated complexes were then washed three times and then boiled at 95 °C in the presence of 1% SDS. The resulting samples were subjected to analysis through western blotting.

**Nuclear fractionation.** Trypsinized cells were centrifuged at 500 g for 5 min at 4 °C. The cell pellets were lysed in buffer I (150 mM NaCl, 50 mM HEPES, 25  $\mu$ g/ml digitonin (Sigma 11024-24-1) with protease and phosphatase inhibitors), pipetted up and down 10 times, and rotated for 30 min at 4 °C. Cells were then centrifuged at 3000 g for 5 min at 4 °C; the supernatant was collected as the cytosolic fraction. The pellets were then lysed with buffer II (150 mM NaCl, 50 mM HEPES, 1% NP40 (Sigma 74285), benzonase (Millipore, 70746) (2 units/ml), 1 mM MgCl<sub>2</sub>, 0.1%SDS, 0.5% sodium deoxycholate with protease and phosphatase inhibitors), pipetted up and down 10 times, vortexed for 10 s, and rotated for 1h at 4 °C. The lysate was centrifuged at 16000 g for 10 min at 4 °C. The supernatant was collected as the nuclear fraction.

**Western blotting.** For immunoblot analysis, cells were harvested in buffer containing 20 mM Tris, pH 7.5, 137 mM NaCl, 1 mM MgCl<sub>2</sub>, 1 mM CaCl<sub>2</sub>, 1% NP-40, supplemented with 1:100 Halt protease and phosphatase inhibitor cocktail (Thermo Fisher Scientific) and benzonase at 12.5 U/ml. The lysates were rotated at 4 °C for 1h, centrifuged at 16000g for 5 min and the supernatant was collected and boiled at 95°C in the presence of 1% SDS. The resulting supernatants were subjected to electrophoresis using SDS-PAGE gels. Proteins were transferred to nitrocellulose membrane (LI-COR, 926-31092) and stained with Ponceau S (Sigma, P35504). The membranes were then blocked in 5% non-fat milk in TBS at room temperature for 1 h. Primary antibodies were diluted in Intercept<sup>®</sup> (TBS) blocking buffer, following incubation at 4°C overnight. Membranes were subsequently washed 4x in TBS containing 0.1% Tween 20 (TBS-T), each for 10 min, followed by incubation of secondary antibodies at room temperature for 1 h, Intercept<sup>®</sup> (TBS) blocking buffer. The membranes were washed again 4x and the signal was detected using the LI-COR Odyssey<sup>®</sup> CLx imaging system. Quantification of the fluorescent signal was done using the ImageStudio software (LI-COR Biosciences-GmbH).

**Immunofluorescent confocal microscopy.** Cells were grown in 24-well plates with #1.5 round 12 mm coverslips (VWR, #631-0150) for immunofluorescence staining and fixed with 4% formaldehyde in PBS for 5 min at 37°C. For immunofluorescence staining, cells were washed once with 1x PBS and then permeabilized with 0.16% Triton X-100 (Sigma, X100) for 5 min. Next, cells were washed 2x with 1x PBS and blocked for 10 min in 3% bovine serum albumin (BSA) (Sigma, A7906). Subsequently, cells were incubated with primary antibodies diluted in 0.3% BSA; and 0.05% saponin in PBS for 1-2h at room temperature. After 5x wash in 1x PBS, cells were incubated with appropriate dilutions of Alexa Fluor secondary antibodies diluted in 0.3% BSA; and 0.05% saponin in PBS for 1h at room temperature. Depending on the experiment, after 5x washes in 1x PBS, cell nuclei were stained with 1 µg/ml DAPI (Thermo Fisher Scientific, #62248) diluted in 1x PBS for 5 min, followed by 2x final washes in 1x PBS. Coverslips were mounted using ProLong<sup>™</sup> Diamond Antifade mountant (Invitrogen, P36970). Cells were imaged using the Zeiss LSM800 (Carl Zeiss Microscopy) using a 40x NA1.2 water immersion lens. Images were collected in ZEN software (Zeiss). Optimal excitation and emission were determined using the Smart Setup function. All fluorescence channels were recorded at non-saturating levels, and settings were kept identical between all samples within replicates used for comparisons or quantifications.

**Image analysis.** For the quantification of the signal of LC3B in the nucleus, cells were treated with SFN at different time points and then imaged. All images within each replicate were taken using identical settings, based on the signal of 24h SFN-treated cells. Next, using the open-source image

analysis CellProfiler software, the nuclei were objectified using the appropriate CellProfiler pipeline and the signal of LC3B overlapping with these nuclei was quantified.

**AlphaFold prediction.** Predictions of protein complexes were performed using the ColabFold tool (Mirdita et al., 2022) via the ChimeraX (Pettersen et al., 2021) software. To optimize the NRF2 – LC3B binding prediction, we also used SWISS MODEL (Bertoline et al., 2023; Guex et al., 2009; Kiefer et al., 2009).

**Statistical analysis.** Statistical analysis was done using GraphPad Prism 10, with the specific statistical tests used being mentioned in the respective figure legend.

## RESULTS

### NRF2, NRF1 and DmCncC are ATG8 interactors

It has been reported previously by our group that the selective autophagy receptor p62/SQSTM1, participates in the antioxidative response by being transcriptionally induced upon oxidative stress, via the direct binding of NRF2 to an antioxidant response element (ARE) in its promoter (Jain et al., 2010). Additionally, it has been reported that p62 competes with NRF2 for binding to KEAP1, resulting in the stabilization of NRF2, while KEAP1 is degraded by autophagy (Jain et al., 2010; Komatsu et al., 2010; Lau et al., 2010; Taguchi et al., 2012). The corresponding mechanism in *D. melanogaster* is different in that Ref(2)P, a *D. melanogaster* orthologue, is unable to interact with DmKEAP1 (Jain et al., 2015). Contrarily, it has been shown that there is a direct interaction between DmAtg8a and DmKeap1 in *D. melanogaster* gut cells. This interaction possibly results in the removal of DmKeap1. Notably, CncC, the NRF2 orthologue in *D. melanogaster*, induces an increase in Atg8a levels and promotes autophagy independently of TFEB in the fat body and larval gut tissues (Jain et al., 2015). Since it was suggested that Ref(2)P is bypassed in the oxidative stress response in *D. melanogaster* and DmAtg8a is a direct interactor of DmKEAP1, we asked whether DmAtg8a or its mammalian homologs, the ATG8 family of proteins, interact directly with CncC or NRF2 respectively, affecting its stability.

As a first step, we confirmed that NRF2 and NRF1, a homolog of NRF2 (Chan et al., 1993), indeed binds to the ATG8 proteins using an in vitro GST pulldown (**Fig. 1A** and **1B**). For this assay, we used human ATG8 proteins tagged with GST. The binding affinity between the two transcription factors and recombinant GST-tagged ATG8 proteins strong for all the ATG8s (**Fig. 1C**). In addition, the interaction between CncC and DmAtg8a was also tested and confirmed (**Fig. 1D** and **1E**). The % binding relative to input for the NRF2-LC3B interaction was found to be above 30%, corresponding to a strong binding

affinity. The strong binding suggested that the interaction is highly likely to be occurring in cellulo. To confirm this, HEK293 cells were treated with 20  $\mu$ M of the NRF2 activator and mild oxidative stress inducer DL-Sulforaphane (SFN) or 10  $\mu$ M of the proteasomal inhibitor MG132 for 6 hours, to stabilize NRF2. Cells were then harvested, followed by endogenous LC3B immunoprecipitation (**Fig. 1F**). The results showed co-immunoprecipitation of NRF2 with LC3B in the SFN- and MG132-treated samples. To confirm the NRF2 – LC3B interaction in a cell line with increased levels of LC3B, we employed the HeLa ATG8KO cell line reconstituted with myc-LC3B. Cells were treated with SFN for 4 and 24 hours and cell extracts were immunoprecipitated using an anti-myc antibody (myc-trap) (**Fig. 1G**). Indeed, NRF2 co-immunoprecipitated with myc-LC3B in the treated samples. These results indicated a strong interaction between ATG8s and NRF2 in vitro and in cells under oxidative stress conditions.

### **LC3B accumulates in the nucleus under oxidative stress**

The nuclear spatiotemporal behavior of the ATG8 family of proteins has been widely unclear and there are only a few studies, focused on LC3B, that have attempted to study it (Drake et al., 2010; Kraft et al., 2014, 2016; Shim et al., 2020; Ying et al., 2009; Zhou et al., 1997). This might be due to their small size and ability to passively diffuse through the nuclear envelope without any requirement for active shuttling. Specifically, the dynamics of LC3B localization under oxidative stress have previously been unexplored. To determine the functionality of the interaction between LC3B and NRF2, we decided to evaluate the spatiotemporal behavior of LC3B under oxidative stress. To examine this, we treated U2OS cells with SFN for 4 and 24 hours and stained for endogenous LC3B (**Fig. 2A and 2B**). We observed a statistically significant increase in the nuclear signal of endogenous LC3B after treatment with SFN for 24 hours. The increased nuclear LC3B signal doesn't necessarily suggest that there is a redistribution of LC3B from the cytoplasm to the nucleus, as the stabilization event of the total LC3B protein would be evident also in the nucleus, due to the LC3B's passive diffusion. This was further assessed by subcellular fractionation of U2OS cells after treatment with SFN for 4, 6 and 8 hours, where LC3B-I was shown to be more prominent in the nucleus in the sample that was treated for 8 hours with SFN (**Fig. 2C**).

Due to the previously studied role of p62/SQSTM1 in the recruitment of nuclear polyubiquitinated proteins to nuclear p62 bodies through nucleocytoplasmic shuttling (Pankiv et al., 2010) and its previously mentioned role in the NRF2-KEAP1 signaling mechanism (Jain et al., 2010, 2015), we decided to evaluate whether LC3B accumulates in the nucleus under oxidative stress because of its interaction with p62/SQSTM1. To examine this, we treated U2OS cells with Leptomycin B (LMB), an irreversible inhibitor of the nuclear export receptor Exportin-1, for 2 hours and stained for endogenous LC3B and p62/SQSTM1 (**Fig. S1A**). While we did observe a strong accumulation of p62/SQSTM1 in the nucleus in cells treated with LMB, the nuclear LC3B signal was not affected (**Fig. S1B**). This suggested that p62/SQSTM1 is not competent of driving nuclear localization of LC3B by itself. At the



same time, we wondered whether NRF2 is degraded by autophagy. As it was previously mentioned, p62/SQSTM1 interacts with KEAP1, NRF2's negative regulator, indirectly affecting NRF2 stability through autophagy (Jain et al., 2010; Taguchi et al., 2012). U2OS cells were treated with either DMSO or SFN for 24 hours, coupled with either Bafilomycin A1 or MG132 for 4 hours (**Fig. 2D**). Interestingly, we observed no statistically significant difference in the NRF2 protein levels between the sample treated with SFN only and the sample treated with SFN and Bafilomycin A1 (**Fig. 2E**). That suggested that NRF2 is not an autophagic substrate under oxidative stress conditions and that its interaction with LC3B is not related to autophagy.

The nucleocytoplasmic transport of LC3B under starvation-induced autophagy has been described to be dependent on an acetylation-deacetylation cycle (Huang et al., 2015). That led us to determine whether the acetylation status of LC3B could play a role in its interaction with NRF2. Huang et al. suggested that under basal conditions, an acetylated pool of LC3B localizes in the nucleus, and during starvation, LC3B is deacetylated at the K49 and K51 residues by sirtuin 1 (SIRT1), which allows LC3B to return to the cytoplasm. To test this, we performed an *in vitro* GST pulldown, testing the interaction between NRF2 and LC3B wild-type, K49Q/K51Q acetyl-mimic or K49R/K51R deacetyl-mimic mutants (**Fig. 2F** and **2G**). We observed that NRF2 showed a clear preference for LC3B wild-type and K49R/K51R but not to LC3B K49Q/K51. This suggested that acetylated LC3B is unable to bind to NRF2.

### **The Neh5 domain of NRF2 is required for its interaction with LC3B**

To acquire a better understanding of the functionality of the interaction between NRF2 and LC3B, we performed an interaction mapping to determine which region of NRF2 is crucial for the binding to LC3B. To this end, we created deletion constructs of NRF2 encompassing different domains and performed an *in vitro* GST pulldown using recombinant GST-tagged LC3B (**Fig. 3A** and **3B**). We identified the aa 86-386 region in NRF2 as the one where the binding occurs, because when it was truncated, the interaction with LC3B was lost. For better resolution, we performed a peptide array screen for potential LC3-interacting region (LIR) motifs in NRF2 (**Fig. 3C**). The peptide array, containing overlapping 20-mer peptides of NRF2 moved by increments of three amino acids to cover the 605 amino acids full-length sequence, was probed with GST-GABARAP, the strongest in binding affinity to NRF2 among the ATG8 proteins (**Fig. 1B** and **1C**). The array revealed four putative LIR motifs (**Fig. 3C**), with putative LIR 2 on the panel being the most prominent, after testing the others in *in vitro* GST pulldown assays (experiments not shown). This particular putative LIR is located on the aa 178-208 or Neh5 domain of NRF2. To assess whether the interaction between NRF2 and LC3B has any differences from the interaction between NRF2 and GABARAP, we performed an *in vitro* GST pulldown assay using myc-tagged NRF2 wild-type or a  $\Delta$ 178–208 truncation and *in vitro* translated LC3B (**Fig. 3D** and

**3E**). Interestingly, we observed that while the binding of LC3B to NRF2  $\Delta$ 178–208 was eliminated, the binding of GABARAP to NRF2  $\Delta$ 178–208 was significantly decreased but not completely abolished, leaving a significant residual binding of  $\approx$  40% when compared to the binding with NRF2 wild-type. This suggested that an additional region of NRF2 different than the aa 178 – 208 Neh5 domain is responsible for the residual binding to GABARAP. For this reason, we decided not to explore the functionality of the interaction between NRF2 and GABARAP. To further study the presence of a canonical LIR in the Neh5 domain, we constructed truncations within this NRF2 domain (**Fig. 3F**) and tested them in an in vitro GST pulldown assay against recombinant GST-LC3B (**Fig. 3G** and **3H**). Among the truncations we tested in the Neh5 domain, only the  $\Delta$ 196–202 was redundant for the binding to GST-LC3B. This suggested that the 20 residues in the region between aa 176 and 196 are required for the interaction between NRF2 and LC3B.

### **Mutational analyses reveal the <sup>188</sup>WEEL<sup>191</sup> residues to be crucial for the binding of NRF2 to LC3B**

Next, we wanted to determine which specific residues of NRF2, in the region between aa 175 and 195, are crucial for binding to LC3B. First, we used a bioinformatics tool called ConSurf, to calculate the evolutionary conservation of amino acid positions in the Neh5 domain (Ashkenazy et al., 2010; Glaser et al., 2003) (**Fig. 4A**). According to the conservation scale, the most conserved region in the Neh5 domain is between the aspartic acid (D) on position 183 and the asparagine (N) on position 204. As previously shown, the aa 196-202 region is less relevant for binding with LC3B, so we focused on the 20 residues in the region between aa 176 and 196. A canonical LIR motif is described by the core sequence: [W/F/Y]<sub>0</sub>-X<sub>1</sub>-X<sub>2</sub>-[I/L/V]<sub>3</sub>, where X is any amino acid (Birgisdottir et al., 2013; Johansen & Lamark, 2020). The LIR-docking site (LDS) is described as the site on the ATG8 protein that is responsible for the interaction with the LIR motif. The LDS contains two hydrophobic pockets where hydrophobic pocket 1 (HP1) accommodates the conserved aromatic residue (W/F/Y) and hydrophobic pocket 2 (HP2) the conserved hydrophobic residue (I/L/V) of the core LIR motif. The binding affinity and specificity of the interaction between the LIR motif of a protein and the ATG8 proteins are also affected by residues N- and C- terminal to the core motif (Wirth et al., 2019). On the Neh5 domain, the sequence that fits the canonical LIR motif core sequence is the W<sup>188</sup>XXL<sup>191</sup>, with tryptophan (W) being in position 0 of the core sequence and leucine (L) being in position 3. Taking these into consideration, we performed a set of alanine substitution mutations in the putative LIR and flanking regions of the Neh5 domain of NRF2, to establish whether the interaction with LC3B is based on a LIR-LDS interaction. To validate this hypothesis, we tested these mutations by in vitro translating the constructs and performing an in vitro GST pulldown assay against recombinant GST-LC3B (**Fig. 4B** and **4C**). Interestingly, while we did observe that the binding of the NRF2 W188A/L191A core LIR mutant to LC3B was significantly reduced as we hypothesized, there were other alanine substitutions on the Neh5 domain that had the same effect, like the NRF2 D183A and the E189A/E190A mutations. This result pointed to a canonical LIR-LDS interaction hypothesis. The F52 and L53 residues have been previously

shown to be important for some LIR-LDS interactions (Behrends et al., 2010; Birgisdottir et al., 2013; Johansen & Lamark, 2020; Rogov et al., 2023), with F52 being among the residues that form the HP2 hydrophobic site and L53 among the residues that form the HP1, on LC3B. We decided to test alanine substitutions of these residues to see if the *in vitro* direct binding of NRF2 to LC3B would be affected. We also decided to include the R69A which is part of a triple arginine motif (R68-70), which has been shown to be important for the size of the slowly diffusing complexes nuclear LC3B associates with (Kraft et al., 2014, 2016), as well as the R10A, R10A/R11A and a combinatorial R10A/R70A. While the F52A and L53A LDS mutants did not affect the binding to NRF2, the R10A, R10A/R11A, R69A and most prominently R10A/R70A strongly reduced the binding (**Fig. 4D** and **4E**).

To get a better understanding of the NRF2-LC3B interaction, we predicted the structure of NRF2 Neh5 domain amino acids 181-212 in complex with full-length LC3B using the ColabFold tool, which utilizes the AlphaFold2 prediction model (Mirdita et al., 2022; Pettersen et al., 2021). The initial prediction model showed that the Neh5 domain of NRF2 has a helical secondary structure docked into the LDS region of LC3B. However, the LIR sequence is oriented in the opposite way of a canonical LIR with the aromatic W188 residue docked into the HP2 hydrophobic pocket which is more narrow than the HP1 (Rogov et al., 2023). We then performed AlphaFold2 predictions using the evolutionarily conserved transactivation regions of NRF1 (NF2EL1) and NFE2 (p45), members of the Cnc family of transcription factors (**Fig. S2A** and **S2B**). We saw that in these predictions, the HP1 and HP2 hydrophobic pockets of LC3B are both engaged in the binding interface with the respective regions of NRF1 and NFE2, which fits with the already described LIR – LDS model. To optimize our NRF2 – LC3B binding prediction, we utilized the SWISS MODEL (Bertoline et al., 2023; Guex et al., 2009; Kiefer et al., 2009) in order to predict the NRF2 – LC3B binding interface using the NFE2 – LC3B prediction as a template (**Fig. 4F**). In this model, the Neh5 domain was not predicted as helical in its entirety, but as a and the HP1 and HP2 hydrophobic pockets are engaged in the interface with the W188 and L191 residues respectively. It also confirmed our mutational analysis which rendered the R10/R11 and R69/R70 residues to be important for the binding interface, as they facilitate electrostatic interactions with different residues on the Neh5 domain. This suggested that the NRF2 – LC3B binding interface has the attributes of a canonical LIR – LDS interaction.

### **NRF2 localizes with nuclear LC3B under oxidative stress conditions**

To further examine the functionality of the interaction between NRF2 and LC3B, we asked in which subcellular compartment is the interaction taking place. As it has previously been established, NRF2 plays a crucial role in initiating the transcription of antioxidative genes by recruiting co-activators and transcription machinery components. Among these, p300/CBP was identified as an early co-activator that interacts with NRF2, with the Neh5 domain being crucial for this interaction (Kato et al., 2001; J. Zhang et al., 2007). It was also shown that following this interaction, the p300/CBP complex acetylates

the C' terminal Neh1 domain under oxidative stress, enhancing NRF2's DNA binding ability (Sun et al., 2009). The acetylation of the Neh3 domain of NRF2 by p300, revealed in another study (Kawai et al., 2011) is also functionally relevant, particularly for the activation of the HO-1 target gene. Other cofactors that are important for the drive of NRF2 target genes transcription are the small musculoaponeurotic fibrosarcoma proteins (sMAFs) (Katsuoka et al., 2005), particularly MafG, which play a key role in the transcriptional activation of the target genes of NRF2. To examine where the interaction occurs, we performed a bimolecular fluorescence complementation (BiFC) assay where the fluorescent protein tag NeonGreen was split into two tags: one with a non-fluorescent  $\beta$  barrel structure of NeonGreen lacking the 11th  $\beta$  strand (NeonGreen 1-10) and another tag with the missing 11th  $\beta$  strand (NeonGreen -11) (Feng et al., 2019). If they are tagged on separate proteins and the NeonGreen fluorescent signal is emitted, then that suggests the proteins are colocalizing and potentially interacting. We tested the complementation by co-expressing NeonGreen 1-10-tagged NRF2 and NeonGreen- 11-tagged LC3B (**Fig. 5A**) and observed that the NRF2 – LC3B complex is localized in the nucleus. As controls for the BiFC assay, we co-expressed NeonGreen 1-10-tagged NRF2 with either NeonGreen -11-tagged KEAP1 or NeonGreen -11-tagged MafG, already studied interactions that are occurring in the cytoplasm and the nucleus respectively (**Fig. S3A** and **S3B**). In addition, we performed endogenous staining for NRF2 and LC3B in U2OS cells treated with SFN for 8 and 24 hours, to confirm the nuclear compartment as the place where the interaction is occurring (**Fig. 5B**). Interestingly, we verified that LC3B is accumulating in the nucleus after 24 hours of SFN treatment, as it was also shown in **Fig. 2A**, and also that some dots of LC3B are colocalizing with NRF2 dots. This suggested that indeed the interaction between NRF2 and LC3B is occurring in the nucleus, leading us to hypothesize that LC3B might have a role in the transcriptional regulation of NRF2 target genes.

### **LC3B and p300 bind competitively to the Neh5 domain of NRF2 to regulate the transcriptional activation of its target genes**

The importance of the Neh5 domain is already established in the transcriptional complex between NRF2 and p300/CBP (Katoh et al., 2001; Kawai et al., 2011; Sun et al., 2009; Zhang et al., 2007). Hence, we hypothesized that LC3B may be competing with p300/CBP for binding to the Neh5 domain to negatively regulate the transcriptional activity of NRF2. To test this, we performed in vitro GST pulldown assays to look for competition between LC3B and full-length p300 as well as p300 amino acids 1660-2414. The latter C-terminal piece of p300 was previously mapped to bind to NRF2 (Sun et al., 2009). We observed that by increasing the amount of full-length p300, or aa 1660-2414 of p300, in the assay, the binding of NRF2 to recombinant GST-LC3B was reduced (**Fig. S4A** and **B**). This suggested that there is a competition between LC3B and p300 for binding to NRF2. In order to increase the resolution when it comes to the interaction between NRF2 and p300, we tested the binding of p300's TAZ2 domain (amino acids 1660 to 1810), known as a protein-protein interaction domain that binds to E1A and various other transcription factors, including B-Myb, C/EPB $\epsilon$ , FOXO3a, HIF-1 $\alpha$ , p53, p63,

p73, STAT1, and STAT2 (Burge et al., 2009; Dames et al., 2002; Delvecchio et al., 2013; Ferreon et al., 2009; Krauskopf et al., 2018; Krois et al., 2016; Miller Jenkins et al., 2015; Oka et al., 2012; Ortega et al., 2018; Wang et al., 2012; Wojciak et al., 2009; L. Xu et al., 2023), to NRF2 using a bimolecular fluorescence complementation assay (**Fig. S3C**). The complementation was positive, and the complex formed dot-like structures in the nucleus. This result, coupled with the *in vitro* competition assay of NRF2, GST-LC3B and the myc-tagged p300 TAZ2 (**Fig. 6A** and **6B**), as well as the sharing of many of the same contact residues in the Neh5 predicted from the AlphaFold2 models for Neh5 bound to LC3B and to p300 TAZ2 (**Fig. 6C**), suggested that LC3B competed with the TAZ2 domain of p300 for binding on the Neh5 domain of NRF2.

To evaluate whether this competition is of functional significance, we stably expressed HA-tagged LC3B in a HEK293T cell line and performed RT-qPCR on target genes of NRF2, after treating the cells with SFN for 18 hours to induce NRF2 protein stabilization (**Fig. S4C** and **S4D**). We observed that the mRNA levels of two NRF2 target genes, HO-1 and TXNRD1, were significantly reduced in the cell line where HA-LC3B was stably expressed. To verify this result, we overexpressed simultaneously HA-tagged p300 full-length and myc-tagged LC3B in U2OS cells, followed by treatment with SFN for 18 hours (**Fig. 6D**). Notably, there was a significant reduction in the mRNA levels of the HO-1, NQO1 and GCLC target genes, as well as a downward trend in G6PD and GCLM. In addition, we performed a luciferase assay using the ARE promoter of the NQO1 target gene to confirm the effect that the competition between LC3B and p300 has on the binding of NRF2 to ARE (**Fig. 6E**). Interestingly, we saw that there was a downward trend in the promoter's induction when LC3B was overexpressed together with NRF2, relative to when NRF2 was overexpressed alone. A downward in the NQO1 promoter's induction was also observed when LC3B was tagged with NLS, validating that the nuclear LC3B is the one responsible for NRF2 transcriptional regulation (**S4E**). These results indicate that LC3B has indeed a negative effect on the transcriptional activation of the target genes of NRF2, which is facilitated by its competition TAZ2 domain of p300 on NRF2's Neh5.

## DISCUSSION

The network of interactions in NRF2's transcriptional complex and how it may affect its transcriptional activity after its translocation to the nucleus has not been extensively studied. Here we show that NRF2 shows a strong binding affinity to LC3B, as well as other members of the ATG8 family of proteins. After mapping the NRF2 – LC3B interaction, we demonstrate that the binding of LC3B to NRF2 was confined to the Neh5 domain of NRF2 (**Fig. 1A**), an important transactivation region which has been shown to be important for NRF2's transcriptional activation by p300/CBP (Katoh et al., 2001; J. Zhang et al., 2007). We also explore the binding between LC3B and NRF2, which, following a mutational analysis and AlphaFold2 predictions, seems to adhere to a canonical LIR-LDS interaction (Birgisdottir et al., 2013; Johansen & Lamark, 2020). In addition, we also show that the competition between LC3B

and p300 for binding on the Neh5 domain is functionally relevant to the transcriptional activity of NRF2, with LC3B taking on the role of a negative regulator. To our knowledge, the present work is the first study demonstrating that a competition between LC3B and p300 modulates the transcriptional complex of NRF2, affecting its ability to induce the antioxidative response.

Our group has spearheaded the discovery that p62/SQSTM1, a selective autophagy receptor, is a target gene of NRF2 and that it generates a positive feedback loop by inducing ARE-driven gene transcription (Jain et al., 2010, 2015). The notion that a central autophagic protein plays a direct role in the antioxidative response mechanism driven by NRF2, pointed us to the direction that other proteins associated with the autophagic pathway might be involved in this process. Following trends in the field of autophagy that demonstrate that ATG8 proteins exhibit autophagy-independent functions in areas that range from genome stability and transcriptional regulation to metabolic homeostasis and senescence (Dou et al., 2015; Jacomin et al., 2020; Jiménez-Moreno et al., 2023; L. Wang et al., 2021; Ying et al., 2009), we decided to test if there is a direct interaction between NRF2 and members of the ATG8 family of proteins (**Fig. 1B**). In the literature, the majority of ATG8 roles involve membrane scaffolding of LIR-containing core autophagy components during autophagy initiation, attachment of selective autophagy receptors (with or without cargo) to the inner surface of the phagophore as well as roles in autophagosome to lysosome fusion and transport (Johansen & Lamark, 2020).

While usually the association between members of the ATG8 family and other proteins, points to an autophagy-dependent degradative role, a recent report provided evidence that LXM1B, a transcription factor that helps sustain efficient cytoplasmic quality control and mitochondrial function in midbrain dopaminergic neurons (Doucet-Beaupré et al., 2016; Laguna et al., 2015), engages the ATG8s via LIR-like interactions as their co-factors, positively influencing transcriptional activities in the nucleus (Jiménez-Moreno et al., 2023; Kournoutis & Johansen, 2023). Looking closely to the Neh5 domain, we initially postulated that the interaction between NRF2 and LC3B is also mediated by a LIR that would bind to the LIR docking site (LDS) of the ATG8s. The amino acidic sequence of the Neh5 domain did have the attributes of a LIR sequence, specifically residues that can fit in the described core sequence:  $[W/F/Y]_0-X_1-X_2-[I/L/V]_3$ , where X is any amino acid (reviewed in Birgisdottir et al., 2013). Our initial hypothesis after the prediction of the NRF2 Neh5 – LC3B interaction using AlphaFold2, was that the Neh5 domain is helical when in complex with LC3B, and that the direction of the Neh5 sequence is reversed when compared to a canonical LIR – LDS interaction (Rogov et al., 2023). However, after utilizing the SWISS MODEL ((Bertoline et al., 2023; Guex et al., 2009; Kiefer et al., 2009) to model the NRF2 – LC3B prediction using the NFE2 (p45) – LC3B prediction as a template, we acquired a structure that fits to a canonical LIR – LDS binding interface. The limitations of structural predictions, including that of AlphaFold2, doesn't allow us to make a concrete hypothesis about how the interaction between NRF2 and LC3B is mediated. Further experiments using a mutational analysis method are

required in order to confidently assess both the direction of the Neh5 domain when bound to LC3B and the specific residues important for the binding interface. It is also important to consider that LIR-flanking residues which can be crucial (Johansen & Lamark, 2020). For example, the D183A alanine substitution did have a strong effect in the binding between NRF2 and LC3B, and D183 was not predicted to be an engaging residue in the AlphaFold2 model. In addition, after mutating the LDS docking site of LC3B using the F52A and L53A alanine substitutions (Pankiv et al., 2007), we observed that the interaction was not affected. We speculate that this is because in the specific binding interface, the F52 and L53 residues are redundant. At the same time, the R10A, R69A and R10A/R70A mutants led to a very strong reduction in binding. This suggests that it is not only the hydrophobic pockets in the LDS of LC3B that are mediating the interaction, but also the R10/R11 residues of the N' terminal arm and the R69/R70 motif, as it was clearly shown in the NRF2 – LC3B complex prediction.

The binding of LC3B to NRF2 on the Neh5 domain strongly indicated that LC3B has a role in the regulation of NRF2's transcriptional activity. Indeed, studies have demonstrated that the Neh5 domain is differentially utilized in the transactivation of cytoprotective genes (Kawai et al., 2011; Sun et al., 2009). These reports show that this transactivation occurs via the initial binding of p300 on the Neh5 and the consecutive acetylations by the later on different residues in the C' terminal regions Nhe1 and Neh3, modifications that augment the binding between NRF2 and the DNA on the promoters of its target genes. In order for LC3B to function as a regulator of the transcriptional activity of NRF2, the interaction between the two would be expected to occur in the nucleus. By using a bimolecular fluorescence complementation assay and confocal microscopy, we verified that the interaction was localized in the nuclear compartment (**Fig. 5A** and **5B**). It is important to question at this point, whether the lipidation of LC3B is playing a role in the interaction with NRF2. In experiments not shown here, we observed that overexpression of an LC3B G120A lipidation-null mutant, had a similar negative transcriptional effect as LC3B wild-type, which points to the conclusion that lipidation has no role in the LC3B's transcriptional activity. We can't exclude the fact that the process of LC3B lipidation affects the available pool of non-lipidated LC3B and its shuttling to the nucleus, thus exerting its functions in collaboration with transcription factors. It would be interesting to test whether, in an ATG4BKO cell line (ATG4B being an important component of the LC3B conjugation system which cleaves the precursor LC3B, leading its non-lipidated soluble form (Betin et al., 2013; Rasmussen et al., 2017; Satoo et al., 2009)), there would be a downregulatory effect in NRF2 target gene regulation. Or that other posttranslational modifications are at play, which either affect the direct interaction of LC3B with nuclear components and proteins or the shuttling of LC3B in and out of the nucleus and hence, its availability in that component.

The next step was to demonstrate that the access of p300/CBP to NRF2 is affected by the competitive interplay of LC3B in the same region. Previous reports showed that the TAZ2 domain is an important structure in the catalytic core of p300, associating with intrinsically disordered proteins but also transcription factors like E1A (Delvecchio et al., 2013; Ibrahim et al., 2022; Xu et al., 2023). We created a myc-tagged p300 aa 1660-1810 (TAZ2) construct and confirmed its binding to NRF2. Next, by employing it in an in vitro competition assay, we demonstrated that increasing amounts of the TAZ2 construct are able to significantly reduce the binding capacity of NRF2 to recombinant LC3B.

Our observation that LC3B competes with the TAZ2 domain of p300 for binding to NRF2, set the groundwork for investigating whether LC3B has a negative effect on the expression of NRF2's target genes. Interestingly, we found that there was a downward trend in the expression levels of most NRF2 target genes we checked following overexpression or stable expression of LC3B under oxidative stress, with that trend being statistically significant mainly for the *HO-1* gene. We are not aware why the significance in the downregulation of the *HO-1* gene is higher compared to other NRF2 target genes but we speculate that it can be because of differences in the co-factor requirements for its activation. For example, the ATF4 transcription factor has been described to lead to a specific *HO-1* activation in collaboration with NRF2 (Raghunath et al., 2018; Rössler & Thiel, 2017). Since the interaction mapping between ATF4 and NRF2 hasn't been performed, it could be possible that LC3B is negatively affecting it in a more prominent way than in its competition with p300. In addition, the Neh5 domain has been shown to be important to other co-factors of NRF2, like the MED16 subunit of the Mediator complex (Sekine et al., 2016) or BRG1, the central ATPase subunit of the SWI/SNF chromatin-remodeling complex (J. Zhang et al., 2006), prompting us to consider that the target genes that we tested in this manuscript are a fraction of those affected by the presence of LC3B in the nucleus and its binding with NRF2.

In contrast to the previously published study (Jiménez-Moreno et al., 2023), where LC3B was shown to function as a co-factor, positively regulating the transcriptional activity of LMX1B on its autophagy-related target genes, in this report we demonstrate that LC3B assumes the role of a negative regulator of the antioxidative response. The reason for this can be that LC3B assists with the recruitment of other co-factors of LMX1B in the first case, while in the case of NRF2, we show that it affects the binding of p300 on the latter. The mechanisms and context for the activation of LMX1 and NRF2 are different, and that could also explain why LC3B has a duality in transcriptional regulation. It is also important to note that LC3B has been associated with heterochromatic domains (Dou et al., 2015), specifically the lamin-associated domains (LADs) which could point to its role being mainly repressive.

The work presented here provides insight into the question of participation of ATG8s in transcriptional mechanisms, as well as into the activity of NRF2 in the nucleus and how such an activity can be



terminated. We posit that the Neh5 domain of NRF2, while the transcriptional factor is in the nucleus, is the potential target of both p300 and LC3B and that the interaction of LC3B with that domain is atypical compared to that of a canonical LDS to LIR interaction. Our results are particularly novel because we demonstrate for the first time that LC3B is negatively affecting NRF2's target gene expression, as well as that it accumulates slowly in the nucleus under oxidative stress, possibly in order to allow the antioxidant response to unfold before introducing a brake, acting as a cytoprotective agent. In order to elucidate the role of ATG8s in transcriptional regulation and association in transcriptional complexes, further studies are required

## **ACKNOWLEDGEMENTS**

We thank the Advanced Microscopy Core Facility at the Faculty of Health Sciences, UiT – The Arctic University of Norway for assistance and use of instruments. We thank Zambarlal Bhujabal for constructing the plasmids: pDest-NeonGreen 1-10, -11. Molecular graphics and analyses were performed using UCSF ChimeraX, developed by the resource for Biocomputing, Visualization and Informatics at the University of California, San Francisco, with support from the National Institutes of Health R01-GM129325 and the Office of Cyber Infrastructure and Computational Biology, National Institute of Allergy and Infectious Diseases. This work was funded by the TOPPFORSK (grant number 249884) program of the Research Council of Norway to T.J.

## **AUTHOR CONTRIBUTIONS**

AK designed the experiments, performed most of the experiments and interpreted the results. BKS performed the initial GST-pulldown and luciferase assays. HLO performed the AlphaFold predictions and the respective interpretation. GE performed repetitions of GST pulldown assays. AØ performed cell work. AK, BKS, AJ, TL and TJ conceived the project and analyzed the data. AK, TL and TJ wrote the manuscript.

## REFERENCES

- Ashkenazy, H., Erez, E., Martz, E., Pupko, T., & Ben-Tal, N. (2010). ConSurf 2010: calculating evolutionary conservation in sequence and structure of proteins and nucleic acids. *Nucleic Acids Research*, *38*(suppl\_2), W529–W533. <https://doi.org/10.1093/NAR/GKQ399>
- Behrends, C., Sowa, M. E., Gygi, S. P., & Harper, J. W. (2010). Network organization of the human autophagy system. *Nature*, *466*(7302), 68–76. <https://doi.org/10.1038/nature09204>
- Bertoline, L. M. F., Lima, A. N., Krieger, J. E., & Teixeira, S. K. (2023). Before and after AlphaFold2: An overview of protein structure prediction. *Frontiers in Bioinformatics*, *3*, 1120370. <https://doi.org/10.3389/FBINF.2023.1120370/BIBTEX>
- Betin, V. M. S., Singleton, B. K., Parsons, S. F., Anstee, D. J., & Lane, J. D. (2013). Autophagy facilitates organelle clearance during differentiation of human erythroblasts. *Autophagy*, *9*(6), 881–893. <https://doi.org/10.4161/AUTO.24172>
- Birgisdottir, Á. B., Lamark, T., & Johansen, T. (2013). The LIR motif - crucial for selective autophagy. In *Journal of Cell Science* (Vol. 126, Issue 15, pp. 3237–3247). J Cell Sci. <https://doi.org/10.1242/jcs.126128>
- Brown, S. L., Sekhar, K. R., Rachakonda, G., Sasi, S., & Freeman, M. L. (2008). Activating transcription factor 3 is a novel repressor of the nuclear factor erythroid-derived 2-related factor 2 (Nrf2)-regulated stress pathway. *Cancer Research*, *68*(2), 364–368. <https://doi.org/10.1158/0008-5472.CAN-07-2170>
- Burge, S., Teufel, D. P., Townsley, F. M., Freund, S. M. V., Bycroft, M., & Fersht, A. R. (2009). Molecular basis of the interactions between the p73 N terminus and p300: Effects on transactivation and modulation by phosphorylation. *Proceedings of the National Academy of Sciences of the United States of America*, *106*(9), 3142–3147. <https://doi.org/10.1073/PNAS.0900383106/ASSET/ECB4966A-5673-4270-9D38-CECAC1E7840B/ASSETS/GRAPHIC/ZPQ9990970240006.JPEG>
- Chan, J. Y., Han, X. L., & Yuet Wai Kan. (1993). Cloning of Nrf1, an NF-E2-related transcription factor, by genetic selection in yeast. *Proceedings of the National Academy of Sciences of the United States of America*, *90*(23), 11371–11375. <https://doi.org/10.1073/PNAS.90.23.11371>
- Chen, Y., McMillan-Ward, E., Kong, J., Israels, S. J., & Gibson, S. B. (2008). Oxidative stress induces autophagic cell death independent of apoptosis in transformed and cancer cells. *Cell Death and Differentiation*, *15*(1), 171–182. <https://doi.org/10.1038/sj.cdd.4402233>
- Cullinan, S. B., Gordan, J. D., Jin, J., Harper, J. W., & Diehl, J. A. (2004). The Keap1-BTB protein is an adaptor that bridges Nrf2 to a Cul3-based E3 ligase: oxidative stress sensing by a Cul3-Keap1 ligase. *Molecular and Cellular Biology*, *24*(19), 8477–8486. <https://doi.org/10.1128/MCB.24.19.8477-8486.2004>
- Dames, S. A., Martinez-Yamout, M., De Guzman, R. N., Jane Dyson, H., & Wright, P. E. (2002). Structural basis for Hif-1 $\alpha$ /CBP recognition in the cellular hypoxic response. *Proceedings of the National Academy of Sciences of the United States of America*, *99*(8), 5271–5276. <https://doi.org/10.1073/PNAS.082121399/ASSET/BDC0A086-4B15-4C3D-8C3B-B8E3B00CA177/ASSETS/GRAPHIC/PQ0821213004.JPEG>

- Delvecchio, M., Gaucher, J., Aguilar-Gurrieri, C., Ortega, E., & Panne, D. (2013). Structure of the p300 catalytic core and implications for chromatin targeting and HAT regulation. *Nature Structural & Molecular Biology*, *20*(9), 1040–1046. <https://doi.org/10.1038/nsmb.2642>
- Dou, Z., Xu, C., Donahue, G., Shimi, T., Pan, J. A., Zhu, J., Ivanov, A., Capell, B. C., Drake, A. M., Shah, P. P., Catanzaro, J. M., Ricketts, M. D., Lamark, T., Adam, S. A., Marmorstein, R., Zong, W. X., Johansen, T., Goldman, R. D., Adams, P. D., & Berger, S. L. (2015). Autophagy mediates degradation of nuclear lamina. *Nature*, *527*(7576), 105–109. <https://doi.org/10.1038/nature15548>
- Doucet-Beaupré, H., Gilbert, C., Profes, M. S., Chabrat, A., Pacelli, C., Giguère, N., Rioux, V., Charest, J., Deng, Q., Laguna, A., Ericson, J., Perlmann, T., Angg, S. L., Cicchetti, F., Parent, M., Trudeau, L. E., & Lévesque, M. (2016). Lmx1a and Lmx1b regulate mitochondrial functions and survival of adult midbrain dopaminergic neurons. *Proceedings of the National Academy of Sciences of the United States of America*, *113*(30), E4387–E4396. [https://doi.org/10.1073/PNAS.1520387113/SUPPL\\_FILE/PNAS.201520387SI.PDF](https://doi.org/10.1073/PNAS.1520387113/SUPPL_FILE/PNAS.201520387SI.PDF)
- Drake, K. R., Kang, M., & Kenworthy, A. K. (2010). Nucleocytoplasmic distribution and dynamics of the autophagosome marker EGFP-LC3. *PLOS ONE*, *5*(3), e9806. <https://doi.org/10.1371/journal.pone.0009806>
- Feng, S., Varshney, A., Coto Villa, D., Modavi, C., Kohler, J., Farah, F., Zhou, S., Ali, N., Müller, J. D., Van Hoven, M. K., & Huang, B. (2019). Bright split red fluorescent proteins for the visualization of endogenous proteins and synapses. *Communications Biology*, *2*(1). <https://doi.org/10.1038/S42003-019-0589-X>
- Ferreon, J. C., Martinez-Yamout, M. A., Dyson, H. J., & Wright, P. E. (2009). Structural basis for subversion of cellular control mechanisms by the adenoviral E1A oncoprotein. *Proceedings of the National Academy of Sciences of the United States of America*, *106*(32), 13260–13265. [https://doi.org/10.1073/PNAS.0906770106/SUPPL\\_FILE/0906770106SI.PDF](https://doi.org/10.1073/PNAS.0906770106/SUPPL_FILE/0906770106SI.PDF)
- Forman, H. J., & Zhang, H. (2021). Targeting oxidative stress in disease: promise and limitations of antioxidant therapy. *Nature Reviews Drug Discovery*, *20*(9), 689–709. <https://doi.org/10.1038/s41573-021-00233-1>
- Glaser, F., Pupko, T., Paz, I., Bell, R. E., Bechor-Shental, D., Martz, E., & Ben-Tal, N. (2003). ConSurf: Identification of Functional Regions in Proteins by Surface-Mapping of Phylogenetic Information. *Bioinformatics*, *19*(1), 163–164. <https://doi.org/10.1093/BIOINFORMATICS/19.1.163>
- Guex, N., Peitsch, M. C., & Schwede, T. (2009). Automated comparative protein structure modeling with SWISS-MODEL and Swiss-PdbViewer: A historical perspective. *Electrophoresis*, *30*(S1), S162–S173. <https://doi.org/10.1002/ELPS.200900140>
- He, W., Hu, C. X., Hou, J. K., Fan, L., Xu, Y. W., Liu, M. H., Yan, S. Y., Chen, G. Q., & Huang, Y. (2014). Microtubule-Associated Protein 1 Light Chain 3 Interacts with and Contributes to Growth Inhibiting Effect of PML. *PLOS ONE*, *9*(11), e113089. <https://doi.org/10.1371/JOURNAL.PONE.0113089>
- Horie, Y., Suzuki, T., Inoue, J., Iso, T., Wells, G., Moore, T. W., Mizushima, T., Dinkova-Kostova, A. T., Kasai, T., Kamei, T., Koshihara, S., & Yamamoto, M. (2021). Molecular basis for the disruption of Keap1–Nrf2 interaction via Hinge & Latch mechanism. *Communications Biology*, *4*(1), 1–11. <https://doi.org/10.1038/s42003-021-02100-6>

- Huang, R., Xu, Y., Wan, W., Shou, X., Qian, J., You, Z., Liu, B., Chang, C., Zhou, T., Lippincott-Schwartz, J., & Liu, W. (2015). Deacetylation of nuclear LC3 drives autophagy initiation under starvation. *Molecular Cell*, *57*(3), 456–466. <https://doi.org/10.1016/j.molcel.2014.12.013>
- Ibrahim, Z., Wang, T., Destaing, O., Salvi, N., Hoghoughi, N., Chabert, C., Rusu, A., Gao, J., Feletto, L., Reynoird, N., Schalch, T., Zhao, Y., Blackledge, M., Khochbin, S., & Panne, D. (2022). Structural insights into p300 regulation and acetylation-dependent genome organisation. *Nature Communications*, *13*(1). <https://doi.org/10.1038/s41467-022-35375-2>
- Itoh, K., Wakabayashi, N., Katoh, Y., Ishii, T., O'Connor, T., & Yamamoto, M. (2003). Keap1 regulates both cytoplasmic-nuclear shuttling and degradation of Nrf2 in response to electrophiles. *Genes to Cells*, *8*(4), 379–391. <https://doi.org/10.1046/J.1365-2443.2003.00640.X>
- Jacomín, A.-C. C., Petridi, S., Di Monaco, M., Bhujabal, Z., Jain, A., Mulakkal, N. C., Palara, A., Powell, E. L., Chung, B., Zampronio, C., Jones, A., Cameron, A., Johansen, T., & Nezis, I. P. (2020). Regulation of Expression of Autophagy Genes by Atg8a-Interacting Partners Sequoia, YL-1, and Sir2 in *Drosophila*. *Cell Reports*, *31*(8), 107695. <https://doi.org/10.1016/j.celrep.2020.107695>
- Jain, A., Lamark, T., Sjøttem, E., Larsen, K. B., Awuh, J. A., Øvervatn, A., McMahon, M., Hayes, J. D., & Johansen, T. (2010). p62/SQSTM1 is a target gene for transcription factor NRF2 and creates a positive feedback loop by inducing antioxidant response element-driven gene transcription. *Journal of Biological Chemistry*, *285*(29), 22576–22591. <https://doi.org/10.1074/jbc.M110.118976>
- Jain, A., Rusten, T. E., Katheder, N., Elvenes, J., Bruun, J. A., Sjøttem, E., Lamark, T., & Johansen, T. (2015). p62/Sequestosome-1, Autophagy-related Gene 8, and Autophagy in *Drosophila* Are Regulated by Nuclear Factor Erythroid 2-related Factor 2 (NRF2), Independent of Transcription Factor TFEB. *Journal of Biological Chemistry*, *290*(24), 14945–14962. <https://doi.org/10.1074/JBC.M115.656116>
- Jiménez-Moreno, N., Kollareddy, M., Stathakos, P., Moss, J. J., Antón, Z., Shoemark, D. K., Sessions, R. B., Witzgall, R., Caldwell, M., & Lane, J. D. (2023). ATG8-dependent LMX1B-autophagy crosstalk shapes human midbrain dopaminergic neuronal resilience. *Journal of Cell Biology*, *222*(5). <https://doi.org/10.1083/jcb.201910133>
- Johansen, T., & Lamark, T. (2020). Selective Autophagy: ATG8 Family Proteins, LIR Motifs and Cargo Receptors. *Journal of Molecular Biology*, *432*, 80–103. <https://doi.org/10.1016/j.jmb.2019.07.016>
- Katoh, Y., Itoh, K., Yoshida, E., Miyagishi, M., Fukamizu, A., & Yamamoto, M. (2001). Two domains of Nrf2 cooperatively bind CBP, a CREB binding protein, and synergistically activate transcription. *Genes to Cells*, *6*(10), 857–868. <https://doi.org/10.1046/j.1365-2443.2001.00469.x>
- Katsuoka, F., Motohashi, H., Engel, J. D., & Yamamoto, M. (2005). Nrf2 Transcriptionally Activates the mafK Gene through an Antioxidant Response Element. *Journal of Biological Chemistry*, *280*(6), 4483–4490. <https://doi.org/10.1074/JBC.M411451200>
- Kawai, Y., Garduño, L. K., Theodore, M., Yang, J., & Arinze, I. J. (2011). Acetylation-deacetylation of the transcription factor Nrf2 (nuclear factor erythroid 2-related factor 2) regulates its transcriptional activity and nucleocytoplasmic localization. *Journal of Biological Chemistry*, *286*(9), 7629–7640. <https://doi.org/10.1074/jbc.M110.208173>

- Kiefer, F., Arnold, K., Künzli, M., Bordoli, L., & Schwede, T. (2009). The SWISS-MODEL Repository and associated resources. *Nucleic Acids Research*, *37*(suppl\_1), D387–D392. <https://doi.org/10.1093/NAR/GKN750>
- Klionsky, D. J., Petroni, G., Amaravadi, R. K., Baehrecke, E. H., Ballabio, A., Boya, P., Pedro, J. M. B.-S., Cadwell, K., Cecconi, F., Choi, A. M. K., Choi, M. E., Chu, C. T., Codogno, P., Colombo, M. I., Cuervo, A. M., Deretic, V., Dikic, I., Elazar, Z., Eskelinen, E.-L., ... Pietrocola, F. (2021). Autophagy in major human diseases. *The EMBO Journal*, *40*(19), e108863. <https://doi.org/10.15252/EMBJ.2021108863>
- Kobayashi, A., Kang, M.-I., Okawa, H., Ohtsuji, M., Zenke, Y., Chiba, T., Igarashi, K., & Yamamoto, M. (2004). Oxidative stress sensor Keap1 functions as an adaptor for Cul3-based E3 ligase to regulate proteasomal degradation of Nrf2. *Molecular and Cellular Biology*, *24*(16), 7130–7139. <https://doi.org/10.1128/MCB.24.16.7130-7139.2004>
- Komatsu, M., Kurokawa, H., Waguri, S., Taguchi, K., Kobayashi, A., Ichimura, Y., Sou, Y. S., Ueno, I., Sakamoto, A., Tong, K. I., Kim, M., Nishito, Y., Iemura, S. I., Natsume, T., Ueno, T., Kominami, E., Motohashi, H., Tanaka, K., & Yamamoto, M. (2010). The selective autophagy substrate p62 activates the stress responsive transcription factor Nrf2 through inactivation of Keap1. *Nature Cell Biology*, *12*(3), 213–223. <https://doi.org/10.1038/ncb2021>
- Kournoutis, A., & Johansen, T. (2023). LC3B is a cofactor for LMX1B-mediated transcription of autophagy genes in dopaminergic neurons. *Journal of Cell Biology*, *222*(5). <https://doi.org/10.1083/JCB.202303008>
- Kraft, L. J., Manral, P., Dowler, J., & Kenworthy, A. K. (2016). Nuclear LC3 Associates with Slowly Diffusing Complexes that Survey the Nucleolus. *Traffic*, *17*(4), 369–399. <https://doi.org/10.1111/tra.12372>
- Kraft, L. J., Nguyen, T. A., Vogel, S. S., & Kenworthy, A. K. (2014). Size, stoichiometry, and organization of soluble LC3-associated complexes. *Autophagy*, *10*(5), 861–877. <https://doi.org/10.4161/auto.28175>
- Krauskopf, K., Gebel, J., Kazemi, S., Tuppi, M., Löhr, F., Schäfer, B., Koch, J., Güntert, P., Dötsch, V., & Kehrloesser, S. (2018). Regulation of the Activity in the p53 Family Depends on the Organization of the Transactivation Domain. *Structure*, *26*(8), 1091-1100.e4. <https://doi.org/10.1016/J.STR.2018.05.013>
- Krois, A. S., Ferreon, J. C., Martinez-Yamout, M. A., Dyson, H. J., & Wright, P. E. (2016). Recognition of the disordered p53 transactivation domain by the transcriptional adapter zinc finger domains of CREB-binding protein. *Proceedings of the National Academy of Sciences of the United States of America*, *113*(13), E1853–E1862. [https://doi.org/10.1073/PNAS.1602487113/SUPPL\\_FILE/PNAS.201602487SI.PDF](https://doi.org/10.1073/PNAS.1602487113/SUPPL_FILE/PNAS.201602487SI.PDF)
- Laguna, A., Schintu, N., Nobre, A., Alvarsson, A., Volakakis, N., Jacobsen, J. K., Gómez-Galán, M., Sopova, E., Joodmardi, E., Yoshitake, T., Deng, Q., Kehr, J., Ericson, J., Svenningsson, P., Shupliakov, O., & Perlmann, T. (2015). Dopaminergic control of autophagic-lysosomal function implicates Lmx1b in Parkinson's disease. *Nature Neuroscience*, *18*(6), 826–835. <https://doi.org/10.1038/nn.4004>
- Lau, A., Wang, X.-J., Zhao, F., Villeneuve, N. F., Wu, T., Jiang, T., Sun, Z., White, E., & Zhang, D. D. (2010). A Noncanonical Mechanism of Nrf2 Activation by Autophagy Deficiency: Direct

- Interaction between Keap1 and p62. *Molecular and Cellular Biology*, 30(13), 3275–3285. <https://doi.org/10.1128/MCB.00248-10>
- Martinez-Lopez, N., Athonvarangkul, D., Mishall, P., Sahu, S., & Singh, R. (2013). Autophagy proteins regulate ERK phosphorylation. *Nature Communications*, 4(1), 1–14. <https://doi.org/10.1038/ncomms3799>
- McMahon, M., Itoh, K., Yamamoto, M., & Hayes, J. D. (2003). Keap1-dependent Proteasomal Degradation of Transcription Factor Nrf2 Contributes to the Negative Regulation of Antioxidant Response Element-driven Gene Expression. *Journal of Biological Chemistry*, 278(24), 21592–21600. <https://doi.org/10.1074/JBC.M300931200>
- Miller Jenkins, L. M., Feng, H., Durell, S. R., Tagad, H. D., Mazur, S. J., Tropea, J. E., Bai, Y., & Appella, E. (2015). Characterization of the p300 Taz2-p53 TAD2 Complex and Comparison with the p300 Taz2-p53 TAD1 Complex. *Biochemistry*, 54(11), 2001–2010. [https://doi.org/10.1021/ACS.BIOCHEM.5B00044/SUPPL\\_FILE/BI5B00044\\_SI\\_001.PDF](https://doi.org/10.1021/ACS.BIOCHEM.5B00044/SUPPL_FILE/BI5B00044_SI_001.PDF)
- Mirdita, M., Schütze, K., Moriwaki, Y., Heo, L., Ovchinnikov, S., & Steinegger, M. (2022). ColabFold: making protein folding accessible to all. *Nature Methods*, 19(6), 679–682. <https://doi.org/10.1038/s41592-022-01488-1>
- Nguyen, T., Sherratt, P. J., Huang, H. C., Yang, C. S., & Pickett, C. B. (2003). Increased Protein Stability as a Mechanism That Enhances Nrf2-mediated Transcriptional Activation of the Antioxidant Response Element: Degradation of NRF2 by the 26S proteasome. *Journal of Biological Chemistry*, 278(7), 4536–4541. <https://doi.org/10.1074/JBC.M207293200>
- Nioi, P., McMahon, M., Itoh, K., Yamamoto, M., & Hayes, J. D. (2003). Identification of a novel Nrf2-regulated antioxidant response element (ARE) in the mouse NAD(P)H:quinone oxidoreductase 1 gene: reassessment of the ARE consensus sequence. *Biochemical Journal*, 374(Pt 2), 337. <https://doi.org/10.1042/BJ20030754>
- Oka, O., Waters, L. C., Strong, S. L., Dosanjh, N. S., Veverka, V., Muskett, F. W., Renshaw, P. S., Klempnauer, K. H., & Carr, M. D. (2012). Interaction of the Transactivation Domain of B-Myb with the TAZ2 Domain of the Coactivator p300: Molecular Features and Properties of the Complex. *PLOS ONE*, 7(12), e52906. <https://doi.org/10.1371/JOURNAL.PONE.0052906>
- Ortega, E., Rengachari, S., Ibrahim, Z., Hoghoughi, N., Gaucher, J., Holehouse, A. S., Khochbin, S., & Panne, D. (2018). Transcription factor dimerization activates the p300 acetyltransferase. *Nature*, 562(7728), 538–544. <https://doi.org/10.1038/s41586-018-0621-1>
- Pankiv, S., Clausen, T. H., Lamark, T., Brech, A., Bruun, J. A., Outzen, H., Øvervatn, A., Bjørkøy, G., & Johansen, T. (2007). p62/SQSTM1 Binds Directly to Atg8/LC3 to Facilitate Degradation of Ubiquitinated Protein Aggregates by Autophagy. *Journal of Biological Chemistry*, 282(33), 24131–24145. <https://doi.org/10.1074/JBC.M702824200>
- Pankiv, S., Lamark, T., Bruun, J. A., Øvervatn, A., Bjørkøy, G., & Johansen, T. (2010). Nucleocytoplasmic shuttling of p62/SQSTM1 and its role in recruitment of nuclear polyubiquitinated proteins to promyelocytic leukemia bodies. *Journal of Biological Chemistry*, 285(8), 5941–5953. <https://doi.org/10.1074/jbc.M109.039925>
- Pettersen, E. F., Goddard, T. D., Huang, C. C., Meng, E. C., Couch, G. S., Croll, T. I., Morris, J. H., & Ferrin, T. E. (2021). UCSF ChimeraX: Structure visualization for researchers, educators, and developers. *Protein Science*, 30(1), 70–82. <https://doi.org/10.1002/pro.3943>

- Pizzino, G., Irrera, N., Cucinotta, M., Pallio, G., Mannino, F., Arcoraci, V., Squadrito, F., Altavilla, D., & Bitto, A. (2017). Oxidative Stress: Harms and Benefits for Human Health. *Oxidative Medicine and Cellular Longevity*, 2017. <https://doi.org/10.1155/2017/8416763>
- Raghunath, A., Sundarraj, K., Nagarajan, R., Arfuso, F., Bian, J., Kumar, A. P., Sethi, G., & Perumal, E. (2018). Antioxidant response elements: Discovery, classes, regulation and potential applications. *Redox Biology*, 17, 297–314. <https://doi.org/10.1016/J.REDOX.2018.05.002>
- Rasmussen, M. S., Moulleron, S., Kumar Shrestha, B., Wirth, M., Lee, R., Bowitz Larsen, K., Abudu Princely, Y., O'Reilly, N., Sjøttem, E., Tooze, S. A., Lamark, T., & Johansen, T. (2017). ATG4B contains a C-terminal LIR motif important for binding and efficient cleavage of mammalian orthologs of yeast Atg8. *Autophagy*, 13(5), 834–853. <https://doi.org/10.1080/15548627.2017.1287651>
- Rogov, V. V., Nezis, I. P., Tsapras, P., Zhang, H., Dagdas, Y., Noda, N. N., Nakatogawa, H., Wirth, M., Moulleron, S., McEwan, D. G., Behrends, C., Deretic, V., Elazar, Z., Tooze, S. A., Dikic, I., Lamark, T., & Johansen, T. (2023). Atg8 family proteins, LIR/AIM motifs and other interaction modes. *Autophagy Reports*, 2(1). <https://doi.org/10.1080/27694127.2023.2188523>
- Rössler, O. G., & Thiel, G. (2017). Specificity of Stress-Responsive Transcription Factors Nrf2, ATF4, and AP-1. *Journal of Cellular Biochemistry*, 118(1), 127–140. <https://doi.org/10.1002/JCB.25619>
- Satoo, K., Noda, N. N., Kumeta, H., Fujioka, Y., Mizushima, N., Ohsumi, Y., & Inagaki, F. (2009). The structure of Atg4B-LC3 complex reveals the mechanism of LC3 processing and delipidation during autophagy. *EMBO Journal*, 28(9), 1341–1350. <https://doi.org/10.1038/EMBOJ.2009.80/ASSET/5FB29A0A-42FB-4DE9-BB83-B53339A6B515/ASSETS/GRAPHIC/EMBJ200980-FIG-0005-M.JPG>
- Sekine, H., Okazaki, K., Ota, N., Shima, H., Katoh, Y., Suzuki, N., Igarashi, K., Ito, M., Motohashi, H., & Yamamoto, M. (2016). The Mediator Subunit MED16 Transduces NRF2-Activating Signals into Antioxidant Gene Expression. *Molecular and Cellular Biology*, 36(3), 407–420. <https://doi.org/10.1128/MCB.00785-15>
- Shim, M. S., Nettesheim, A., Hirt, J., & Liton, P. B. (2020). The autophagic protein LC3 translocates to the nucleus and localizes in the nucleolus associated to NUFIP1 in response to cyclic mechanical stress. *Autophagy*, 16(7), 1248–1261. <https://doi.org/10.1080/15548627.2019.1662584>
- Sies, H. (1985). Oxidative Stress: Introductory Remarks. *Academic Press*, 1–8. <https://doi.org/10.1016/B978-0-12-642760-8.50005-3>
- Sies, H. (1997). Oxidative stress: oxidants and antioxidants. *Experimental Physiology*, 82(2), 291–295. <https://doi.org/10.1113/EXPPHYSIOL.1997.SP004024>
- Sun, Z., Chin, Y. E., & Zhang, D. D. (2009). Acetylation of Nrf2 by p300/CBP Augments Promoter-Specific DNA Binding of Nrf2 during the Antioxidant Response. *Molecular and Cellular Biology*, 29(10), 2658–2672. <https://doi.org/10.1128/mcb.01639-08>
- Taguchi, K., Fujikawa, N., Komatsu, M., Ishii, T., Unno, M., Akaike, T., Motohashi, H., & Yamamoto, M. (2012). Keap1 degradation by autophagy for the maintenance of redox homeostasis. *Proceedings of the National Academy of Sciences of the United States of America*, 109(34), 13561–13566. [https://doi.org/10.1073/PNAS.1121572109/SUPPL\\_FILE/PNAS.201121572SI.PDF](https://doi.org/10.1073/PNAS.1121572109/SUPPL_FILE/PNAS.201121572SI.PDF)

- Takaya, K., Suzuki, T., Motohashi, H., Onodera, K., Satomi, S., Kensler, T. W., & Yamamoto, M. (2012). Validation of the multiple sensor mechanism of the Keap1-Nrf2 system. *Free Radical Biology and Medicine*, 53(4), 817–827. <https://doi.org/10.1016/j.freeradbiomed.2012.06.023>
- Tonelli, C., Chio, I. I. C., & Tuveson, D. A. (2018). Transcriptional Regulation by Nrf2. *Antioxidants & Redox Signaling*, 29(17), 1727–1745. <https://doi.org/10.1089/ars.2017.7342>
- Wang, F., Marshall, C. B., Yamamoto, K., Li, G. Y., Gasmi-Seabrook, G. M. C., Okada, H., Mak, T. W., & Ikura, M. (2012). Structures of KIX domain of CBP in complex with two FOXO3a transactivation domains reveal promiscuity and plasticity in coactivator recruitment. *Proceedings of the National Academy of Sciences of the United States of America*, 109(16), 6078–6083. [https://doi.org/10.1073/PNAS.1119073109/SUPPL\\_FILE/PNAS.201119073SI.PDF](https://doi.org/10.1073/PNAS.1119073109/SUPPL_FILE/PNAS.201119073SI.PDF)
- Wang, L., Xu, C., Johansen, T., Berger, S. L., & Dou, Z. (2021). SIRT1—a new mammalian substrate of nuclear autophagy. *Autophagy*, 17(2), 593–595. <https://doi.org/10.1080/15548627.2020.1860541>
- Wirth, M., Zhang, W., Razi, M., Nyoni, L., Joshi, D., O'Reilly, N., Johansen, T., Tooze, S. A., & Moulleron, S. (2019). Molecular determinants regulating selective binding of autophagy adapters and receptors to ATG8 proteins. *Nature Communications*, 10(1). <https://doi.org/10.1038/s41467-019-10059-6>
- Wojciak, J. M., Martinez-Yamout, M. A., Dyson, H. J., & Wright, P. E. (2009). Structural basis for recruitment of CBP/p300 coactivators by STAT1 and STAT2 transactivation domains. *EMBO Journal*, 28(7), 948–958. [https://doi.org/10.1038/EMBOJ.2009.30/SUPPL\\_FILE/EMBJ200930-SUP-0001.DOC](https://doi.org/10.1038/EMBOJ.2009.30/SUPPL_FILE/EMBJ200930-SUP-0001.DOC)
- Xu, L., Xuan, H., He, W., Zhang, L., Huang, M., Li, K., Wen, H., Xu, H., & Shi, X. (2023). TAZ2 truncation confers overactivation of p300 and cellular vulnerability to HDAC inhibition. *Nature Communications*, 14(1), 1–12. <https://doi.org/10.1038/s41467-023-41245-2>
- Ying, L., Lau, A., Alvira, C. M., West, R., Cann, G. M., Zhou, B., Kinnear, C., Jan, E., Sarnow, P., Van de Rijn, M., & Rabinovitch, M. (2009). LC3-mediated fibronectin mRNA translation induces fibrosarcoma growth by increasing connective tissue growth factor. *Journal of Cell Science*, 122(9), 1441–1451. <https://doi.org/10.1242/JCS.025957>
- Zhang, D. D., Lo, S.-C., Cross, J. V., Templeton, D. J., & Hannink, M. (2004). Keap1 Is a Redox-Regulated Substrate Adaptor Protein for a Cul3-Dependent Ubiquitin Ligase Complex. *Molecular and Cellular Biology*, 24(24), 10941–10953. <https://doi.org/10.1128/MCB.24.24.10941-10953.2004>
- Zhang, J., Hosoya, T., Maruyama, A., Nishikawa, K., Maher, J. M., Ohta, T., Motohashi, H., Fukamizu, A., Shibahara, S., Itoh, K., & Yamamoto, M. (2007). Nrf2 Neh5 domain is differentially utilized in the transactivation of cytoprotective genes. *Biochemical Journal*, 404(3), 459–466. <https://doi.org/10.1042/BJ20061611>
- Zhang, J., Ohta, T., Maruyama, A., Hosoya, T., Nishikawa, K., Maher, J. M., Shibahara, S., Itoh, K., & Yamamoto, M. (2006). BRG1 Interacts with Nrf2 To Selectively Mediate HO-1 Induction in Response to Oxidative Stress. *Molecular and Cellular Biology*, 26(21), 7942–7952. <https://doi.org/10.1128/mcb.00700-06>
- Zhou, B., Boudreau, N., Coulber, C., Hammarback, J., & Rabinovitch, M. (1997). Microtubule-associated protein 1 light chain 3 is a fibronectin mRNA-binding protein linked to mRNA



translation in lamb vascular smooth muscle cells. *The Journal of Clinical Investigation*, 100(12), 3070–3082. <https://doi.org/10.1172/JCI119862>

**Table 1: Plasmids used in study**

Plasmids	Source
<b>Gateway cloning vectors</b>	
pENTR1A, -2B and -3C	Invitrogen
pDONR221	Invitrogen
pDest15	Invitrogen
pDest-myc	(Lamark et al., 2003)
pDest-NeonGreen 1-10	This study
pDest-NeonGreen -11	This study
<b>Promoter constructs used in reporter gene assays</b>	
pGL3-Basic	Promega
Nqo1-ARE-luc	(Nioi et al., 2003)
<b>cDNA constructs made by Gateway cloning, InFusion cloning or site-directed mutagenesis</b>	
pDONR221-DmCncC	(Jain et al., 2015)
pENTR-DmAtg8a	(Alemu et al., 2012)
pDONR221-NRF1-V5/His	This study
pDONR221-NRF2	(Jain et al., 2010)
pDONR221-NRF2 1-86	This study
pDONR221-NRF2 87-386	This study
pDONR221-NRF2 87-605	This study
pDONR221-NRF2 1-386	This study
pDONR221-NRF2 $\Delta$ 175-188	This study
pDONR221-NRF2 $\Delta$ 175-191	This study
pDONR221-NRF2 $\Delta$ 178-208	This study
pDONR221-NRF2 $\Delta$ 191-204	This study
pDONR221-NRF2 $\Delta$ 196-202	This study
pDONR221-NRF2 Q182A/D183A	This study
pDONR221-NRF2 I184A/E185A	This study
pDONR221-NRF2 W188A/L191A	This study
pDONR221-NRF2 E189A/E190A	This study
pDONR221-NRF2 D176A	This study
pDONR221-NRF2 D178A	This study
pDONR221-NRF2 D183A	This study
pDONR221-NRF2 E196A	This study
pDONR221-MafG	DF/HCC DNA Resource Core, Harvard
pENTR-KEAP1	(Jain et al., 2010)
pENTR-p62	(Lamark et al., 2003)
<b>cDNA constructs made by Gateway LR reactions</b>	
pDest-myc-NRF2	This study
pDest-myc-NRF2 1-86	This study

pDest-myc-NRF2 87-386	This study
pDest-myc-NRF2 87-605	This study
pDest-myc-NRF2 1-386	This study
pDest-myc-NRF2 386-606	This study
pDest-myc-NRF2 Δ175-188	This study
pDest-myc-NRF2 Δ175-191	This study
pDest-myc-NRF2 Δ178-208	This study
pDest-myc-NRF2 Δ191-204	This study
pDest-myc-NRF2 Δ196-202	This study
pDest-myc-NRF2 Q182A/D183A	This study
pDest-myc-NRF2 I184A/E185A	This study
pDest-myc-NRF2 W188A/L191A	This study
pDest-myc-NRF2 E189A/E190A	This study
pDest-myc-NRF2 D176A	This study
pDest-myc-NRF2 D178A	This study
pDest-myc-NRF2 D183A	This study
pDest-myc-NRF2 E196A	This study
pDest15-LC3A	(Pankiv et al., 2007)
pDest15-LC3B	(Pankiv et al., 2007)
pDest15-LC3B R10A	(Kirkin et al., 2009)
pDest15-LC3B R10A/R11A	(Kirkin et al., 2009)
pDest15-LC3B R10A/R70A	(Kirkin et al., 2009)
pDest15-LC3B F52A	(Kirkin et al., 2009)
pDest15-LC3B L53A	This study
pDest15-LC3B R69A	This study
pDest15-LC3C	(Kirkin et al., 2009)
pDest15-GABARAP	(Pankiv et al., 2007)
pDest15-GABARAPL1	(Pankiv et al., 2007)
pDest15-GABARAPL2	(Pankiv et al., 2007)
pDest-NeonGreen 1-10 – NRF2	This study
pDest-NeonGreen 1-10 – MafG	This study
pDest-NeonGreen 1-10 – KEAP1	This study
pDest-NeonGreen 1-10 – p300 1660-1810 (TAZ2)	This study
pDest-NeonGreen -11 – LC3B	This study

\* All plasmids contain human genes, unless otherwise specified as *Drosophila melanogaster* genes (Dm).

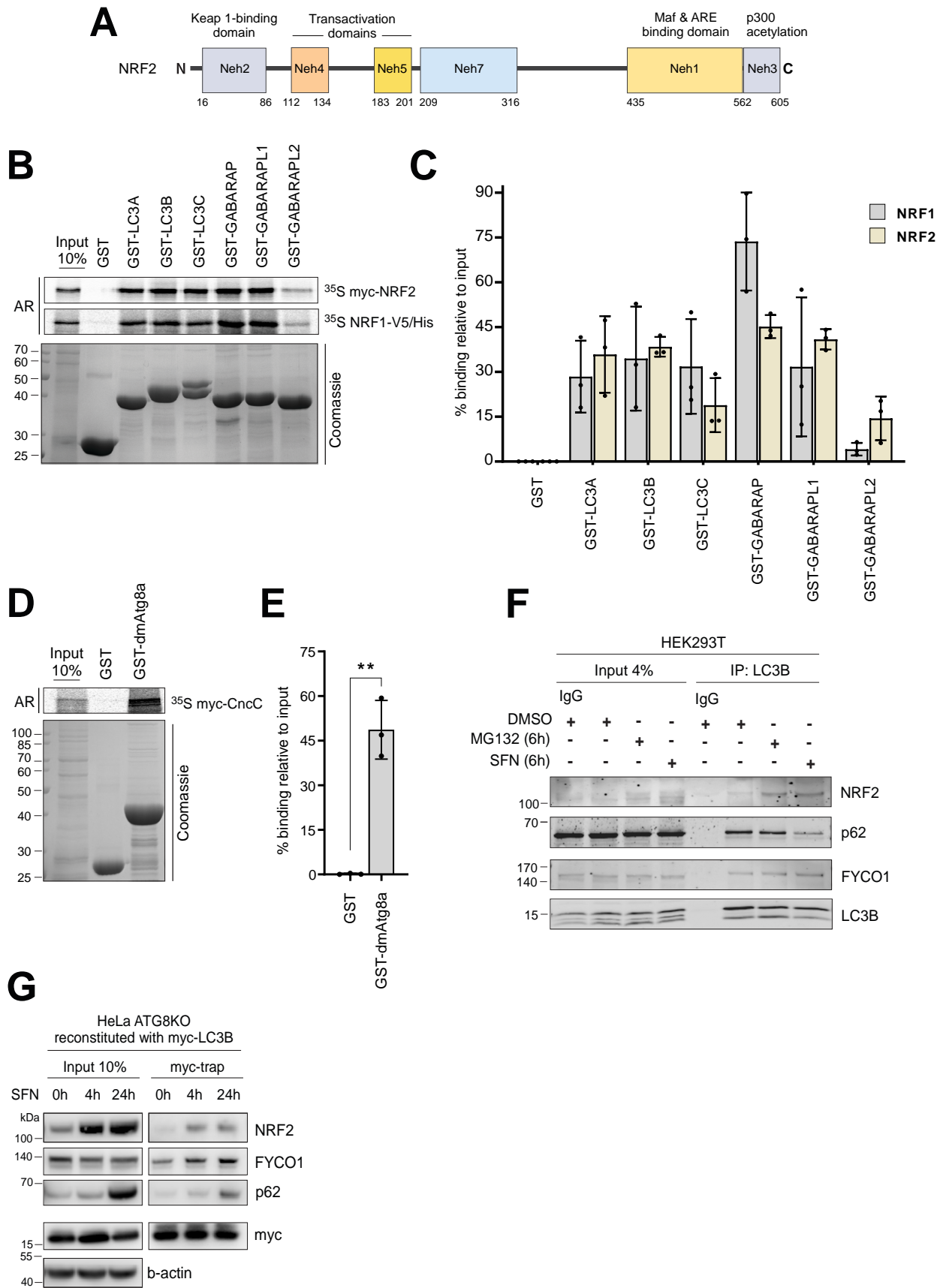
**Table 2: RT-qPCR primers used in this study (5'→3')\***  
(F: Forward Primer, R: Reverse Primer)

NRF2	F: AGCCAGCCCAGCACATCCAG R: ACAAACGGGAATGTCTGCGCC
HO-1	F: CTGAAGGAGGCCACCAAGGA R: TCCTCCTCCAGGGCCACATA
NQO1	F: AATCAGCGCCCCGGACTGC R: TCCGACTCCACCACCTCCCA

TXNRD1	F: CCTTGCCTTACTGCCCGGGT R: ACCAGCAAGAAATCCAGCGCAC
p62	F: AAAAGAAGCCGCCTGACCCC R: CCTCAACATTCCCACCCGGC
G6PD	F: AAGCCGGGCATGTTCTTCAA R: GCGTCAGGGAGCTTCACGTT
GCLC	F: GCTGAGCTGGGAGGAAACCA R: GGCCTTGACGGCGTGGTAG
GCLM	F: ACGGGGAACCTGCTGAACTG R: CATGAAGCTCCTCGCTGTGC
Lamin A/C	F: AGCTGAAAGCGCGCAATACC R: GGCCTCCTTGGAGTTCAGCA

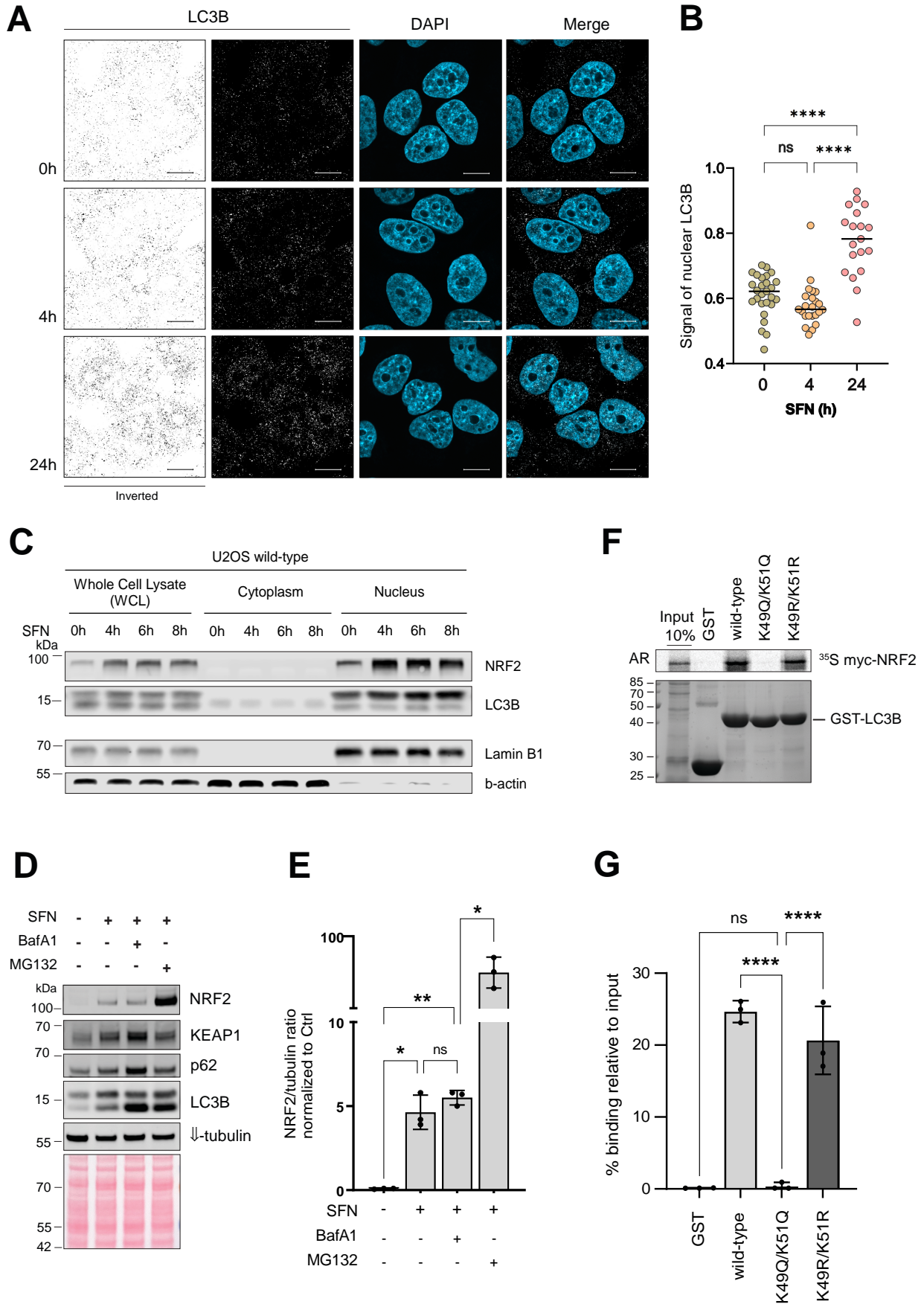
\* All are human genes, unless otherwise specified.

FIGURE 1



**Figure 1. NRF2, NRF1, and dmCncC interact with the human ATG8 family of proteins. (A)** Schematic representation of the domain architecture of NRF2, showing its six Neh domains. **(B)** In vitro GST pulldown assay using <sup>35</sup>S-labeled myc-NRF2 and V5/His-NRF1 against recombinant GST and GST-tagged human ATG8s. Bound myc-NRF2 and V5/His-NRF1 were detected by autoradiography (AR). **(C)** Quantification of GST-pulldown from B. Relative % binding was quantified against 10% input (n = 3). ns = P > 0.05 (non-significant), based on one-way ANOVA (post hoc Tukey test). Error bars indicate SEM. Values from each independent experiment are shown as dots. **(D)** In vitro GST pulldown assay using <sup>35</sup>S-labeled myc-CncC against recombinant GST and GST-tagged dmAtg8a. **(E)** Quantification of GST-pulldown from D. Relative % binding was quantified against 10% input (n = 3). \*\* = P < 0.01 (non-significant), based on one-way ANOVA (post hoc Tukey test). Error bars indicate SEM. Values from each independent experiment are shown as dots. **(F)** Treatment with MG132 or SFN amplified the in vivo interaction between NRF2 and LC3B. Proteins were co-immunoprecipitated with anti-LC3B in HEK293T cells, treated with MG132 or SFN for 6h, and analyzed by Western blot (n = 2). **(G)** Proteins were co-immunoprecipitated with myc-trap in HeLa ATG8 KO, reconstituted with myc-LC3B, treated with SFN for 4 and 24h, and analyzed by Western blot (n = 2).

FIGURE 2



**Figure 2. LC3B accumulates under oxidative stress.** (A) Endogenous LC3B increases in the nucleus in HeLa cells under treatment with SFN for 4 and 24h. Cells were imaged using Zeiss LSM800 and representative images based on two independent experiments are shown. Scale bar = 10  $\mu$ m. (B) Quantification of A. The nuclear signal of LC3B was quantified using a CellProfiler pipeline based on one-way ANOVA (post hoc Tukey test), where each cell corresponds to one value. ns =  $P > 0.05$  (non-significant), \*\*\*\* =  $P < 0.0001$ . Error bars indicate SEM. (C) U2OS cells were treated with either vehicle (DMSO) or SFN for 4h, 6h and 8h and subjected to subcellular fractionation, followed by Western blot analysis of the indicated proteins (n = 2). Lamin B1 and b-actin were used as controls for the nuclear and cytoplasmic fractions respectively. (D) U2OS cells were treated as indicated with either vehicle (DMSO) or SFN for 6h alone or complemented with either BafA1 for 6h or MG132 for 6h. Cell lysates were analyzed by Western blot using the indicated antibodies. (E) Quantification of D. Bar graphs show relative intensities of the NRF2 and LC3B proteins normalized against loading control ( $\beta$ -tubulin) (n = 3). ns =  $P > 0.05$  (non-significant), \* =  $P < 0.05$ , based on unpaired t-test. Error bars indicate SEM. Values from each independent experiment are shown as dots. (F) In vitro GST pulldown assay using  $^{35}$ S-labeled myc-NRF2 against recombinant GST and GST-tagged LC3B wild-type, K49Q/K51Q and K49R/K51R. Bound myc-NRF2 was detected by autoradiography (AR). (G) Quantification of GST-pulldown from F. Relative % binding was quantified against 10% input (n = 3). ns =  $P > 0.05$  (non-significant), \*\*\*\* =  $P < 0.0001$ , based on one-way ANOVA (post hoc Tukey test). Error bars indicate SEM. Values from each independent experiment are shown as dots.



**FIGURE 3**

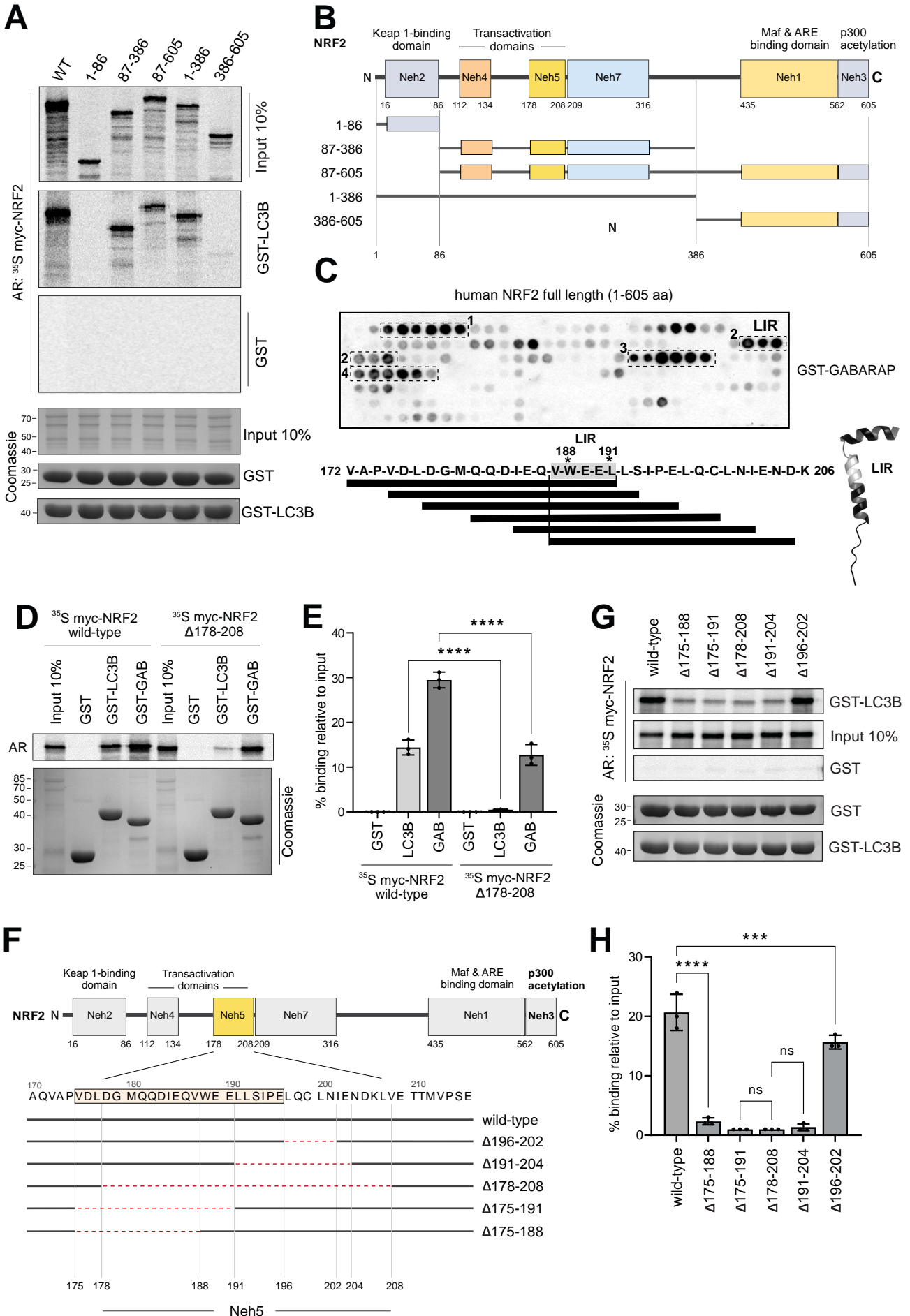
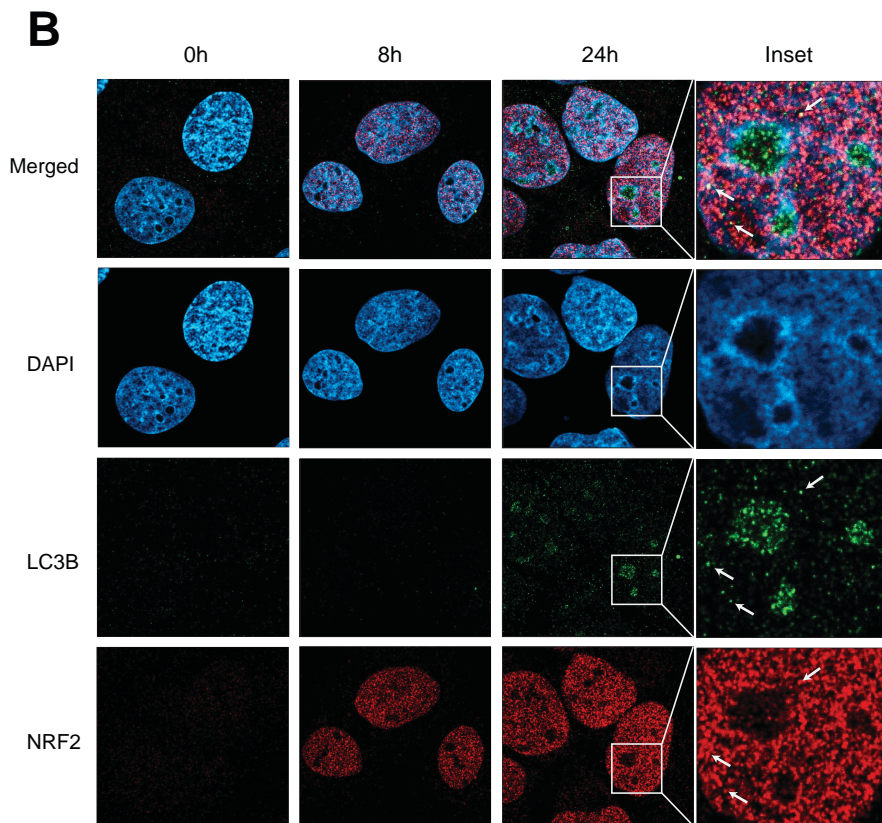
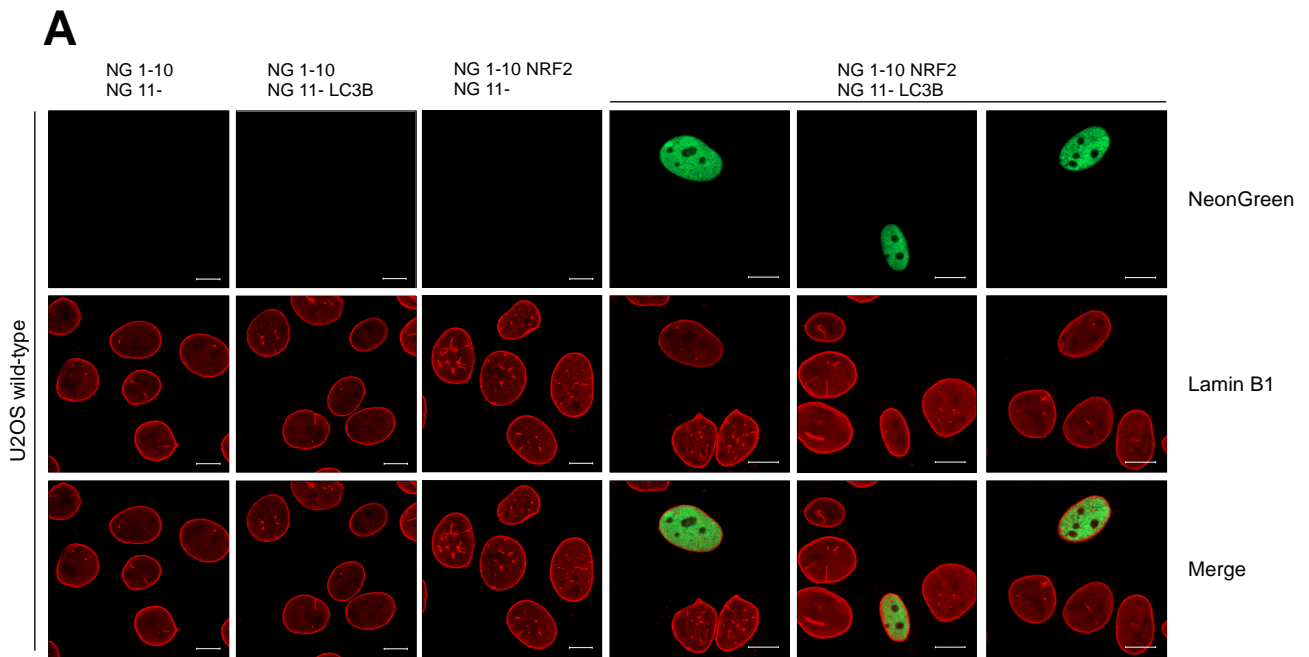


**Figure 3. The Neh5 domain of NRF2 is required for its interaction with LC3B.** (A) In vitro GST pulldown assay using <sup>35</sup>S-labeled myc-NRF2 and its indicated truncations against recombinant GST and GST-tagged human LC3B. Bound myc-NRF2 was detected by autoradiography (AR). (B) Schematic representation of the domain architecture of NRF2, indicating the truncated constructs used in A. (C) A peptide array of 20-mer peptides covering the full length of human NRF2 was used to probe for possible LIRs, using GST-GABARAP. (D) In vitro GST pulldown assay using <sup>35</sup>S-labeled myc-NRF2 and myc-NRF2 Δ178-208 against recombinant GST and GST-tagged human LC3B and GABARAP. (E) Quantification of GST-pulldown from D. Relative % binding was quantified against 10% input (n = 3). \*\*\*\* = P < 0.0001, based on one-way ANOVA (post hoc Tukey test). Error bars indicate SEM. Values from each independent experiment are shown as dots. (F) Schematic representation of the domain architecture of NRF2 showing the amino acid sequence of the Neh5 domain and the truncations used in G. (G) In vitro GST pulldown assay using <sup>35</sup>S-labeled myc-NRF2 wild-type and Neh5 domain truncations against recombinant GST and GST-tagged human LC3B. (H) Quantification of GST-pulldown from G. Relative % binding was quantified against 10% input (n = 3). ns = P > 0.05 (non-significant), \*\*\*\* = P < 0.0001, based on one-way ANOVA (post hoc Tukey test). Error bars indicate SEM. Values from each independent experiment are shown as dots.



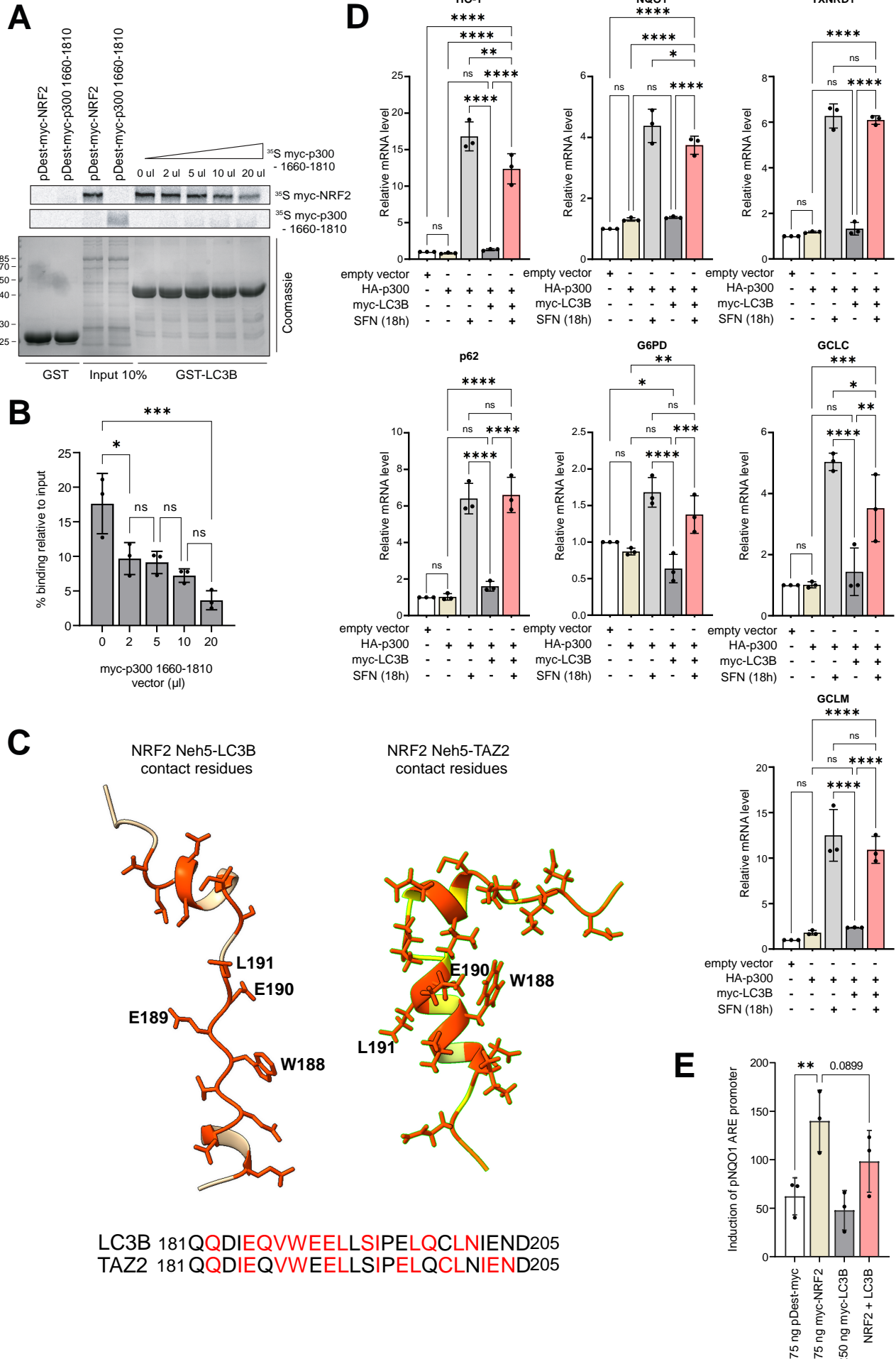
**Figure 4. Mutational analyses reveal the <sup>188</sup>WEEL<sup>191</sup> residues to be crucial for the binding of NRF2 to LC3B.** (A) Schematic representation for the estimation of the evolutionary conservation of amino acid positions in the Neh5 domain of NRF2, produced using the ConSurf web server (Ashkenazy et al., 2010; Glaser et al., 2003). (B) In vitro GST pulldown assay using <sup>35</sup>S-labeled myc-NRF2 and its indicated mutants in its Neh5 domain against recombinant GST and GST-tagged human LC3B. Bound myc-NRF2 was detected by autoradiography (AR). (C) Quantification of GST-pulldown from B. Relative % binding was quantified against 10% input (n = 3). \* = P < 0.05, \*\* = P < 0.01, based on one-way ANOVA (post hoc Tukey test). Error bars indicate SEM. Values from each independent experiment are shown as dots. (D) In vitro GST pulldown assay using <sup>35</sup>S-labeled myc-NRF2 against recombinant GST and GST-tagged human LC3B and its mutants. Bound myc-NRF2 was detected by autoradiography (AR). (E) Quantification of GST-pulldown from D. Relative % binding was quantified against 10% input (n = 3). ns = P > 0.05 (non-significant), \* = P < 0.05, \*\*\* = P < 0.001, \*\*\*\* = P < 0.0001, based on one-way ANOVA (post hoc Tukey test). Error bars indicate SEM. Values from each independent experiment are shown as dots. (F) AlphaFold prediction of the structure of the complex of human NRF2 aa 181-212 and full-length LC3B. (Left) Cartoon of NRF2 colored in green. (Right) Surface of LC3B colored by electrostatic potential. Residues of NRF2 in white text, and of LC3B in orange text.

FIGURE 5



**Figure 5. The interaction between NRF2 and LC3B is facilitated in the nucleus. (A)** Bimolecular fluorescence complementation (BiFC) analysis of the NRF2-LC3B interaction. U2OS cells were transfected with the indicated combination of split NeonGreen constructs, followed by endogenous staining of Lamin B1 as a nuclear control and imaging using Zeiss LSM800. Representative images based on two independent experiments are shown. Scale bar = 10  $\mu\text{m}$ . **(B)** Endogenous LC3B and NRF2 co-localize in the nucleus in U2OS cells under treatment with SFN for 24h. Cells were imaged using Zeiss LSM800. Representative images are shown and supplemented with line plots illustrating the co-localization of detected proteins. Scale bar = 10  $\mu\text{m}$ .

**FIGURE 6**

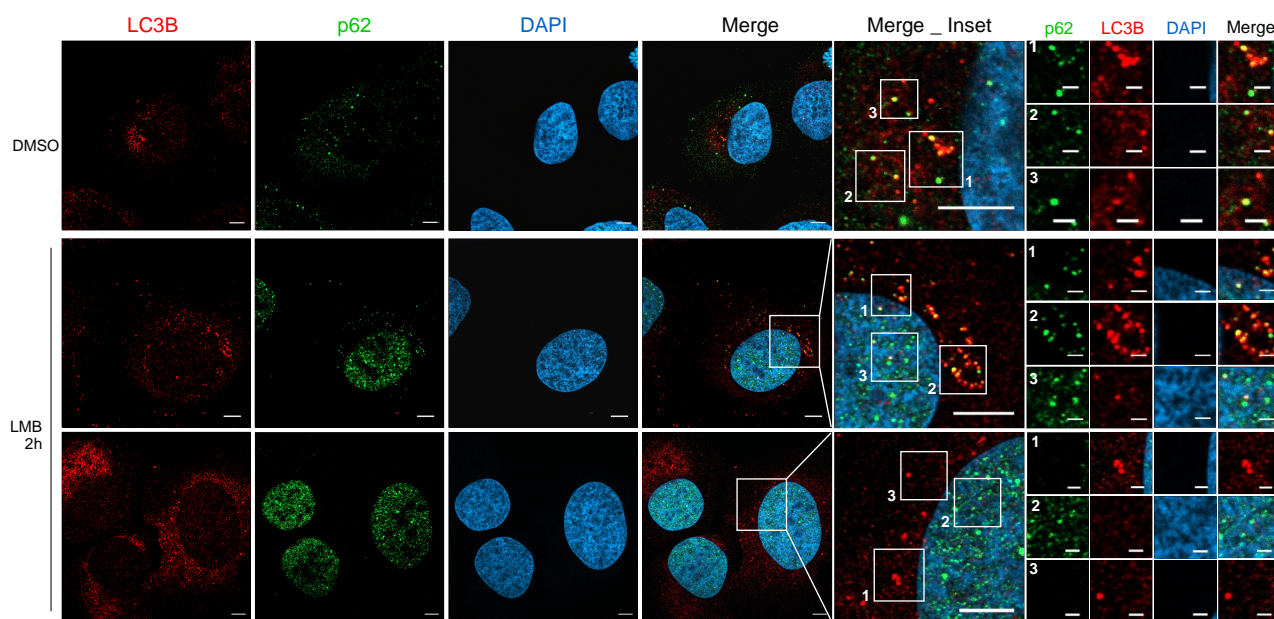


**Figure 6. LC3B competes with p300 for binding on the Neh5 domain of NRF2 and negatively regulates transcriptional activation of its target genes.** (A) In vitro GST pulldown assay demonstrating competition between LC3B and p300 1660-1810 for binding to NRF2. Recombinant GST-tagged LC3B was incubated with in vitro translated <sup>35</sup>S-labeled myc-NRF2, in the presence or absence of increasing amounts of in vitro translated <sup>35</sup>S-labeled myc-p300 1660-1810. The amount of <sup>35</sup>S-labeled myc-NRF2 and GST-LC3B is constant in all reactions. (B) Quantification of GST-pulldown from A. Relative % binding was quantified against 10% input (n = 3). ns = P > 0.05 (non-significant), \* = P < 0.05, \*\*\* = P < 0.001, based on one-way ANOVA (post hoc Tukey test). Error bars indicate SEM. Values from each independent experiment are shown as dots. (C) Comparison of the AlphaFold2 predictions of the structure of the Neh5 domain of human NRF2 (aa 181-212) in complex with full-length LC3B (left) or with the TAZ2 domain of p300 (right). Only the part of Neh5 interacting with LC3B and p300 TAZ2 is shown with the contact residues depicted in orange. Nine of the Neh5 contact residues are shared between the interaction models for LC3B and p300 TAZ2 domain. (D) RT-qPCR analyses of HO-1, NQO1, TXNRD1, p62, G6PD, GCLC and GCLM in HEK293T cells in which HA-tagged p300 or myc-tagged LC3B or both were overexpressed, with or without SFN treatment for 18h. Results were normalized to Lamin A/C and presented as mean values with s.d. (n = 3). ns = P > 0.05 (non-significant), \* = P < 0.05, \*\* = P < 0.01, \*\*\* = P < 0.001, \*\*\*\* = P < 0.0001 based on one-way ANOVA (Fisher's LSD test). (E) Reporter gene assay testing the activation of the Nqo1-ARE-Luc reporter by co-expression with either empty vector (pDest-myc), myc-tagged NRF2, myc-tagged LC3B or both, as indicated. Cells were co-transfected with the indicated myc-tagged proteins together with 60 ng of Nqo1-ARE-Luc reporter and were analyzed 24h after transfection. Results were normalized to β-gal and presented as mean values with s.d. (n = 3). \*\* = P < 0.01, based on one-way ANOVA (Fisher's LSD test).

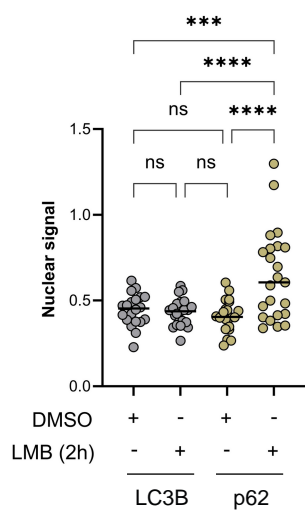


FIGURE S1

**A**



**B**



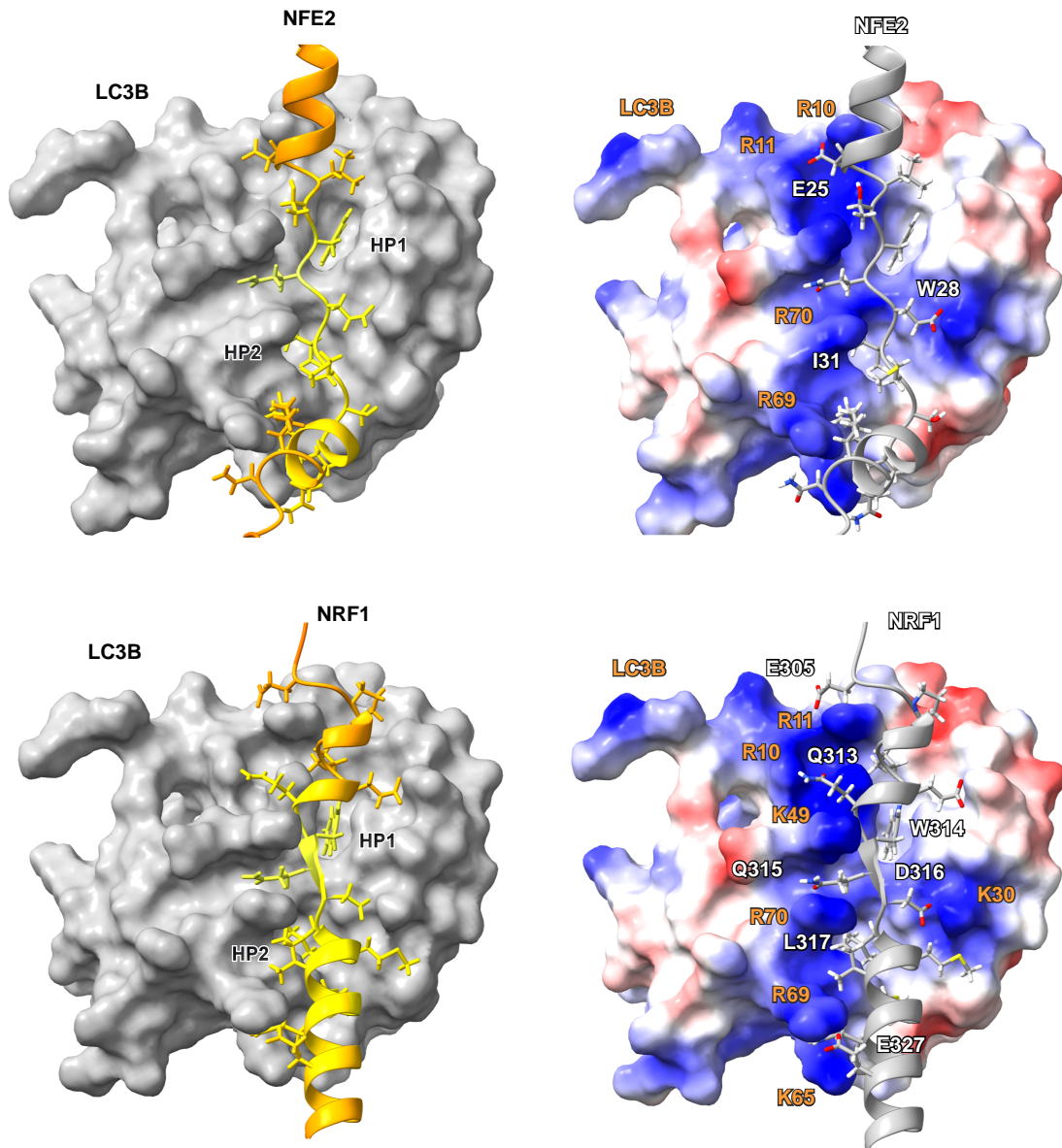
**Figure S1. p62 is not capable of inducing nuclear shuttling of LC3B.** (A) U2OS cells were treated with either vehicle (DMSO) or LMB for 2h, followed by immunostaining of endogenous p62 and LC3B. Cells were imaged using Zeiss LSM800 and representative images based on two independent experiments are shown. Scale bar = 10  $\mu$ m. (B) Quantification of A. The nuclear signal of LC3B and p62 were quantified using a CellProfiler pipeline based on one-way ANOVA (post hoc Tukey test), where each cell corresponds to one value. ns =  $P > 0.05$  (non-significant), \*\*\*\* =  $P < 0.0001$ . Error bars indicate SEM.

FIGURE S2

**A**

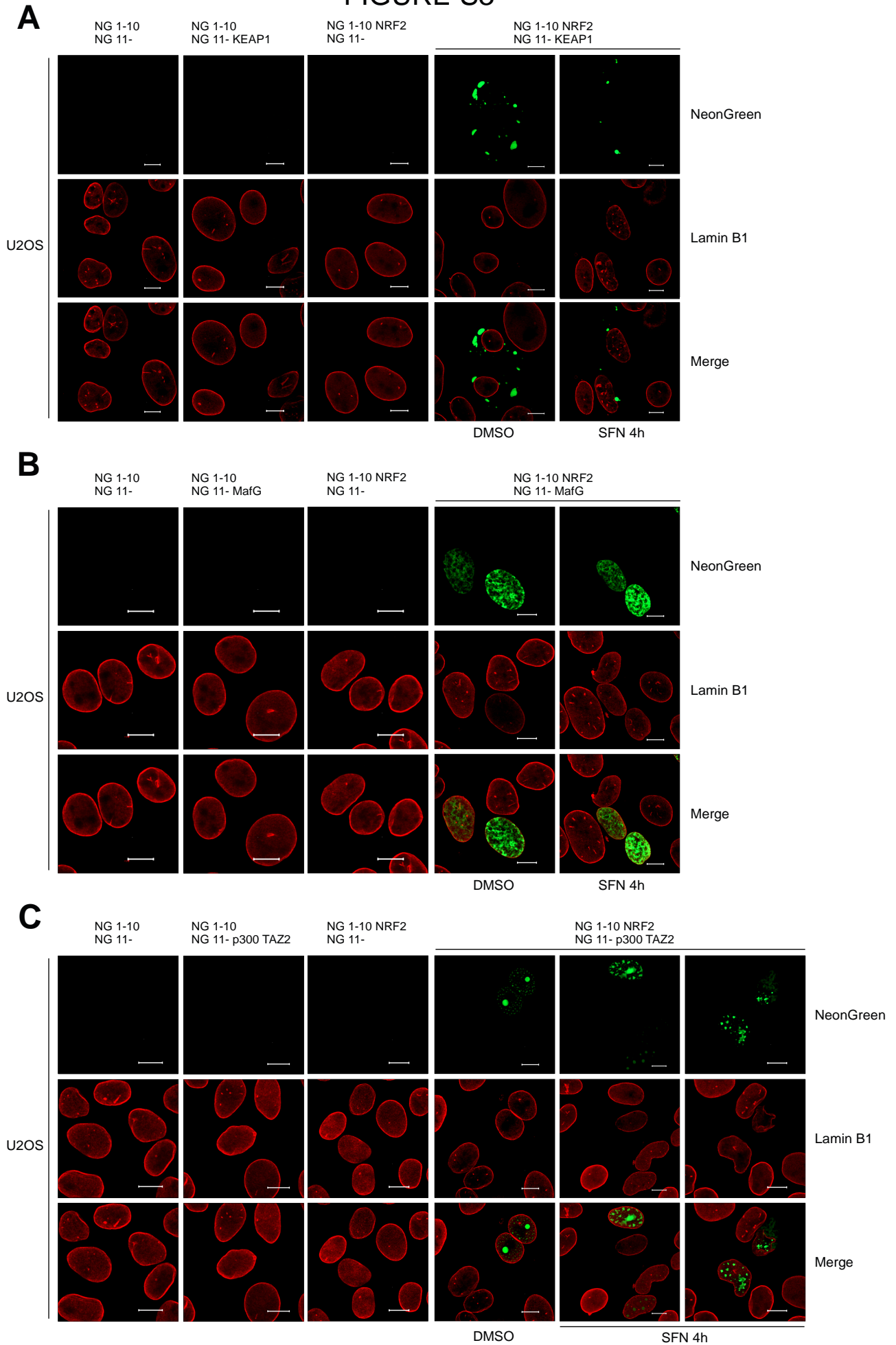
sp	Q9Y4A8	NF2L3_HUMAN	1	10	20	30																										
sp	Q16236	NF2L2_HUMAN	NG	T	D	T	S	F	S	L	E	D	L	F	Q	L	L	S	Q	P	E	N	S	L	E	G	I	S	L	G		
sp	Q16621	NFE2_HUMAN	D	L	D	G	M	Q	Q	D	I	E	Q	V	W	E	L	L	S	I	P	E	L	Q	C	L	N	I	E	N	D	
sp	Q14494	NF2L1_HUMAN	L	S	T	S	E	L	G	E	M	E	L	T	W	Q	E	I	M	S	I	T	E	L	Q	G	L	N	A	P	S	E
			T	G	T	E	S	P	F	D	L	E	Q	Q	W	Q	D	L	M	S	I	M	E	M	A	M	E	V	N	T	S	

**B**



**Figure S2. AlphaFold2 structure predictions of NRF1 and p45. (A)** Comparison of the Neh5 domain in NRF2 aligned with transactivation regions in NRF1, NRF3 and NFE2 (p45). Conserved residues are boxed, and highly conserved residues are indicated by red color. **(B)** (Upper) AlphaFold prediction of the structure of the complex of human NFE2 (p45) aa 21-48 and full-length LC3B. (Upper Left) Cartoon of NFE2 (p45) colored by predicted local distance difference test (pLDDT) (Light blue>70, orange>50, yellow<50). (Upper Right) Surface of LC3B colored by electrostatic potential. Residues of NFE2 in white/grey text, and of LC3B in orange text. (Lower) AlphaFold prediction of the structure of the complex of human NRF1 aa 302-331 and full-length LC3B. (Lower Left) Cartoon of NRF1 colored by predicted local distance difference test (pLDDT) (Light blue>70, orange>50, yellow<50). (Lower Right) Surface of LC3B colored by electrostatic potential. Residues of NRF1 in white/grey text, and of LC3B in orange text.

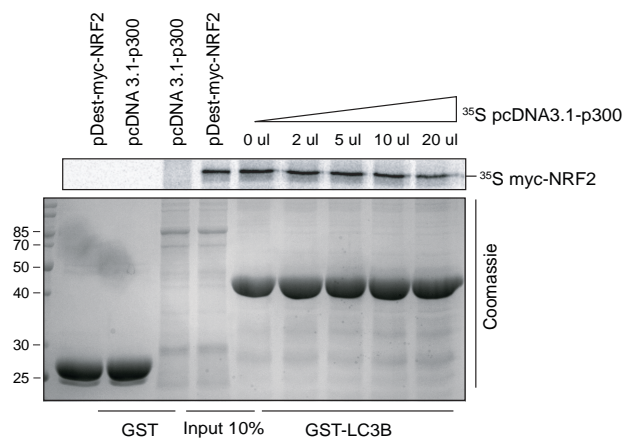
FIGURE S3



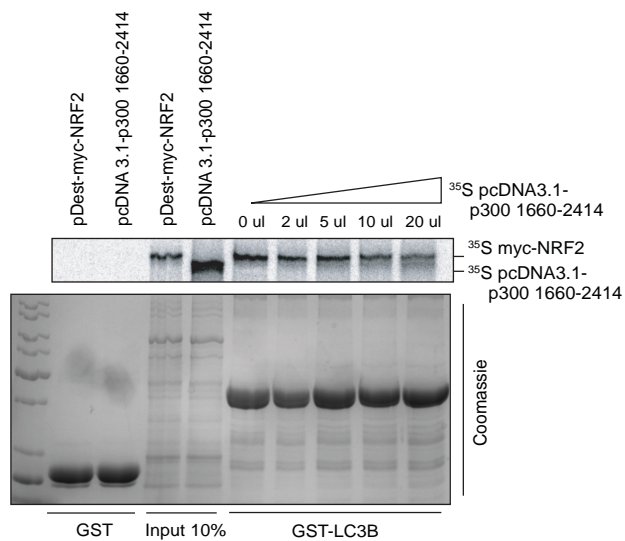
**Figure S3. Bimolecular fluorescence complementation assays for different NRF2 interactors. (A)** Bimolecular fluorescence complementation (BiFC) analysis of the NRF2-KEAP1 interaction. U2OS cells were transfected with the indicated combination of split NeonGreen constructs, followed by endogenous staining of Lamin B1 as a nuclear control and imaging using Zeiss LSM800. Representative images based on two independent experiments are shown. Scale bar = 10  $\mu$ m. **(B)** BiFC assay for the NRF2 – MafG interaction. **(C)** BiFC assay for the NRF2 – p300 1660-1810 (TAZ2) interaction.

FIGURE S4

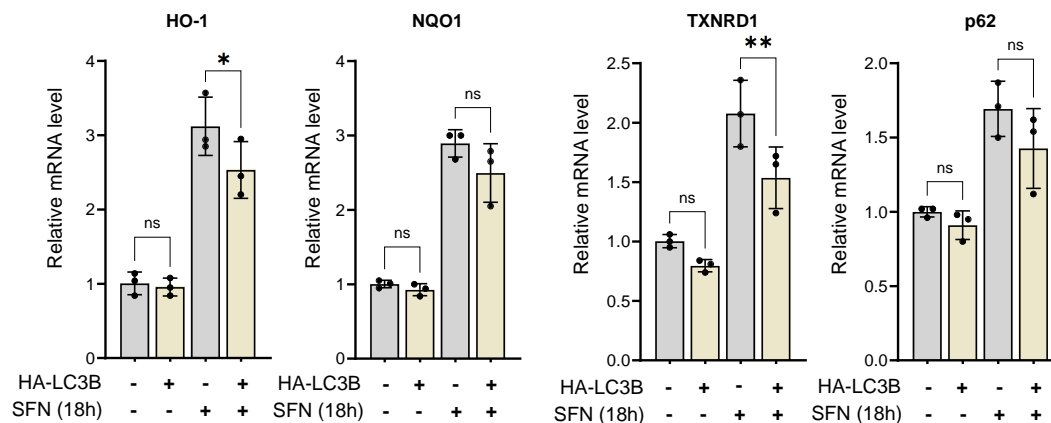
**A**



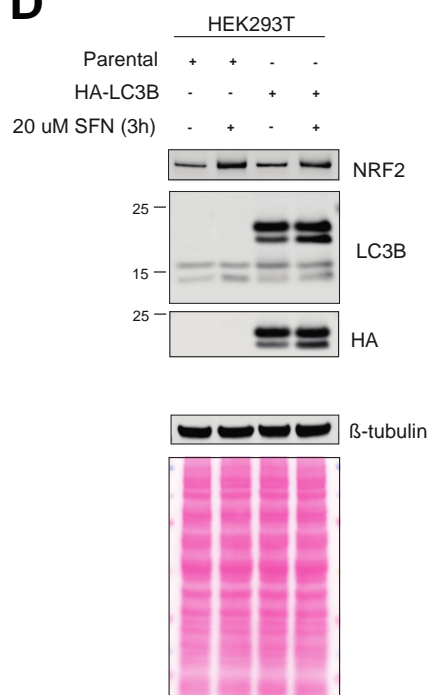
**B**



**C**



**D**



**E**

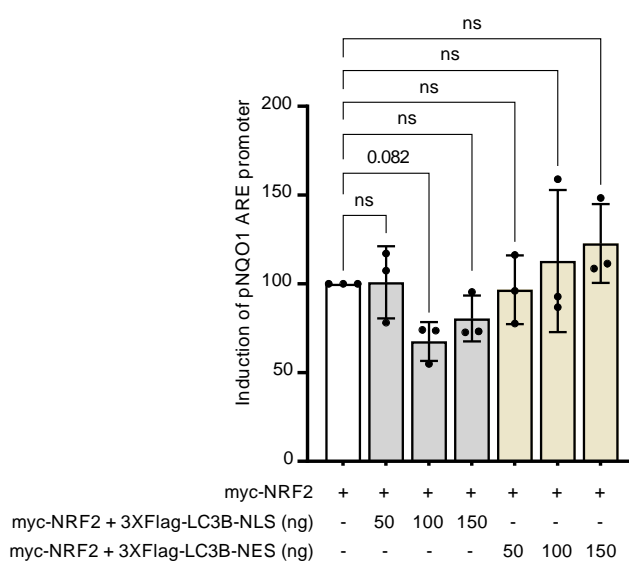


**Figure S4. LC3B competes with p300 in vitro.** (A) In vitro GST pulldown assay demonstrating competition between LC3B and p300 (full length) for binding to NRF2. Recombinant GST-tagged LC3B was incubated with in vitro translated <sup>35</sup>S-labeled myc-NRF2, in the presence or absence of increasing amounts of in vitro translated <sup>35</sup>S-labeled myc-p300. The amount of <sup>35</sup>S-labeled myc-NRF2 and GST-LC3B is constant in all reactions. (B) In vitro GST pulldown assay demonstrating competition between LC3B and p300 1660-2414 for binding to NRF2. (C) RT-qPCR analyses of HO-1, NQO1, TXNRD1 and p62 in HEK293T stably expressing HA-LC3B. Results were normalized to Lamin A/C and presented as mean values with s.d. (n = 3). ns = P > 0.05 (non-significant), \* = P < 0.05, \*\* = P < 0.01, based on one-way ANOVA (Fisher's LSD test). (D) Confirmation of HA-LC3B stable expression in HEK293T cells using Western blot analysis. (E) Reporter gene assay testing the activation of the Nqo1-ARE-Luc reporter by expression with either 75 ng of myc-tagged NRF2 or co-expression of 75 ng myc-tagged NRF2 with different concentrations of myc-tagged LC3B-NLS or myc-tagged LC3B-NES, as indicated. HEK293 were co-transfected with the indicated myc-tagged proteins together with 60 ng of Nqo1-ARE-Luc reporter and were analyzed 24h after transfection. Results were normalized to β-gal and presented as mean values with s.d. (n = 3). ns = P > 0.05, based on one-way ANOVA (Fisher's LSD test).



## PAPER II

## **Nuclear autophagy interactome unveils WSTF as a constitutive nuclear inhibitor of inflammation**

Yu Wang<sup>1,2,3,4</sup>, Vinay V. Eapen<sup>5</sup>, Athanasios Kournoutis<sup>4</sup>, Angelique Onorati<sup>1,2,3</sup>, Xianting Li<sup>6</sup>, Xiaoting Zhou<sup>6</sup>, Murat Cetinbas<sup>7</sup>, Lu Wang<sup>8</sup>, Jihe Liu<sup>9</sup>, Corey Bretz<sup>10</sup>, Zhuo Zhou<sup>11,12</sup>, Shannan J. Ho Sui<sup>9</sup>, Srinivas Vinod Saladi<sup>13</sup>, Ruslan I. Sadreyev<sup>7</sup>, Peter D. Adams<sup>10</sup>, Robert E. Kingston<sup>14,15</sup>, Zhenyu Yue<sup>6</sup>, Terje Johansen<sup>4,\*</sup>, Zhixun Dou<sup>1,2,3,\*</sup>

<sup>1</sup> Center for Regenerative Medicine, Massachusetts General Hospital, Boston, MA, USA.

<sup>2</sup> Harvard Stem Cell Institute, Harvard University, Cambridge, MA, USA.

<sup>3</sup> Department of Medicine, Massachusetts General Hospital, Harvard Medical School, Boston, MA, USA.

<sup>4</sup> Autophagy Research Group, Department of Medical Biology, University of Tromsø - The Arctic University of Norway, Tromsø, Norway.

<sup>5</sup> Department of Cell Biology, Harvard Medical School, Boston, MA, United States.

<sup>6</sup> Department of Neurology, Department of Neuroscience, Friedman Brain Institute, Icahn School of Medicine at Mount Sinai, New York, NY, USA.

<sup>7</sup> Department of Molecular Biology, Department of Pathology, Massachusetts General Hospital, Harvard Medical School, Boston, MA, USA.

<sup>8</sup> Department of Cell and Developmental Biology, Perelman School of Medicine, University of Pennsylvania, Philadelphia, PA, USA.

<sup>9</sup> Bioinformatics Core, Department of Biostatistics, Harvard T.H. Chan School of Public Health, Boston, MA, USA.

<sup>10</sup> Aging, Cancer and Immuno-oncology Program, Sanford Burnham Prebys Medical Discovery Institute, La Jolla, CA, USA.

<sup>11</sup> Institute of Systems Medicine, Chinese Academy of Medical Sciences & Peking Union Medical College, Beijing, China.

<sup>12</sup> Suzhou Institute of Systems Medicine, Suzhou, Jiangsu, China.

<sup>13</sup> Department of Otolaryngology, Massachusetts Eye and Ear Infirmary, Harvard Medical School, Boston, MA, USA.

<sup>14</sup> Department of Molecular Biology and MGH Research Institute, Massachusetts General Hospital, Boston, MA, USA.

<sup>15</sup> Department of Genetics, Harvard Medical School, Boston, MA, USA.

\* Correspondence: Zhixun Dou (zdou@mgh.harvard.edu) or Terje Johansen (terje.johansen@uit.no)

## **Abstract**

Macroautophagy (hereafter referred to as autophagy) degrades a variety of cellular components. A poorly understood area is autophagic degradation of nuclear substrates, or “nuclear autophagy”. It remains unclear what can be degraded by autophagy from the mammalian nuclei. We began our study by investigating the nuclear binding partners of ATG8 family proteins that play important roles in recognizing autophagy substrates. We systematically evaluated the ATG8 nuclear interactome in primary human cells and in mouse brain, identifying hundreds of novel interactions. We continued our study by evaluating the nuclear proteomes of cellular senescence, a stable form of cell cycle arrest program associated with inflammation, in which nuclear autophagy is involved. Combined with the ATG8 nuclear interactome data, we identified WSTF, a component of the ISWI chromatin remodeling complex, as a novel substrate of nuclear autophagy. The degradation of WSTF, mediated by a direct interaction with the GABARAP isoform of ATG8, promotes chromatin accessibility of inflammatory genes and induces senescence-associated inflammation. Furthermore, WSTF directly binds the p65 subunit of NF- $\kappa$ B and inhibits its acetylation, thus blocking inflammatory gene expression in the setting of senescence, cancer, and pathogen infection. In addition, we show that loss of WSTF is required for the immuno-surveillance of oncogenic Ras in mouse liver; forced expression of WSTF inhibited tumor-suppressive inflammation and led to the development of liver tumors. Taken together, our study provides a global view of mammalian nuclear autophagy and reveals a novel nuclear inhibitor of inflammation implicated in diverse pathological contexts. Targeting WSTF may be broadly valuable as therapeutic intervention of inflammatory diseases.

Keywords: autophagy, nuclear autophagy, senescence, SASP, WSTF, ISWI, inflammation

## Introduction

Mammalian ATG8 family proteins (including LC3A, LC3B, LC3C, GABARAP, GABARAPL1, and GABARAPL2) bind to selective autophagy receptors or directly to autophagy substrates and help mediate their delivery to autophagosomes for degradation<sup>1</sup>. While yeasts have one single ATG8 protein, the six isoforms of mammalian ATG8 family proteins have both distinct and redundant roles in autophagosome formation, expansion, maturation, vesicle transport, docking of autophagy receptors, and in direct recognition of autophagy substrates<sup>2,3</sup>. ATG8 proteins are present in the nucleus with low mobilities<sup>4,5</sup>, suggesting that they interact with large molecular weight complexes. We recently reported that nuclear ATG8s directly bind to nuclear Lamin B1 and SIRT1, facilitating their shuttling to the cytoplasm for autophagic degradation upon cellular senescence<sup>6,7</sup>, suggesting that autophagy has a previously unappreciated role in degrading nuclear constituents, termed as “nuclear autophagy”. Beyond Lamin B1 and SIRT1, whether nuclear autophagy can degrade other substrates is unclear, which represents a major open area for investigation.

Cellular senescence is a pro-inflammatory condition in which nuclear autophagy is induced<sup>6,7</sup>. Senescent cells accumulate in aged and diseased tissues, where they impair tissue renewal and promote inflammation<sup>8,9</sup>. While senescence is a potent tumor-suppressive mechanism, it paradoxically contributes to aging and the progression of many diseases<sup>10,11,12</sup>. Clearing senescent cells using pharmacological or genetic approaches ameliorates several diseases in mice and humans<sup>13,14</sup>. A key feature of senescence is the secretion of a large array of pro-inflammatory cytokines, chemokines, growth factors, and proteases, collectively referred to as senescence-associated secretory phenotype (SASP)<sup>11,12,8,9</sup>. The SASP program recruits immune cells and alters tissue microenvironment, leading to inflammation<sup>11,12,8,9</sup>. Targeting the SASP program is an important biomedical objective to intervene in diseases. The roles of nuclear autophagy in senescence are poorly understood, largely due to our limited knowledge of the substrates of nuclear autophagy.

To fill the major gaps in our understanding of nuclear autophagy, we examined the nuclear binding partners of ATG8s as well as the nuclear proteome of senescent cells. These proteomic studies offer a comprehensive resource to study nuclear autophagy. We further focused on WSTF, which we identified as a new substrate of nuclear autophagy, and discovered an unexpected role of WSTF in regulating inflammation.

## Results

### The nuclear ATG8 interactome

While ATG8 interactomes using whole cell extracts have been reported by several groups<sup>15,16,17</sup>, very few nuclear interactions have been identified. We reason that this is likely due to the poor lysis efficiency of the nuclear and chromatin fraction. Most interactomics studies used NP40 or

Triton X-100 to lyse cells; after a centrifugation step, the supernatants were collected for subsequent co-immunoprecipitation (co-IP). These standard lysis conditions led the chromatin fraction to become pelleted and discarded for the subsequent IP steps. Using histone H3 as a marker for the chromatin fraction, we found that 1% NP40 lysis showed a minimal signal of H3 in the supernatant (Fig. 1a). To resolve the poor solubility issue of the chromatin fraction, we used benzonase, an endonuclease that digests chromatin DNA, to facilitate the release of chromatin proteins to the supernatant. The efficiency is similar to that of adding 1% SDS followed by sonication (Fig. 1a). Thus, we generated a new procedure suitable for nuclear interactome studies.

We then stably expressed the six ATG8 isoforms in IMR90 primary human fibroblasts, cultured in physiological 3% oxygen, and performed nuclear fractionation and co-IPs (Fig. 1b and 1c). As a positive control, an interaction with Lamin B1 was detected (Fig. 1b and 1c). We subsequently performed tandem mass tag (TMT)-based mass-spectrometry analyses, with three biological replicates of each ATG8 isoform and two biological replicates of GFP as negative controls (scheme shown in Fig. 1d). A total of 422 statistically significant nuclear interactions were identified for LC3A, LC3B, LC3C, and 568 for GABARAP, GABARAPL1, GABARAPL2 (Fig. 1e). As expected, these isoforms showed overlapping yet distinct binding partners (Fig. 1e). Top interaction partners are presented in interaction maps (Extended data Fig. 1a and 1b). When comparing with a previous autophagy interaction network (AIN) focusing on cytoplasmic interactions<sup>15</sup>, we found that the majority of the binding partners of ATG8 from our nuclear AIN are unique and previously unknown (Extended data Fig. 1c). Hence, we generated a new database of nuclear ATG8 interactome in primary human cells.

To further explore ATG8 binding partners *in vivo*, we used a GFP-LC3B transgenic mouse strain<sup>18</sup> and performed GFP co-IPs in mouse brain, in both cytoplasmic and nuclear fractions (scheme shown in Fig. 1f). Wild-type (not expressing GFP-LC3B) mice were used as negative controls. Similar to the nuclear fractionation of primary human cells, a benzonase treatment step was included, leading to successful solubilization of histone H3 (Extended data Fig. 1d). Compared with the negative control using wild-type mice, GFP co-IPs in GFP-LC3B mice precipitated specific proteins (Extended data Fig. 1e). Three biological replicates for cytoplasmic GFP co-IPs were included, and due to the low protein concentrations of the nuclear fractions, the three nuclear fractions were combined for TMT-based mass-spectrometry analyses (Fig. 1f). Although LC3B was present much less in the nucleus than in the cytoplasm, specific binding with nuclear proteins was detected from nuclear GFP co-IPs.

We went on further to analyze the nuclear binding partners of ATG8s in primary human cells and mouse brain, and discovered the overlapping and unique interactions in the two biological models (Fig. 1g and specific proteins listed in Extended data Fig. 1g). Gene ontology (GO) analyses revealed similar profiles of the nuclear binding partners of ATG8s in the two models, with substantial proteins within the categories of RNA binding, mRNA splicing and transport (Fig. 1h). The binding between ATG8s and RNA-related proteins is supported by recent studies showing LC3 mediates RNA secretion<sup>19</sup> and degradation<sup>20</sup>. In addition, proteins involved in chromatin

remodeling, nucleosomal binding, and transcription were identified (Fig. 1h). The overlapping nuclear proteins from the two unrelated biological models suggest conserved roles for nuclear ATG8s across tissues in mammals in regulating these biological processes. Of our particular interest is the chromatin remodeling complexes that bind to both human and mouse ATG8s (Fig. 1i), as these proteins regulate nucleosome positioning and chromatin structures, thereby affecting gene expression and silencing.

Taken together, we have generated a systematic resource of nuclear ATG8 interactomes in primary human cells and mouse brain, and identified chromatin remodeling complexes as putative ATG8 binding partners in mammalian nuclei.

### **Nuclear proteomes of cellular senescence**

We previously reported that nuclear Lamin B1 and SIRT1 autophagic degradation occurs in cellular senescence, in which cells respond to cellular insults such as oncogene activation and telomere attrition and upregulate autophagy activities<sup>6,7</sup>. To explore novel substrates of nuclear autophagy under senescence, we induced senescence of primary IMR90 cells using two different means, oncogene activation and sub-lethal dose of DNA damage, and searched for overlapping hits with ATG8 nuclear interactomes.

We began by investigating the whole cell proteome of HRasV12-induced senescence (Fig. 2a), using TMT-based mass-spectrometry, done with three biological replicates (Fig. 2b and Extended data Fig. 2a). Consistent with our existing knowledge of senescence, the proteome of senescent cells harbors significantly upregulated proteins, most of which are involved in the SASP program and the DNA damage responses, as well as significantly downregulated proteins involved in cell cycle and DNA replication (Fig. 2c and Extended data Fig. 2b). Among the downregulated proteins, 718 are nuclear proteins (Fig. 2d), and 89 of them (including Lamin B1) overlap with ATG8 nuclear interactome of IMR90 cells (Fig. 2e and listed in Extended data Fig. 2c).

We further examined the proteome of etoposide-induced senescence, in both autophagy-competent and autophagy-deficient cells, using shRNA-mediated silencing of ATG7, focusing on nuclear fractions (Fig. 2f-2h and Extended data Fig. 2d). As expected, inhibition of ATG7 suppressed LC3 lipidation and impaired Lamin B1 downregulation in senescence (Fig. 2f and 2g). The nuclear fractions of these cells were subjected to TMT-based mass-spectrometry analyses (Fig. 2h and Extended data Fig. 2e). 309 proteins were downregulated in the autophagy competent cells and 199 of them (including Lamin B1) overlap with ATG8 nuclear interactome of IMR90 cells (listed in Extended data Fig. 2f). We did not detect SIRT1 in these proteomic studies, likely due to the higher sensitivity of SIRT1 antibodies than that of mass-spectrometry.

While HRasV12 and etoposide-induced senescence both revealed putative downregulated nuclear proteins that bind to ATG8, we reason that the 27 overlapping targets in the two senescence models (Fig. 2k) are of greater generalizability in senescence. We thus investigated these targets in greater

detail, and further asked whether their downregulation is linked to ATG7 and/or their mRNA levels using our previously established RNA-seq datasets<sup>7,21</sup>. We grouped these targets in four categories: (1) rescued by ATG7 deficiency while their mRNA levels are unaltered, (2) not rescued by ATG7 deficiency while their mRNA levels are reduced; (3) rescued by ATG7 deficiency while their mRNA levels are also reduced in senescence, and (4) not linked to ATG7 or mRNA downregulation (Fig. 2l and 2m). As a control, Lamin B1 is known to be downregulated at both mRNA and protein levels<sup>6</sup>, and is listed in group (3). The proteins that are lost in senescence and are rescued by ATG7 deficiency are further presented in a heatmap (Fig. 2n) and overlapped with ATG8 nuclear interactome (Fig. 2o).

Because our ATG8 nuclear interactome studies identified chromatin remodeling proteins as putative binding partners of ATG8 (Fig. 1h and 1i), we examined their protein levels in senescence (Extended data Fig. 2g). Our results showed that WSTF is a consistent target in all our proteomic datasets: WSTF binds to ATG8 in both human fibroblasts and mouse brain (Fig. 1i and Extended data Fig. 1b and 1g) and is downregulated in senescent cells, which can be rescued by ATG7 deficiency (Fig. 2m-2o and Extended data 2g). Further, while WSTF protein is reduced in senescence, its mRNA levels remain unchanged (Fig. 2m and 2p), making it a strong candidate as a substrate of nuclear autophagy. WSTF (also known as BAZ1B, hereafter referred to as WSTF for both gene and protein), is a subunit of imitation switch (ISWI) chromatin remodeling complex<sup>22</sup>. The ISWI chromatin remodeling complex regulates nucleosome spacing, changing the chromatin from an “open” state to a “closed” state, by forming ordered nucleosome arrays on chromatin, thereby repressing gene expression<sup>23,24,25</sup>. WSTF has not been investigated in the context of autophagy or senescence. In summary, we generated nuclear proteomic datasets in two forms of senescence, and revealed new potential substrates of nuclear autophagy. We will focus on WSTF for the rest of this study, investigating its autophagic degradation and its biological functions.

### **WSTF is degraded by autophagy in senescence**

We induced senescence by multiple means, in multiple cell systems, to investigate the behavior of WSTF. WSTF protein levels are dramatically reduced in senescent IMR90 cells induced by etoposide (Fig. 3a), HRasV12 (Fig. 3b), or replication exhaustion (Fig. 3c). The loss of WSTF protein is also observed in senescent primary BJ fibroblasts, induced by etoposide, ionizing irradiation (IR), or HRasV12, as well as in senescent primary MEFs induced by etoposide or IR (Extended data Fig. 3a). In addition, therapy-induced senescence of A549 cancer cells exhibited loss of WSTF protein (Extended data Fig. 3b). In contrast to the loss of WSTF in senescence, WSTF protein levels remain unchanged upon quiescence or starvation (Extended data Fig. 3c-3e). We further examined other proteins of the ISWI complex. SNF2H (also known as SMARCA5), the ATPase of the ISWI complex that binds to WSTF, is largely unaltered in senescence (Fig. 3a). Another subunit of the ISWI complex, ACF1 (also known as BAZ1A) that also binds to SNF2H, is reduced in senescence (Fig. 3a). However, ACF1 is also reduced upon quiescence or starvation (Extended data Fig. 3c and 3d), and the loss of ACF1 cannot be rescued by ATG7 deficiency (Extended data Fig. 3e), suggesting that ACF1 is not a selective autophagy substrate upon

senescence. While WSTF protein is consistently lost in senescence, its mRNA levels are unchanged (Fig. 3d-3f), consistent with our proteomic and transcriptomic results (Fig. 2m and 2p). We therefore went on to investigate whether the loss of WSTF is mediated by autophagy.

We inhibited autophagy by both genetic and pharmacological approaches, and examined the behavior of WSTF in senescence. First, we stably inactivated ATG7 using shRNA, and found that while WSTF was lost in non-targeting control shRNA cells, its protein levels were largely retained upon etoposide or IR-induced senescence in cells where ATG7 was knocked down (Fig. 3g and 3h, Extended data Fig. 3f). By contrast, the loss of ACF1 was not impaired by ATG7 deficiency (Extended data Fig. 3f). Second, we inhibited autophagy degradation using bafilomycin A1 that blocks lysosomal acidification. This led to a restoration of WSTF protein levels in senescence (Fig. 3i and Extended data Fig. 3g). By contrast, inhibition of proteasomal degradation by MG132 failed to rescue WSTF in senescence (Fig. 3j).

We further observed WSTF localization using imaging approaches. While WSTF is localized in the nucleus of proliferating control cells, cytoplasmic localization of WSTF was observed in senescence, colocalizing with autophagosome markers LC3 or GABARAP as well as lysosomal markers LAMP1 or LysoTracker (Fig. 3k and 3l, Extended data Fig. 3h and 3i, and quantified in Fig. 3m and 3n). Addition of bafilomycin A1 accumulated WSTF in the cytoplasm, colocalizing with LAMP1 (Extended data Fig. 3h). In contrast to senescence, starvation did not induce WSTF cytoplasmic localization (Extended data Fig. 3h), consistent with our immunoblotting results showing that WSTF was not lost upon starvation (Extended data Fig. 3d and 3e). Taken together, these results collectively indicate that WSTF is a selective nuclear autophagy substrate upon senescence.

### **A GABARAP-WSTF interaction mediates WSTF autophagic degradation**

We subsequently investigated the molecular mechanisms underlying WSTF autophagic degradation. Because ATG8 proteins bind to autophagy receptors or substrates and aid in delivering them to autophagosomes for degradation, we tested the binding between WSTF and the six ATG8 proteins. Using *in vitro* translated WSTF subjected to pull down with bacterially expressed and purified GST-ATG8 proteins, we found that GABARAP is the main ATG8 isoform that directly binds to WSTF (Fig. 4a). The binding with LC3B is quantitatively much less than that of GABARAP (Fig. 4a and 4b) in these *in vitro* pulldowns, which was further validated by co-IPs from cell extracts (Fig. 4c). These results are consistent with our ATG8 nuclear interactome data in which WSTF was detected via GABARAP co-IP (Extended data Fig. 1b and Fig. 2o). We further performed co-IP of endogenous proteins, and found that GABARAP IP brought down WSTF and its binding partner SNF2H in the ISWI chromatin remodeling complex (Fig. 4d). By contrast, GABARAP IP precipitated much less of BRG1 and BRM, components of the SWI/SNF chromatin remodeling complex<sup>26,27,28</sup>. Further examination using *in vitro* translated WSTF and SNF2H revealed that WSTF, and not SNF2H, is a direct binding partner of GABARAP (Extended



data Fig. 4a and 4b). Taken together, these results strongly support a direct GABARAP-WSTF interaction.

We next interrogated the regions or amino acid residues that mediate the GABARAP–WSTF interaction. On the GABARAP end, we found that the GABARAP F77A mutant significantly impaired the binding with WSTF from both *in vitro* pull-down (Fig. 4e) and co-IP from cell extracts (Fig. 4f). On the WSTF end, we constructed a series of truncations (summarized in Fig. 4g) and found that the region encompassing amino acids 474-691 of WSTF is both necessary and sufficient for interaction with GABARAP (Fig. 4h, Extended data Fig. 4c-4f). We further interrogated this region in greater detail (summarized in Fig. 4i) and found that WSTF 474-483 region, and in particular, the L476 residue, is essential for GABARAP binding in both *in vitro* pulldown and in co-IPs from cells (Fig. 4i-4k and Extended data Fig. 4g). While deletion of 474-483 or mutation of L476 abolished the binding to GABARAP, these mutants of WSTF did not affect the binding to SNF2H (mediated by the BAZ1&2 domain of WSTF) or to histone H3 (mediated by the PHD and bromodomain of WSTF) (Extended data Fig. 5a). Hence, we have discovered the critical residues on both ends that mediate the GABARAP-WSTF interaction.

To further investigate the interaction, we synthesized a series of WSTF peptides corresponding to the WSTF 474-483 region (Fig. 4l), and asked whether these peptides could block the GABARAP-WSTF interaction. The peptide corresponding to 474-483 of WSTF along with its flanking sequence at the amino and carboxy (N and C) termini (PP4, residues 466-492) effectively inhibited GABARAP-WSTF binding in *in vitro* pulldown (Fig. 4m). Introducing L476A mutation into this peptide giving PP5 abrogated this effect (Fig. 4n).

Several interaction surfaces are known for binding to ATG8 family proteins with the LC3-interacting region (LIR) docking site (LDS) being the most used surface for interaction partners<sup>29</sup>. Recently, another binding surface named ubiquitin-interacting motif (UIM)-docking site (UDS) was suggested<sup>30</sup>. Using point mutations, we can compromise the two binding surfaces selectively (Extended data Fig. 5b). We used the Y49A mutation to render the LDS binding deficient and the F77A mutation to cripple the UDS in GABARAP. Our results clearly implicate the UDS in binding to WSTF (Fig. 4e and 4f). We next investigated the structure of the WSTF region binding to GABARAP using *in silico* modeling. The 474-484 region of WSTF is predicted to form an alpha-helix, similar to a helix of the Cav2.2 protein<sup>31</sup>, based on PHYRE2 server that predicts protein structure<sup>32</sup> (Extended data Fig. 5c). Furthermore, structural modeling of WSTF by AlphaFold2<sup>33,34</sup> predicts with high confidence that the 473-485 region of WSTF forms an alpha-helix, with the L476 residue exposed at the outer surface of WSTF (Extended data Fig. 5d). Employing the ClusPro web server for automatic protein-protein docking<sup>35</sup>, we obtained a top ranked model placing the WSTF helix with the L476 residue firmly into the UDS of GABARAP (Extended data Fig. 5d). The UDS surfaces of LC3B and GABARAP are different with a wider and more shallow pocket in GABARAP than in LC3B, which helps explain why WSTF binds GABARAP with higher affinity than LC3B (Extended data Fig. 5e, Fig. 4b). Together, these results provided

mechanistic insights into the WSTF-GABARAP interaction and prompted us to investigate the behavior of WSTF mutants in senescence.

We stably expressed the WSTF  $\Delta$ 474-483 mutant or the WSTF L476A mutant defective in binding to GABARAP, and investigated their degradation and localization. While the protein levels of wild-type WSTF were reduced upon senescence, both mutants showed impaired downregulation in senescence, measured at two time points post IR (Fig. 4o). By contrast, the loss of Lamin B1 was not affected by the two mutants (Fig. 4o). In addition, we found that while wild-type WSTF was translocated to the cytoplasm, colocalizing with GABARAP puncta, both mutants showed impaired ability to do so (Fig. 4p and quantified in Fig. 4q, Extended data Fig. 5b). The WSTF mutants did not affect the formation of senescence-associated heterochromatin foci (SAHF), a marker for senescence (Fig. 4q). Taken together, these results strongly suggest that WSTF binding to GABARAP is required for its autophagic degradation in senescence.

### **WSTF represses the SASP program**

We subsequently investigated the biological significance of autophagic degradation of WSTF in senescence. To counteract the loss of WSTF, we overexpressed WSTF, and examined the key features of senescence (Fig. 5a). We found that WSTF overexpression did not affect the loss of Lamin B1 (Fig. 5a), induction of p16Ink4a (hereafter referred to as p16) (Fig. 5a), or senescence-associated beta-galactosidase (SA- $\beta$ -gal) (Extended data Fig. 6a). However, the induction of IL8, a SASP factor, was reduced by WSTF overexpression (Fig. 5a). RT-qPCR analyses of senescence and SASP genes confirmed that while WSTF overexpression did not affect Lamin B1, p16, or p21, the induction of key factors of the SASP program was significantly reduced, including IL6, IL8, IL1 $\alpha$ , and IL1 $\beta$  (Fig. 5b). The impaired SASP program was further confirmed at the secreted level, measuring the conditioned media of senescent cells overlaid to a cytokine array (Fig. 5c). While multiple SASP factors showed reduced levels in the conditioned media, TIMP-2, a soluble factor constitutively secreted by proliferating and senescent IMR90 cells, was not altered by WSTF overexpression (Fig. 5c and quantified in Fig. 5d). In addition to WSTF overexpression, we also asked whether disruption of WSTF promotes the SASP program. shRNA-mediated WSTF inactivation, using two independent hairpins, enhanced SASP gene expression, while not affecting Lamin B1 or p16 upon IR-induced senescence (Fig. 5e and 5f, Extended data Fig. 6b and 6c). Furthermore, we found that WSTF overexpression blocks the SASP program of oncogene-induced senescence triggered by HRasV12 (Fig. 5g and 5h). Moreover, expression of WSTF in established senescent cells that already lost WSTF inhibited IL8 expression (Extended data Fig. 6d). Taken together, these data collectively suggest that WSTF is a negative regulator of the SASP program.

To further examine the SASP program in an unbiased manner, we performed an RNA-seq study, including proliferating control and HRasV12-induced senescence, expressing vector control or WSTF (following the design of Fig. 5g). Analysis of differentially expressed genes (DEGs) in senescent cells suggested that WSTF substantially inhibited the expression of a large panel of pro-inflammatory genes (Fig. 5i). Pathway enrichment analysis using EnrichR<sup>36</sup> revealed that genes

downregulated by WSTF are strongly enriched in the categories of cytokines, growth factors, and chemokines, characteristic of the SASP program (Fig. 5j and specific genes listed in Extended data Fig. 6e). Genes related to other processes like cell cycle arrest are not affected by WSTF. The global reduction of the SASP gene expression is also presented in a heatmap, including established SASP factors<sup>37</sup> (Fig. 5k). These results strongly support that WSTF specifically represses the SASP program of senescence.

Lastly, we asked whether inhibition of WSTF autophagic degradation affects the SASP. To this end, we expressed a short region of WSTF (406-552) that binds to GABARAP, using deletion of the core amino acids for GABARAP interaction 466-492 as a negative control (illustrated in Fig. 5l). We tagged these peptides with a nuclear localization signal (NLS), leading to their expression in the nucleus (Extended data Fig. 6f). While WSTF 406-552 peptide strongly inhibited the binding between full-length WSTF and GABARAP, likely due to its competition with WSTF for GABARAP binding, WSTF 406-552  $\Delta$ 466-492 showed impaired binding to GABARAP, accompanied by its inability to block full-length WSTF-GABARAP interaction. Upon induction of senescence, the 466-492 peptide inhibited WSTF downregulation and the expression of IL6, while the 406-552  $\Delta$ 466-492 mutant peptide failed to do so. Hence, these data indicate that autophagic degradation of WSTF, mediated by GABARAP, is critical for the induction of the SASP program of senescence.

### **WSTF suppresses chromatin accessibility of SASP genes**

We next investigated how WSTF suppresses the SASP program of senescence. We first asked whether WSTF affects the established mechanisms of the SASP<sup>38,39,21,40,41,42,43,44,45</sup>, and found that while WSTF blocked the SASP gene expression (Extended data Fig 7a), it did not alter the status of p38MAPK, DNA damage response, mTOR, cytoplasmic chromatin fragments (CCF), cGAS-STING pathway, NF- $\kappa$ B p65 subunit nuclear translocation and phosphorylation at S536, or senescence-associated heterochromatin foci (SAHF) (Extended data Fig. 7a to 7c). These data suggest that WSTF employs a previously uncharacterized mechanism to regulate the SASP program.

We truncated the domains of WSTF with established biological functions and asked which activities of WSTF are involved in the SASP program. WSTF harbors a WAC domain with tyrosine kinase activity<sup>46</sup>, a BAZ1&2 domain that binds to SNF2H, and PHD & bromodomains that bind to histones (illustrated in Extended data Fig. 7d). We generated a series of truncation mutants of WSTF, and confirmed that the BAZ1&2 truncation impaired the binding to SNF2H while the PHD & bromodomain truncation impaired the binding to histones (Extended data Fig. 7d and 7e). Upon induction of senescence, we found that the BAZ1&2 domain as well as PHD & bromodomains are required for WSTF to inhibit the SASP (Fig. 6a and 6b). By contrast, the WAC domain of WSTF is not required to inhibit the SASP (Extended data Fig. 7f and 7g). These results suggest that the binding of SNF2H and association with chromatin are necessary for WSTF to suppress the SASP program of senescence.

We thus investigated the connection with SNF2H in greater detail, and discovered that SNF2H-WSTF complex is critical in repressing the SASP. First, CRISPR-mediated inactivation of SNF2H abrogated the effect of WSTF in blocking the SASP (Fig. 6c and 6d), consistent with the results that the BAZ1&2 domain of WSTF is involved (Fig. 6a and 6b). Second, overexpression of SNF2H inhibited the SASP (Fig. 6e and 6f), suggesting that SNF2H, like WSTF, is also a repressor of the SASP. Third, inactivation of WSTF abrogated the effect of SNF2H in blocking the SASP (Fig. 6g and 6h). Together, these results indicate that the ISWI chromatin remodeling complex has a previously unappreciated role in suppressing the SASP program of senescence.

Because the ISWI complex represses gene expression by forming ordered nucleosomes on chromatin, we assessed whether WSTF regulates chromatin accessibility over SASP genes by ATAC-seq<sup>47</sup>. Chromatin accessibility at SASP genes was low in control cells but was massively increased in senescence (Fig. 6i showing genomic tracks of ATAC-seq read density at IL8, MMP3, and IL1 $\beta$ ). Importantly, expression of WSTF substantially reduced chromatin accessibility at these SASP genes (Fig. 6i). We subsequently performed peak calling and evaluated the differentially accessible regions (DARs) at the genome-wide scale. GO analysis of the DARs revealed strong enrichment of functional gene categories involving cytokines, growth factors, and acute inflammation, characteristics of the SASP program (Fig. 6j and specific genes listed in Extended data Fig. 8a). The global reduction of chromatin accessibility at representative SASP genes is also presented in a heatmap (Extended data Fig. 8b). Further, the DARs with reduced chromatin accessibility located at the genes with downregulated RNA-seq expression in senescence were strongly enriched with genes of the SASP program (Extended data Fig. 8c). In sum, our results strongly suggest that WSTF in cooperation with SNF2H suppresses chromatin accessibility of pro-inflammatory genes of senescence.

### **WSTF is a broad inhibitor of inflammation**

Senescence shares several features with cancer. Senescent cells induced by activated oncogenes or loss of tumor suppressor proteins can generate neoplastic lesions *in vivo*. Both senescence and cancer are associated with DNA damage, and they share similar features of genome methylation<sup>48</sup>. Using cancer cell line encyclopedia (CCLE), we previously showed that the cGAS-STING pathway, required for the SASP program of senescence, is also strongly linked to cancer-associated pro-inflammatory gene expression<sup>21</sup>. These connections prompted us to investigate whether WSTF is involved in pro-inflammatory gene expression in cancer.

We inactivated WSTF using shRNA, and found that loss of WSTF increased the expression of IL6 and IL8 in Caco2, HeLa, MDA-MB-231, HCT116, and A549 cells (Fig. 7a and Extended data Fig. 9a). To robustly examine the connection between WSTF and pro-inflammatory gene expression in cancer at a larger scale, we exploited the proteomic resource of CCLE database that contains the proteomes of over 300 cancer cell lines<sup>49</sup>. Cell lines with lowest and highest 50% of WSTF expression were grouped and the expression of key pro-inflammatory genes was compared between WSTF-low and WSTF-high subsets. This analysis revealed that higher WSTF expression

is linked to higher expression of SNF2H, and importantly, lower expression of pro-inflammatory genes, while the housekeeping gene Lamin A does not follow this pattern (Fig. 7b). Together with our WSTF knockdown in cancer cell results, these data collectively suggest that WSTF is a negative regulator of pro-inflammatory genes in broad scenarios of cancer cells.

The results in cancer prompted us to examine a hypothesis that WSTF is a broad inhibitor of inflammatory gene expression. We exposed the control and WSTF deficient cells with a variety of pro-inflammatory conditions, including dsDNA (ISD) and dsRNA (poly I:C) transfection, tumor necrosis factor alpha (TNF $\alpha$ ), and bacterial lipopolysaccharides (LPS). In all these conditions, WSTF deficiency led to significantly higher expression of pro-inflammatory cytokines (Fig. 7c and Extended data Fig. 9b-9d). Moreover, we examined viral infection, using DNA virus (HSV-1) and RNA virus (SeV). In both cases, WSTF deficiency led to significantly higher expression of pro-inflammatory genes (Fig. 7d). The induction of interferon gene (IFN $\beta$ ) was not upregulated by WSTF deficiency (Fig. 7c and 7d). Together with our results in senescence and cancer, these data strongly suggest that WSTF is a broad negative regulator of inflammation.

### **WSTF directly binds to p65 and inhibits p65 acetylation**

The specific inhibition of inflammatory genes by WSTF, in a variety of contexts, sparked us to further examine the molecular mechanisms by which WSTF blocks inflammation. While we presented results showing that WSTF inhibits chromatin accessibility of SASP genes in senescence, it remains unclear what instructs WSTF to specifically affect inflammatory genes. A clue is provided from our RNA-seq and ATAC-seq data, exploring the transcription factors associated with the downregulated genes by WSTF. In both datasets, a strong enrichment of NF- $\kappa$ B and RelA (p65) subunit of NF- $\kappa$ B was detected (Extended data Fig. 10a and 10b). We subsequently investigated how WSTF is connected to NF- $\kappa$ B, a key transcription factor for inflammatory genes.

We first asked whether WSTF interacts with the p65 subunit of NF- $\kappa$ B. In basal condition, p65 is in the cytoplasm while WSTF is in the nucleus, thus an interaction was not detected; upon stimulation by TNF $\alpha$ , p65 is translocated to the nucleus, and an interaction with WSTF was detected by co-IP (Fig. 7e). The WSTF-p65 interaction was further confirmed by co-IPs at the endogenous level upon TNF $\alpha$  (Fig. 7f) or poly I:C stimulation (Fig. 7g), and in WSTF overexpressed senescent cells (Fig. 7h, of note, endogenous WSTF is lost in senescent cells and thus overexpressed WSTF was used). Importantly, using *in vitro* translated WSTF and p65, a direct interaction was detected (Fig. 7i). By contrast, p65 failed to bind to *in vitro* translated SNF2H (Fig. 7i). In sum, we found that WSTF of the ISWI complex directly binds to the p65 subunit of NF- $\kappa$ B.

We went on further to examine whether WSTF regulates p65 activity. In basal condition, p65 binds to I $\kappa$ B in the cytoplasm. Upon inflammatory stimulation, I $\kappa$ B is phosphorylated, leading to its proteasomal degradation and p65 translocation to the nucleus<sup>50</sup>. Nuclear p65 undergoes a series of modifications, such as phosphorylation and acetylation, facilitating p65 binding to chromatin and stimulation of the transcription of inflammatory genes<sup>51</sup>. We found that p65 nuclear translocation and phosphorylation at S536 were not affected by WSTF deficiency (Extended data Fig. 10c-10g),

consistent with the behavior of p65 in senescent cells overexpressed with WSTF (Extended data Fig. 7a and 7b).

An important modification of p65 is the reversible acetylation<sup>52</sup>. Acetylation of p65, catalyzed by p300 or CBP, stimulates p65 binding to DNA and its transcription activity<sup>53</sup>. Acetylation at K310 of p65 is important for recruitment of BRD4 and transcription of inflammatory genes<sup>54,55</sup>. Using T7-tagged p65 coupled with WSTF knockdown and p300 overexpression, we found that WSTF deficiency substantially increased p65 overall acetylation and acetylation at K310 (referred to as K310ac, Fig. 7j). Consistent with the increased acetylation of p65, enhanced p65 binding to p300 was detected (Fig. 7j). We further examined p65 K310ac at the endogenous level, and found that WSTF deficiency increased K310ac upon TNF $\alpha$  stimulation (Fig. 7k), accompanied by increased mRNA levels of IL6 and IL8 (Extended data Fig. 10h). Likewise, K310ac was increased in WSTF-deficient cells upon poly I:C stimulation (Fig. 7l) and in senescence (Fig. 7m).

Lastly, we examined the binding between WSTF and acetylated p65. In addition to K310, other important sites of acetylation have also been reported, including K218 and K221<sup>53</sup>. Mutation of the three acetylation sites to R (termed as 3KR)<sup>53</sup> substantially increased the binding to WSTF upon TNF $\alpha$  stimulation (Fig. 7n). Using individual K to R mutations, we found that K221 is the predominant residue that mediates the interaction with WSTF (Fig. 7n). These data suggest that WSTF preferentially binds to unmodified lysine residues on p65 to prevent p65 acetylation. We thus envision two-step events for NF- $\kappa$ B activation in the nucleus (illustrated in Extended data Fig. 10i). Upon p65 translocation to the nucleus, WSTF directly binds to non-acetylated p65 and inhibits p300 binding, serving as an inhibitor of p65 acetylation and activation (Extended data Fig. 10i, left). When stimulation further propagates, p300 eventually acetylates p65, leading to WSTF dissociation from p65 and transcription activation by NF- $\kappa$ B (Extended data Fig. 10i, right).

### **Loss of WSTF is required for immuno-surveillance of activated Ras *in vivo***

We investigated the importance of WSTF in regulating inflammation *in vivo*. An important role of inflammation is to restrain tumorigenesis in response to oncogene activation. The SASP program triggered by activated oncogenes can alarm the immune system to induce immuno-surveillance and clearance of the pre-malignant cells, acting as a potent tumor suppressive mechanism<sup>11,12</sup>. In particular, many primary cell types cope with oncogenic Ras activation by inducing cellular senescence, which, via the SASP, activates an initial state of tumor suppressive inflammation<sup>11,12</sup>. An established model for oncogene-induced senescence and the SASP in mice is liver expression of NRasV12, which induces hepatocyte senescence, the SASP, immune cell infiltration, and clearance of the NRasV12-expressing hepatocytes<sup>56</sup>. We previously reported that ablation of STING blocked the SASP program, leading to impaired immuno-surveillance and formation of liver tumors<sup>21</sup>.

A vector with a Sleeping Beauty transposon that co-expresses NRasV12 and GFP, together with a transposase construct, was co-injected into the mouse tail vein through hydrodynamic injection (illustrated in Fig. 8a). WSTF was cloned to co-express with NRasV12 to investigate the role of

WSTF in this system (Fig. 8b). This approach leads to specific and stable hepatocyte expression of NRasV12 together with GFP or WSTF (Fig. 8a and 8b). The liver was analyzed 6 days after injection for inflammation and the SASP, and 12 days after injection for NRasV12 hepatocyte clearance (outlined in Fig. 8c).

NRasV12 expression in the liver led to specific loss of WSTF in NRasV12-positive hepatocytes, but not in NRasV12-negative cells (Fig. 8d and Extended data Fig. 11a), consistent with our results that oncogene-induced senescence lost WSTF in primary human cells (Fig. 3b). We therefore overexpressed WSTF together with NRasV12 in the same vector (Fig. 8b and 8d) to investigate the SASP and inflammation in the liver.

6 days post injection, NRasV12/GFP mice induced infiltration of CD45-positive immune cells surrounding NRasV12-positive hepatocytes (Fig. 8e). Clusters of immune cells can also be observed by DAPI staining (Fig. 8e). These responses are consistent with what we and others previously reported in this model<sup>56,21</sup>. By sharp contrast, NRasV12/WSTF mice showed dramatically impaired infiltration of immune cells and formation of immune clusters, although NRasV12 was expressed at comparable levels to the NRasV12/GFP group (Fig. 8f and quantified in Fig. 8j and 8k). In addition, we performed RT-qPCR analyses to quantify the transcripts of SASP genes and immune cell genes. The critical pro-inflammatory factors IL1 $\alpha$ , IL1 $\beta$ , IL6, and CXCL1 were all significantly reduced in WSTF group, accompanied by reduced CD45 (a marker for all immune cells), CD3 (T cells), and KLRD1 (NK cells) (Fig. 8g). These results indicate that NRasV12-induced loss of WSTF is required for the induction of SASP and inflammation in the liver.

12 days post the injection, NRasV12-positive hepatocytes showed reduced positivity, due to immune-mediated clearance of the pre-malignant cells (Fig. 8h and quantified in Fig. 8j and 8k). By contrast, NRasV12/WSTF group exhibited persistence of NRasV12-positive hepatocytes, accompanied by reduced infiltration of CD45-positive immune cells (Fig. 8i and quantified in Fig. 8j and 8k). Impaired clearance of NRasV12-positive hepatocytes can lead to malignant growth of these cells and progression to liver tumors that express NRasV12<sup>56,21</sup>. Six months following the hydrodynamic injection, while none of the GFP group developed liver tumors (0 out of 10) (Fig. 8l and Extended data Fig. 11b), severe intrahepatic tumors were observed in all mice of the WSTF group (10 out of 10) (Fig. 8m and Extended data Fig. 11c). These data strongly indicate that loss of WSTF is a critical event to induce immuno-surveillance of oncogenic Ras in mice.

## Discussion

In this study, we generated a nuclear ATG8 interaction network in primary human fibroblasts and in mouse brain, uncovering hundreds of novel interactions. Combined with the nuclear proteomes in senescence, we identified WSTF as a previously unknown nuclear substrate of autophagy. Autophagic degradation of WSTF, via interaction with GABARAP, stimulates senescence-associated inflammation, by promoting chromatin accessibility over inflammatory genes. In

addition to senescence, we uncovered that WSTF is a broad repressor of inflammation, via direct binding to the NF- $\kappa$ B p65 subunit and inhibiting its acetylation. Lastly, we demonstrated that loss of WSTF is essential for immuno-surveillance of activated oncogene in mice. A schematic model summarizing our findings is presented in Fig. 9a.

Our study offers new perspectives and insights in several fields of research. First, our nuclear ATG8 interactome offers a systematic resource for studying nuclear autophagy. While ATG8 interactomics studies have been conducted before<sup>15,16,17</sup>, we reason that, due to technical issues in lysing nuclear and chromatin fractions (Fig. 1a), prior resources were in fact limited to cytoplasmic interactions. Our nuclear autophagy interaction network differs substantially from a previously established autophagy-interaction network<sup>15</sup> (Extended data Fig. 1c), which we hope will spark other investigators to explore nuclear autophagy, an area still in its infancy. Second, our proteomic datasets in senescence provide a new resource to investigate senescence. We present a whole cell proteome in HRasV12-induced senescence as well as nuclear proteomes of etoposide-induced senescence, in wild-type and ATG7-deficient cells. Together with our RNA-seq datasets in prior<sup>7,21</sup> and current studies, these resources will allow investigators to discover new RNA and protein alterations in senescence. Third, we uncovered a new mechanism regulating senescence-associated inflammation (the SASP program). While the roles of SASP in cancer, wound healing, and aging have been documented<sup>11,12</sup>, the mechanisms that initiate the robust and sustained inflammation are not fully understood. We showed that WSTF altering chromatin accessibility over inflammatory genes is a new mechanism to initiate the SASP program. This mechanism is distinct from cGAS-STING and other established mechanisms of the SASP. Fourth, we unveiled a novel activity of the ISWI chromatin remodeling complex. While WSTF and ISWI complex have been reported to be involved in regulating development and other biological processes<sup>57,58,59,60</sup>, our study is the first to connect ISWI complex with senescence and inflammation, thus suggesting a new strategy to target inflammatory disorders. Lastly and importantly, this study discovers a novel regulatory mechanism of NF- $\kappa$ B and inflammation, from the nucleus (described below).

Inflammation is considered a “double-edged sword”. Although inflammation is essential for restraining infection and tumorigenesis, chronic and uncontrolled inflammation contributes to autoimmunity and many other diseases, including most age-associated diseases<sup>61</sup>. Hence, investigation of negative regulators of inflammation is of critical importance. Our discovery of WSTF as a negative regulator of NF- $\kappa$ B sheds a new light on the complex role of inflammation. We showed that while WSTF competent cells are able to properly resolve inflammation, WSTF deficient cells, such as in senescent cells, exhibited robust and sustained inflammation (illustrated in Fig. 9b). Mechanistically, besides the ISWI activity, WSTF binds to p65 in the nucleus, suppressing its acetylation and activation. This role of WSTF is distinct from other reported negative regulators of p65 in the nucleus, such as enzymes that remove acetylation or phosphorylation marks of p65<sup>51</sup>, which require p65 to be activated first. By contrast, WSTF preferentially binds to unmodified lysine residues of p65 (Fig. 7n), preventing p65 activation. This mechanism of WSTF is similar to I $\kappa$ B in the cytoplasm, serving as a constitutive nuclear inhibitor of NF- $\kappa$ B. Hence, WSTF acts as a “checkpoint” to raise the threshold of signals that can produce inflammatory gene expression. This ensures that (1) only bona-fide inflammatory signals can



produce successful inflammation, and (2) inflammation can be properly resolved to prevent tissue damage. We noted that the pro-inflammatory conditions under acute setting did not show loss of WSTF, unlike the loss of WSTF in cellular senescence which takes days to weeks to establish. Future studies are needed to investigate autophagic degradation of WSTF under chronic inflammatory conditions besides senescence. We envision that WSTF is likely to be involved in other inflammatory disorders, such as age-associated diseases, metabolic disorders, and cytokine-associated toxicity. Our study further suggests that targeting WSTF autophagic degradation may hold promise to intervene in inflammation-associated diseases.

### **Acknowledgements**

The nuclear autophagy interactome studies in human fibroblasts were conducted in collaboration with J. Wade Harper and Joseph D. Mancias. We thank Maria Grazia Vizioli for contributing part of the western blots in Fig. 3a as well as Yuting Tan for generating the sgRNA constructs targeting SNF2H and the next-gen sequencing samples in control cells. We thank Yanxin Xu, Takuya Kumazawa, Yaosi Liang, and Yuting Tan for technical support and discussions. We acknowledge the microscopy core facility of Center for Regenerative Medicine at Massachusetts General Hospital for assistance on confocal microscopy, and the next-gen sequencing core at Massachusetts General Hospital for assistance on RNA-seq. We thank Riley Graham for advice on ATAC-seq. Z.D. is supported by National Institute of Health (NIH) awards R35GM137889, R00AG053406, UG3CA268117, R21AG073894, and Glenn Foundation for Medical Research and AFAR Grant for Junior Faculty. T.J. is supported by a strategic thematic grant from UiT and by TOPPFORSK (grant 249884) program of the Research Council of Norway. Work by J.L. and S.H.S. is supported in part by the Harvard Stem Cell Institute and Harvard Catalyst NIH UL1TR002541.

### **Author contributions**

Z.D. conceived the project. Y.W. conducted most of the experiments unless stated. V.V.E. contributed the mass-spectrometry results of ATG8 nuclear interactomes and proteomes in human fibroblasts, performed in J. Wade Harper and Joseph D. Mancias laboratories. A.K. contributed part of the GABARAP-WSTF interaction results. A.O. contributed part of the autophagy and senescence data. X.L., X.Z., and Z.Y. contributed mouse brain LC3 interactome. M.C. and R.I.S. contributed computational analyses of RNA-seq and ATAC-seq. L.W. contributed experimental design and part of the next-gen sequencing data. J.L. and S.H.S. contributed part of the protein interaction maps. C.B. and P.D.A. contributed part of the mouse liver tissue samples and *in vivo* data. Z.D. generated samples for next-gen sequencing in senescent cells and contributed part of the autophagy, senescence, and inflammation results. Z.D. and Z.Z. conceived and supervised inflammation experiments. S.V.S. and R.E.K. contributed novel reagents of ISWI complex and supervised epigenetic experiments. T.J. and Z.D. supervised the study and provided funding support. Y.W., T.J. and Z.D. wrote the paper. All authors discussed the manuscript.

The authors declare no competing financial interests.

## Materials and methods

### Cell culture and treatment

Primary IMR90, BJ fibroblasts and MEFs were described previously<sup>6,21</sup>. The cells were cultured in DMEM supplemented with 10% fetal bovine serum (FBS), 100 units/mL penicillin, and 100 µg/mL streptomycin (Invitrogen), and were intermittently cultured with plasmocin (Invivogen) and tested for mycoplasma using MycoAlert™ PLUS Mycoplasma Detection Kit (Lonza). The cells were cultured under physiological oxygen (3%), and were used within population doubling of 35, except for replicative senescence experiments where cells were cultured till replication exhaustion (around population doubling 80). For etoposide-induced senescence, IMR90 cells at approximately 60–70% confluency were treated with 50 µM etoposide for 48 hours and harvested at days indicated in figure legends. To establish senescence of BJ cells, the cells at approximately 60–70% confluency were treated with 40 µM etoposide for 24 h and harvested at days indicated in figure legends. For ionizing radiation (IR), cells were irradiated with X-Rad 320 (Precision X-Ray Irradiator) at 20 Gy and harvested as described in figure legends. For HRasV12-induced senescence, retrovirus from retroviral vector encoding HRasV12 was used to infect cells. Following hygromycin selection, cells were cultured for 7 or more days as described in figure legends. These conditions reproducibly induced senescence, confirmed by cell cycle arrest measured by lack of Cyclin A and phosphorylated Rb, EdU less than 5% positivity, and SA-β-gal over 95% positivity, as described in our previous studies (Dou et al., 2017; Dou et al., 2015; Vizioli et al., 2020; Xu et al., 2020). HeLa (American Type Culture Collection; CCL2) and A549 (ATCC CCL185) were grown in DMEM (Sigma-Aldrich; D5796) supplemented with 10% FBS (Biochrom AG; S0615) and 1% streptomycin-penicillin (Sigma-Aldrich; P4333). HEK293T and MEFs were grown in DMEM (Sigma-Aldrich; D6046) supplemented with 10% FBS and 1% streptomycin-penicillin. Caco2 cells (ATCC HTB-37) from a colorectal adenocarcinoma were grown in DMEM (Sigma-Aldrich; D6046) supplemented with 10% FBS and 1% streptomycin-penicillin. HCT116 cells (ATCC CCL-247) from a colorectal carcinoma were grown in McCoy's 5A (Sigma-Aldrich; M9309) supplemented with 10% FBS and 1% streptomycin-penicillin. MDA-MB-231 cells (ATCC HTB-26) from a breast adenocarcinoma were grown in high glucose DMEM (Sigma-Aldrich; D6046) supplemented with 10% FBS, 2mM glutamine and 1% streptomycin-penicillin. 0.2 µM BafA1 or 10 µM MG132 were used in experiments described in Fig. 3i and 3j.

### Mice experiments

All mice experiments were performed in compliance with the Institutional Animal Care and Use Committee at Icahn School of Medicine at Mount Sinai and Massachusetts General Hospital. GFP-LC3 transgenic mice were described elsewhere<sup>18</sup>. Both sexes were included for mice studies. Hydrodynamic tail vein injection was performed as previously described<sup>21</sup>. In brief, 20

µg of NRasV12 and 10 µg of transposase constructs were injected to C57BL/6 mice that were 8–12 weeks old in Ringer solution that corresponded to 10% of the body weight (for example, 2.0 ml for a 20 g mouse, but not over 2.5 ml if the mouse was more than 25 g) within 6 s. Liver tumor experiments were conducted following institutional protocol in Massachusetts General Hospital. Mice were euthanized with CO<sub>2</sub> followed by cervical dislocation. Tissues were harvested post euthanasia and analyzed as indicated.

### **Mouse brain homogenization and nuclear isolation**

The mouse brain was harvested and rinsed with cold PBS. Homogenization buffer A (0.32 M sucrose, 1 mM NaHCO<sub>3</sub>, 0.25 mM CaCl<sub>2</sub>, 1 mM MgCl<sub>2</sub>, 50 mM Tris HCl, pH 7.5) supplied with halt proteinase and phosphatase inhibitors (78442, Invitrogen) was added as 2 ml buffer A per mouse brain. The tissue was homogenized with a Dounce homogenizer 20 times before being centrifuged at 1000g for 10 min. The supernatant was transferred to a new 15 ml falcon tube labeled as the cytoplasmic sample. For the pellet, 1 ml buffer A was used to resuspend it prior to further homogenization with a Dounce homogenizer 10 times. The sample was centrifuged (1000g, 10 minutes), and supernatant was collected and placed in a new tube to separate the pellet and supernatant.

The pellet was resuspended in 2 ml buffer B (0.32 M sucrose, 1 mM NaHCO<sub>3</sub>, 5 mM CaCl<sub>2</sub>, 3 mM MgCl<sub>2</sub>, 0.1 mM EDTA, 1 mM DTT, 0.1% NP40, 10 mM Tris HCl, pH 8.0), before being homogenized with a Dounce homogenizer 20 times. The sample was then centrifuged at 1000g for 10 minutes. The supernatant was discarded, and the pellet was resuspended with 5 ml buffer B and transferred into a 14 ml ultracentrifuge tube (331372, Beckman Coulter). 9 ml Buffer C (1.8 M sucrose, 3 mM MgCl<sub>2</sub>, 1 mM DTT, 10 mM Tris HCl, pH 8.0) was carefully added into the bottom of the tube. The samples were then ultracentrifuged at 24,000 rpm (106803.1x g RCF) for 1 hour prior to discarding of the supernatant (Thermo Scientific Sorvall WX floor ultra centrifuge and Surespin 630 swinging bucket rotor). Next, 1 ml cold PBS was added into the tube and kept on ice for 10 minutes. The pellet was then carefully resuspended and transferred into a new Eppendorf tube, prior to being centrifuged at 1000 g for 10 min. Finally, the supernatant was discarded; the pellet contains the nuclear fraction.

### **Mouse brain immunoprecipitation**

For the cytoplasm sample, 2X buffer D (300 mM NaCl, 2% NP40, 1% Sodium Deoxycholate, 2 mM EDTA, 2 mM EGTA, 100 mM Tris HCl, pH 7.5) was added and the sample was rotated for 1 hour. Next, the sample was centrifuged at 20,800g for 20 minutes and the supernatant was transferred into a new falcon tube. The sample was then centrifuged a second time under the same conditions, with the supernatant being collected. Of the sample (about 5 ml), 100 µl was saved as input and to test protein concentration. 25 µl GFP-trap beads (gmta-20 GFP-Trap ChromoTek GmbH) per mouse brain was added and the sample was incubated overnight. The next day, beads

were washed three times (10 minutes each, 500  $\mu$ l 1X buffer D). After the final wash, the protein was eluted at 70°C with 30  $\mu$ l 1X LDS-PAGE sample buffer (NP0007). 3  $\mu$ l of the IP sample was used for SDS-PAGE and Silver staining (LC6070, Invitrogen). The rest of the IP samples were subjected to mass-spectrometry analyses.

For the nuclear sample, 150  $\mu$ l buffer E (Invitrogen (1861754) buffer with 1 mM MgCl<sub>2</sub>, 1 mM CaCl<sub>2</sub>, 10 mM ZnCl<sub>2</sub>, 1X halt proteinase and phosphatase inhibitor) was added. The sample was vortexed for 15 seconds at full speed, then incubated at 4°C for 30 minutes. Next, 1  $\mu$ l benzonase (70746-4, Lot# 2705583, Millipore) was added and the sample was incubated for a further 30 minutes. Then 2X buffer D was added prior to an additional 30 minutes incubation on a rotator. The sample was then centrifuged at 20,800g for 10 minutes and the supernatant was transferred into a new Eppendorf tube. 10  $\mu$ l GFP-trap beads were used per mouse brain to pull down the GFP-LC3 binding protein. The binding protein was eluted at 70°C with 20  $\mu$ l 1X LDS-PAGE sample buffer. 2  $\mu$ l of the IP sample was used for SDS-PAGE and Silver staining. The rest of the IP samples were subjected to mass-spectrometry analyses.

### **Protein digestion and tandem-mass-tag (TMT) labeling of mouse brain**

The analysis was performed with a previously optimized protocol<sup>62,63,64</sup>. For whole proteome profiling, quantified protein samples (1 mg in the lysis buffer with 8 M urea) for each TMT channel were proteolyzed with Lys-C (Wako, 1:100 w/w) at 21 °C for 2 h, diluted by 4-fold to reduce urea to 2 M for the addition of trypsin (Promega, 1:50 w/w) to continue the digestion at 21°C overnight. The insoluble debris was kept in the lysates for the recovery of insoluble proteins. The digestion was terminated by the addition of 1% trifluoroacetic acid. After centrifugation, the supernatant was desalted with the Sep-Pak C18 cartridge (Waters), and then dried by Speedvac. Each sample was resuspended in 50 mM HEPES (pH 8.5) for TMT labeling, and then mixed equally, followed by desalting for the subsequent fractionation. For whole proteome analysis alone, 0.1 mg protein per sample was used.

### **Extensive two-dimensional liquid chromatography-tandem mass spectrometry (LC/LC-MS/MS) for mouse brain**

The TMT labeled samples were fractionated by offline basic pH reverse phase LC, and each of these fractions was analyzed by the acidic pH reverse phase LC-MS/MS<sup>65,66</sup>. The offline basic pH LC was performed with an XBridge C18 column (3.5  $\mu$ m particle size, 4.6 mm  $\times$  25 cm, Waters), buffer A (10 mM ammonium formate, pH 8.0), buffer B (95% acetonitrile, 10 mM ammonium formate, pH 8.0), using a 2–3 h gradient of 15–35% buffer B<sup>62</sup>. In the acidic pH LC-MS/MS analysis, fractions were analyzed sequentially on a column (75  $\mu$ m  $\times$  15–30 cm, 1.9  $\mu$ m C18 resin from Dr. Maisch GmbH, 65 °C to reduce backpressure) coupled with a Fusion or Q Exactive HF Orbitrap mass spectrometer (Thermo Fisher Scientific). Peptides were analyzed with a 1–3 h gradient (buffer A: 0.2% formic acid, 5% DMSO; buffer B: buffer A plus 65% acetonitrile). For mass spectrometer settings, positive ion mode and data-dependent acquisition were applied with

one full MS scan followed by a 20 MS/MS scans. MS1 scans were collected at a resolution of 60,000,  $1 \times 10^6$  AGC and 50 ms maximal ion time; higher energy collision-induced dissociation (HCD) was set to 32–38% normalized collision energy;  $\sim 1.0$  m/z isolation window with 0.3 m/z offset was applied; MS2 spectra were acquired at a resolution of 60,000, fixed first mass of 120 m/z, 410–1600 m/z,  $1 \times 10^5$  AGC, 100–150 ms maximal ion time, and  $\sim 15$  s of dynamic exclusion.

### **Protein identification and quantification by the JUMP software suite for mouse brain**

The bioinformatics processing of protein identification and quantification were carried out with the JUMP software suite<sup>67,68,69</sup>. In brief, MS/MS raw data were searched against a target-decoy database to estimate false discovery rate (FDR)<sup>70</sup>. We combined the downloaded Swiss-Prot, TrEMBL, and UCSC databases and removed redundancy (human: 83,955 entries) to create the database. Main search parameters were set at precursor and product ion mass tolerance ( $\pm 15$  ppm), full trypticity, maximal modification sites ( $n = 3$ ), maximal missed cleavage ( $n = 2$ ), static mass shift including carbamidomethyl modification (+ 57.02146 on Cys), TMT tags (+ 229.16293 on Lys and N-termini), and dynamic mass shift for oxidation (+ 15.99491 on Met). Peptide-spectrum matches (PSM) were filtered by mass accuracy, clustered by precursor ion charge, and the cutoffs of JUMP-based matching scores (J-score and  $\Delta J_n$ ). The peptide was represented by the protein with the highest PSMs according to the rule of parsimony when one peptide was matched to multiple homologous proteins<sup>71</sup>. Protein quantification was performed based on the reporter ions from MS2 using our previously optimized method<sup>65</sup>.

### **RNA-seq analysis**

RNA quality was checked using Agilent TapeStation. RNA-seq libraries were prepared from total RNA using polyA selection followed by the NEBNext Ultra II Directional RNA library kit workflow (New England Biolabs). Sequencing was performed on the Illumina HiSeq 2500 instrument, resulting in approximately 30 million 50 bp reads per sample. Sequencing reads were mapped in a splice-aware fashion to the human reference transcriptome (hg19 assembly) using STAR<sup>72</sup>. Read counts over transcripts were calculated using HTSeq<sup>73</sup> based on the Ensembl annotation for GRCh38/hg19 assembly. For the differential expression analysis, we used the EdgeR method<sup>73,74</sup> and defined differentially expressed genes (DEGs) based on the cutoffs of 2-fold change in expression value and false discovery rates (FDR) below 0.05. GO analysis was performed using EnrichR<sup>36</sup>. For heatmap visualization of SASP genes, the SASP factors curated previously were used as a reference<sup>37</sup>. The genes upregulated in HRasV12 samples ( $\geq 2$  fold change compared to vector untreated samples) to a substantive expression level (RPKM  $\geq 1$  in HRasV12 samples) were used to generate heatmaps by an online tool<sup>75</sup>. Transcription factor predictions were performed using EnrichR<sup>36</sup>.

### **ATAC-seq analysis**

Sample preparations were done using established procedures<sup>76,47</sup>. ATAC-seq libraries were sequenced on Illumina HiSeq 2500 instrument, resulting in approximately 40 million paired-end 50 bp reads per sample. Reads were mapped to the hg19 human reference genome using BWA<sup>73,74,77</sup>. The fragments with both ends unambiguously mapped to the genome that were longer than 100 bp were used in further analysis. Hotspot<sup>78</sup> was used to detect significant peaks of read density with FDR cutoff of 0.05. Differentially accessible chromatin regions (DARs) were detected using the DiffBind package<sup>79</sup> with FDR cutoff of 0.05. Pathway enrichment analysis was performed using EnrichR<sup>36</sup>. Heatmap visualization of ATAC-seq signal density at selected genes was based on RPKM values calculated over the regions including gene body and 1 kb flanks. In the comparison between vector HRasV12 and WSTF HRasV12 groups, cytokine and secreted factor genes with significant signal change ( $P < 0.05$ ) were used. Genes with fold change  $>1.5$  between HRasV12 and control were included in the heatmap.

### **Fractionation and immunoprecipitation for primary human fibroblasts**

Trypsinized cells were centrifuged at 500 g for 5 min at 4 °C. The cell pellets were lysed in buffer 1, pipetted up and down 10 times, and rotated for 30 min at 4 °C. Cells were then centrifuged at 500 g for 5 min at 4 °C; the collected supernatant is cytosolic fractionation. The pellets were further lysed with buffer 2, pipetted up and down 10 times, vortexed for 5 s, and rotated for 10 min at 4 °C, followed by centrifugation at 3000 g for 5 min at 4 °C. The collected supernatant is membrane fractionation. The pellets were lysed with buffer 3, pipetted up and down 10 times, vortexed for 10 s, and rotated for 1h at 4 °C. The product was centrifuged at 5000 g for 5 min at 4 °C. The collected supernatant is nuclear fractionation. Buffer 1: 150 mM NaCl, 50 mM HEPES, 25 ug/ml digitonin (Sigma 11024-24-1) with protease and phosphatase inhibitors (Roche); Buffer 2: 150 mM NaCl, 50 mM HEPES, 0.5% IGEPAL (Sigma I3021) with protease and phosphatase inhibitors (Roche); Buffer 3: 150 mM NaCl, 50 mM HEPES, 1% NP40 (Sigma 74285), benzonase (2 units/ml), 1 mM MgCl<sub>2</sub>, 0.1% SDS, 0.5% sodium deoxycholate with protease and phosphatase inhibitors (Roche). The nuclear fractionation was dialyzed using Amicon Ultra-0.5 Centrifugal Filter Unit (Millipore), followed by reconstitution and immunoprecipitation with buffer (20mM Tris HCl, pH 7.5, 137 mM NaCl, 1 mM CaCl<sub>2</sub>, 3 mM MgCl<sub>2</sub>, benzonase (2 units/ml), 0.5% NP40, with protease and phosphatase inhibitors (Roche)). Anti-HA magnetic beads (Thermo Fisher) were used for immunoprecipitation.

### **Nuclear proteome analyses for primary human fibroblasts**

For mass spectrometry of nuclear fractions and ATG8 immunoprecipitated, samples were alkylated and reduced using chloroacetamide, 20 mM at room temperature for 30 min and TCEP, 5 mM for 10 min at 55°C followed by TCA precipitation. TCA was added to eluates at final concentration of 20% and placed on ice at 4°C for at least an hour after which the samples were pelleted for 30 min. The pellets were washed three times using ice cold methanol. Dried pellets were resuspended in 50 µl, 200 mM EPPS, pH 8.0. Peptide digestion was carried out using LysC (Wako cat. # 129-02541, 0.25 µg) for 2 h at 37°C followed by trypsin (0.5 µg) overnight. Digested

peptides were then labeled with 4  $\mu$ l of TMT reagent (at 20  $\mu$ g/ $\mu$ l stock) for 1 hr and the reaction was quenched using hydroxylamine at a final concentration of 0.5 % (wt/vol) for 20 min. The samples were then combined and dried in a vacuum centrifuge. This combined sample was then subjected to fractionation using the high pH reversed-phase peptide fractionation kit (Thermo Fisher) for a final of six fractions for the nuclear eluates. The dried fractions were processed by C18 stage tip desalting prior mass spectrometry.

Quantitative whole-cell proteomics of HRasV12 expressing cells was performed as per<sup>80,81</sup>. After induction of senescence, cells were lysed in 8 M urea buffer (8 M urea, 1 M Tris pH 7.4, 5 M NaCl) containing protease and phosphatase inhibitors (Roche) followed by sonication at 4°C. The sonicated lysate was clarified by centrifugation at 13,000 rpm for 10 min at 4°C. Protein concentration was estimated by Bradford assay and 100  $\mu$ g of total protein was used for each replicate. 100  $\mu$ g of clarified lysate for each sample was then reduced and alkylated by the addition of 5 mM TCEP for 30 min at 37°C and 20 mM chloroacetamide for 20 min at room temperature, followed by methanol-chloroform precipitation at a 3:1 ratio to the lysate. The protein precipitate was washed thrice with ice cold methanol and resuspended in 200 mM HEPES pH 8.5 for protein digestion. Protein digestion was carried out by 1:100 protease to protein ratio of Lys-C for 2 h at 37°C followed by trypsin overnight. Each sample was then labeled with TMT reagent (TMT10 reagent, ThermoFisher Scientific, 90110) for 1 h, and the reaction was quenched with hydroxylamine at a final concentration of 0.3% w/v. 1% of each sample was mixed in a 1:1:1:1:1:1:1:1:1 ratio and a 'ratio-check' analysis using LC-MS/MS was performed to determine if the samples were present in equal ratios. Based on this result, the volumes of the remaining sample were adjusted and combined so as to maintain the 1:1:1:1:1:1:1:1:1 ratio. This combined sample was then dried to completeness using a vacuum centrifuge and acidified with 5% w/v formic acid. Digested peptides were cleaned up using C18 SPE (Sep-Pak, Waters) and separated using basic pH reversed-phase HPLC and pooled into 24 fractions. All 24 fractions were vacuum dried to completeness and subject to the C18 stage tip method prior to loading on the mass-spectrometer. Data was obtained using an Orbitrap fusion Lumos mass spectrometer linked with a Proxeon EASY-nLC 1200 LC pump. Peptides were separated on a 75  $\mu$ m inner diameter microcapillary tube packed with 35 cm of Accucore C18 resin (2.6  $\mu$ m, 100A, Thermo Fisher Scientific). The data were acquired using the MS3 method as outlined in previous study<sup>82</sup>.

Raw mass spectra obtained were processed using an in-house software pipeline as described previously<sup>83,84</sup>. Values for protein quantification were exported and processed using Perseus to calculate Log fold changes and p values. The interaction maps were generated by Cytoscape software<sup>85</sup>.

## Reagents and antibodies

All reagents were purchased from Sigma, unless otherwise stated. Odyssey ladder (Licor 928-60000). Primary antibodies used include: WSTF (Abcam ab51256), Lamin B1 (Abcam ab16048),

phospho-Rb (Cell Signaling Technology 9308S), CyclinB1 (Cell Signaling Technology 12231S), phospho-S6 (Cell Signaling Technology 2215), GAPDH (Cell Signaling Technology 5174), IL8 (Abcam ab18672), p21 (Santa Cruz Biotechnology sc-271532), p16 (BD Biosciences G175-405), p-ATM (Abcam ab81292), IL6 (Cell Signaling Technology 12153), NF- $\kappa$ B p65 (Cell Signaling Technology 8242S and 6956S), phospho-p65 (Cell Signaling Technology 3033), IL1 alpha (Abcam ab18672), p38 MAPK (Cell Signaling Technology 9212), phospho-p38MAPK (Cell Signaling Technology 9211), phospho-ATF2 (Cell Signaling Technology 9221), phospho-p53 (Cell Signaling Technology 9284T), STING (Cell Signaling Technology 13647), Beta-tubulin (Sigma T8328-25UL), SNF2H (Abcam ab72499), HA-Tag (Sigma H3663-200UL), ACF1 (Abcam ab187670), Cyclin A2 (Cell Signaling Technology 4656), ATG7 (Cell Signaling Technology 8558S), BRG1 (Cell Signaling Technology 49360), ATG5 (Cell Signaling Technology 12994S), Histone 3 (H3) (Active Motif 39763), Histone H3K4me3 (Active Motif 39160), T7 Tag (MilliporeSigma 69522-3), H4K16ac (Millipore 07-329), Acetylated-Lysine (Cell Signaling Technology 9814S), IgG (Cell Signaling Technology 3900), Flag (Sigma F-1804), p65 K310Ac (Cell Signaling Technology 3045S), Ras (Cell Signaling Technology 14412), and CD45 (Biolegend 103101).

Secondary antibodies used for western blots include: Goat anti-Mouse IgG, IRDye® 680RD (Licor 926-68070), Goat anti-Mouse IgG, IRDye® 800RD (Licor 926-32210), Goat anti-Rabbit IgG, IRDye® 680CW (Licor 926-68071), Goat anti-Rabbit IgG, IRDye® 800CW (Licor 926-32211), Goat Anti-Mouse IgG (H + L)-HRP Conjugate (Bio Rad 1706516), Goat Anti-Rabbit IgG (H + L)-HRP Conjugate (Bio Rad 1706515), and Mouse Anti-Rabbit IgG (Light-Chain Specific) (Cell Signaling Technology 93702).

Secondary antibodies used for immunofluorescence (IF) include: Goat anti-Mouse IgG Alexa Fluor 488 (Thermo Fisher Scientific A-11001), Goat anti-Mouse IgG Alexa Fluor 532 (Thermo Fisher Scientific A-11002), Goat anti-Mouse IgG Alexa Fluor 555 (Thermo Fisher Scientific A-21422), Goat anti-Mouse IgG Alexa Fluor 647 (Thermo Fisher Scientific A-21236), Goat anti-Rabbit IgG, Alexa Fluor 488 (Thermo Fisher Scientific R-37116), Goat anti-Rabbit IgG Alexa Fluor 555 (Thermo Fisher Scientific A-21428), Goat anti-Rabbit IgG Alexa Fluor 647 (Thermo Fisher Scientific A-21446), Donkey anti-Rat IgG Alexa Fluor 647 (Thermo Fisher Scientific A-78947), Donkey anti-Goat IgG Alexa Fluor 555 (Thermo Fisher Scientific A-21432), and Donkey anti-Goat IgG Alexa Fluor 647 (Thermo Fisher Scientific A-21447).

### **Retrovirus and lentivirus**

Retroviral WZL-HRasV12 construct was transfected to the phoenix packaging cell line, and production of virus for stable expression was performed as previously described<sup>21</sup>. Lentiviral vectors were transfected with packaging plasmids to HEK293T cells, as described previously<sup>21</sup>. Viral supernatant was filtered through a 0.45- $\mu$ m filter and mixed with trypsinized recipient cells. The infected cells were then selected with puromycin or hygromycin.



pLKO-shRNA constructs were purchased from Sigma. The following shRNA sequences were used: WSTF#1 (TRCN0000013341: GCAGATGACTTTGTTGGATAT) and WSTF#2 (TRCN0000013338: CCCACAACAAATCTAGCTCTA). Non-targeting control and ATG7 shRNA were described previously<sup>6</sup>. pLentiCRISPRv2 construct was used for CRISPR-mediated gene silencing. The following sequences were used: sgRNA targeting SNF2H #1 (CACCGAATCTTCAGTCAAATGACAA, AAACCTTGTCATTTGACTGAAGATTC). sgRNA targeting SNF2H #2 (CACCGATAGCCTGAAGATCTACTTG, AAACCAAGTAGATCTTCAGGCTATC). Control sgRNA was described previously<sup>6,7</sup>.

### Plasmids

GST, GST-LC3A, B, C, GABARAP, GABARAPL1 and GABARAPL2 were described elsewhere<sup>86</sup>. HA-tagged LC3A, B, C, GABARAP, GABARAPL1 and GABARAPL2 cDNA were described previously<sup>15</sup> and were cloned into lentiviral vectors for stable expression. GABARAP truncations/mutations were made from GST-GABARAP. WSTF and SNF2H cDNA were cloned into the *in vitro* translation (IVT) vectors for *in vitro* translation (1-Step IVT Systems, Thermo Fisher) and lentiviral/retroviral vectors for stable expression. WSTF truncations/mutations were made from plenti-HA-WSTF. All new constructs in this study were verified by DNA sequencing. T7-tagged p65 WT and mutants were purchased from Addgene: T7-RelA (#21984), T7-RelA(3KR) (#23251), T7-RelA(K310R) (#23250), T7-RelA(K221R) (#23248), T7-RelA(K218R) (#23247). HA-p300 was purchased from Addgene (#89094).

### Immunoblotting

Western blotting was described previously<sup>21</sup> with slight modifications. Cells were lysed in buffer containing 20 mM Tris, pH 7.5, 137 mM NaCl, 1 mM MgCl<sub>2</sub>, 1 mM CaCl<sub>2</sub>, 1% NP-40, supplemented with 1:100 Halt protease and phosphatase inhibitor cocktail (Thermo) and benzonase (Novagen) at 12.5 U/mL. The lysates were rotated at 4 °C for 30 min and boiled at 95 °C in the presence of 1% SDS. The resulting supernatants were subjected to electrophoresis using NuPAGE Bis-Tris precast gels (Thermo). After transferring to nitrocellulose membrane, 5% milk in TBS was used to block the membrane at room temperature for 1 h. Primary antibodies were diluted in 5% BSA in TBS supplemented with 0.1% Tween 20 (TBST) and incubated at 4 °C overnight. The membrane was washed 3 times with TBST, each for 10 min, followed by incubation of secondary antibodies at room temperature for 1 h, in 5% milk in TBST. The membrane was washed again 3 times and imaged by film or by an Odyssey imager (Licor Odyssey CLx 2000).

### Immunofluorescence

Immunofluorescence was performed as described previously<sup>21</sup>. Briefly, cells were fixed in 4% paraformaldehyde in PBS for 30 min at room temperature. Cells were washed twice with PBS, and permeabilized with 0.5% Triton X-100 in PBS for 10 min. After washing twice, cells were blocked with 10% BSA in PBS for 1 h at room temperature. Cells were then incubated with

primary antibodies in 5% BSA in PBS supplemented with 0.1% Tween 20 (PBST) overnight at 4 °C. The next day, the cells were washed four times with PBST, each for 10 min, followed by incubation with Alexa Fluor-conjugated secondary antibody (Thermo), in 5% BSA/PBST for 1 h at room temperature. The cells were then washed four times with PBST, incubated with 1 µg/mL DAPI in PBS for 10 min, and washed twice with PBS. The slides were mounted with ProLong Diamond (Thermo) and imaged with a Leica TCS SP8 fluorescent confocal microscope. Quantification of % positive cells was done under identical microscopy settings between samples. Over 200 cells from 4 randomly selected fields were analyzed.

### ***In vitro* translation**

*In vitro* translation was performed using the One Step *In Vitro* Translation Kit (Thermo Scientific). Target proteins were cloned into pT7CFE1-NHA vector (with N-terminal HA tag) and translated *in vitro* at 30 °C for 6 hours.

The other *in vitro* translation was done in the presence of radioactive [<sup>35</sup>S]methionine using the TNT T7 Reticulocyte Lysate System (Promega 14610). *In vitro*-translated proteins were then precleared by incubation with empty glutathione Sepharose beads in NETN buffer (50 mM Tris, pH 8.0, 150 mM NaCl, 1 mM EDTA, and 0.5% NP-40) supplemented with protease inhibitors for 30 min at 4°C to remove nonspecific binding. The precleared lysates were incubated with the GST fusion protein-loaded beads for subsequent GST pulldown experiments.

### **Bacterial expression and GST pulldown**

cDNA of target proteins were cloned into GST fusion expression vectors. GST-tagged vectors were transformed in BL21-CodonPlus *Escherichia coli*, then expressed and purified with glutathione beads (Thermo Scientific #78602) at 4 °C for 2 h and washed four times with the wash buffer containing 50 mM Tris, pH 7.5, 150 mM NaCl, 1% Triton X-100, 1 mM DTT, supplemented with 100 µM PMSF. The purified proteins or *in vitro* translated proteins were diluted in binding buffer (20 mM Tris, pH 7.5, 137 mM NaCl, 1 mM MgCl<sub>2</sub>, 1 mM CaCl<sub>2</sub>, 1% NP-40, supplemented with 1:1000 Halt Protease inhibitor cocktail) and then pre-cleared with GST at 4 °C for 1 h. The resulting supernatant was then subjected to GST pull-down with GST or GST fusion proteins. The product was washed four times with the wash buffer and boiled with NuPAGE loading dye for immunoblotting analysis. WSTF peptides were purchased from Genscript and purified by Pierce™ C-18 Spin Columns (Thermo Fisher 89870).

### **Immunohistochemistry**

Mouse liver was buried in O.C.T. Compound (Thermo Fisher 23-730-571) and frozen on dry ice. The frozen tissues were sectioned into desired thickness using a cryostat (35 µm) (Leica). The tissue sections were placed onto glass slides suitable for immunohistochemistry, and oaked in 4% PFA for 20 min. The slides were rinsed twice gently with PBS, followed by permeabilization and blocking using filtered (by a 0.45 µM syringe filter) 10% BSA and 0.5% Triton X100 in PBS for

2 h. A circle was drawn surrounding the tissue sample using a hydrophobic pen. Primary antibody was added (1:100-500) into the circle with filtered 10% BSA in PBST (Tween-20 0.1%) and incubated in a humid box overnight at 4 degrees. The slides were gently rinsed 3 times with PBST on a shaker for 10 min each. 2nd fluorescent antibodies (1:500) were incubated for 2 h at room temperature on a shaker with gentle shaking. The slides were then gently rinsed 4 times with PBST for 10 min each, followed by incubation with DAPI (1 ug/ml in PBS) for 20 min. The samples were then gently rinsed twice with PBS for 10 min each, and mounted with sufficient ProLong™ Diamond Antifade Mountant (Thermo Fisher P36961). The slides were dried in a dark place overnight and imaged by a confocal microscopy.

## RT-qPCR

mRNA was extracted from cells or tissues using RNeasy Mini Kit (Qiagen), with a DNase I (Qiagen) digestion step to minimize genomic DNA contamination. Reverse transcription (RT) was done using High-Capacity RNA-to-cDNA Kit (Thermo), and then quantitative PCR (qPCR) was performed using a qPCR machine (BioRad CFX 384 Real-Time System). Results were normalized to Lamin A/C for both human cells and mouse cells. The following primers were used for RT-qPCR of human cells:

WSTF:	GCCAAAGGCACGCAGAAGAT,
GGCTGCAGGAGGCAGATGTT;	LaminB1: CTCGTCGCATGCTGACAGAC,
GATCCCTTATTTCCGCCATCT;	p16: CCAACGCACCGAATAGTTACG,
CCATCATCATGACCTGGATCG;	IL6: CACCGGGAACGAAAGAGAAG,
TCATAGCTGGGCTCCTGGAG;	p21: CTCAGGGGAGCAGGCTGAAG,
AGAAGATCAGCCGGCGTTTG;	IL8: ACATGACTTCCAAGCTGGCC,
CAAATCAGGAAGGCTGCC	

IL1 $\alpha$ : AGTGCTGCTGAAGGAGATGCCTGA, CCCCTGCCAAGCACACCCAGTA

IL1 $\beta$ : CTCTCTCCTTTCAGGGCCAA, GAGAGGCCTGGCTCAACAAA.

Lamin A/C: AGCTGAAAGCGCGCAATACC, GGCCTCCTTGGAGTTCAGCA; SNF2H: TGATGCGTCACCTGGAAAGC, GCCCGGTCAGTTTGCATTTT.

For mouse tissues, RNeasy Mini Kit (Qiagen) was used to extract the RNA. For mouse liver NRasV12 related RT-qPCR, three pieces of liver from the same mouse were combined as one sample (n = 1), and the mRNA extraction and reverse transcription were performed as previously described<sup>21</sup>. The results of SASP/immune cell factors were normalized to the value of NRasV12 as an internal control for NRas abundance. The following primers were used for RT-qPCR of mouse cells/tissues:

WSTF:	TGCGGGAAAAAGCCAAAGAA,	
CAGCCTGAATGCTGGGAGGT;	IL-1 $\alpha$ :	TTCAAGGAGAGCCGGGTGAC,
TGCTGATCTGGGTTGGATGG;	IL1 $\beta$ :	TCGCAGCAGCACATCAACAA,
GCTGCCACAGCTTCTCCACA;	IL6:	CCGTGTGGTTACATCTACCCT,
CGTGGTTCTGTTGATGACAGTG;	CXCL1:	CCATGGCTGGGATTCACCTC,
CCAAGGGAGCTTCAGGGTCA;	NRasV12:	CCTCAGCCAAGACCAGACAGG,
CATCACCACACATGGCAATCC;	GAPDH:	TGCATCCTGCACCACCAACT,
ACGCCACAGCTTTCAGAGG;	CD45:	CTGGAAGGCCTGGAAGCAGA,
TGTGCCTCCACTTGCACCAT;	CD3:	CGAGGAACCGGTGCTGGTAG,

CTGGGTTGGGAACAGGTGGT; Klr1: GCCTTCTTCAGCCCCAATCC,  
TGTGCCATCCTCCCATAGCC. Lamin A/C: TTCCTGGAGACCGAGAACG,  
CACCTCTCGGCTGACCACCT.

### **Conditioned media and cytokine arrays**

Control or senescent cells were cultured in regular media for 2 to 3 days before use. The media were then collected and filtered with a 0.45  $\mu$ m PVDF filter (Millipore) to remove cells and debris. The resulting supernatant was used for immunoblotting. The amounts of media used for immunoblotting were quantified based on the protein concentrations of cell lysates, and media corresponding to equal amounts of total cellular proteins were loaded into protein gels. Cytokine arrays were performed as described previously<sup>21</sup>. The serum-free conditioned media were analyzed by a cytokine array (RayBiotech, Human Cytokine Array C3) following the manufacturer's guidelines. The intensities of array dots were quantified with Fiji and normalized against the positive controls on the blots.

### **Data mining from published resources**

Quantitative proteomic data of the Cancer Cell Line Encyclopedia (CCLE) were based on a previous report<sup>49</sup>. Cancer types from solid tissues were used. For box plots displayed in this study, the central rectangle spans a range from the first quartile to the third quartile, also called the Interquartile Range. A line inside the rectangle shows the median. The whiskers are drawn down to the 10th percentile and up to the 90th. Points below and above the whiskers are drawn as individual dots. Outliers were defined as data points that were either  $1.5 \times$  interquartile range or more above the third quartile, or  $1.5 \times$  interquartile range or more below the first quartile. Unpaired t test with Welch's correction (do not assume equal SDs) was used to compute statistical significance. P values less than 0.05 were considered significant.

### **Statistical analyses**

Unpaired two-tailed Student's t-test was used for comparison between two groups. One-way ANOVA coupled with Tukey's post hoc test was used for comparisons over two groups. Two-way ANOVA coupled with post hoc test was used for comparisons whereas there are two independent variables. Significance was considered when p value was less than 0.05.

### **Data availability**

RNA-seq and ATAC-seq data have been deposited in the NCBI Gene Expression Omnibus (GEO) database under accession number GSE214410. Other original data are available upon reasonable request.

## References

1. Lamark, T. & Johansen, T. Mechanisms of Selective Autophagy. *Annu. Rev. Cell Dev. Biol.* **37**, 143–169 (2021).
2. Johansen, T. & Lamark, T. Selective autophagy mediated by autophagic adapter proteins. *Autophagy* **7**, 279–296 (2011).
3. Kirkin, V. & Rogov, V. V. A Diversity of Selective Autophagy Receptors Determines the Specificity of the Autophagy Pathway. *Mol. Cell* **76**, 268–285 (2019).
4. Kraft, L. J., Manral, P., Dowler, J. & Kenworthy, A. K. Nuclear LC3 Associates with Slowly Diffusing Complexes that Survey the Nucleolus. *Traffic* **17**, 369–399 (2016).
5. Drake, K. R., Kang, M. & Kenworthy, A. K. Nucleocytoplasmic distribution and dynamics of the autophagosome marker EGFP-LC3. *PLoS One* **5**, e9806 (2010).
6. Dou, Z. *et al.* Autophagy mediates degradation of nuclear lamina. *Nature* **527**, 105–109 (2015).
7. Xu, C. *et al.* SIRT1 is downregulated by autophagy in senescence and ageing. *Nat. Cell Biol.* **22**, 1170–1179 (2020).
8. Young, A. R. J. & Narita, M. SASP reflects senescence. *EMBO Rep.* **10**, 228–230 (2009).
9. Olan, I. & Narita, M. Senescence: An Identity Crisis Originating from Deep Within the Nucleus. *Annu. Rev. Cell Dev. Biol.* (2022) doi:10.1146/annurev-cellbio-120420-013537.
10. Sharpless, N. E. & DePinho, R. A. P53: Good cop/bad cop. *Cell* **110**, 9–12 (2002).
11. Campisi, J. Cellular senescence: putting the paradoxes in perspective. *Curr. Opin. Genet. Dev.* **21**, 107–112 (2011).
12. Velarde, M. C., Demaria, M. & Campisi, J. Senescent cells and their secretory phenotype as targets for cancer therapy. *Interdiscip. Top. Gerontol.* **38**, 17–27 (2013).
13. Kirkland, J. L. & Tchkonina, T. Clinical strategies and animal models for developing senolytic agents. *Exp. Gerontol.* **68**, 19–25 (2015).
14. Baker, D. J. *et al.* Clearance of p16Ink4a-positive senescent cells delays ageing-associated disorders. *Nature* **479**, 232–236 (2011).
15. Behrends, C., Sowa, M. E., Gygi, S. P. & Harper, J. W. Network organization of the human autophagy system. *Nature* **466**, 68–76 (2010).
16. Wild, P., McEwan, D. G. & Dikic, I. The LC3 interactome at a glance. *J. Cell Sci.* **127**, 3–9 (2014).
17. Le Guerroué, F. *et al.* Autophagosomal Content Profiling Reveals an LC3C-Dependent Piecemeal Mitophagy Pathway. *Mol. Cell* **68**, 786–796.e6 (2017).
18. Mizushima, N., Yamamoto, A., Matsui, M., Yoshimori, T. & Ohsumi, Y. In vivo analysis of autophagy in response to nutrient starvation using transgenic mice expressing a fluorescent autophagosome marker. *Mol. Biol. Cell* **15**, 1101–1111 (2004).
19. Leidal, A. M. *et al.* The LC3-conjugation machinery specifies the loading of RNA-binding proteins into extracellular vesicles. *Nat. Cell Biol.* **22**, 187–199 (2020).
20. Hwang, H. J. *et al.* LC3B is an RNA-binding protein to trigger rapid mRNA degradation during autophagy. *Nat. Commun.* **13**, 1436 (2022).
21. Dou, Z. *et al.* Cytoplasmic chromatin triggers inflammation in senescence and cancer. *Nature* **550**, 402–406 (2017).

22. Bozhenok, L., Wade, P. A. & Varga-Weisz, P. WSTF-ISWI chromatin remodeling complex targets heterochromatic replication foci. *EMBO J.* **21**, 2231–2241 (2002).
23. Zhou, S. *et al.* Epigenetic regulation of melanogenesis. *Ageing Res. Rev.* **69**, 101349 (2021).
24. Goodwin, L. R. & Picketts, D. J. The role of ISWI chromatin remodeling complexes in brain development and neurodevelopmental disorders. *Mol. Cell. Neurosci.* **87**, 55–64 (2018).
25. Toto, M., D'Angelo, G. & Corona, D. F. V. Regulation of ISWI chromatin remodelling activity. *Chromosoma* **123**, 91–102 (2014).
26. Mittal, P. & Roberts, C. W. M. The SWI/SNF complex in cancer - biology, biomarkers and therapy. *Nat. Rev. Clin. Oncol.* **17**, 435–448 (2020).
27. Wilson, B. G. & Roberts, C. W. M. SWI/SNF nucleosome remodellers and cancer. *Nat. Rev. Cancer* **11**, 481–492 (2011).
28. Ribeiro-Silva, C., Vermeulen, W. & Lans, H. SWI/SNF: Complex complexes in genome stability and cancer. *DNA Repair* **77**, 87–95 (2019).
29. Johansen, T. & Lamark, T. Selective Autophagy: ATG8 Family Proteins, LIR Motifs and Cargo Receptors. *J. Mol. Biol.* **432**, 80–103 (2020).
30. Marshall, R. S., Hua, Z., Mali, S., McLoughlin, F. & Vierstra, R. D. ATG8-Binding UIM Proteins Define a New Class of Autophagy Adaptors and Receptors. *Cell* **185**, 1101–1102 (2022).
31. Kim, E. Y. *et al.* Structures of CaV2 Ca<sup>2+</sup>/CaM-IQ domain complexes reveal binding modes that underlie calcium-dependent inactivation and facilitation. *Structure* **16**, 1455–1467 (2008).
32. Kelley, L. A., Mezulis, S., Yates, C. M., Wass, M. N. & Sternberg, M. J. E. The Phyre2 web portal for protein modeling, prediction and analysis. *Nat. Protoc.* **10**, 845–858 (2015).
33. Jumper, J. *et al.* Highly accurate protein structure prediction with AlphaFold. *Nature* **596**, 583–589 (2021).
34. Varadi, M. *et al.* AlphaFold Protein Structure Database: massively expanding the structural coverage of protein-sequence space with high-accuracy models. *Nucleic Acids Res.* **50**, D439–D444 (2022).
35. Kozakov, D. *et al.* The ClusPro web server for protein-protein docking. *Nat. Protoc.* **12**, 255–278 (2017).
36. Kuleshov, M. V. *et al.* Enrichr: a comprehensive gene set enrichment analysis web server 2016 update. *Nucleic Acids Res.* **44**, W90–7 (2016).
37. Freund, A., Orjalo, A. V., Desprez, P.-Y. & Campisi, J. Inflammatory networks during cellular senescence: causes and consequences. *Trends Mol. Med.* **16**, 238–246 (2010).
38. Freund, A., Patil, C. K. & Campisi, J. p38MAPK is a novel DNA damage response-independent regulator of the senescence-associated secretory phenotype. *EMBO J.* **30**, 1536–1548 (2011).
39. Zhao, J. *et al.* ATM is a key driver of NF- $\kappa$ B-dependent DNA-damage-induced senescence, stem cell dysfunction and aging. *Ageing* **12**, 4688–4710 (2020).
40. Yang, H., Wang, H., Ren, J., Chen, Q. & Chen, Z. J. cGAS is essential for cellular senescence. *Proc. Natl. Acad. Sci. U. S. A.* **114**, E4612–E4620 (2017).
41. Narita, M. *et al.* Rb-mediated heterochromatin formation and silencing of E2F target genes during cellular senescence. *Cell* **113**, 703–716 (2003).

42. Laberge, R.-M. *et al.* mTOR regulates the pro-tumorigenic senescence-associated secretory phenotype by promoting IL1A translation. *Nat. Cell Biol.* **17**, 1049–1061 (2015).
43. Glück, S. *et al.* Innate immune sensing of cytosolic chromatin fragments through cGAS promotes senescence. *Nat. Cell Biol.* **19**, 1061–1070 (2017).
44. Chien, Y. *et al.* Control of the senescence-associated secretory phenotype by NF- $\kappa$ B promotes senescence and enhances chemosensitivity. *Genes Dev.* **25**, 2125–2136 (2011).
45. Rodier, F. *et al.* Persistent DNA damage signalling triggers senescence-associated inflammatory cytokine secretion. *Nat. Cell Biol.* **11**, 973–979 (2009).
46. Xiao, A. *et al.* WSTF regulates the H2A.X DNA damage response via a novel tyrosine kinase activity. *Nature* **457**, 57–62 (2009).
47. Buenrostro, J. D., Wu, B., Chang, H. Y. & Greenleaf, W. J. ATAC-seq: A Method for Assaying Chromatin Accessibility Genome-Wide. *Curr. Protoc. Mol. Biol.* **109**, 21.29.1–21.29.9 (2015).
48. Cruickshanks, H. A. *et al.* Senescent cells harbour features of the cancer epigenome. *Nat. Cell Biol.* **15**, 1495–1506 (2013).
49. Nusinow, D. P. *et al.* Quantitative Proteomics of the Cancer Cell Line Encyclopedia. *Cell* **180**, 387–402.e16 (2020).
50. Karin, M. How NF-kappaB is activated: the role of the IkappaB kinase (IKK) complex. *Oncogene* **18**, 6867–6874 (1999).
51. Huang, B., Yang, X.-D., Lamb, A. & Chen, L.-F. Posttranslational modifications of NF-kappaB: another layer of regulation for NF-kappaB signaling pathway. *Cell. Signal.* **22**, 1282–1290 (2010).
52. Chen Lf, Fischle, W., Verdin, E. & Greene, W. C. Duration of nuclear NF-kappaB action regulated by reversible acetylation. *Science* **293**, 1653–1657 (2001).
53. Chen, L.-F., Mu, Y. & Greene, W. C. Acetylation of RelA at discrete sites regulates distinct nuclear functions of NF-kappaB. *EMBO J.* **21**, 6539–6548 (2002).
54. Huang, B., Yang, X.-D., Zhou, M.-M., Ozato, K. & Chen, L.-F. Brd4 coactivates transcriptional activation of NF-kappaB via specific binding to acetylated RelA. *Mol. Cell. Biol.* **29**, 1375–1387 (2009).
55. Tasdemir, N. *et al.* BRD4 Connects Enhancer Remodeling to Senescence Immune Surveillance. *Cancer Discov.* **6**, 612–629 (2016).
56. Kang, T.-W. *et al.* Senescence surveillance of pre-malignant hepatocytes limits liver cancer development. *Nature* **479**, 547–551 (2011).
57. Barnett, C. & Krebs, J. E. WSTF does it all: a multifunctional protein in transcription, repair, and replication. *Biochem. Cell Biol.* **89**, 12–23 (2011).
58. Barnett, C. *et al.* Williams Syndrome Transcription Factor is critical for neural crest cell function in *Xenopus laevis*. *Mech. Dev.* **129**, 324–338 (2012).
59. Percipalle, P. *et al.* The chromatin remodelling complex WSTF-SNF2h interacts with nuclear myosin 1 and has a role in RNA polymerase I transcription. *EMBO Rep.* **7**, 525–530 (2006).
60. Zanella, M. *et al.* Dosage analysis of the 7q11.23 Williams region identifies as a major human gene patterning the modern human face and underlying self-domestication. *Sci Adv* **5**, eaaw7908 (2019).

61. Franceschi, C., Garagnani, P., Parini, P., Giuliani, C. & Santoro, A. Inflammaging: a new immune-metabolic viewpoint for age-related diseases. *Nat. Rev. Endocrinol.* **14**, 576–590 (2018).
62. Bai, B. *et al.* Deep Profiling of Proteome and Phosphoproteome by Isobaric Labeling, Extensive Liquid Chromatography, and Mass Spectrometry. *Methods Enzymol.* **585**, 377–395 (2017).
63. Xu, P., Duong, D. M. & Peng, J. Systematical optimization of reverse-phase chromatography for shotgun proteomics. *J. Proteome Res.* **8**, 3944–3950 (2009).
64. Pagala, V. R. *et al.* Quantitative protein analysis by mass spectrometry. *Methods Mol. Biol.* **1278**, 281–305 (2015).
65. Niu, M. *et al.* Extensive Peptide Fractionation and y Ion-Based Interference Detection Method for Enabling Accurate Quantification by Isobaric Labeling and Mass Spectrometry. *Anal. Chem.* **89**, 2956–2963 (2017).
66. Wang, H. *et al.* Systematic optimization of long gradient chromatography mass spectrometry for deep analysis of brain proteome. *J. Proteome Res.* **14**, 829–838 (2015).
67. Wang, X. *et al.* JUMP: a tag-based database search tool for peptide identification with high sensitivity and accuracy. *Mol. Cell. Proteomics* **13**, 3663–3673 (2014).
68. Li, Y. *et al.* JUMPg: An Integrative Proteogenomics Pipeline Identifying Unannotated Proteins in Human Brain and Cancer Cells. *J. Proteome Res.* **15**, 2309–2320 (2016).
69. Shi, H. *et al.* Amino Acids License Kinase mTORC1 Activity and Treg Cell Function via Small G Proteins Rag and Rheb. *Immunity* **51**, 1012–1027.e7 (2019).
70. Peng, J., Elias, J. E., Thoreen, C. C., Licklider, L. J. & Gygi, S. P. Evaluation of multidimensional chromatography coupled with tandem mass spectrometry (LC/LC-MS/MS) for large-scale protein analysis: the yeast proteome. *J. Proteome Res.* **2**, 43–50 (2003).
71. Nesvizhskii, A. I. & Aebersold, R. Interpretation of shotgun proteomic data: the protein inference problem. *Mol. Cell. Proteomics* **4**, 1419–1440 (2005).
72. Dobin, A. *et al.* STAR: ultrafast universal RNA-seq aligner. *Bioinformatics* **29**, 15–21 (2013).
73. Anders, S., Pyl, P. T. & Huber, W. HTSeq—a Python framework to work with high-throughput sequencing data. *Bioinformatics* **31**, 166–169 (2015).
74. Robinson, M. D., McCarthy, D. J. & Smyth, G. K. edgeR: a Bioconductor package for differential expression analysis of digital gene expression data. *Bioinformatics* **26**, 139–140 (2010).
75. Babicki, S. *et al.* Heatmapper: web-enabled heat mapping for all. *Nucleic Acids Res.* **44**, W147–53 (2016).
76. Buenrostro, J. D., Giresi, P. G., Zaba, L. C., Chang, H. Y. & Greenleaf, W. J. Transposition of native chromatin for fast and sensitive epigenomic profiling of open chromatin, DNA-binding proteins and nucleosome position. *Nat. Methods* **10**, 1213–1218 (2013).
77. Li, H. & Durbin, R. Fast and accurate short read alignment with Burrows-Wheeler transform. *Bioinformatics* **25**, 1754–1760 (2009).
78. John, S. *et al.* Chromatin accessibility pre-determines glucocorticoid receptor binding patterns. *Nat. Genet.* **43**, 264–268 (2011).
79. Ross-Innes, C. S. *et al.* Differential oestrogen receptor binding is associated with clinical outcome in breast cancer. *Nature* **481**, 389–393 (2012).



80. An, H. *et al.* TEX264 Is an Endoplasmic Reticulum-Resident ATG8-Interacting Protein Critical for ER Remodeling during Nutrient Stress. *Mol. Cell* **74**, 891–908.e10 (2019).
81. Paulo, J. A., Mancias, J. D. & Gygi, S. P. Proteome-Wide Protein Expression Profiling Across Five Pancreatic Cell Lines. *Pancreas* **46**, 690–698 (2017).
82. McAlister, G. C. *et al.* MultiNotch MS3 enables accurate, sensitive, and multiplexed detection of differential expression across cancer cell line proteomes. *Anal. Chem.* **86**, 7150–7158 (2014).
83. Huttlin, E. L. *et al.* A tissue-specific atlas of mouse protein phosphorylation and expression. *Cell* **143**, 1174–1189 (2010).
84. Paulo, J. A., Gaun, A. & Gygi, S. P. Global Analysis of Protein Expression and Phosphorylation Levels in Nicotine-Treated Pancreatic Stellate Cells. *J. Proteome Res.* **14**, 4246–4256 (2015).
85. Shannon, P. *et al.* Cytoscape: a software environment for integrated models of biomolecular interaction networks. *Genome Res.* **13**, 2498–2504 (2003).
86. Kirkin, V. *et al.* A role for NBR1 in autophagosomal degradation of ubiquitinated substrates. *Mol. Cell* **33**, 505–516 (2009).

## Figure Legends

### Figure 1. Generation of nuclear ATG8 interaction network.

**a**, Primary IMR90 cells were subjected to protein extraction using different approaches. Supernatants were blotted with indicated antibodies. **b, c**, Primary IMR90 cells cultured in 3% oxygen were stably infected by lentiviral constructs encoding HA-tagged GFP or ATG8 genes. The cells were subjected to subcellular fractionation, and the nuclear and chromatin fractions (collectively referred to as “nucleus”) were subjected to co-immunoprecipitation using anti-HA antibody. The input and IP products were analyzed by immunoblotting. **d**, Scheme depicting the workflow of TMT proteomic analysis, using cells as described in **b** and **c**. **e**, ATG8 nuclear interactomes were analyzed and targets with P values less than 0.05 (compared to GFP negative control) and  $\log_2 \text{ATG8/GFP} > 0$  were included in the Venn diagrams. The numbers of nuclear binding partners of each ATG8 member, and the overlap of LC3 or GABARAP subgroups are shown. **f**, Scheme depicting the workflow of TMT proteomic studies using the brain of GFP-LC3B transgenic mice. WT (non-transgenic) mice were also included in these experiments (not shown in the scheme). **g**, Venn diagram showing the numbers of nuclear binding partners of human LC3A, LC3B and LC3C (hLC3s), and human GABARAP, GABARAPL1 and GABARAPL2 (hGABARAPs), and LC3B from mouse brain. **h**, Gene Ontology (GO) analyses of ATG8 nuclear binding proteins in human fibroblasts and LC3B nuclear binding proteins in mouse brain. Top biological processes, together with protein numbers and P values, are shown. **i**, Protein-protein interaction map presentation of ATG8 nuclear binding partners in human fibroblasts and mouse brain, focusing on proteins involved in chromatin remodeling.

### Figure 2. Nuclear proteome analyses of senescent cells.

**a**, Primary low passage IMR90 cells cultured in 3% oxygen were infected with retrovirus encoding HRasV12 or vector control. 7 days post the infection, cell lysates were analyzed by western blotting with indicated antibodies. Three independent replicates were used for each condition. **b**, Scheme depicting the workflow for TMT proteomic analysis, using cells as described in **a**. **c**, Bar graph showing the numbers of upregulated and downregulated proteins in HRasV12 cells compared to vector control cells. For upregulated, proteins that meet  $\log_2 \text{HRasV12/Vector} > 0.5$ ,  $p < 0.05$  were included; for downregulated, proteins that meet  $\log_2 \text{HRasV12/Vector} < -0.5$ ,  $p < 0.05$  were included. **d**, Pie chart showing the numbers of nuclear and non-nuclear proteins within the downregulated proteins in HRasV12 cells from **c**, as defined by GO term cellular component. **e**, Venn diagram showing the numbers of downregulated nuclear proteins upon HRasV12 overlapping with ATG8 nuclear interactome from human fibroblasts. **f**, Primary low passage IMR90 cells were infected with lentivirus expressing non-targeting control hairpin (sh-NTC) or sh-Atg7 hairpin. The cells were treated with 50  $\mu\text{M}$  etoposide for 2 days and then cultured without etoposide for 7 days. Whole cell extract (WCE) was analyzed by western blotting with antibodies shown. **g**, IMR90 cells as described in **f** were subjected to subcellular fractionation. Whole cell extract (WCE) and nuclear fraction were analyzed by western blotting with antibodies indicated.

**h**, Scheme depicting the workflow of the TMT proteomic analyses, using nuclear fractions as described in **g**. **i**, Bar graph showing the numbers of upregulated and downregulated nuclear proteins in etoposide-treated cells compared to control cells. For upregulated, proteins meet  $\log_2 \text{Eto/CT} > 0.5$ ,  $p < 0.05$  were included; for downregulated, proteins meet  $\log_2 \text{Eto/CT} < -0.5$ ,  $p < 0.05$  were included. **j**, Venn diagram showing the numbers of downregulated nuclear proteins upon etoposide overlapping with ATG8 nuclear interactome from primary human fibroblasts. **k**, Venn diagram showing the numbers of downregulated nuclear proteins in HRasV12-induced senescence overlapping with etoposide-induced senescence. **l**, Venn diagram showing the numbers of decreased nuclear proteins regulated by ATG7 and/or mRNA. **m**, Related to **l**, table showing the names of decreased nuclear proteins regulated by ATG7 and/or mRNA. **n**, Heatmap presentation of relative protein levels from indicated groups. Note that sh-ATG7 rescued the protein downregulation in sh-NTC etoposide group. **o**, Proteins as in **n** were overlapped with ATG8 nuclear interactomes from human fibroblasts. The overlapped proteins were analyzed for their binding affinities with ATG8 and were presented as heatmaps. **p**, Bar graphs showing the protein and mRNA levels of WSTF upon HRasV12 and etoposide-induced senescence.

**Figure 3. WSTF is degraded by autophagy during cellular senescence.**

**a**, IMR90 cells were treated with 50  $\mu\text{M}$  etoposide for 2 days, then cultured in the medium without etoposide, and harvested at indicated days after the etoposide treatment. Cell lysates were subjected to immunoblotting. **b**, IMR90 cells were infected with vector control or retrovirus expressing HRasV12 for 7 days. Cell lysates were analyzed by western blotting. **c**, IMR90 cells under proliferating or replicative senescence conditions were analyzed by western blotting. **d-f**, RT-qPCR analyses of BAZ1B/WSTF (**d**), LMNB1/Lamin B1 (**e**), and CDKN2A/p16 (**f**) in proliferating, etoposide, HRasV12, replicative, or ionizing radiation (IR, 20 Gy then cultured for 14 days) induced senescence conditions. Results were normalized to Lamin A/C and presented as mean values with s.d.;  $n=3$ ;  $p$  values were calculated from unpaired two-tailed Student's  $t$  test. \*  $P < 0.05$ ; \*\*  $P < 0.01$ ; \*\*\*  $P < 0.001$ ; **g and h**, IMR90 cells stably expressing non-targeting control (sh-NTC) or sh-ATG7 were treated with IR (**g**) or etoposide (**h**). The cells were harvested at indicated days and analyzed by western blotting with indicated antibodies. **i and j**, IMR90 cells were infected with vector control or retrovirus expressing HRasV12 for 7 days. The cells were then treated with bafilomycin A1 (Baf A1, **i**) or MG132 (**j**) for 2 days. The lysates were analyzed by western blotting. **k**, IMR90 cells stably expressing GFP-LC3B were left untreated or induced to senesce with etoposide for a week, stained with WSTF and LAMP1 antibodies, and then imaged by confocal microscopy. WSTF signals in senescent cells were deliberately overexposed to allow our examination of its localization, and representative images are shown. Arrows indicate cytoplasmic WSTF. **l**, IMR90 cells stably expressing HA-GABARAP were incubated in growth media with 200 nM LysoTracker™ Red DND-99 for 2 h, followed by staining with WSTF and HA antibodies. The cells were imaged under a confocal microscopy. WSTF signals in senescent cells were deliberately overexposed to allow our examination of its localization, and representative images are shown. **m**, Bar graphs showing the percentage of cells with cytoplasmic WSTF in proliferating or etoposide-induced senescent cells. Data are from four randomly selected fields with over 200 cells. Results shown are mean values with s.d.; \*\*\*\*  $p < 0.0001$ ; unpaired two-tailed

Student's t-test. **n**, Bar graph showing the percentage of cytoplasmic WSTF co-localizing with autophagy vesicles (defined as LC3B, GABARAP, LAMP1, or LysoTracker positive) in proliferating or etoposide-induced senescent cells. Results shown are mean values with s.d.; \*\*\*\*  $p < 0.0001$ ; unpaired two-tailed Student's t-test.

**Figure 4. Direct binding of WSTF to GABARAP is essential for its autophagic degradation in senescence.**

**a**, *In vitro* translated and  $^{35}\text{S}$ -methionine labeled HA-WSTF protein was subjected to GST pull-down assays using bacterially expressed and purified GST-ATG8 proteins. **b**, *In vitro* translated WSTF protein was subjected to GST pull-down of bacterially expressed and purified GST-LC3B or GST-GABARAP. Quantification of the relative binding to WSTF is shown on the right. Data shown are mean values with s.d.; \*\*  $p < 0.01$ ; unpaired two-tailed Student's t-test. **c**, HEK293T cells were transfected with HA-tagged constructs, followed by HA immunoprecipitation and immunoblotting with indicated antibodies. **d**, HEK293T cells were subjected to endogenous GABARAP immunoprecipitation followed by immunoblotting with indicated antibodies. **e**, *In vitro* translated and  $^{35}\text{S}$ -methionine labeled HA-WSTF protein were subjected to GST pulldown of bacterially expressed and purified GABARAP and its mutants. \*  $P < 0.05$ ; \*\*\*  $P < 0.001$ ; one-way ANOVA coupled with Tukey's post hoc test. **f**, HEK293T cells were transfected with HA-tagged GABARAP or its mutant and subjected to HA immunoprecipitation followed by immunoblotting with indicated antibodies. **g**, Scheme of WSTF mutants binding to GABARAP, summarizing the key findings. "+" means positive binding; "-" means negative binding. **h**, *In vitro* translated WSTF wild-type and mutants were subjected to GST-tagged GABARAP pulldown. **i**, Detailed schematic illustration of WSTF mutants in binding to GABARAP. **j**, HEK293T cells were transfected with HA-tagged WSTF constructs and subjected to GABARAP immunoprecipitation followed by immunoblotting with indicated antibodies. **k**, *In vitro* translated WSTF constructs were subjected to GST-tagged GABARAP pulldown. **l**, Scheme of synthesized peptides derived from fragments of WSTF protein, to be used in competition binding assays. **m** and **n**, *In vitro* translated WSTF protein were subjected to GST-tagged GABARAP pulldown in the presence of competing peptides illustrated in **l**. **o**, IMR90 cells were stably infected with HA-tagged WSTF constructs, subjected to IR and harvested at indicated days, then immunoblotted with indicated antibodies. **p**, IMR90 cells stably expressing HA-WSTF constructs were treated with IR and harvested at day 23, stained with HA and GABARAP antibodies, then analyzed by confocal microscopy. Representative images are shown. Note the colocalization between GABARAP and cytoplasmic WSTF in wild-type but not WSTF mutants. **q**, Related to **p**, bar graph showing the percentage of cells with senescence-associated heterochromatin foci (SAHF, measured by DAPI foci in the nucleus), cytoplasmic HA-WSTF, and cytoplasmic HA-WSTF colocalization with GABARAP. More than 400 cells in 4 fields were randomly selected and counted. Results shown are mean values with s.d.; \*\*\*\*  $P < 0.0001$ ; one-way ANOVA coupled with Tukey's post hoc test.

**Figure 5. WSTF negatively regulates the SASP program of senescence.**

**a**, IMR90 cells stably expressing vector control or WSTF were treated by IR and harvested at indicated days, and then analyzed by western blotting. **b**, RT-qPCR analyses of IL6, IL8, IL $\alpha$ , IL1 $\beta$ , WSTF, p16, p21 and Lamin B1 in proliferating vector cells, IR vector cells and IR WSTF cells, harvested at Day 14 post IR. Results were normalized to Lamin A/C and presented as mean values with s.d.; n=3; n.s. non-significant; \*\*\* P < 0.001; \*\*\*\* P < 0.0001; one-way ANOVA coupled with Tukey's post hoc test. **c**, The conditioned media from IR-induced senescence of vector or WSTF-expressing cells were analyzed by a cytokine array. Representative results with different exposures are shown. **d**, Related to **c**, quantification of the relative amounts of cytokines from the cytokine array assays. Results shown are mean  $\pm$  s.e.m.; n=3; n.s. non-significant; \*\*\*\* P < 0.0001; unpaired two-tailed Student's t-test. **e**, sh-NTC and sh-WSTF IMR90 cells were treated by IR and harvested at indicated days, followed by analyses of western blotting. Conditioned media were analyzed as well. **f**, RT-qPCR analyses of IL6, IL8, IL $\alpha$ , IL1 $\beta$ , WSTF, and Lamin B1 in untreated sh-NTC cells, untreated sh-WSTF cells, IR sh-NTC cells, and IR sh-WSTF cells. Cells were harvested 14 days post IR. Results were normalized to Lamin A/C and presented as mean values with s.d.; n=4; n.s. non-significant; \*\*\* P < 0.001; \*\*\*\* P < 0.0001; One-way ANOVA coupled with Tukey's post hoc test. **g**, Stably overexpressed vector or WSTF IMR90 cells were infected by HRasV12 retrovirus and were harvested at indicated days. The cells were analyzed by western blotting. **h**, RT-qPCR analyses of IL $\alpha$ , IL1 $\beta$ , IL6, IL8, WSTF and Lamin B1 in untreated vector cells, HRasV12 vector cells, and HRasV12 WSTF cells. Results were normalized to Lamin A/C and presented as mean values with s.d.; n=3; \*\*\*\* P < 0.0001; one-way ANOVA coupled with Tukey's post hoc test. **i**, Cells generated as in **g** were analyzed by RNA-seq. Differentially expressed genes (DEGs) were plotted in the HRasV12 condition. Representative genes up/down-regulated by WSTF in HRasV12-induced senescence are annotated. **j**, The DEGs downregulated by WSTF were analyzed by EnrichR, showing the top enriched GO biological processes with numbers of genes and P values. **k**, Heatmap presentation of the relative expression values of SASP genes. Refer to Materials and Methods for parameters used in this analysis. **l**, Scheme of WSTF peptides (PP) binding to GABARAP. "+" means positive binding; "-" means negative binding. **m**, HEK293T cells were transfected with vector, Flag-GABARAP, NLS-HA-PP6, or NLS-HAPP7 constructs and subjected to Flag immunoprecipitation followed by immunoblotting with indicated antibodies. **n**, Stably expressed vector, NLS-HA-PP6, or NLS-HA-PP7 IMR90 cells were left untreated or treated with etoposide to induce senescence and analyzed by western blotting; the conditioned media were also analyzed by western blotting.

**Figure 6. WSTF inhibits chromatin accessibility over SASP genes.**

**a**, Full-length WSTF or WSTF truncations were stably expressed in IMR90 cells and were left untreated or induced to senescence by IR. Cells were harvested at day 14 post IR and analyzed by western blotting (**a**) or RT-qPCR (**b**). **b**, RT-qPCR analyses of IL $\alpha$ , IL1 $\beta$ , IL6, IL8, Lamin B1 and p21. Results were normalized to Lamin A/C and presented as mean values with s.d.; n=3; letters (e.g., a, b, and c) to highlight significant differences. Groups that are not significantly different are assigned a common letter. In other words, two treatments without a common letter are statistically significant at the chosen level of significance ( $P \leq 0.05$ ), one-way ANOVA coupled with Tukey's post hoc test. **c and d**, SNF2H inactivation by CRISPR abrogates the effect of WSTF

overexpression. IMR90 cells were engineered to express control sg-RNA or sg-RNA against SNF2H, combined with vector or WSTF overexpression. The cells were left untreated or induced to senescence by IR and were harvested at Day 14. The samples were analyzed by immunoblotting (c) or RT-qPCR (d). d, RT-qPCR analyses of IL6, IL8, IL $\alpha$ , IL1 $\beta$ , p21 and Lamin B1. Results were normalized to Lamin A/C and presented as mean values with s.d.; n=3; \* P < 0.05; \*\* P < 0.01; \*\*\* P < 0.001; one-way ANOVA coupled with Tukey's post hoc test. e and f, Vector and SNF2H-overexpressing cells were left untreated or induced to senescence by IR or etoposide. The samples were analyzed by western blotting (e) or RT-qPCR (f). f, RT-qPCR analyses of SNF2H, p16, Lamin B1, IL $\alpha$ , IL1 $\beta$ , IL6, and IL8. Results were normalized to Lamin A/C and presented as mean values with s.d.; n=3; \*\* P < 0.01; \*\*\* P < 0.001; \*\*\*\* P < 0.0001; one-way ANOVA coupled with Tukey's post hoc test. g and h, IMR90 cells were engineered to overexpress SNF2H in combination with WSTF knockdown, and were left untreated or induced to senescence by IR. The samples were analyzed by immunoblotting (g) or RT-qPCR (h). h, RT-qPCR analyses of IL6, IL8, IL1 $\beta$ , SNF2H, WSTF and Lamin B1. Results were normalized to Lamin A/C and presented as mean values with s.d.; n=3; n.s. non-significant; \* P < 0.05; \*\* P < 0.01; \*\*\* P < 0.001; \*\*\*\* P < 0.0001; one-way ANOVA coupled with Tukey's post hoc test. i and j, ATAC-seq analyses of vector control and WSTF-overexpressing cells. i, Scheme of experimental design is noted on top, and ATAC-seq genomic tracks of IL8, IL1 $\beta$  and MMP3 are presented. j, Enrichment analysis showing the top GO categories enriched among genes at or proximal to differential accessible regions (DARs) whose chromatin accessibility decreased in WSTF-HRasV12 compared to Vec-HRasV12. The numbers of genes corresponding to the DARs and the P values are shown.

**Figure 7. WSTF is a broad inhibitor of NF- $\kappa$ B-mediated pro-inflammatory gene expression.**

a, RT-qPCR analyses of IL6, IL8, and WSTF in sh-NTC and sh-WSTF stably expressing cancer cells, including CaO.2, HeLa, MDA-MB-231, HCT116, and A549. Results were normalized to Lamin A/C and presented as mean values with s.d.; n=3; n.s. non-significant; \* P < 0.05; \*\* P < 0.01; \*\*\* P < 0.001; \*\*\*\* P < 0.0001; unpaired two-tailed Student's t-test. b, Cancer Cell Line Encyclopedia (CCLE) analyses of WSTF and inflammatory gene correlation, which contains proteomic datasets from over 300 cancer cell lines. Based on the protein levels of WSTF, we grouped these cancer cell lines into the lowest 50% subset and the highest 50% subset, then compared the expression of SNF2H, IL1 $\beta$ , IL6, IL8, IL18, SERPINE1 and Lamin A between these two subsets. For box plots displayed in this study, the central rectangle spans a range from the first quartile to the third quartile, also called the Interquartile Range. A line inside the rectangle shows the median. The whiskers are drawn down to the 10th percentile and up to the 90th. Points below and above the whiskers are drawn as individual dots. Outliers were defined as data points that were either  $1.5 \times$  interquartile range or more above the third quartile, or  $1.5 \times$  interquartile range or more below the first quartile. Unpaired t test with Welch's correction (do not assume equal SDs) was used to compute statistical significance. P values were shown as indicated. c, RT-qPCR analyses of IL6, IL8, IL $\alpha$ , IL1 $\beta$ , and IFN $\beta$  in sh-NTC and sh-WSTF BJ-hTERT cells for ISD, poly I:C, TNF $\alpha$  stimulation, and THP1 cells for LPS stimulation. Results were normalized to Lamin A/C and presented as mean values with s.d.; n=3; n.s. non-significant; \* P < 0.05; \*\* P < 0.01; \*\*\* P < 0.001; \*\*\*\* P < 0.0001; unpaired two-tailed Student's t-test. d, RT-qPCR analyses of IL6,

IL $\alpha$ , IL1 $\beta$  and IFN $\beta$  in sh-NTC and sh-WSTF BJ-hTERT cells for SeV infection, and THP1 cells for HSV infection. Results were normalized to Lamin A/C and presented as mean values with s.d.; n=3; n.s. non-significant; \* P < 0.05; \*\* P < 0.01; \*\*\* P < 0.001; \*\*\*\* P < 0.0001; unpaired two-tailed Student's t-test. **e**, HEK293T cells were transfected with a Flag-p65 construct and treated with or without TNF $\alpha$  (20 ng/ml) for 30min, then fractionated into cytoplasm and nucleus, followed by Flag immunoprecipitation and immunoblotting with indicated antibodies. **f**, HEK293T cells were treated with TNF $\alpha$  and fractionated into cytoplasm and nucleus, then subjected to p65 immunoprecipitation at the endogenous level, followed by immunoblotting with indicated antibodies. **g**, IMR90 cells were treated with poly I:C (30 ug/ml) for 1.5h, and fractionated into cytoplasm and nucleus, then subjected to p65 immunoprecipitation at the endogenous level, followed by immunoblotting with indicated antibodies. **h**, IMR90 cells stably expressing HA-WSTF were treated with etoposide to induce senescence, and fractionated into cytoplasm and nucleus, then subjected to p65 immunoprecipitation and immunoblotting with indicated antibodies. **i**, *In vitro* translated Flag-p65, HA-WSTF, and HA-SNF2H were subjected to Flag immunoprecipitation and immunoblotting with indicated antibodies. Note that WSTF binds quantitatively more to p65 than that of SNF2H. **j**, HEK293T cells stably expressing sh-NTC or sh-WSTF were transfected with constructs encoding T7-p65 or HA-p300, then subjected to T7 immunoprecipitation and immunoblotting with indicated antibodies. **k**, HEK293T cells stably expressing sh-NTC or sh-WSTF were treated with TNF $\alpha$  for indicated minutes, then subjected to p65 K310Ac immunoprecipitation and immunoblotting with indicated antibodies. **l and m**, IMR90 cells stably expressing sh-NTC or sh-WSTF were transfected with poly I:C (**l**) or induced to senescence by etoposide (**m**). The cells were subjected to p65 K310Ac immunoprecipitation and immunoblotting with indicated antibodies. **n**, HEK293T cells were transfected with constructs encoding HA-WSTF, T7-p65 wild-type or its mutants (K218R, K221R, K310R, and 3KR), treated with TNF $\alpha$ , and then subjected to HA immunoprecipitation and immunoblotting with indicated antibodies.

**Figure 8. Loss of WSTF is required for immunosurveillance of activated Ras in mouse liver.**

**a, b, c**, Schematic illustration of constructs and experimental design. **d**, Liver sections 6 days post injection were stained with NRasV12 and WSTF antibodies, followed by imaging under a confocal microscopy. NRasV12-positive cells were highlighted. Note the expression level of WSTF was reduced in the GFP group and increased in the WSTF group. **e and f**, Liver sections 6 days post injection were stained with NRasV12 and CD45 antibodies, then analyzed by a confocal microscopy. The immune cells are highlighted with arrows. Scale bars are shown as indicated. **g**, RT-qPCR analyses of liver from the GFP and WSTF groups. The relative expression levels of pro-inflammatory genes and immune cell genes were measured. 10 mice in each group were used, P values were shown as indicated, calculated by unpaired two-tailed Student's t-test. **h and i**, Liver sections 12 days post injection were stained with NRasV12 and CD45 antibodies, then analyzed by a confocal microscopy. Scale bars were shown as indicated. **j**, Bar graphs showing the quantification of NRasV12 positive cells in different experimental groups and presented as mean values with s.d.; n = 6; n.s.: non-significant. \*\*\* P < 0.001; \*\*\*\* P < 0.0001; one-way ANOVA coupled with Tukey's post hoc test. **k**, Bar graph showing the quantification of immune cell

clusters in different experimental groups and presented as mean values with s.d.; n = 6; n.s.: non-significant. \*\*\*\* P < 0.0001; one-way ANOVA coupled with Tukey's post hoc test. **l** and **m**, Representative images of liver tumors from NRasV12/GFP and NRasV12/WSTF groups, 6 months after the injection. The numbers of mice with liver tumors are shown at the bottom.

### **Figure 9. Schematic illustration for the roles of WSTF in regulating inflammation**

**a**, Autophagic degradation of WSTF induces inflammation. WSTF, via SNF2H, represses chromatin accessibility over inflammatory genes. In addition, WSTF competes with p300 for p65 binding, inhibiting p65 acetylation and transcription of inflammatory genes. WSTF binding to GABARAP leads to nucleus-to-cytoplasm translocation of WSTF and its autophagic degradation, which promotes inflammation. **b**, Biological roles for WSTF in regulating inflammation. In WSTF competent conditions, inflammation can be induced and properly resolved in a timely manner. In WSTF-deficient conditions, rapid and robust inflammation is induced, which causes a longer period of sustained inflammation.

### **Extended Data Figure Legends**

#### **Extended data figure 1. Nuclear ATG8 interactome.**

**a**, Interaction maps showing the nuclear binding partners of human MAP1LC3 isoforms (MAP1LC3A, MAP1LC3B and MAP1LC3C) from the proteomic analysis, generated by Cytoscape software. **b**, Interaction maps showing the nuclear binding partners of human GABARAP isoforms (GABARAP, GABARAPL1 and GABARAPL2) from proteomic analysis. **c**, Venn diagrams showing the overlap of autophagy interaction network (AIN) from a previous study versus the ATG8 nuclear interaction network from this study. **d**, Western blotting showing the fractionation of cytoplasm and nucleus from the brain of GFP-LC3B transgenic mice. **e and f**, The cytoplasm (**e**) and nucleus (**f**) fractions of the mouse brain were subjected to GFP IP. Silver-stained protein gels are shown. **g**, A list showing the overlap of ATG8 interacted nuclear proteins among the human LC3s (MAP1LC3A, MAP1LC3B and MAP1LC3C), human GABARAPs (GABARAP, GABARAPL1 and GABARAPL2), and *in vivo* mouse LC3.

#### **Extended data figure 2. Proteomic analyses of nuclear proteomes in oncogene-induced senescence and etoposide-induced senescence.**

**a**, PCA analysis of the whole-cell proteomes from control and oncogene-induced senescent cells. **b**, GO analysis showing the top biological processes for upregulated and downregulated proteins in HRasV12-induced senescent cells. **c**, Related to Fig. 2e, a list showing the overlapping proteins between downregulated nuclear proteins upon HRasV12 and ATG8 nuclear interactome in human fibroblasts. **d**, Related to Fig. 2f, western blotting showing the fractionation of cytoplasm and nucleus. **e**, PCA analysis of the nuclear proteomes from untreated, etoposide-treated, and etoposide-treated IMR90 cells with ATG7 knockdown. **f**, Related to Fig. 2j, a list showing the overlapping proteins between downregulated nuclear proteins upon etoposide and ATG8 nuclear



interactome in human fibroblasts. **g**, Heatmap presentation of the protein levels of chromatin remodeling proteins upon HRasV12 and etoposide-induced senescence with sh-NTC or sh-ATG7.

### **Extended data figure 3. WSTF is degraded by autophagy during cellular senescence.**

**a**, Primary BJ fibroblasts and primary MEFs were induced to senescence using various means, and were analyzed by western blotting using indicated antibodies. **b**, A549 cells were treated with etoposide to induce senescence, and then analyzed by western blotting using indicated antibodies. **c**, IMR90 cells were induced to quiescence by contact inhibition, and were harvested at indicated days and analyzed by western blotting. **d**, IMR90 cells were treated by amino acid starvation for 24 hours and analyzed by western blotting. **e**, Wild-type and ATG5 knockout MEFs were treated by amino acid starvation for 24 hours and analyzed by western blotting. **f**, IMR90 cells stably expressing sh-NTC or sh-ATG7 were treated by etoposide and harvested at indicated days, followed by western blotting analyses. **g**, IMR90 cells were induced to senescence by etoposide, and bafilomycin A was added to the media of senescent cells, followed by western blotting analyses. **h**, IMR90 cells were left untreated or treated with etoposide to induce senescence, or serum starvation for 24 hours, with or without bafilomycin A1 added for 24 hours as indicated, and were stained with WSTF and LAMP1 antibodies, followed by imaging under a confocal microscopy. Representative images and scale bars are shown. **i**, IMR90 cells were induced to senescence by etoposide, then stained with Lyso-tracker and WSTF antibody, followed by imaging

under a confocal microscopy. Representative images and scale bars are shown.

### **Extended data figure 4. Characterization of GABARAP and WSTF association.**

**a**, *In vitro* translated WSTF were subjected to GST-tagged GABARAP pulldown and analyzed by western blotting. **b**, *In vitro* translated SNF2H were subjected to GST-tagged GABARAP pulldown and analyzed by western blotting. **c to g**, *In vitro* translated WSTF wild-type and mutants as shown were subjected to GST-tagged GABARAP pulldown followed by western blotting analyses.

### **Extended data figure 5. Molecular mechanisms for GABARAP and WSTF association.**

**a**, WSTF wild-type and mutants as shown were subjected to HA IP and analyzed by western blotting. **b**, Surface model (grey) and secondary structure of GABARAP (PDB code:1GNU) showing the locations of the LDS and UDS and the mutants compromising the respective sites indicated. **c**, PHYRE2 prediction of the hydrophobic helix of WSTF aligned with the published structure of Cav2.2. **d**, Upper part, Alphafold2 prediction of WSTF protein structure (UniProt:Q9UIG0). The helix 1 predicted by PHYRE2 is here predicted with high confidence. Lower part, model with helix1 and the exposed L476 docked into the UDS pocket of GABARAP. The region of the Alphafold2 model encompassing amino acids 460 to 550 of WSTF with the helices 1,2 and 3 was used as input with the solved structure of GABARAP (PDB code: 1GNU) for automatic protein-protein docking on the ClusPro web server. WSTF region 460-550 is shown in magenta, the L476 residue in red, and the contact surface with the UDS of GABARAP shown in yellow. Helices 1-3 are indicated. **e**, Surface models of structures of GABARAP (PDB code:

1GNU) and LC3B (PDB code: 5D94) showing the UDS pockets with some directly aligned residues (ALFFFV for GABARAP and AFFLLV for LC3B) in green. **f**, Related to Fig. 4 **p,q**, Proliferating IMR90 cells expressing WSTF mutants were stained with HA and GABARAP antibodies, followed by imaging under a confocal microscopy. Representative images and scale bars are shown.

### **Extended data figure 6. WSTF is a negative regulator of the SASP program.**

**a**,  $\beta$ -gal staining of IMR90 cells with vector control or WSTF overexpression. The cells were left untreated or subjected to IR-induced senescence and fixed at day 14. Bar graphs showing the quantification of the percentage of  $\beta$ -gal positive cells from 4 randomly selected fields. n.s.: non-significant. **b and c**, IMR90 cells were stably expressed with sh-NTC or sh-WSTF #2 hairpin, and treated with or without IR as indicated in the scheme, followed by analyses of western blotting (**b**) and RT-qPCR (**c**). **c**, RT-qPCR analyses of IL $\alpha$ , IL1 $\beta$ , IL6, IL8, and Lamin B1. Results were normalized to Lamin A/C and presented as mean values with s.d.; n=3; \*\*\*\* P < 0.0001; unpaired two-tailed Student's t-test. **d**, IMR90 cells were treated with IR or HRasV12 to establish senescence, and then were infected with lentivirus encoding vector or WSTF, followed by western blotting analyses. **e**, Related to Fig. 5j, a list showing the genes downregulated by WSTF upon HRasV12-induced senescence, from RNA-seq studies. **f**, HEK293T cells were transfected with NLS-HA-PP6 and NLS-HA-PP7 constructs, and then stained with DAPI and HA antibody, followed by imaging under a confocal microscopy. Representative images are shown.

### **Extended data figure 7. Molecular mechanisms underlying WSTF regulation of the SASP program.**

**a**, IMR90 cells stably expressing vector control or WSTF were left untreated or treated with IR (20 Gy), and were harvested at day 10. The lysates were analyzed by immunoblotting using indicated antibodies. **b**, Vector and WSTF stably expressing IMR90 cells were left untreated or induced to senescence with IR, then stained with a p65 antibody, followed by imaging under a confocal microscopy. Representative images are shown. Bar graphs showing the quantification of the percentage of nuclear p65 positive cells in vector and WSTF cells with or without IR treatment. Results shown are the mean values from four randomly selected fields with over 200 cells. Error bars: s.d.; n.s.: non-significant. **c**, IMR90 cells were left untreated or induced to senescence with IR, and stained with  $\gamma$ H2AX and H3K27me3 antibodies, followed by imaging under a confocal microscopy. Representative images are shown. Arrows indicate CCF. Bar graphs showing the quantification of the percentage of SAHF and CCF positive cells in vector and WSTF cells with or without IR treatment. Results shown are the mean values from four randomly selected fields with over 200 cells. Error bars: s.d.; n.s.: non-significant. **d**, Related to Fig. 6a, schematic illustrations of WSTF full-length and truncations. **e**, HEK293T cells were transfected with HA-tagged wild-type or mutant WSTF constructs, and then subjected to HA immunoprecipitation and immunoblotting with indicated antibodies. **f and g**, IMR90 cells stably expressing WSTF wild-type or mutant were treated with or without IR, then the cell lysates and conditioned media were analyzed by western blotting (**f**) or RT-qPCR (**g**). **g**, RT-qPCR analyses of IL6, IL8, IL $\alpha$ , IL1 $\beta$ ,

p16 and Lamin B1. Results were normalized to Lamin A/C and presented as mean values with s.d.; n=3; \*\* P < 0.01; \*\*\* P < 0.001; \*\*\*\* P < 0.0001; one-way ANOVA coupled with Tukey's post hoc test.

#### **Extended data figure 8. WSTF reduces chromatin accessibility at SASP genes.**

**a**, Related to Fig. 6j, list of genes corresponding to DARs whose chromatin accessibility was decreased by WSTF in HRasV12-induced senescence. **b**, Heatmap of the ATAC-seq signal density (RPKM) at TSS-proximal region, gene body, and TES-proximal region of inflammatory genes from. **c**, DEGs downregulated by WSTF according to RNA-seq were overlapped with genes of DARs with chromatin accessibility decreased by WSTF based on ATAC-seq. The GO terms enriched among these genes are shown with the corresponding numbers of genes and P values.

#### **Extended data figure 9. WSTF restrains the transcription of pro-inflammatory genes in cancer and other conditions.**

**a**, Related to Fig. 7a, RT-qPCR analyses of IL6, IL8 and WSTF in sh-NTC and sh-WSTF #2 cancer cells, including CaO.2, MDA-MB-231, and A549. Results were normalized to Lamin A/C and presented as mean values with s.d.; n=3; n.s. non-significant; \* P < 0.05; \*\* P < 0.01; \*\*\* P < 0.001; \*\*\*\* P < 0.0001; unpaired two-tailed Student's t-test. **b**, Related to Fig. 7c and **d**, RT-qPCR analyses of WSTF in sh-NTC and sh-WSTF#1 BJ-hTERT cells for ISD, poly I:C, TNF $\alpha$  and SeV, and THP1 cells for LPS and HSV-1. Results were normalized to Lamin A/C and presented as mean values with s.d.; n=3; n.s. non-significant; \*\*\*\* P < 0.0001; unpaired two-tailed Student's t-test. **c**, RT-qPCR analyses of WSTF in sh-NTC and sh-WSTF #2 BJ-hTERT cells for ISD stimulation. Results were normalized to Lamin A/C and presented as mean values with s.d.; n=3; \*\* P < 0.01; unpaired two-tailed Student's t-test. **d**, RT-qPCR analyses of IL6, IL8 and IFN $\beta$  in sh-NTC and sh-WSTF #2 BJ-hTERT cells transfected with ISD. Results were normalized to Lamin A/C and presented as mean values with s.d.; n=3; \*\* P < 0.01; \*\*\*\* P < 0.0001; unpaired two-tailed Student's t-test.

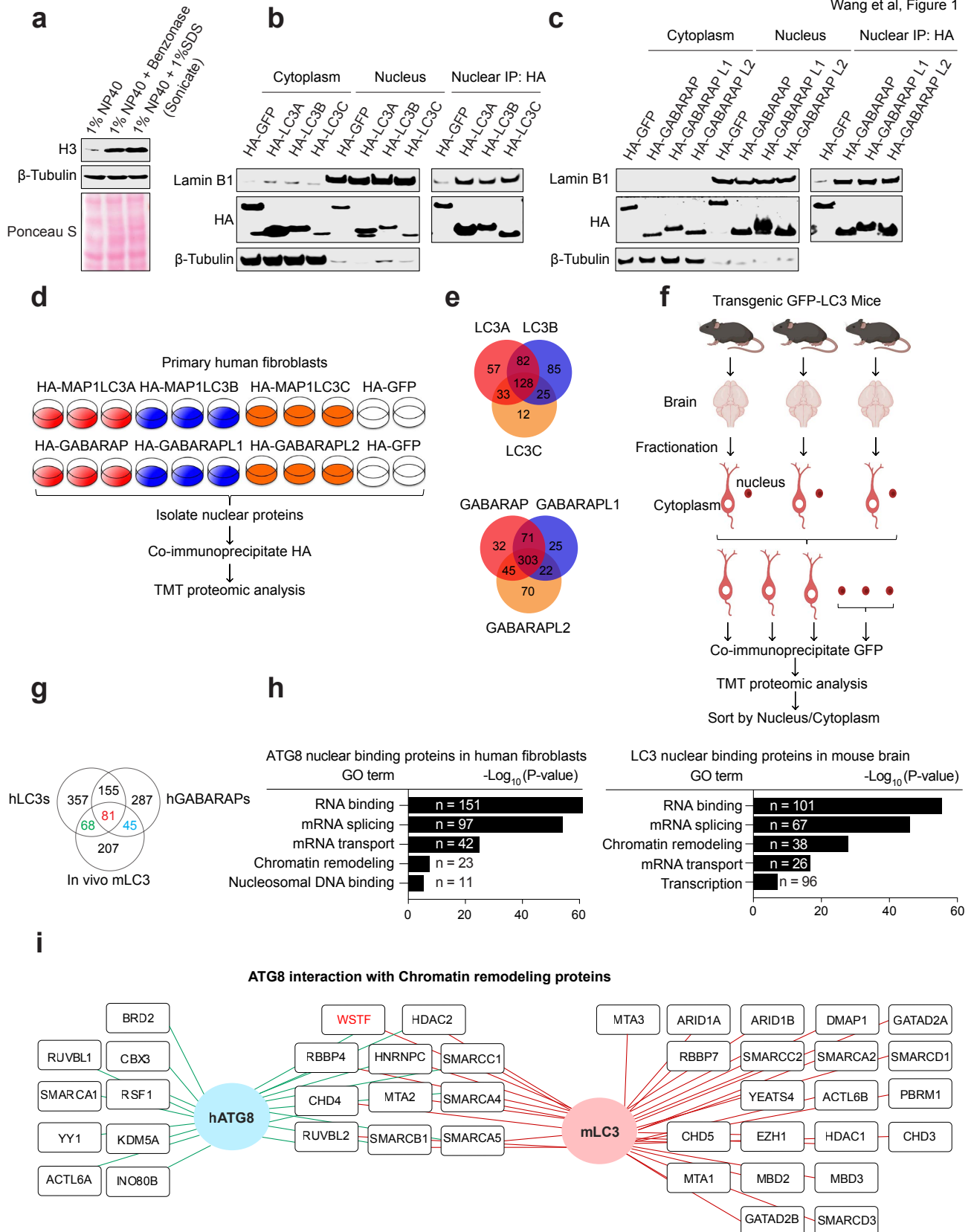
#### **Extended data figure 10. WSTF inhibits p65-mediated pro-inflammatory gene expression.**

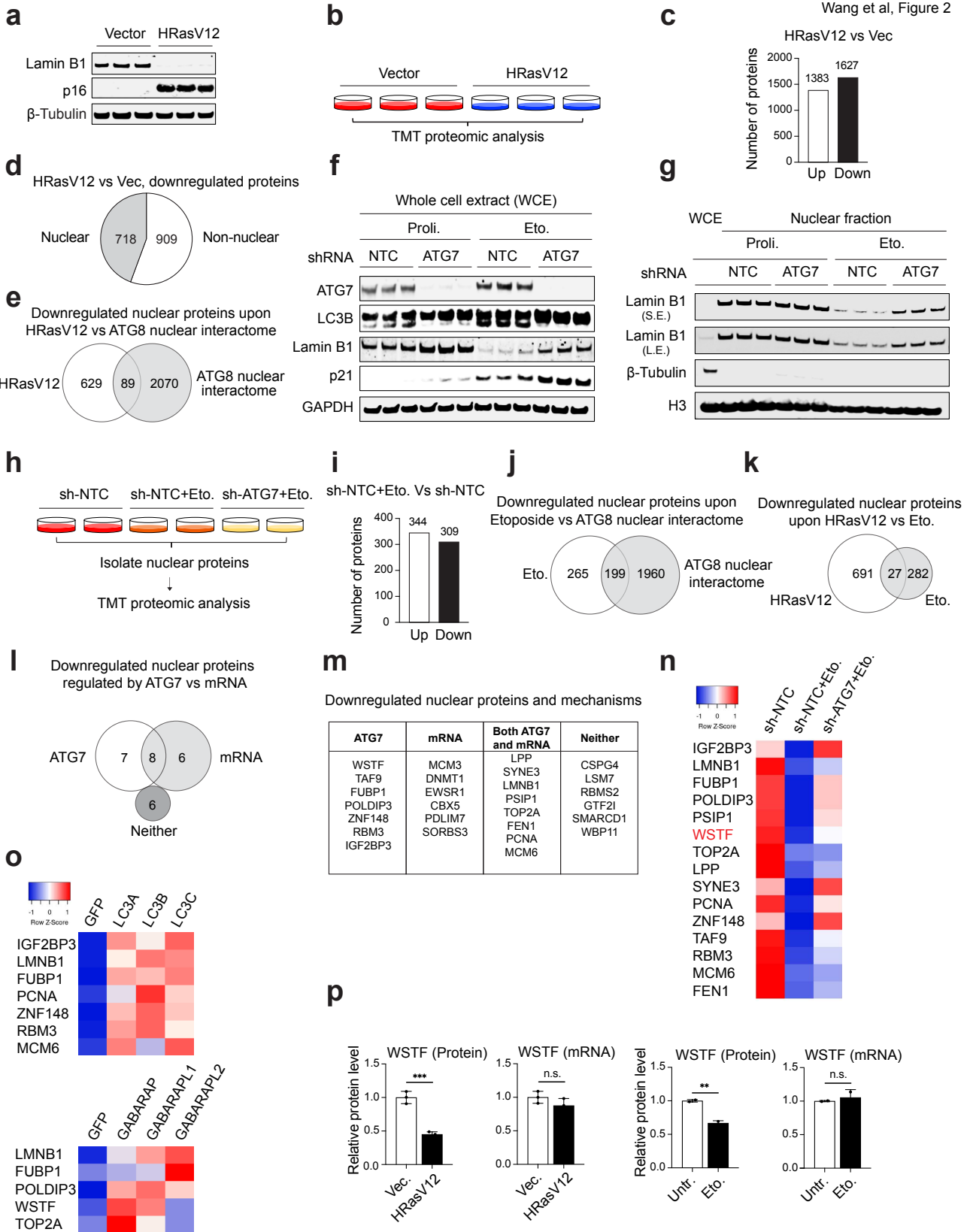
**a, b**, Transcription factor prediction from RNA-seq using DEGs and ATAC-seq from DARs that are downregulated by WSTF in HRasV12-induced senescence. **c-e**, sh-NTC and sh-WSTF IMR90 (**c** and **e**) or HEK293T (**d**) were left untreated or treated with poly I:C 30 ug/ml for 1.5h, TNF $\alpha$  20 ng/ml for 30min, or etoposide-induced senescence, then stained with a p65 antibody, followed by imaging under a confocal microscopy. Representative images are shown. Bar graphs showing the quantification of the percentage of cells with nuclear p65. Results are from four randomly selected fields with over 200 cells, presented as mean with s.d.; n.s.: non-significant. **f**, IMR90 cells were stably expressed with sh-NTC or sh-WSTF, and were treated with or without poly I:C, then analyzed by western blotting using indicated antibodies. **g**, 293T cells were stably expressed with sh-NTC or sh-WSTF, and treated with or without TNF $\alpha$ , then analyzed by western blotting using indicated antibodies. **h**, RT-qPCR analyses of IL6 and IL8 in sh-NTC and sh-WSTF 293T cells

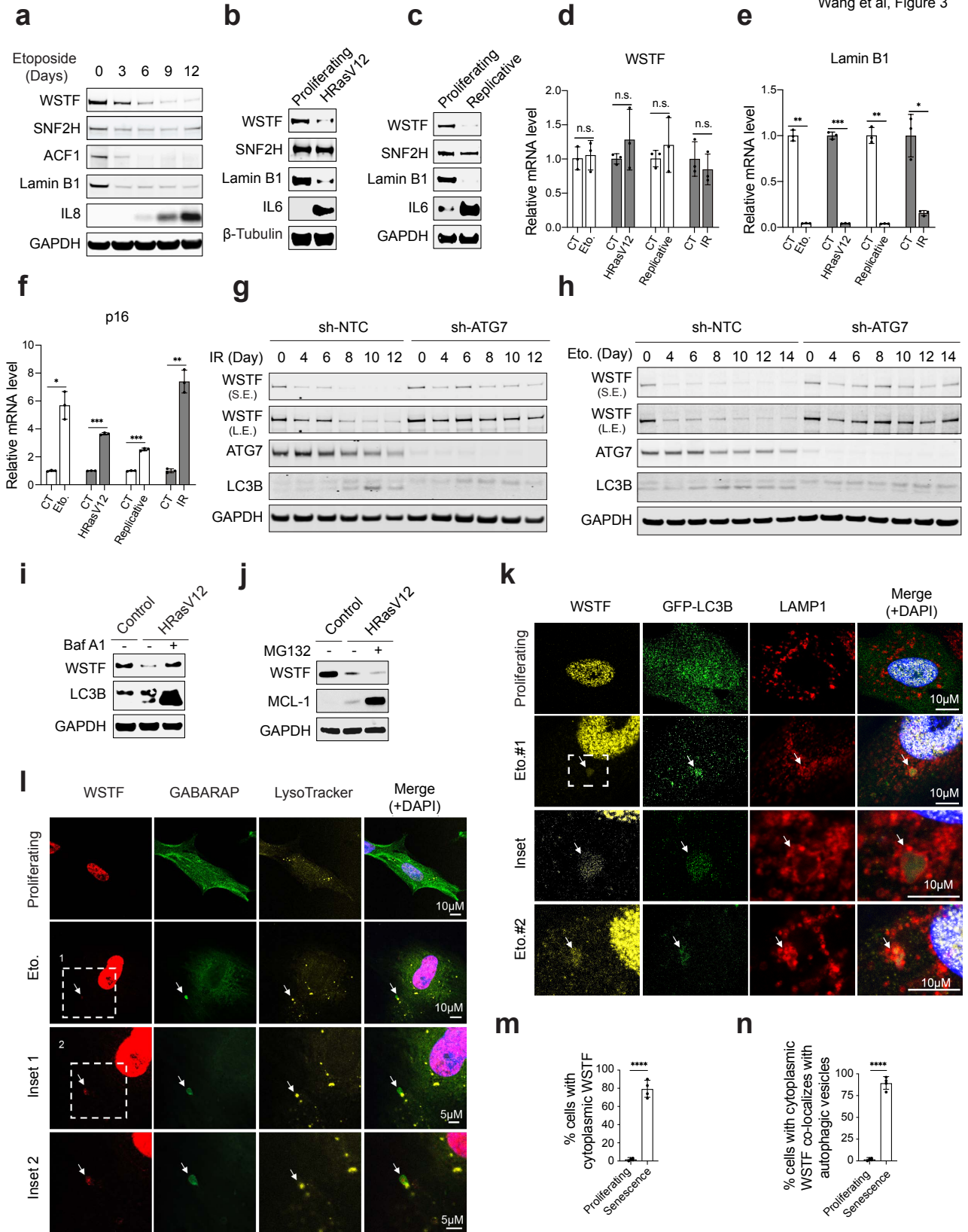
upon TNF $\alpha$  treatment. Results were normalized to Lamin A/C and presented as mean values with s.d.; n=3; n.s. non-significant; \* P < 0.05; \*\*\*\* P < 0.0001; one-way ANOVA coupled with Tukey's post hoc test. **i**, Schematic illustration of WSTF interaction with non-acetylated p65. Upon p65 translocation to the nucleus, WSTF binds to non-acetylated p65 and inhibits p300 binding to p65. Upon further stimulation, p300 acetylates p65, leading to dissociation between WSTF and p65, promoting p65 transcriptional activation of pro-inflammatory genes.

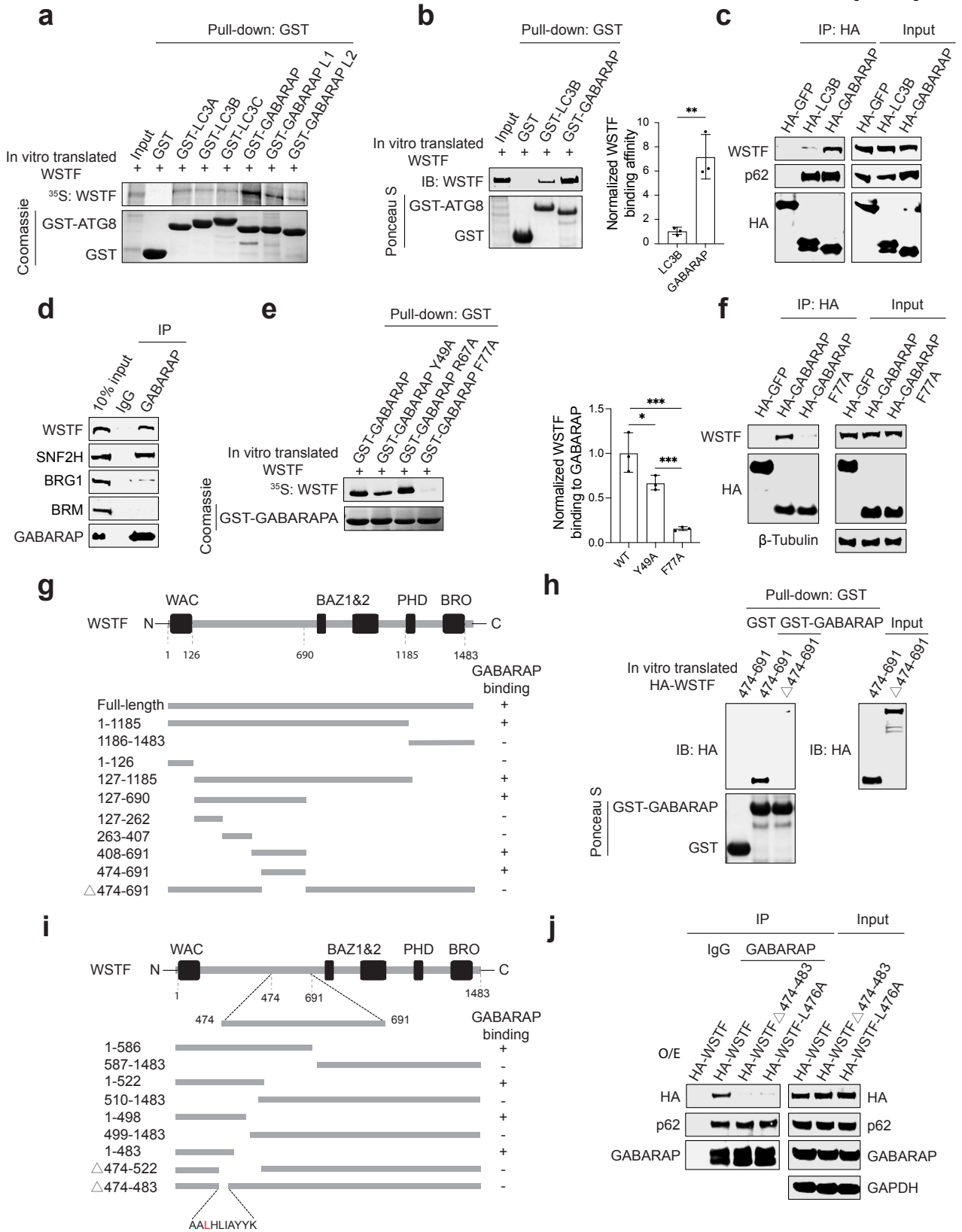
**Extended data figure 11. WSTF inhibits immuno-surveillance of NRasV12 in mouse liver.**

**a**, Liver sections 6 days post injection were stained with GFP and WSTF antibodies, and then analyzed by a confocal microscopy. Scale bars are shown. Note the GFP-positive cell showed reduced WSTF. **b** and **c**, Related to Fig. 8**l** and **m**, Images showing liver from NRasV12/GFP and NRasV12/WSTF groups 6 months post injection. Note while the GFP group did not develop liver tumors, all mice in the WSTF group developed liver tumors.





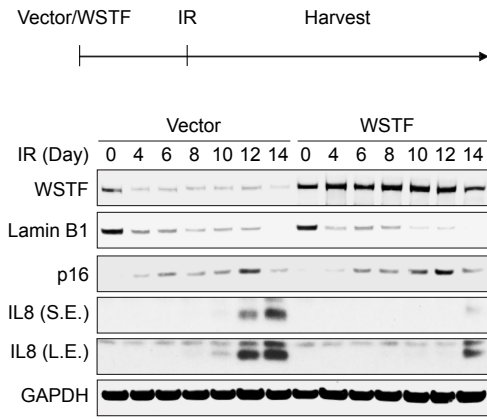




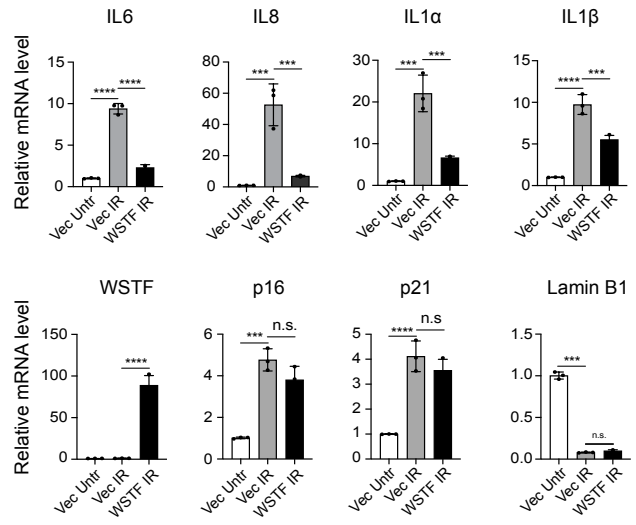




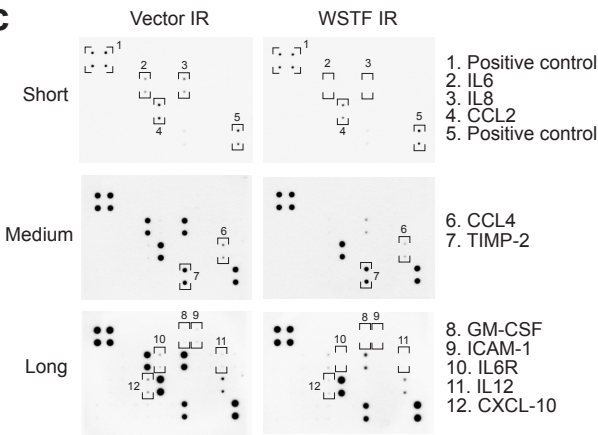
**a**



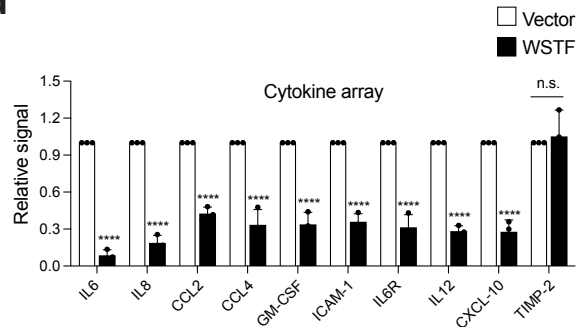
**b**



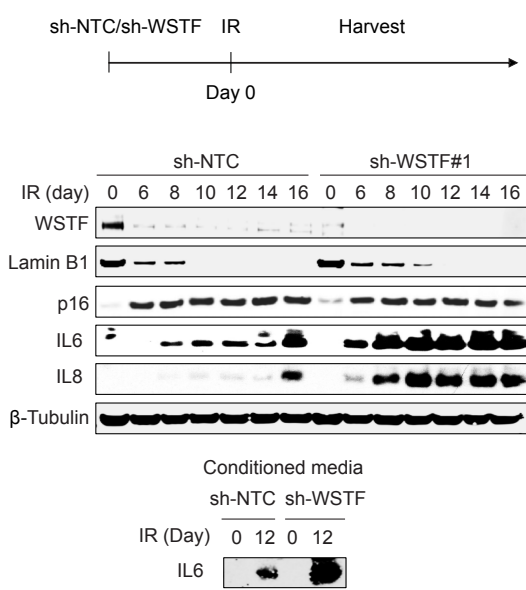
**c**



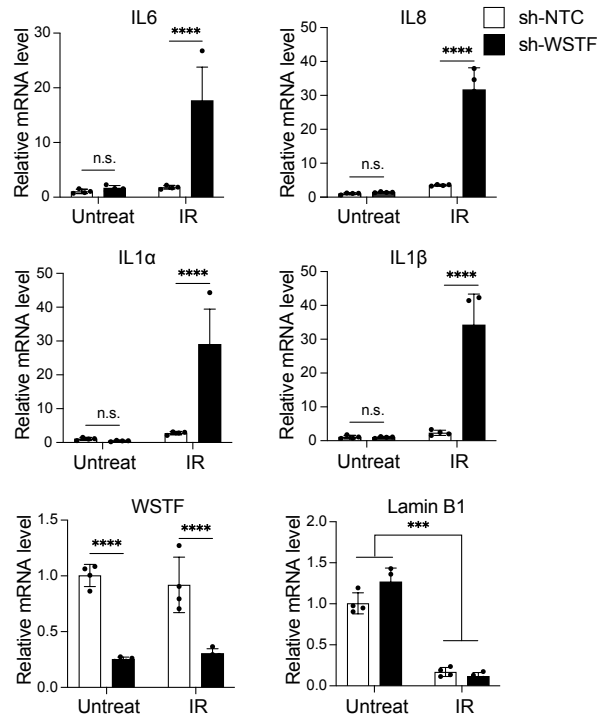
**d**

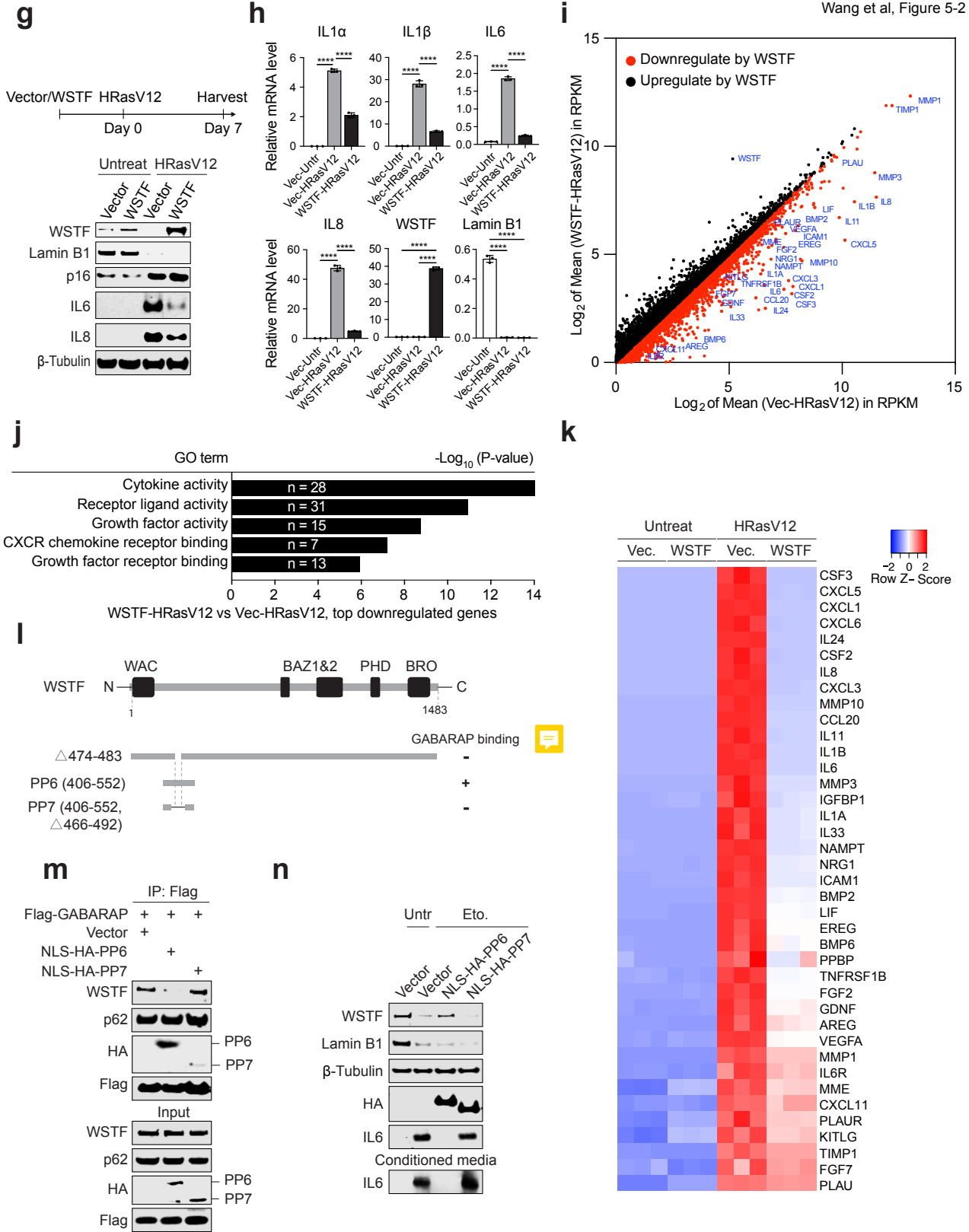


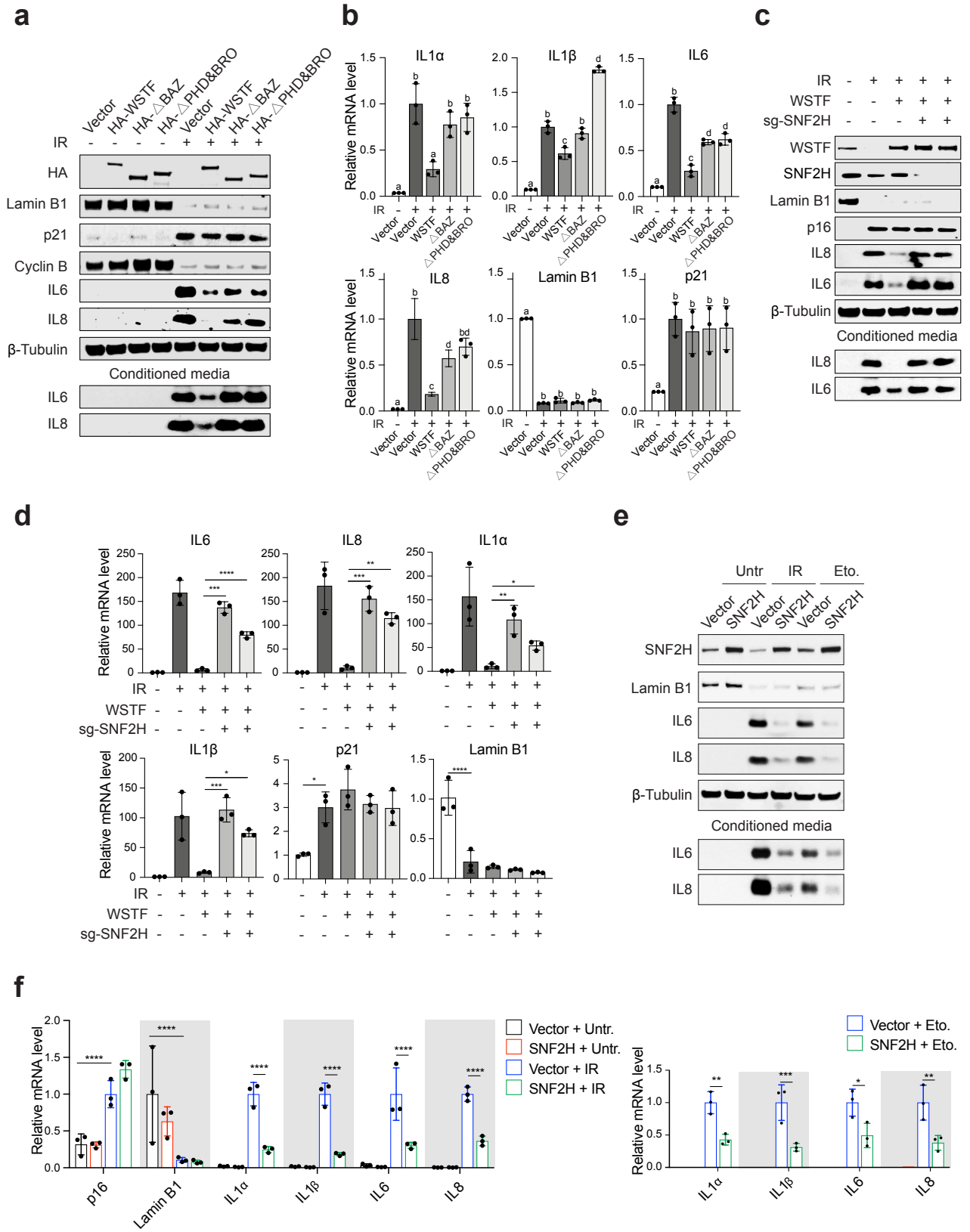
**e**



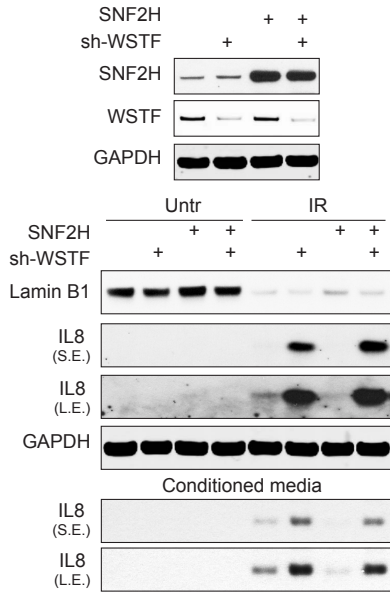
**f**



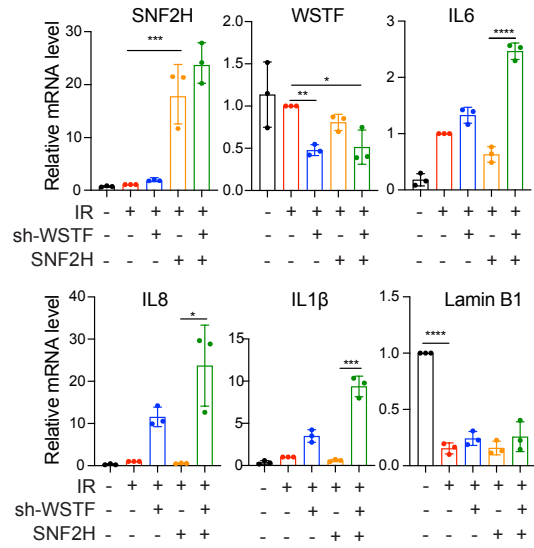




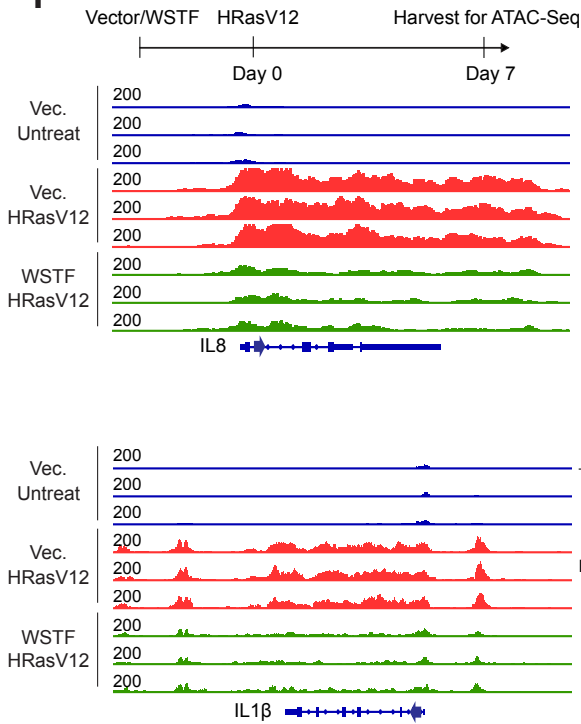
**g**



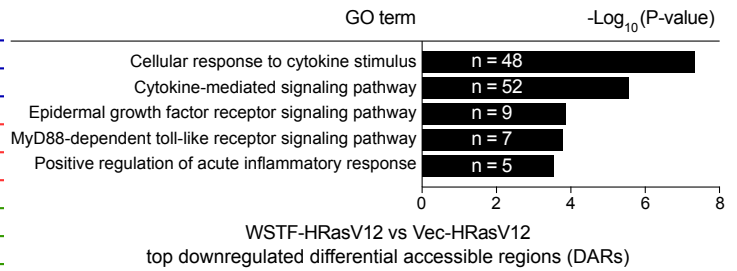
**h**

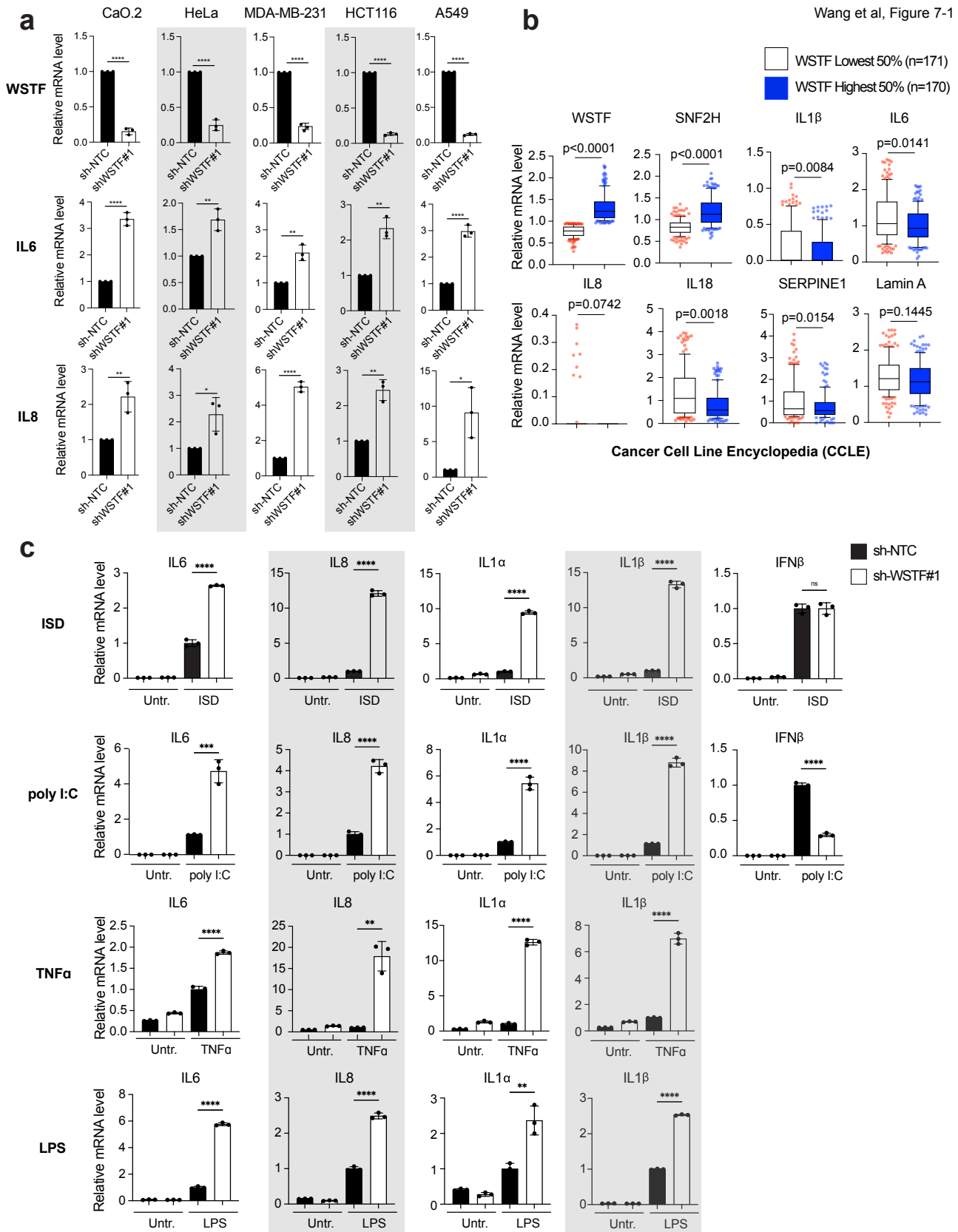


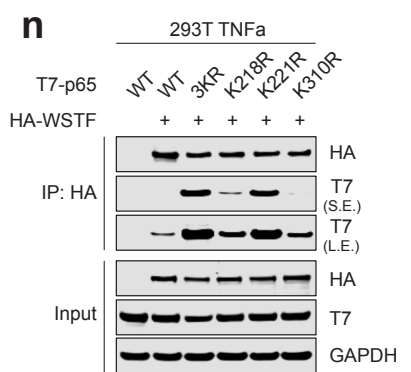
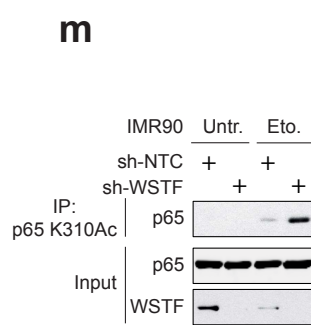
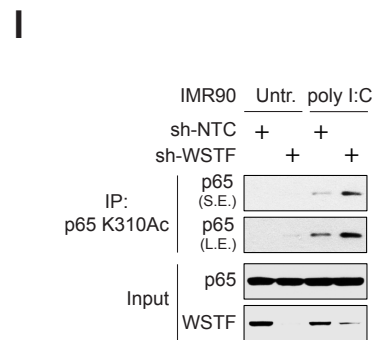
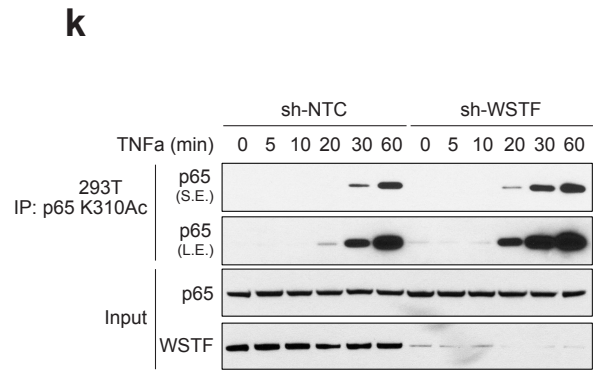
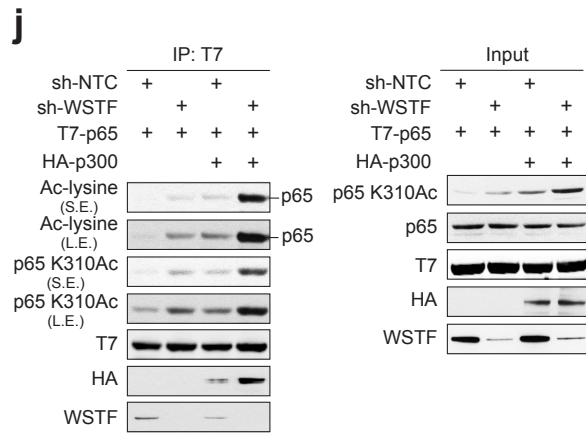
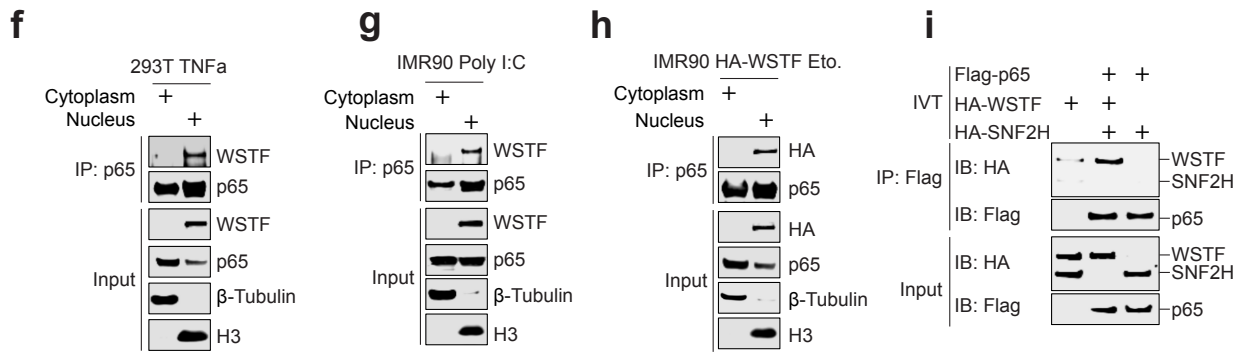
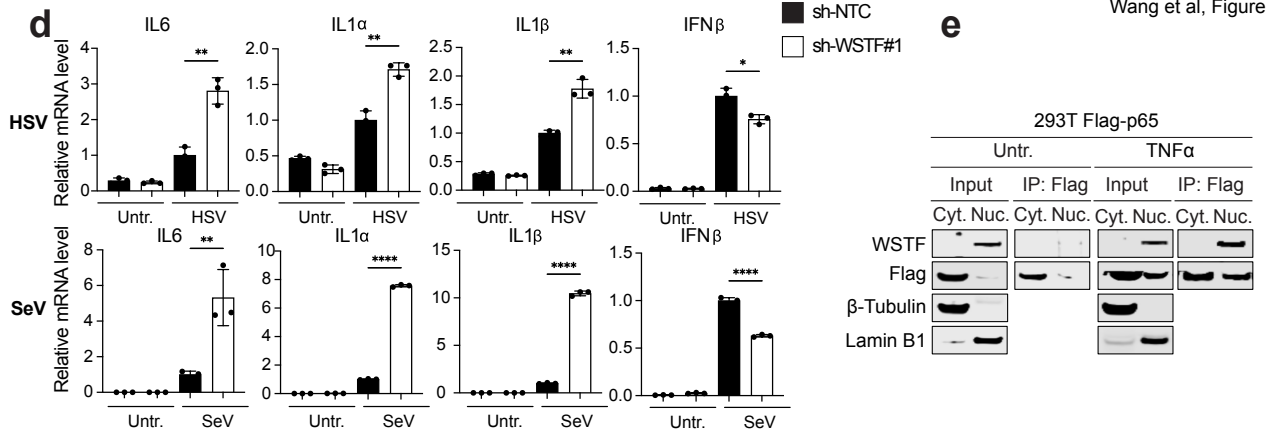
**i**



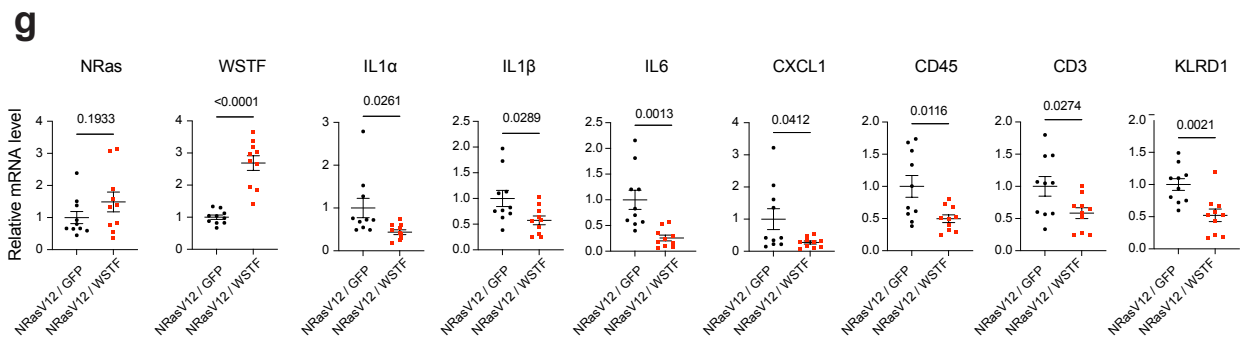
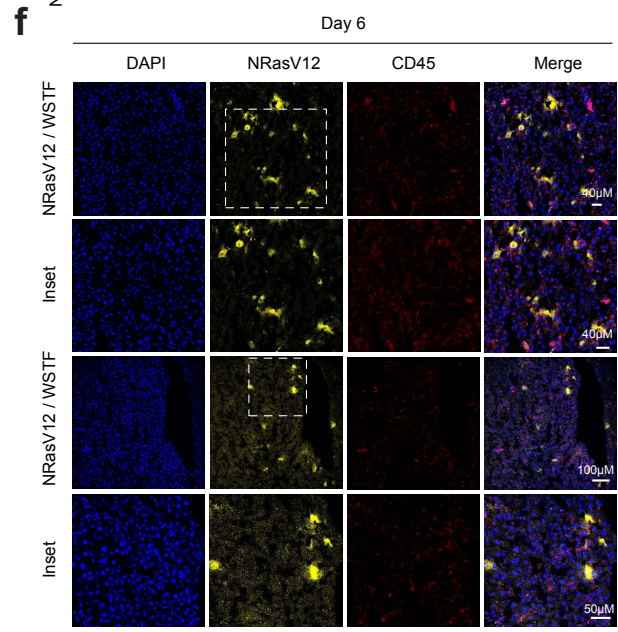
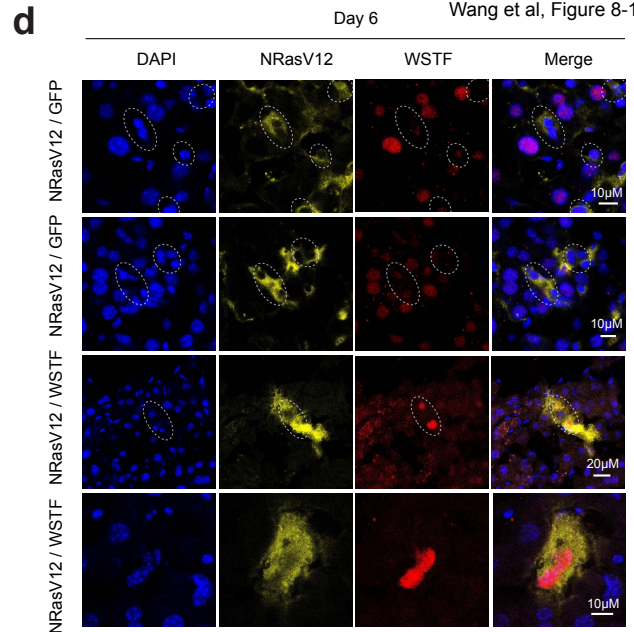
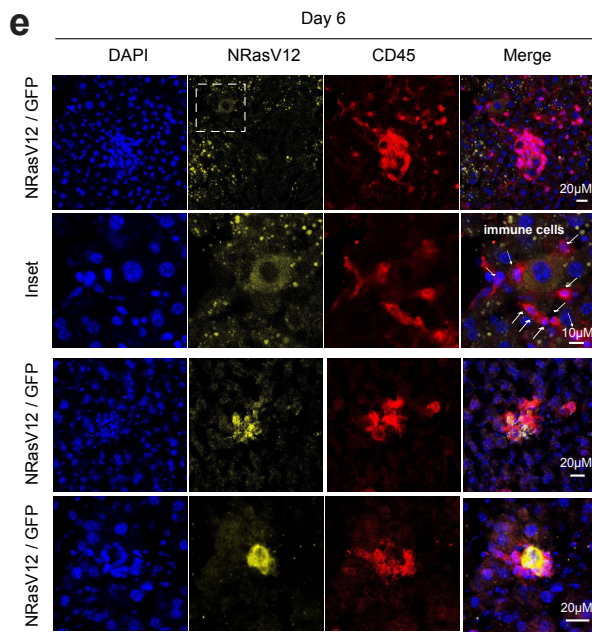
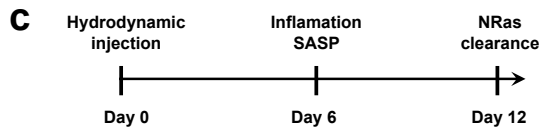
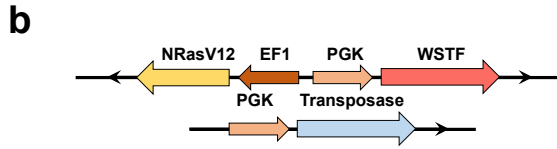
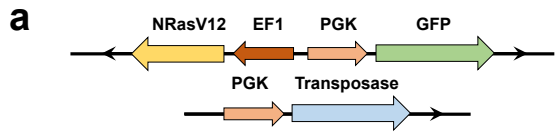
**j**



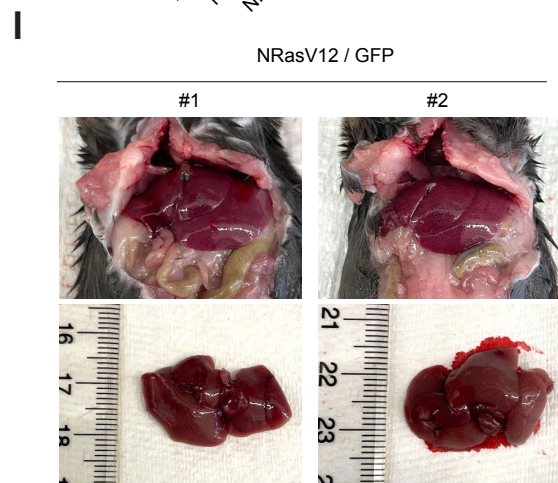
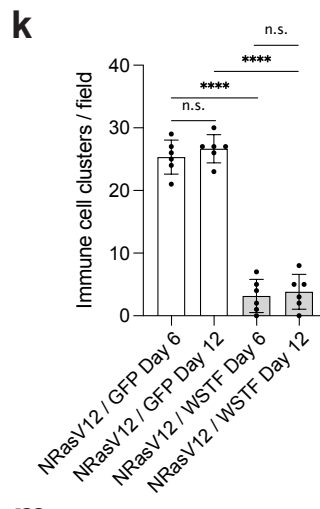
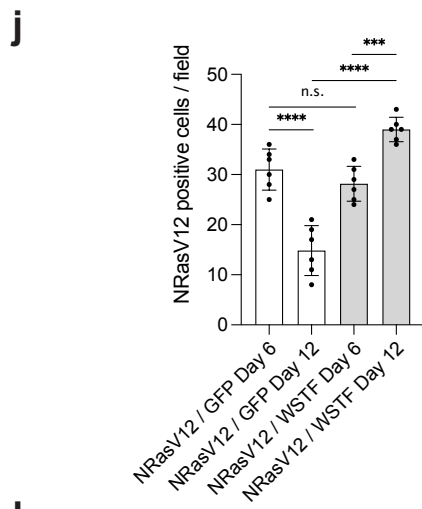
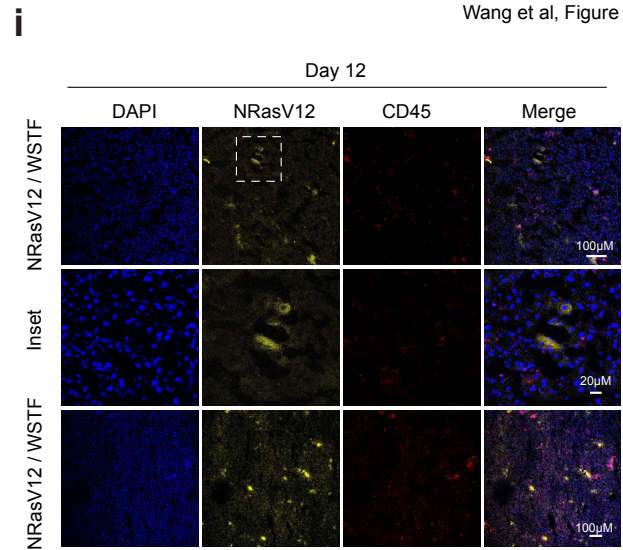
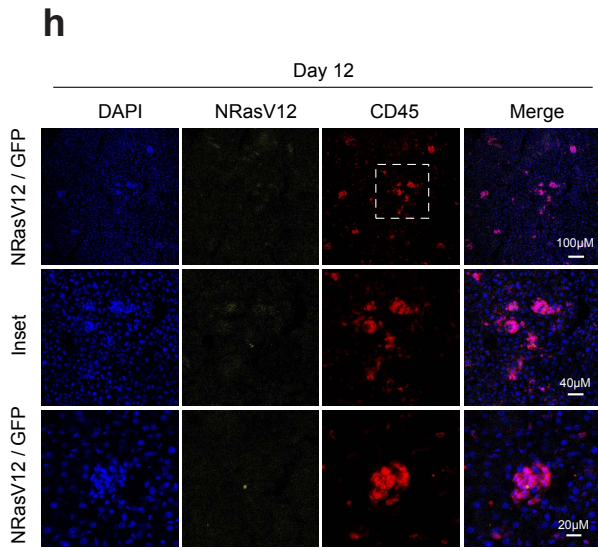




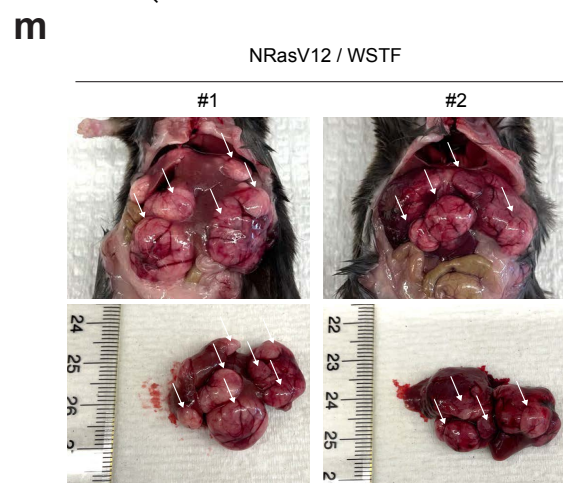






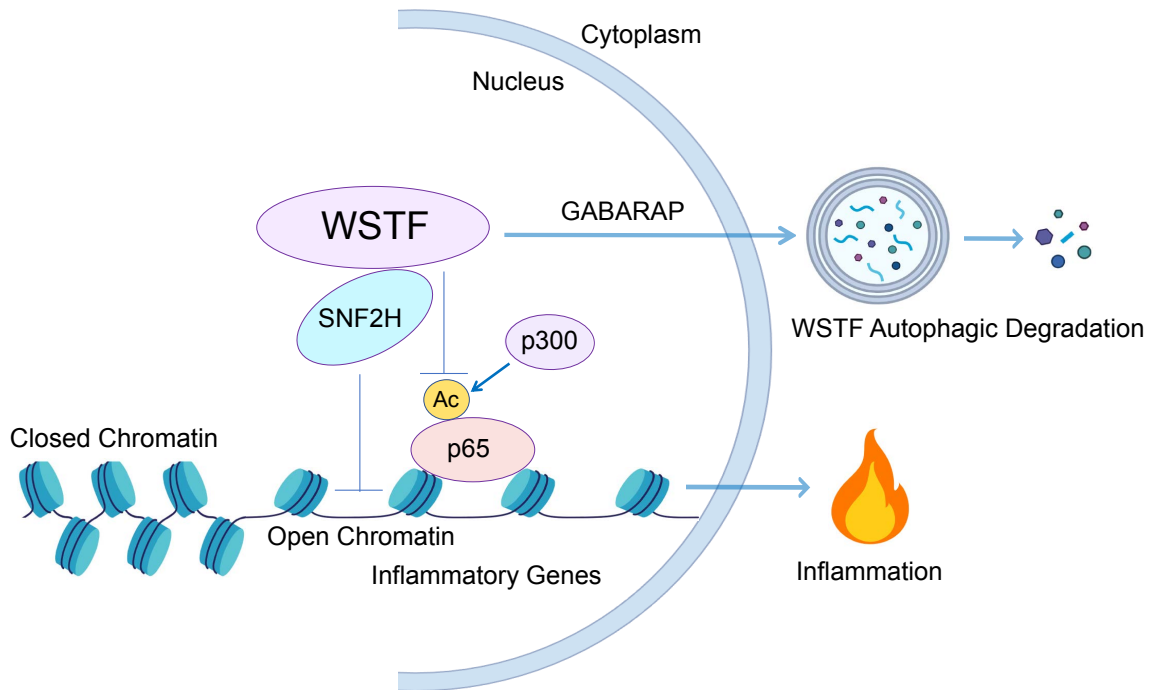


Mice with liver tumor: 0% 0/10

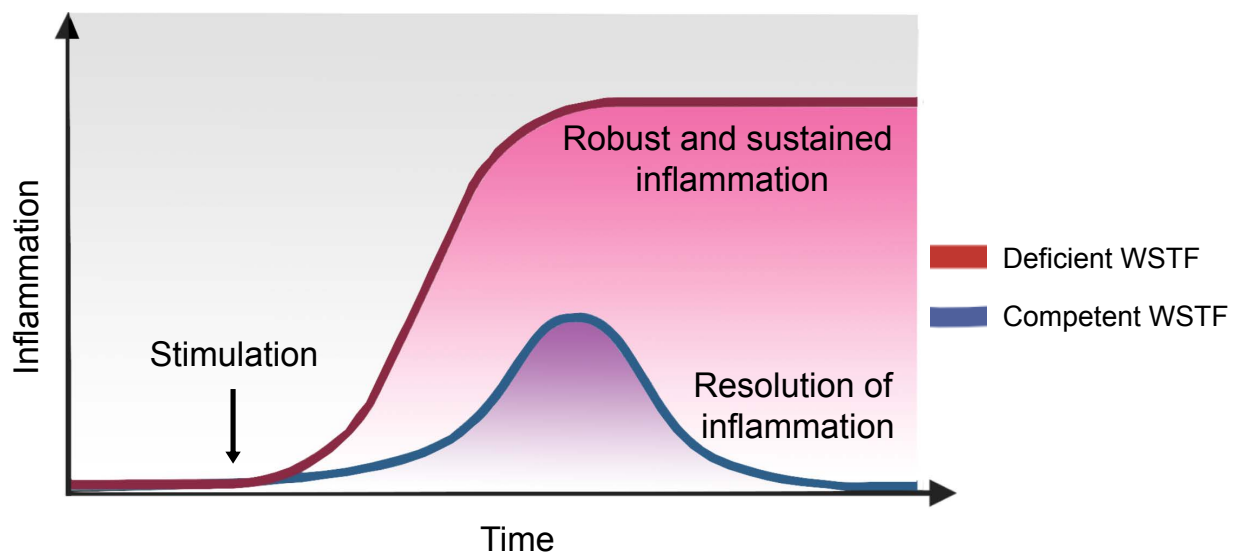


Mice with liver tumor: 100% 10/10

**a**

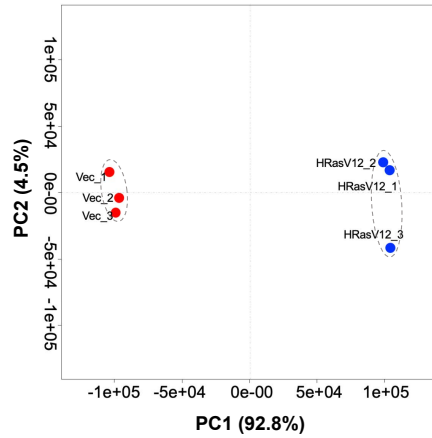


**b**



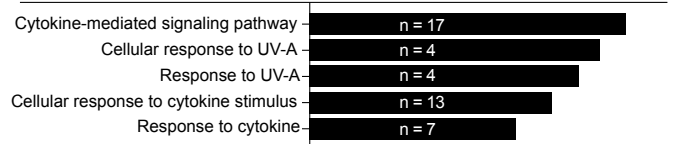


**a**

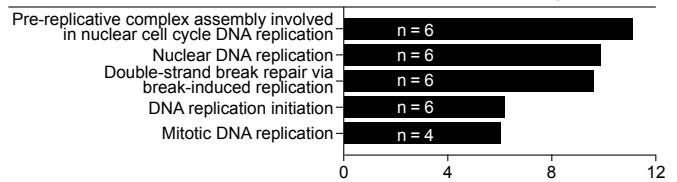


**b**

**HRasV12 vs Vector (Log2 HRasV12/Vector>2), top upregulated proteins**



**HRasV12 vs Vector (Log2 HRasV12/Vector<-2), top downregulated proteins**

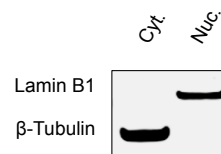


**c**

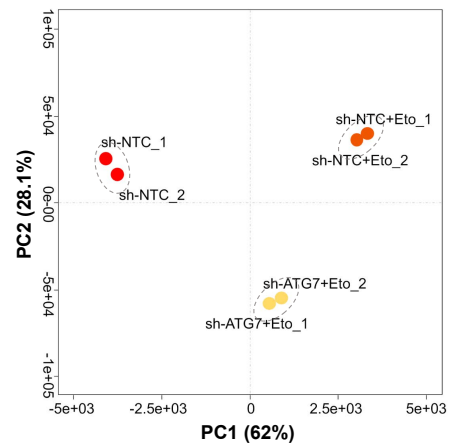
**Downregulated nuclear proteins upon HRasV12 vs ATG8 nuclear interactome**

SYNCRIP	MCM2	H2AFX	ZMYND11	CCDC137	UHRF1
HSPB1	SMARCA4	UTRN	NIFK	NF2	FUBP1
RBM3	PWP1	CTDSP2	ADD1	LOX	FLOT1
CAMK2D	FLNA	MYH9	WSTF	FXR1	EPPK1
LBR	SUN1	GTF2I	EWSR1	GSN	LOXL2
CENPV	ZNF148	HSPA1A	RBM34	DNAJB4	POLDIP3
ZFR	CSRP1	NAP1L1	TCOF1	H2AFV	PPP1R12A
MCM4	AZ1	CBX5	HP1BP3	FYTTD1	WIZ
LMNB1	NOLC1	CTNBN1	CSRP2	TJP1	MSH6
TOP2A	MYOF	SYNPO	HIST2H2BC	PCNA	CBX8
AHNAK	SLC2A1	PHC2	LMNA	MYEF2	IGF2BP3
EPB41L2	GLUL	HIST1H1C	RAI14	TOP2B	CIRBP
DAG1	UBTF	CAV2	WBP11	MPHOSPH10	DEK
KPNA3	NUCKS1	LRP1	HNRNPA0	PDGFRB	HNRNPA1
ACIN1	SPATS2L	HIST1H2AD	HDGFRP3	ACTN4	

**d**



**e**

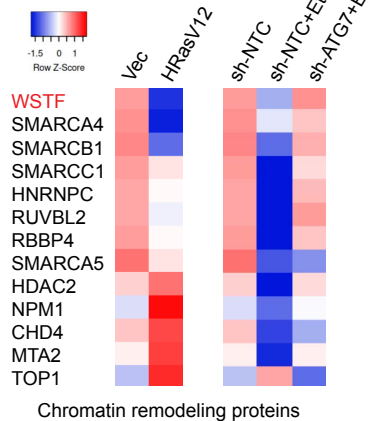


**f**

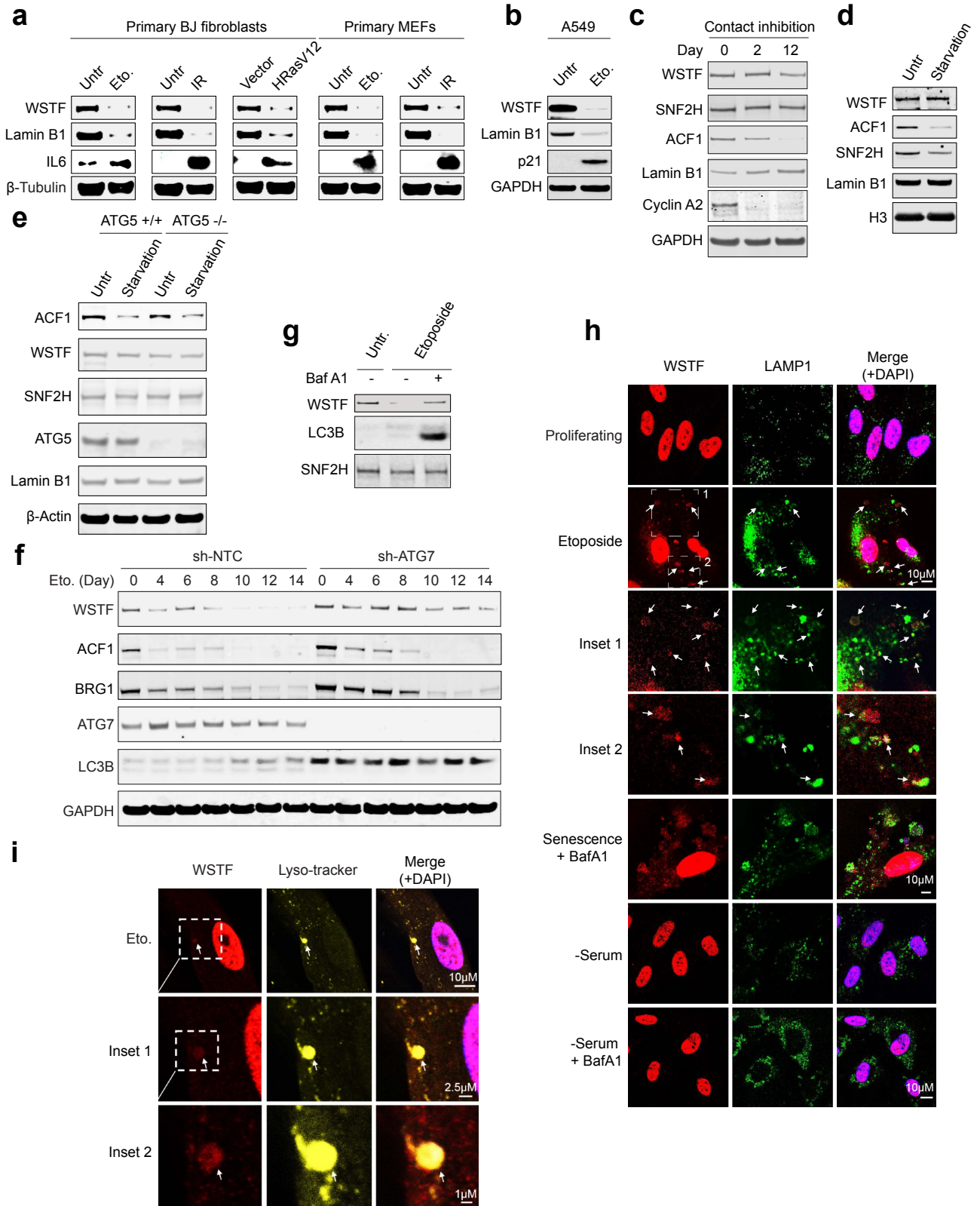
**Downregulated nuclear proteins upon Etoposide vs ATG8 nuclear interactome**

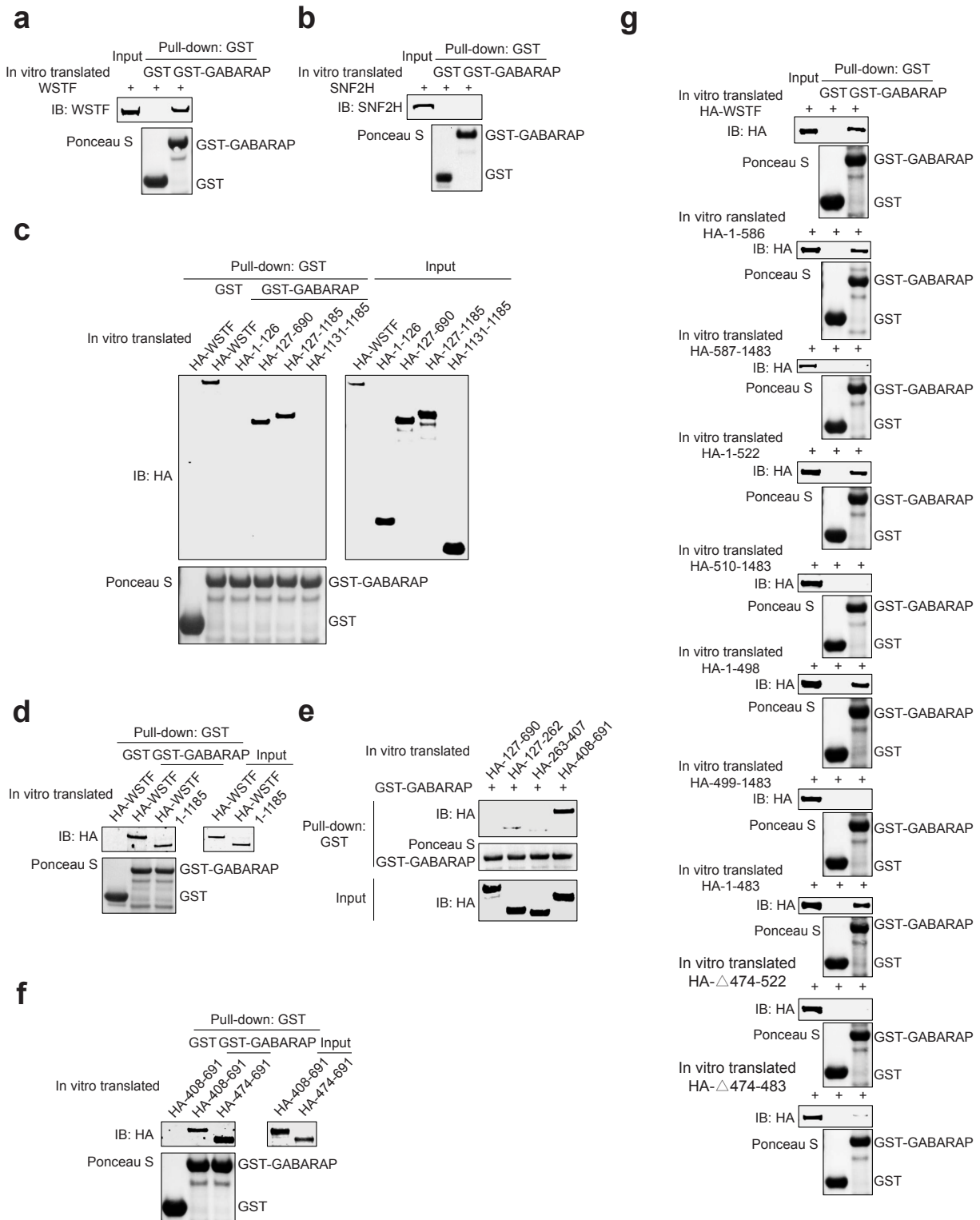
LMNB1	WSTF	CBX5	YBX3	GTF2I	WDR18
YBX1	RANGAP1	STRAP	RPS3	EIF4A3	CPSF3
SNRPD3	PFN1	SNRNP200	EIF3A	BUB3	SMC1A
DBP1	RANBP2	PPIH	RUVBL1	RUVBL2	PCBP2
ENO1	TPR	EFTUD2	CTBP1	KHSRP	CENPB
ZNF148	SFPQ	SERBP1	EIF3L	RPS15	HNRNPR
FXR2	SYNCRIP	LUZP1	WBP11	EEF2	WDR75
SRSF1	HNRNPK	TARDBP	PRPF6	CDC5L	RPL11
ALYREF	IGF2BP1	EIF3A	SMU1	RBBP4	PCNA
UBC	DDX17	MTA2	IGF2BP2	PWP2	RALY
DHX9	HNRNPD	ITGA2	MEAF6	ACTN4	SRRT
AQR	RPS3A	TAF15	CTNBN1	HNRNPD	CIRH1A
PRPF3	SF3A2	DDX47	RBM3	FXR1	NONO
HNRNPL	CCAR2	USP10	TAF15	EXOSC10	POLDIP3
TOP2A	EIF5A	HMGA2	STAG2	U2AF2	DDX21
SNW1	XRN2	CTNBL1	SART1	TRIM28	NUMA1
TIAL1	RBM8A	XRCC6	HNRNPC	FUS	ACTL6A
PLRG1	ILF2	TMPO	MAGOHB	THOC3	DDX3X
KPNA2	CTBP2	RPS13	HNRNPM	SCAF11	HNRNPA0
ADAR	HNRNPF	CDC73	HNRNPA1	HMG1	POLR2A
STRAP	IGF2BP3	HNRNPA3	KHDRBS1	SMARCC1	CIRBP
HNRNPAB	SQSTM1	DDX21	EPHB2	ELAVL1	HSP90AB1
SMNDC1	RBM6	NUP50	AKAP8	XRCC5	SMC6
ASH2L	MATR3	CCDC9	SF3A1	HNRNPA2B1	TNKS1BP1
SMC3	SNRNP70	USP10	RPS7	PABPC4	SNRNP40
SUN2	FUBP1	RRP9	NUFIP2	MPHOSPH10	KPNB1
PHF14	UTP18	SRSF3	NOL11	HSPA4	PRPF19
TMA16	HDAC2	PRPF4	NACA	EWSR1	PDS5B
MME					

**g**

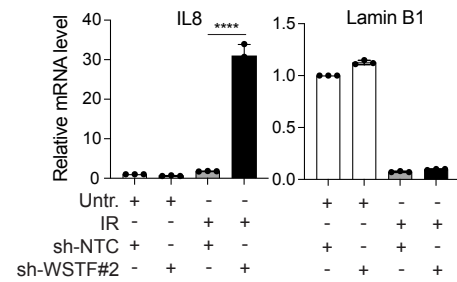
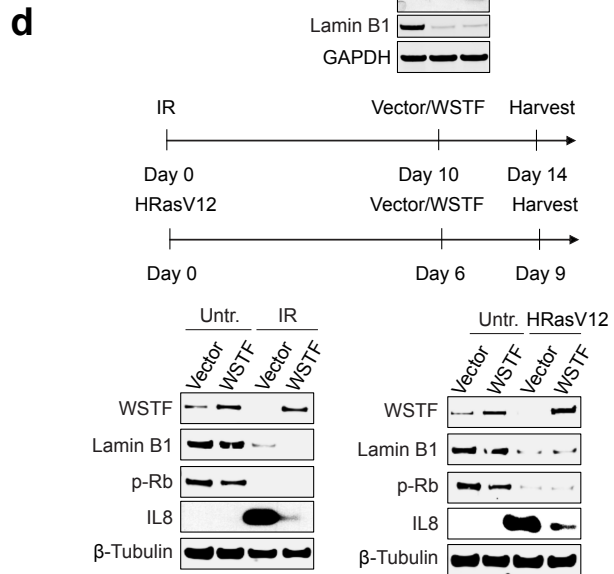
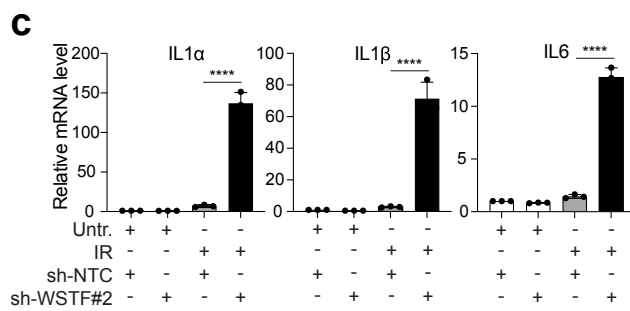
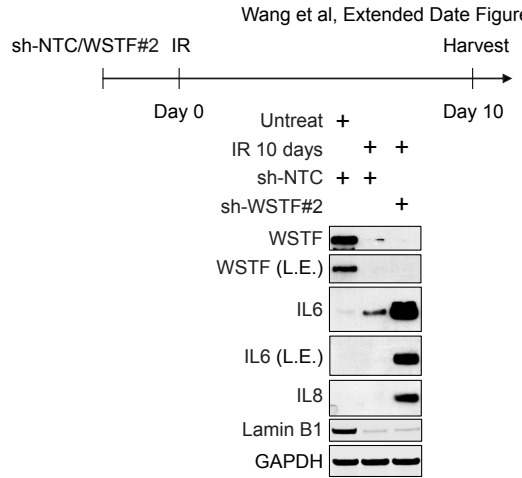
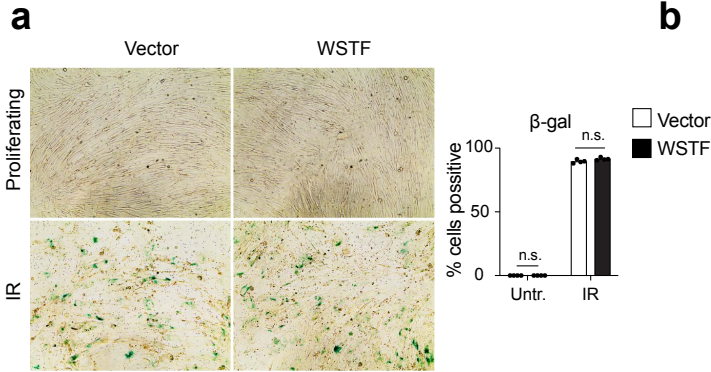










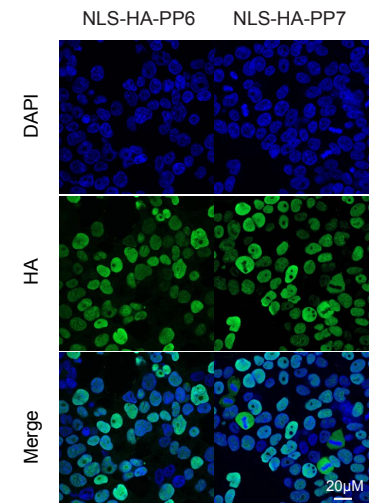


**e**

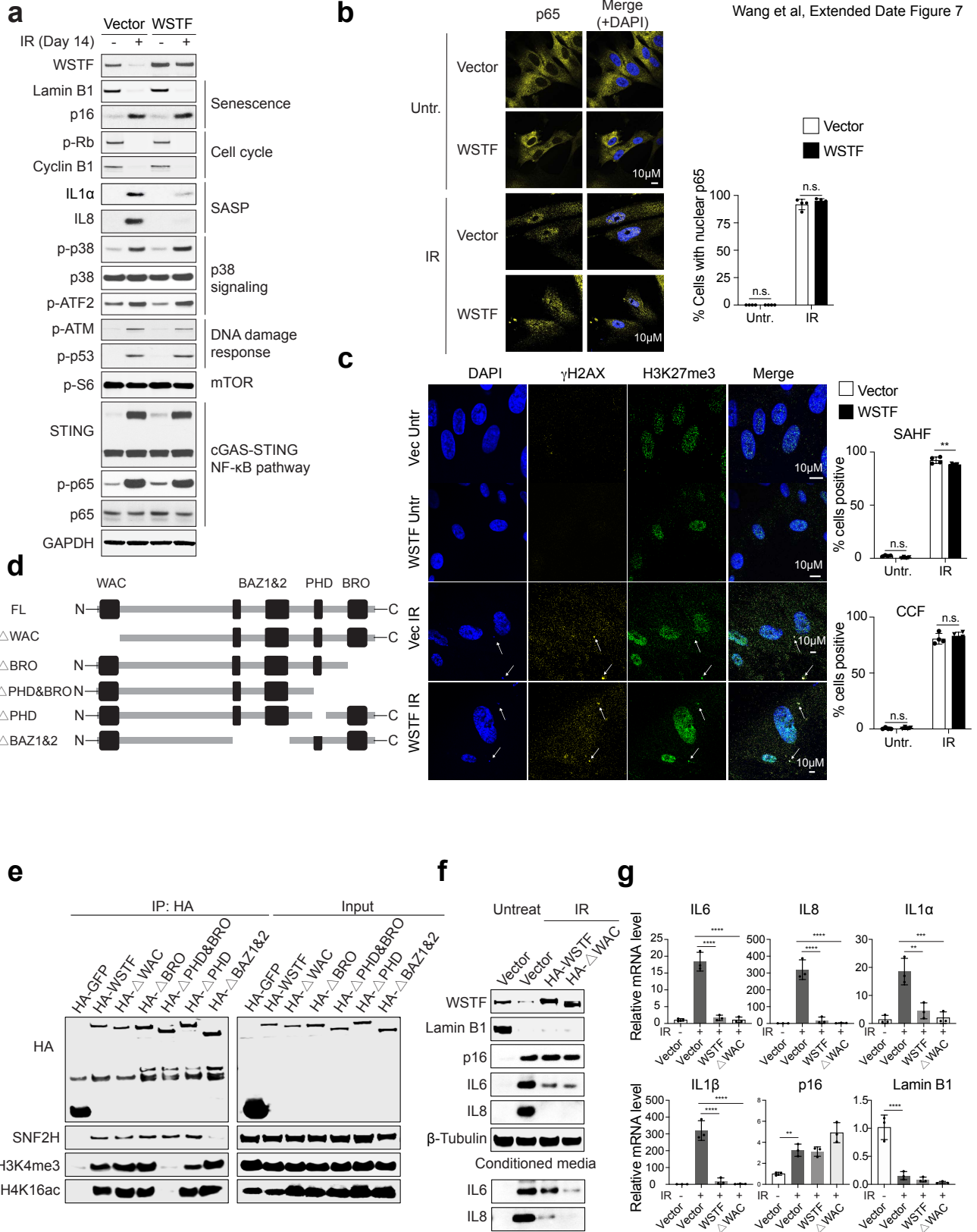
WSTF-HRasV12 vs Vec-HRasV12, list of top downregulated genes from RNA-Seq

GO term	Genes
Cytokine activity (GO:0005125)	CXCL6, CSF3, CSF2, IL8, CXCL1, CXCL3, FGF2, CXCL2, CXCL5, WNT11, IL36B, NDP, IL11, IL33, TSLP, CCL20, WNT7B, LIF, NRG1, INHBA, BMP7, BMP6, VEGFA, IL1A, BMP2, IL6, IL1B, PF4
Receptor ligand activity (GO:0048018)	CSF3, COLEC10, CSF2, PDGFB, TGFA, CXCL1, AREG, FGF2, SHH, WNT11, IL36B, NDP, IL11, IL33, EPHA7, TSLP, WNT7B, SEMA6D, LIF, NRG1, OSGIN2, INHBA, BMP7, BMP6, EREG, VEGFA, IL1A, BMP2, IL6, GDNF, IL1B
Growth factor activity (GO:0008083)	IL11, CSF3, PDGFB, LIF, TGFA, CXCL1, NRG1, INHBA, OSGIN2, AREG, FGF2, EREG, VEGFA, IL6, GDNF
CXCR chemokine receptor binding (GO:0045236)	CXCL6, IL8, CXCL1, CXCL3, CXCL2, CXCL5, PF4
Growth factor receptor binding (GO:0070851)	IL11, CSF3, TSLP, PDGFB, TGFA, FGF2, AREG, EREG, VEGFA, IL6, ESM1, IL36B, IL1B

**f**





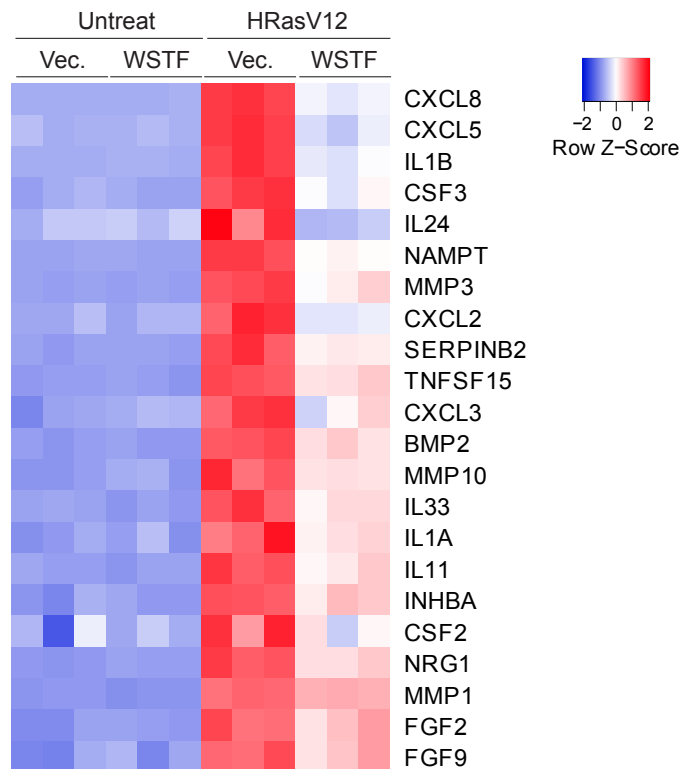
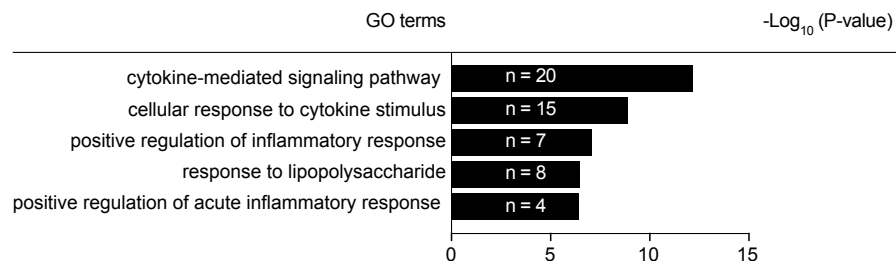


**a**

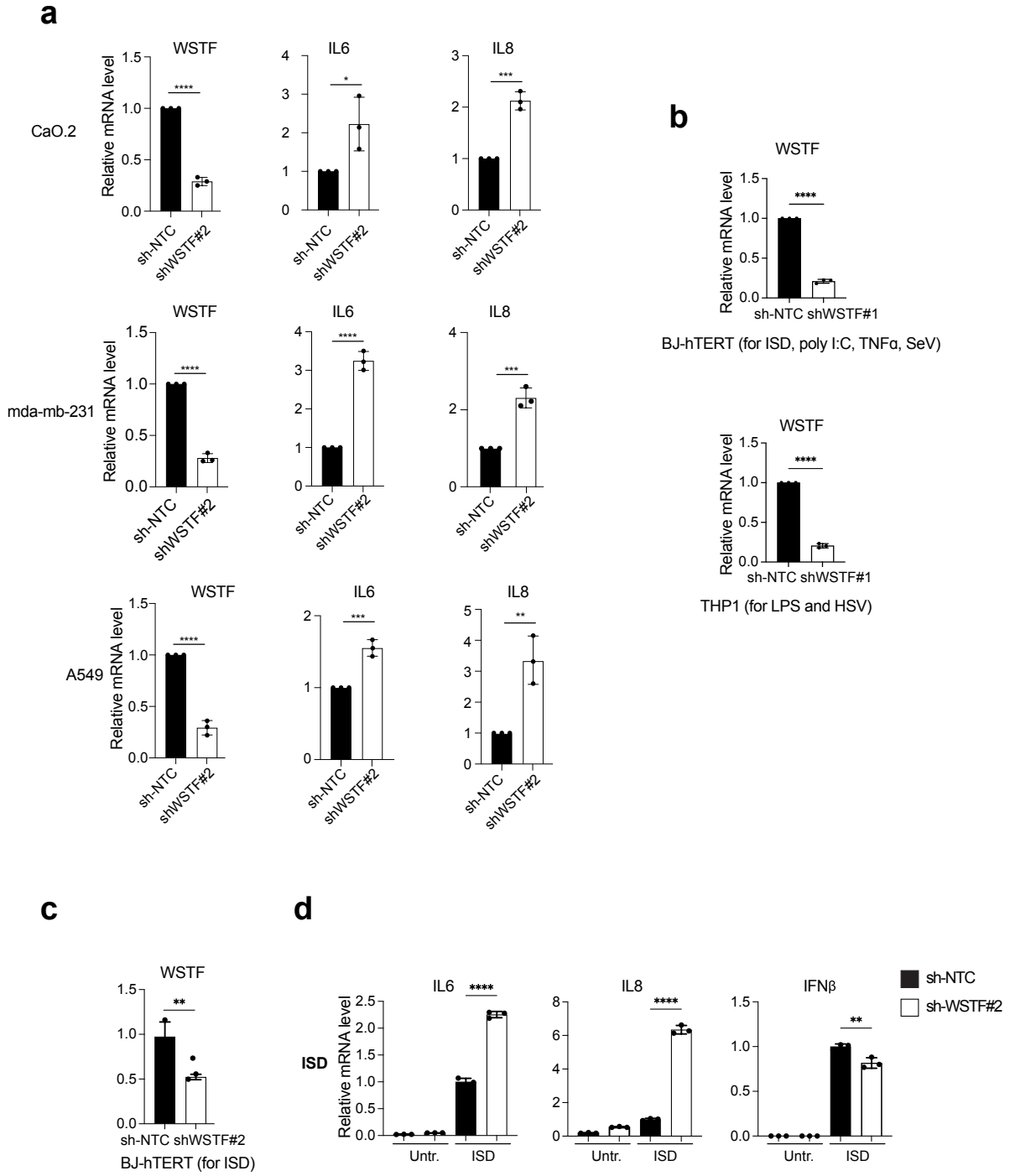
Wang et al, Extended Data Figure 8

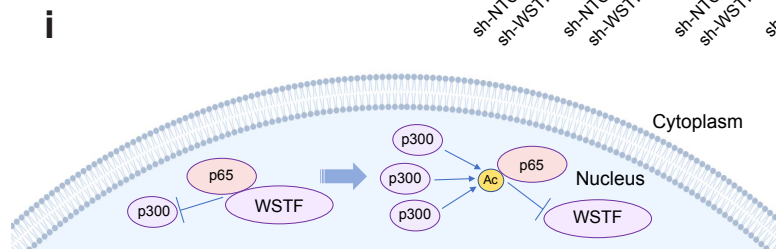
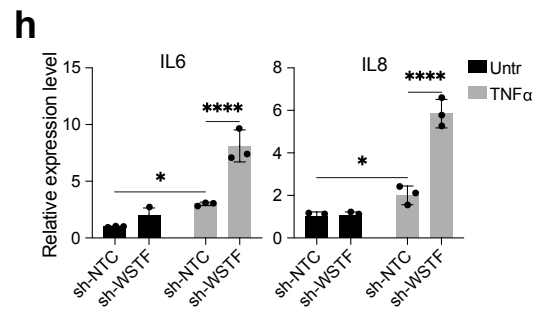
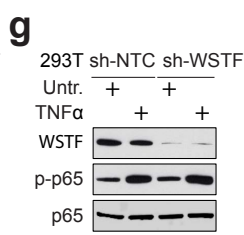
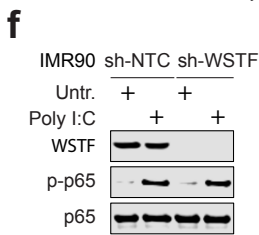
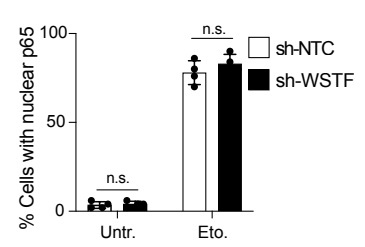
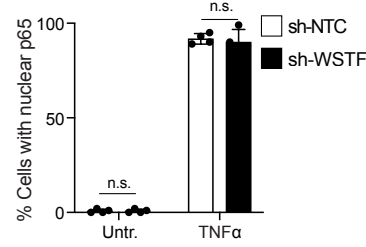
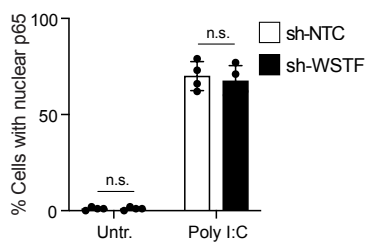
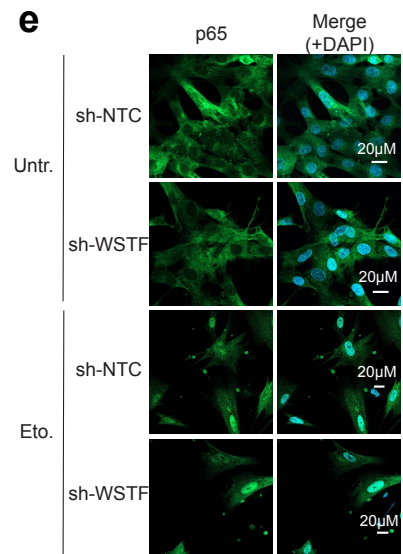
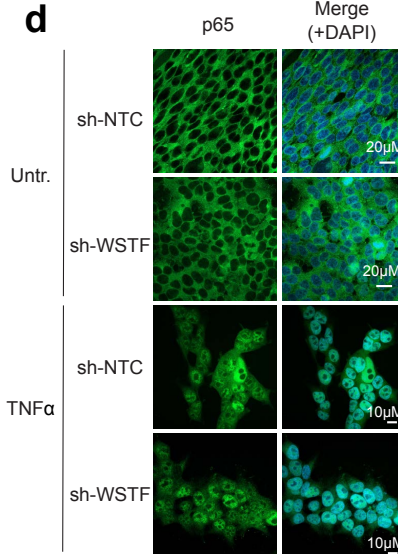
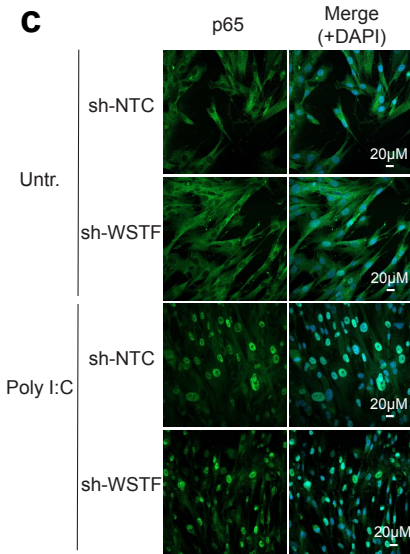
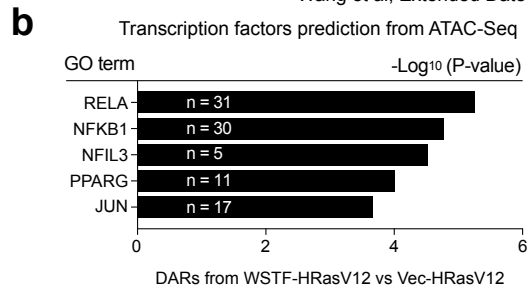
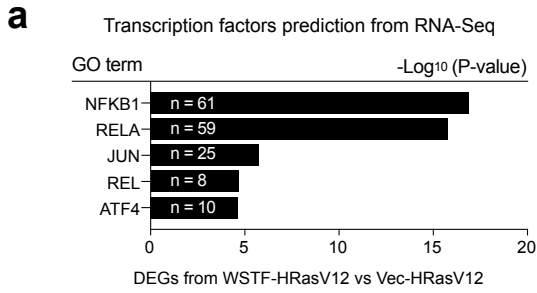
WSTF-HRasV12 versus Vec-HRasV12, list of top downregulated DAR-associated genes

GO Term	Genes
Cellular response to cytokine stimulus (GO:0071345)	CEBPA;CSF2;CXCL8;CSF1;CEBPD;IL24;TCF7;RORA;PTPRJ;CXCL1;PIK3R1;PTGS2;CRKL;SOCS3;SOCS1;IRAK2;STAT4;HAS2;FYN;SOX9;SOCS6;SH2B3;IL10;IL11;ANXA1;EDN2;POU2F1;SMAD3;DUSP1;CCL20;IL37;MMP1;IL1R2;MMP3;IRAK3;OXSR1;OSMR;PRLR;YWHAZ;POU4F2;NFKB1;EREG;LRCH1;IL1B;FSCN1;IFNK;CD47;TLR2
Cytokine-mediated signaling pathway (GO:0019221)	CSF2;CXCL8;CSF1;IL24;RORA;PTPRJ;CXCL1;EDA2R;CXCL5;CRKL;TRIM25;MAP3K7;IL10;IL11;ANXA1;SERPINB2;EDN2;RIPK2;FBXW11;MMP1;IL1R2;MMP3;IRAK3;OSMR;PRLR;YWHAZ;EREG;IL1B;PELI1;FSCN1;IFNK;CEBPA;SP100;CEBPD;PIK3R1;PTGS2;SOCS3;SOCS1;IRAK2;STAT4;FYN;SOCS6;SH2B3;TNFSF18;IL33;POU2F1;CCL20;IL37;NFKB1;TNFSF8;IL7R;LIMS1
Epidermal growth factor receptor signaling pathway (GO:0007173)	SHC3;KIF16B;PLCE1;PIK3R1;SOX9;AREG;EGFR;FAM83B;EREG
MyD88-dependent toll-like receptor signaling pathway (GO:0002755)	TNIP1;IRAK2;LY96;IRAK3;TLR5;MAP3K7;TLR2
Positive regulation of acute inflammatory response (GO:0002675)	IL1B;C2CD4A;C2CD4B;OSMR;PTGS2

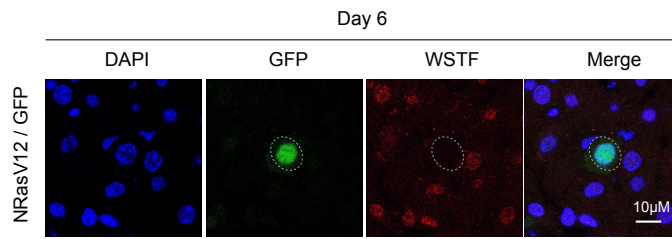
**b****c**

WSTF-HRasV12 versus Vec-HRasV12, top downregulated genes in both RNA-Seq and ATAC-Seq

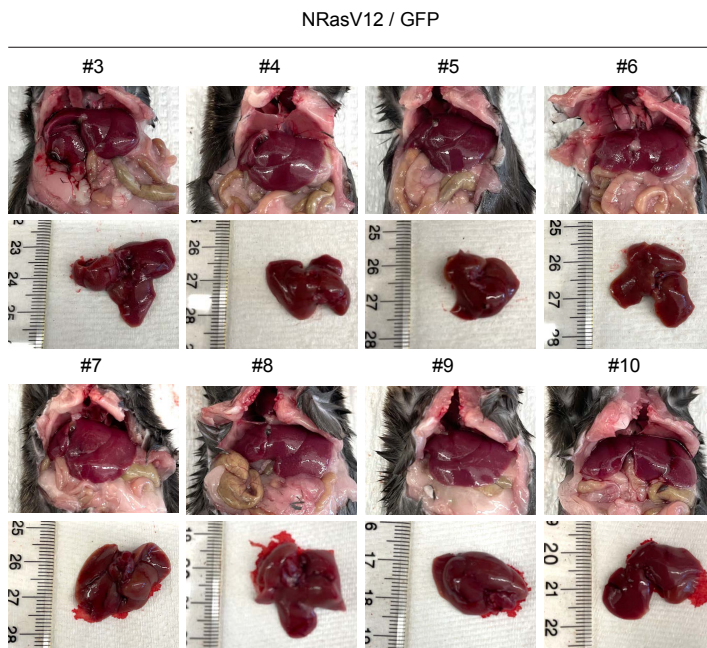




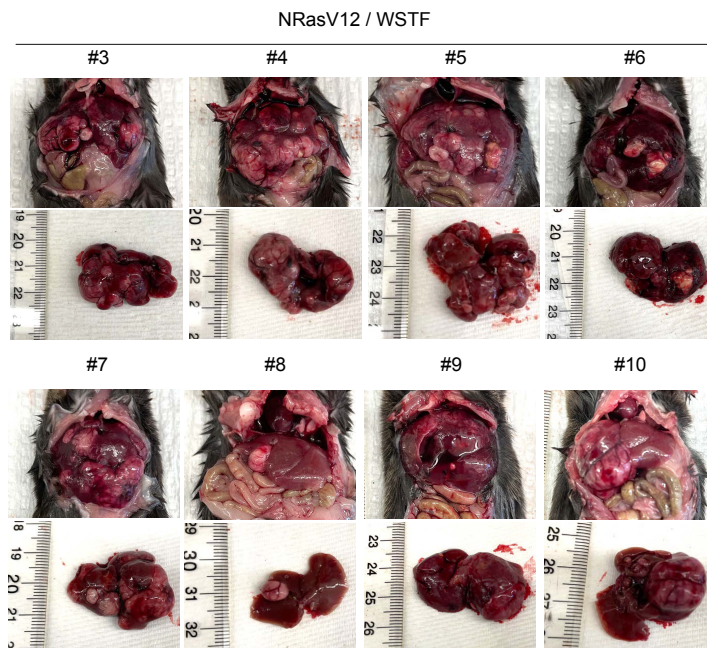
**a**



**b**



**c**




# PAPER III



SPOTLIGHT

# LC3B is a cofactor for LMX1B-mediated transcription of autophagy genes in dopaminergic neurons

Athanasios Kournoutis<sup>1</sup> and Terje Johansen<sup>1</sup> 

**It is becoming increasingly clear that the Atg8 family of autophagy proteins have roles not only in the cytoplasm, but also in the cell nucleus. In this issue, Jiménez-Moreno et al. (2023. *J. Cell Biol.* <https://doi.org/10.1083/jcb.201910133>) report that nuclear LC3B binds to the LIM homeodomain transcription factor LMX1B and acts as a cofactor for LMX1B-mediated transcription of autophagy genes, providing stress protection and ensuring survival of midbrain dopaminergic neurons.**

Macroautophagy (hereafter autophagy) is an evolutionary conserved lysosomal degradation pathway crucial for maintaining macromolecular and organellar homeostasis important for cell survival and organismal fitness in response to stress (1). Toxic protein aggregates, damaged or surplus organelles, and intracellular pathogens exposed to the cytoplasm are recognized as cargo by autophagy receptors, binding components of the basal autophagy apparatus to nucleate formation of autophagosomes on the cargo, which then fuse with lysosomes. Among about 40 conserved autophagy-related (ATG) proteins orchestrating this multistep process is the Atg8 family of 120 amino acid-long ubiquitin-like proteins that in humans consists of LC3A, -B, -B2, -C, GABARAP, GABARAPL1, and GABARAPL2 (2). Atg8 proteins act as membrane scaffold for other ATG proteins involved in autophagosome formation and fusion with the lysosome, help expand the autophagosome membrane, aid in transport of autophagosomes, and participate in cargo sequestration by bridging autophagy receptors to the autophagosomal membrane in selective autophagy (3). Atg8 proteins also have tasks outside autophagy and roles in the cell nucleus, as exemplified by the autophagic degradation of lamin B1 mediated by nuclear LC3B during oncogene-induced senescence (4). Autophagy receptors and most other

proteins that bind directly to Atg8 family proteins do so via a 10–15 amino acid-long LC3 interacting region (LIR) motif with a core sequence W/F/Y-X-X-L/I/V with the aromatic residue docking into a hydrophobic pocket 1 (HP1) and the hydrophobic residue into a hydrophobic pocket 2 (HP2) in the LIR docking site of the Atg8 protein (3).

Autophagy is a pro-longevity mechanism, and autophagy dysfunction is linked to the pathogenesis of major human disorders including cancer and neurodegenerative diseases, like Parkinson's disease (PD; 1, 5). In PD, degeneration of midbrain dopaminergic neurons (mDANs) in the substantia nigra is a characteristic feature. The PD mDANs have compromised autophagy,  $\alpha$ -synuclein aggregates, often in strongly ubiquitin-positive Lewy bodies, and mitochondrial defects with increased oxidative stress (1, 5). Mitochondrial dysfunction in PD can be linked to the role of the PD familial genes PTEN-induced putative kinase 1 (*PINK1*) and parkin (*PRKN*) in mediating autophagic degradation (mitophagy) of damaged mitochondria (6). Hence, it is important to determine how autophagy responses are regulated in mDANs, both short term and long term. Short-term responses, like induction of autophagy in response to nutrient or oxidative stress, is regulated by posttranslational modifications of proteins

and protein–protein interactions in the cytoplasm. Transcriptional regulation of autophagy genes is important for more long-term changes in autophagy activity, like prolonged starvation.

Transcription factors and transcriptional networks that regulate autophagy in mDANs and possible relevance to PD pathogenesis need to be determined. As shown in a rat model, mDANs can be rescued from  $\alpha$ -synuclein toxicity by increasing autophagy through overexpressing transcription factor TFEB, a master regulator of the autophagy–lysosome pathway (ALP; 7). Conditional inactivation of LIM homeodomain transcription factors *LMX1A* and *-B* in the postmitotic dopamine neurons of mice led to loss of mDANs. Abnormally large mDAN axon terminals with strong accumulation of autophagosomes and lysosomes concomitant with reduction of mRNA levels to around 50% for a number of autophagy- and lysosomal-associated genes were observed (8). This was mainly caused by the loss of *LMX1B*. Overexpression of *LMX1B* in cultured primary neurons from ventral midbrain increased expression of ALP genes while overexpression of *LMX1A* did not. Loss- and gain-of-function experiments strongly indicated that *LMX1B* regulates transcription of autophagy genes in mDANs and that *LMX1B* is required for maintenance of mDANs (8).

<sup>1</sup>Department of Medical Biology, Autophagy Research Group, UiT The Arctic University of Norway, Tromsø, Norway.

Correspondence to Terje Johansen: [terje.johansen@uit.no](mailto:terje.johansen@uit.no).

© 2023 Kournoutis and Johansen. This article is distributed under the terms of an Attribution–Noncommercial–Share Alike–No Mirror Sites license for the first six months after the publication date (see <http://www.rupress.org/terms/>). After six months it is available under a Creative Commons License (Attribution–Noncommercial–Share Alike 4.0 International license, as described at <https://creativecommons.org/licenses/by-nc-sa/4.0/>).



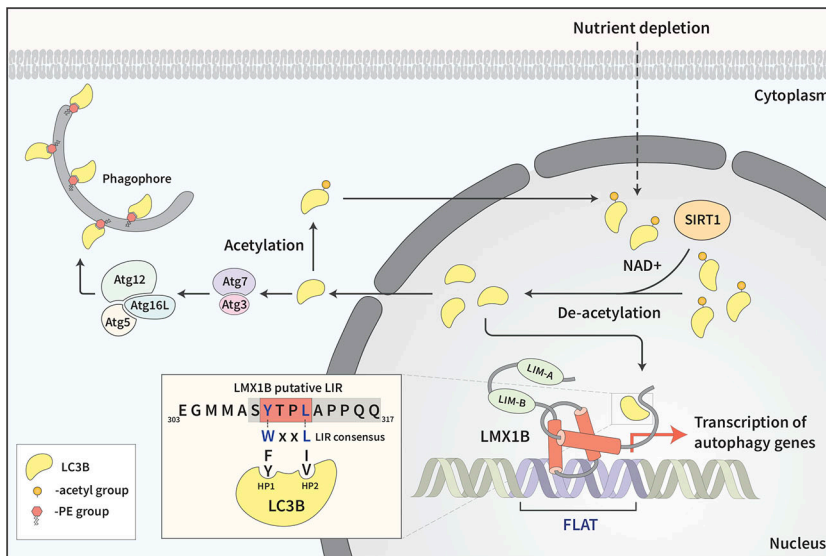


**Figure 1. LMX1B interacts with de-acetylated nuclear LC3B via a LIR-like sequence to stimulate transcription of autophagy genes in mDANs.** LMX1B binds to FLAT elements in promoters of autophagy genes. Nuclear LC3B, de-acetylated on K49 and K51, binds to the LIR-like sequence of LMX1B in a non-canonical manner to enhance transcription of autophagy genes. Nutrient depletion is known to induce SIRT1-mediated de-acetylation of LC3B (10). The de-acetylated LC3B exported out of the nucleus will be conjugated to phosphatidyl ethanolamine (PE) and incorporated in the membranes of the forming autophagosomes (phagophore).

In this issue of *JCB*, Jiménez-Moreno et al. (9) used siRNA and shRNA knock-down and CRISPR/CAS9-mediated knock-out of *LMX1B* in cells combined with rescue experiments with WT and mutants to confirm that *LMX1B* is indeed a transcriptional regulator of a number of autophagy genes. To address the knowledge gap on the role of *LMX1B* in regulating autophagy in mDANs, the authors first used bioinformatic analyses to identify *LMX1B* binding sites, called FLAT elements, in the promoters of autophagy genes. Subsequently, they verified promoter occupancy by *LMX1B* and positive regulation of mRNA levels of genes encoding proteins involved in initiation (ULK1) and expansion (ATG7, ATG3, ATG16L1) of the forming autophagosome, autophagy receptors (OPTN and NDP52, not p62/SQSTM1), *PINK1* (which is involved in mitophagy), and *TFEB* (important for ALP). Very interestingly, the authors found that *LMX1B* interacts directly with human Atg8 proteins and that LC3B acts as a nuclear cofactor to stimulate transcription of autophagy genes (Fig. 1). All this was demonstrated in HEK293T cells and in in vitro induced pluripotent stem cell-derived human mDANs. However, direct binding of *LMX1B* to LC3B was not directly demonstrated in mDANs, only in HEK293T cells.

Jiménez-Moreno et al. (9) identified a putative LIR motif in *LMX1B* located C-terminal to the homeodomain (Fig. 1). Mutation of the core amino acids binding to HPI and HP2 to alanine, in this case Y and L, usually abolish binding. This did not occur in this case. However, the deletion,  $\Delta$ 308-317, encompassing the core LIR and some flanking residues, did abolish binding. This LIR lacks the acidic residues flanking the core LIR that usually are present to ensure strong binding and contains a proline that is often inhibitory for binding by canonical LIRs (3). Hence, it will be interesting to solve the structure of the complex between LC3B and the *LMX1B* LIR to reveal how this non-canonical binding occurs. *LMX1B*  $\Delta$ 308-317 could neither effectively stimulate expression from FLAT element reporters, nor rescue the expression of autophagy genes in mDANs (or HEK293T) upon knockdown of endogenous *LMX1B*, nor protect against rotenone-induced cell death in mDANs with *LMX1B* shRNA knockdown. Another case of nuclear Atg8 acting as a cofactor to regulate autophagy genes is reported in *Drosophila* where Sequoia, a repressor of autophagy gene transcription, binds in a LIR-dependent manner to nuclear Atg8a, thereby repressing autophagy genes (11). Hence, Atg8-

transcription factor interactions can have different outcomes. The complexity involved is suggested by the observation that *Drosophila* mutants lacking Atg8a show reduced expression of autophagy genes.

Nuclear LC3B is deacetylated at K49 and K51 by SIRT1 to enable its redistribution to the cytoplasm to mediate starvation-induced autophagy (10; Fig. 1). Upon 2 h starvation, the cytoplasmic fraction of *LMX1B* decreased and the nuclear fraction increased, likely in order to meet the demand of increased autophagy gene expression upon starvation. Consistently, *LMX1B* bound to deacetylated nuclear LC3B. Sequoia also preferentially bound to deacetylated Atg8a (11). Hence, Atg8 binding in the nucleus is regulated by acetylation, and nucleo-cytoplasmic shuttling of these transcription factors and Atg8s is likely also regulated to coordinate starvation stress with transcriptional regulation of autophagy genes.

In future experiments it would be interesting to see if co-occupancy of *LMX1B* and LC3B on target gene promoters can be verified. How does LC3B act to enhance transcription? Is it an adaptor binding to established transcriptional cofactors? The authors show that siRNA knockdown of *GABARAPL1* results in reduced *LMX1B*-mediated reporter gene expression, suggesting that other Atg8 proteins may also act as nuclear cofactors.

The study by Jiménez-Moreno et al. (9) represents a very important contribution to our understanding of transcriptional regulation of autophagy genes with particular relevance to PD. Several layers of interconnectivity between *LMX1B* and LC3B in the regulation of autophagy are revealed. This study also highlights that upregulation of autophagy by modulating the activity of transcription factors like *LMX1B* and *TFEB* needs exploration for possibility of drug development to combat or slow progression of PD and other neurodegenerative diseases.

#### Acknowledgments

We thank Trond Lamark for critical reading of the manuscript.

We acknowledge the support of the Research Council of Norway (grant 249884), the Norwegian Cancer Society (grant



190214) and UiT The Arctic University of Norway (grant eph 2021/929).




## References

1. Klionsky, D.J., et al. 2021. *EMBO J.* <https://doi.org/10.15252/embj.2021108863>
2. Yamamoto, H., et al. 2023. *Nat. Rev. Genet.* <https://doi.org/10.1038/s41576-022-00562-w>
3. Johansen, T., and T. Lamark. 2020. *J. Mol. Biol.* <https://doi.org/10.1016/j.jmb.2019.07.016>
4. Dou, Z., et al. 2015. *Nature.* <https://doi.org/10.1038/nature15548>
5. Karabiyik, C., et al. 2017. *Essays Biochem.* <https://doi.org/10.1042/EBC20170023>
6. Malpartida, A.B., et al. 2021. *Trends Biochem. Sci.* <https://doi.org/10.1016/j.tibs.2020.11.007>
7. Decressac, M., et al. 2013. *Proc. Natl. Acad. Sci. USA.* <https://doi.org/10.1073/pnas.1305623110>
8. Laguna, A., et al. 2015. *Nat. Neurosci.* <https://doi.org/10.1038/nn.4004>
9. Jiménez-Moreno, N., et al. 2023. *J. Cell Biol.* <https://doi.org/10.1083/jcb.201910133>
10. Huang, R., et al. 2015. *Mol. Cell.* <https://doi.org/10.1016/j.molcel.2014.12.013>
11. Jacomin, A.C., et al. 2020. *Cell Rep.* <https://doi.org/10.1016/j.celrep.2020.107695>

# PAPER IV

REVIEW

# NBR1: The archetypal selective autophagy receptor

Nikoline Lander Rasmussen<sup>1</sup> , Athanasios Kournoutis<sup>1</sup>, Trond Lamark<sup>1</sup> , and Terje Johansen<sup>1</sup> 

**NBR1 was discovered as an autophagy receptor not long after the first described vertebrate autophagy receptor p62/SQSTM1. Since then, p62 has currently been mentioned in >10,000 papers on PubMed, while NBR1 is mentioned in <350 papers. Nonetheless, evolutionary analysis reveals that NBR1, and likely also selective autophagy, was present already in the last eukaryotic common ancestor (LECA), while p62 appears first in the early Metazoan lineage. Furthermore, yeast-selective autophagy receptors Atg19 and Atg34 represent NBR1 homologs. NBR1 is the main autophagy receptor in plants that do not contain p62, while most animal taxa contain both NBR1 and p62. Mechanistic studies are starting to shed light on the collaboration between mammalian NBR1 and p62 in the autophagic degradation of protein aggregates (aggrephagy). Several domains of NBR1 are involved in cargo recognition, and the list of known substrates for NBR1-mediated selective autophagy is increasing. Lastly, roles of NBR1 in human diseases such as proteinopathies and cancer are emerging.**

## The selective autophagy receptor NBR1

Selective autophagy consists of a set of evolutionarily conserved pathways for targeted lysosomal degradation of macromolecules, protein aggregates, lipid droplets, viral capsids, intracellular pathogens, and organelles. The different pathways of selective autophagy depend on either soluble or membrane-bound selective autophagy receptors (SARs; Lamark and Johansen, 2021). The first SAR discovered, p62/SQSTM1 (sequestosome-1), belongs to a family of soluble SARs including NBR1, CALCOCO1, CALCOCO2 (aka NDP52), TAX1BP1 (aka CALCOCO3), and OPTN (optineurin). This group of SARs, commonly referred to as sequestosome-1 like receptors (SLRs; Deretic, 2012), are typically characterized by the presence of (1) an LC3 interacting region (LIR) motif, (2) homo- or heterooligomerization domains, and (3) a C-terminal ubiquitin-binding domain for engaging ubiquitinated substrates (Johansen and Lamark, 2020; Nthiga et al., 2020). The SLR-LIR motifs bind to ATG8 family proteins anchored in the autophagosomal double membrane through a covalent conjugation to phosphatidylethanolamine (Lystad and Simonsen, 2019; Mizushima et al., 2011). Substrates and cargos for selective autophagy are usually labeled with ubiquitin or other “eat me” signals recognized by the ubiquitin-binding domain or other domains found in SLRs. When bound to cargo, some SLRs can themselves initiate autophagosome formation in situ by interacting with components of the core autophagy machinery (Chang et al., 2021; Goodall et al., 2022). Further, SLRs can facilitate the expansion of the autophagosome membrane (phagophore) by multivalent interactions with ATG8 proteins (Johansen and Lamark, 2020). The most studied SLR p62 forms

phase-separated bodies in cells that are called p62 bodies (Lamark and Johansen, 2021). The formation of p62 bodies depends on polymerization mediated by the N-terminal Phox/Bem1p (PB1) domain (Lamark et al., 2003; Wilson et al., 2003), with p62 forming helical filaments (Ciuffa et al., 2015; Jakobi et al., 2020), and is induced by binding of p62 to polyubiquitin, causing a phase separation (Sun et al., 2018; Zaffagnini et al., 2018). Phase separation of p62 filaments is also induced by increased p62 expression or by posttranslational modifications increasing the binding of p62 to ubiquitin (Lamark and Johansen, 2021).

NBR1 (neighbor of BRCA1 gene 1) was discovered as a selective autophagy receptor due to its interaction with and similarity in domain organization to p62 and direct binding to ATG8 proteins and ubiquitin (Kirkin et al., 2009; Waters et al., 2009). Mammalian NBR1 acts as a SAR involved in degrading protein aggregates (aggrephagy; Kirkin et al., 2009), peroxisomes (pexophagy; Deosaran et al., 2013), midbody remnants (Isakson et al., 2013; Kuo et al., 2011), focal adhesions (Kenific et al., 2016), and major histocompatibility complex (MHC) class I receptor (Yamamoto et al., 2020). In plants, NBR1 degrades protein aggregates upon heat-, oxidative-, salt-, and drought stress (Zhou et al., 2013; Zhou et al., 2014), viral capsids (Hafren et al., 2017), a viral RNA silencing suppressor (Hafren et al., 2018), and acts in defense against bacterial infections (Leong et al., 2022; Ustun and Hofius, 2018). In fungi, NBR1 homologs transport lysosomal enzymes from the cytoplasm into the vacuole as shown in the fission yeast *Schizosaccharomyces pombe* (Liu et al., 2015; Wang et al., 2021), and they act as a pexophagy receptor in the filamentous fungus *Sordaria macrospora* (Werner et al., 2019).

<sup>1</sup>Autophagy Research Group, Department of Medical Biology, University of Tromsø-The Arctic University of Norway, Tromsø, Norway.

Correspondence to Terje Johansen: [terje.johansen@uit.no](mailto:terje.johansen@uit.no).

© 2022 Rasmussen et al. This article is available under a Creative Commons License (Attribution 4.0 International, as described at <https://creativecommons.org/licenses/by/4.0/>).

Substrates of NBR1 in mammals, plants, and yeast are summarized in Fig. 1. In this review, we will elaborate on the roles of NBR1 in selective autophagy processes in plants, fungi, and mammals, and its roles in human disease. But first, we will focus on the domain structure and evolution of NBR1.

### Domain structure of NBR1

Vertebrate NBR1 and p62 share an N-terminal PBI domain, the ZZ zinc finger domain, LIR motif, and C-terminal UBA domains. In addition, NBR1 contains the four tryptophan (FW) domains involved in protein-protein interactions, two coiled-coil (CC) domains, and an amphipathic helix (AH) domain not found in p62 (Deosaran et al., 2013; Mardakheh et al., 2010; Svenning et al., 2011; Fig. 2 A). The PBI domain is involved in interactions with other PBI domain-containing proteins (notably p62, see below), while the CC1 domain mediates self-interaction. The UBA domain binds to ubiquitin and ubiquitinated cargo, while the LIR binds to ATG8 family proteins (Johansen and Lamark, 2020). Human NBR1 has two LIR motifs. Both bind ATG8 proteins in vitro, but only LIR1 binds strongly in cell extracts and is required for efficient autophagic degradation of NBR1 (Kirkin et al., 2009).

The FW domain was so named because it contains four highly conserved tryptophan (W) residues (Svenning et al., 2011). It is also referred to as NBR1-like or NBR1 domain (Kraft et al., 2010). Some bacterial proteins also contain FW domains, which precede the eukaryotic NBR1 that first appeared in protists (Marchbank et al., 2012; Svenning et al., 2011; Fig. 2 A). The FW domain is present in only one other eukaryotic protein called ILRUN (inflammation and lipid regulator with UBA-like and NBR1-like domains; Fig. 2 A). The FW domain of human NBR1 binds to microtubule-associated protein MAPIB and TAX1BP1 (Marchbank et al., 2012; Turco et al., 2021). The recent finding that the FW domain of the filamentous fungus *Chaetomium thermophilum* binds specifically to vacuolar  $\alpha$ -mannosidase (Ams1) and delivers Ams1 to the vacuole by autophagy in the fission yeast *S. pombe* shows that this domain can be involved in cargo recognition (Zhang et al., 2022a).

The same group previously showed that the *S. pombe* NBR1 homolog uses its ZZ domains to transport aminopeptidases Ape4, Ape2, and Lap2, and Ams1 from the cytosol into the vacuole, analogous to Atg19 acting as a receptor in the biosynthetic cytoplasm to vacuole transfer (Cvt) pathway in *S. cerevisiae* (Liu et al., 2015; Wang et al., 2021; Fig. 1 B). Ams1 and Ape4 bind competitively to ZZ1. Lap2 and Ape2 bind to ZZ2 and ZZ3. Surprisingly, this Nbr1-mediated vacuolar targeting (NVT) pathway in *S. pombe* is not mediated by autophagy components but by endosomal-sorting complexes required for transport (ESCRTs) in a process similar to microautophagy (Hama et al., 2021; Wang et al., 2021). Interestingly, the ZZ domain of mammalian p62, but not that of mammalian NBR1, is also used for cargo recognition by binding to N-arginylated proteins (Cham-Molstad et al., 2017).

The AH domain of mammalian NBR1 was identified as a 22 amino-acid amphipathic  $\alpha$ -helical structure based on secondary structure predictions (Mardakheh et al., 2010). It is located adjacent to the UBA domain and was initially called the

JUBA domain for juxta-UBA. Since JUBA and UBA are confusingly similar names both verbally and written, we propose to call this domain simply AH for amphipathic  $\alpha$ -helix. Circular dichroism spectroscopy showed the AH domain to be an unfolded structure that folds into an  $\alpha$ -helix in the presence of membranes containing phosphatidylinositol-phosphates (PIPs; Mardakheh et al., 2010). AH displayed no specificity toward a specific PIP. Both the AH and UBA domains are needed for the co-localization of NBR1 with LAMP2 (late endosomes; Mardakheh et al., 2010) and peroxisomes (Deosaran et al., 2013), suggesting AH is required for membrane localization of NBR1.

### Evolution of NBR1: The archetypal soluble autophagy receptor

Autophagy-related (ATG) genes have experienced expansions and losses during the evolution of different eukaryotic lineages, enabling functional diversification and specialization. Remote homologs of ATG proteins and the evolutionarily conserved protein domains are found in bacteria and archaea. These were likely recruited into the developing autophagy pathway during eukaryogenesis (Zhang et al., 2021). Phylogenetic and biochemical analyses reveal the evolutionary relationship between NBR1 and p62. Using the presence of the FW domain to distinguish between p62 and NBR1 homologs, we found NBR1 orthologs to be distributed throughout the eukaryotic kingdom, while p62 is confined to the metazoans (Svenning et al., 2011; Fig. 2, B and C). Most non-metazoan organisms have only a single NBR1 homolog and no p62 homolog. Metazoans generally contain both NBR1 and p62, but NBR1 has been secondarily lost in some animal lineages including nematodes, insects, and crustaceans. Clearly, NBR1 preceded p62 in evolution, and p62 likely arose through gene duplication of the ancestral NBR1 gene, which happened early in the metazoan lineage (Fig. 2 C). This is illustrated by the fact that the choanoflagellate *Monosiga brevicollis* and the amoeban protist *Capsaspora owczarzaki*, representing the closest living unicellular relatives of metazoans (King et al., 2008; Ruiz-Trillo et al., 2004), have only a single NBR1 homolog and no p62 homolog (Svenning et al., 2011).

Autophagy is a very fundamental pathway appearing at the root of eukaryote evolution and is likely present in the last eukaryotic common ancestor (LECA; Zhang et al., 2021). LECA is defined as the ancestor of all existing eukaryotes, plus extinct post-LECA lineages. LECA likely arose 1.9–1.6 billion years ago, with all the main features of a eukaryotic cell (Spang et al., 2022). With a few exceptions like red algae, microsporidia, and the flagellate intestinal parasite *Giardia lamblia*, ATG genes and autophagy are found throughout eukaryotes (Zhang et al., 2021; Zhang et al., 2022b). Although gene loss and expansions occur in many lineages, the two conjugation systems with ATG8 and ATG12 are conserved in most eukaryotic clades (Zhang et al., 2022b). The origin of selective autophagy likely occurred with the first SAR, and NBR1 is the pioneer soluble SAR. None of the other vertebrate SARs have been found in protists or plants. Defining NBR1 homologs as proteins that as a minimum contain an FW domain and a PBI or ZZ-type zinc finger domain, we find NBR1 homologs in five of the supergroups of the newly proposed tree of eukaryotes (Burki et al., 2020). Specifically, representatives of the TSAR supergroup (including Stramenopila,

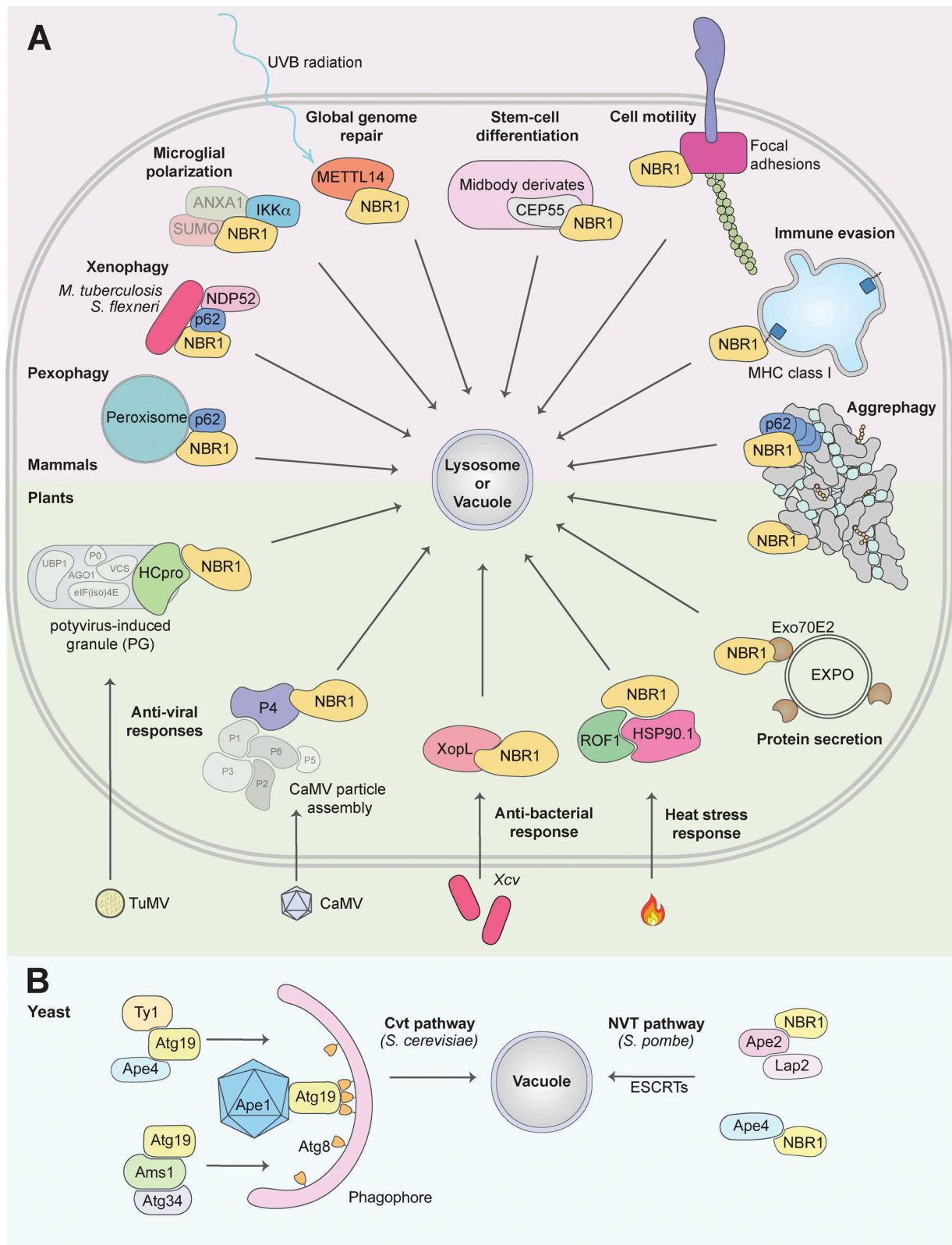


Figure 1. **NBR1 as a selective autophagy receptor in mammals, plants, and yeast.** Summary of identified substrates of NBR1-mediated selective autophagy, indicated by immediate vicinity to NBR1. This does not distinguish direct or indirect interaction. Transparent proteins are part of a complex. **(A)** In mammals, NBR1 has been shown to mediate the degradation of peroxisomes (pexophagy), bacteria (xenophagy), and protein aggregates (aggrephagy) in



conjunction with p62 (and NDP52 for xenophagy). Furthermore, NBR1 has been shown to affect several processes through selective autophagic degradation of the following substrates: the proinflammatory kinase IKK $\alpha$ , affects microglial polarization following ischemia (Li et al., 2021); METTL14 (methyltransferase-like 14) upon ultraviolet B radiation, consequently affecting global genome repair (Yang et al., 2021); the midbody protein CEP55 upon stem-cell differentiation (Kuo et al., 2011); turnover of focal adhesions, promoting cell motility; and MHC class I proteins in PDAC cells, promoting immune evasion. In plants, NBR1 regulates several plant stress responses: clearance of aggregates (aggrephagy), restricting TuMV infection by targeting the viral RNA silencing suppressor component HCpro; restricting CaMV infection by targeting the viral particle protein P4; targeting the bacteria effector protein XopL for degradation, restricting Xcv infection; promoting heat stress recovery by targeting ROF1 and HSP90.1; targeting Exo70E2, a marker for the exocyst-positive organelle (EXPO; Ji et al., 2020). **(B)** In *S. cerevisiae*, the NBR1 homolog Atg19 mediates the degradation of Ty1, Ape4, Ape1, and Ams1 through the Cvt pathway. The second NBR1 homolog Atg34, only targets Ams1. In *S. pombe*, the NBR1 homolog targets Ape2, Lap2, and Ape4 to the vacuole. This Nbr1-mediated vacuolar targeting (NVT) pathway is mediated by ESCRTs, not macroautophagy. Only references not cited in the main text are cited here.

Alveolata, and Rhizaria), Haptista (Haptophyta), Archaeplastida (Chloroplastida), Amorphea (including Apusomonada, Amoebozoa, and Ophisthokonta), and Discoba all have NBR1 homologs (Fig. 2 B). Opisthokonta includes animals, fungi, and some protist lineages that are most closely related to either animals or fungi. Chloroplastida includes green algae and land plants. All the remaining supergroup taxa mentioned represent protists (Burki et al., 2020). The lack of sequence data for some important species defining a few of the taxa presently precludes an exhaustive analysis. However, the coincident presence of important core ATG proteins makes it tempting to suggest that the ancestor NBR1 may have been present in LECA, representing the first SAR that evolved. Hence, selective autophagy may have originated in the LECA and co-evolved with unselective autophagy.

Apart from NBR1, ILRUN is the only other eukaryotic protein containing an FW domain (Fig. 2 A). It is not clear if there is a functional relationship between NBR1 and ILRUN. Human ILRUN is a 298 amino acid protein (formerly known as C6orf106) containing an N-terminal UBA-like domain (residues 23–64) and a central FW domain (residues 71–180). We traced the homologs of ILRUN protein in the evolution, guided by the eukaryotic tree of life, and found that ILRUN is present in all metazoans including the simplest metazoan *Trichoplax adhaerens* and the closest unicellular relatives to metazoans *Monosiga brevicollis* and *Capsaspora owczarzaki*. ILRUN homologs are also found in the Stramenopila of the TSAR supergroup, Haptophyta of the Haptista supergroup, and Apusomonada, but not the sister group Amoebozoa of the Amorphea supergroup (Fig. 2 B). Intriguingly, distinct from NBR1, ILRUN is not found in plants and fungi. This suggests a secondary loss of ILRUN in these taxa.

### Atg19 and Atg34 are yeast NBR1 homologs

*S. cerevisiae*, *D. melanogaster*, and *C. elegans* are extremely valuable model organisms. However, due to long divergent evolution with gene duplications and loss they are often the “odd ones out” when it comes to sequence-based evolutionary studies of proteins. A seminal perspective article suggested that Atg19 is the NBR1 homolog in *S. cerevisiae* (Kraft et al., 2010). Acting as a receptor in the Cvt pathway, yeast Atg19 was the first selective autophagy receptor discovered (Leber et al., 2001; Scott et al., 2001). The primary cargo in the Cvt pathway is the precursor form of the vacuolar aminopeptidase 1 (preApe1), which forms a tetrahedral dodecameric structure that is recognized by the CC domain of Atg19. Atg19 recruits Atg8 via its C-terminal LIR (often called Atg8-family interaction motif [AIM] in yeast) and

the selective autophagy adapter Atg11. This Cvt complex recruits the core autophagy machinery to initiate membrane formation and expansion to form the Cvt vesicle, a special type of autophagosome only 150 nm in diameter (reviewed in Yamasaki and Noda, 2017). In addition to Ape1, Atg19 also transports the vacuolar aspartyl aminopeptidase Ape4, the vacuolar  $\alpha$ -mannosidase Ams1, and even the Ty1 retrotransposon particle to the vacuole. Almost 10 yr after the discovery of Atg19, its paralog Atg34 was discovered (Suzuki et al., 2010). Atg19 and Atg34 have the same domain organization (Fig. 3 A) and show 31% overall sequence identity (49% similarity), but Atg34 can only target Ams1. Hence, Atg34 cannot compensate for Atg19 in the Cvt pathway (Yamasaki and Noda, 2017).

Atg19 has lost the ZZ zinc-finger domain and has no sequence similarity to NBR1 homologs in other phyla. However, Kraft, Peter, and Hofmann noted that Atg19 has the LIR domain and predicted that highly divergent PB1 and NBR1 folds were present in *S. cerevisiae* Atg19, as well as a CC domain (Kraft et al., 2010). Their argument also rested on the evolutionary analysis of NBR1 with emphasis on fungal homologs, where some fungal lineages had retained NBR1 with PB1, ZZ, FW, LIR, and UBA domains although having two or three copies of the ZZ domain. Most fungi lost the UBA domain, and PB1 and FW domains could not be identified by sequence conservation in evolved lineages such as *Saccharomyces*, but a similar fold was predicted, suggesting the presence of PB1-like and FW-like domains in *S. cerevisiae* Atg19 (Kraft et al., 2010; Fig. 3 A). The solution structures of the  $\alpha$ -mannosidase binding domains (ABD) of Atg19 and Atg34 are solved (Watanabe et al., 2010). The Atg19 and Atg34 ABD structures are very similar, with a root mean square difference (RMSD) of 2.1 Å for 102 residues, forming an immunoglobulin-like  $\beta$ -sandwich fold with two  $\beta$ -sheets, each with four anti-parallel  $\beta$ -strands. The ABD of the NBR1 homolog of the filamentous fungus *C. thermophilum* has an FW domain very similar in structure to those found in human NBR1 and ILRUN (Zhang et al., 2022a). Structural comparison of FW domain structures of NBR1 and ILRUN with the ABD of Atg19 and Atg34 revealed the latter to be FW-like domains (Fig. 3 B). A VAST structural alignment search of the Protein Database with the Atg34 ABD revealed the human ILRUN FW domain as a structural homolog of the ABD. With the ABD of Atg19 and -34 being structurally homologous to FW domains, we asked if the N-terminal regions of these two yeast proteins may be PB1-like domains. Comparing the PB1 domain structure of *Arabidopsis* NBR1 (Jakobi et al., 2020) to AlphaFold structure prediction with 90% confidence of the *S. cerevisiae* Atg34 N-terminal region

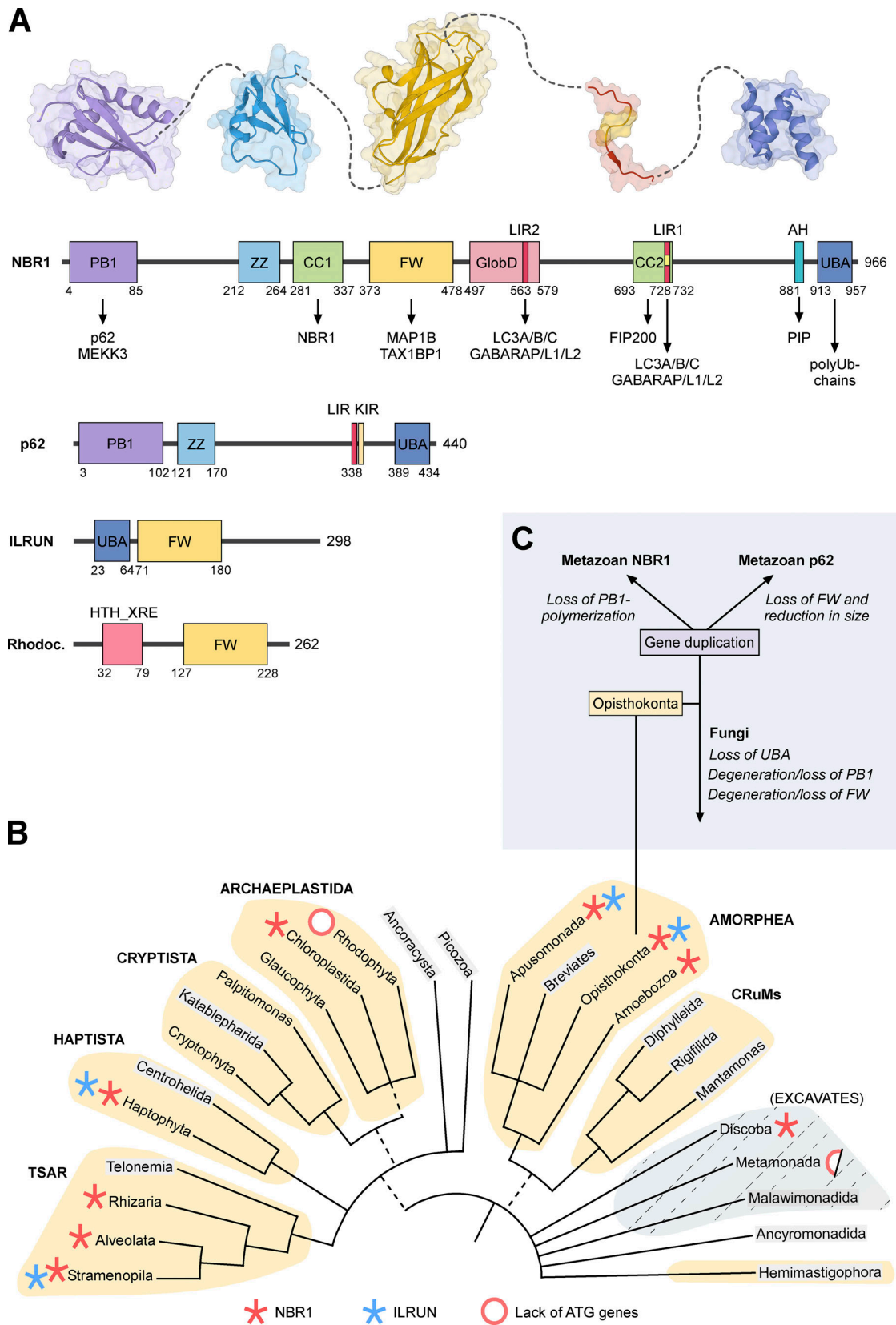


Figure 2. **Domain structure and evolution of NBR1.** (A) Domain architectures of human NBR1, p62, and ILRUN, and HTH-XRE (Helix-turn-helix XRE-family like protein) from *Rhodococcus fascians*. The amino acid positions of the domain borders and the length of the proteins are indicated by numbers below and to

the right of the cartoons, respectively. Structures of PB1, ZZ, FW, LIR, and UBA domains are shown above the NBR1 domain architecture. **(B)** Distribution of NBR1 (red asterisk) and ILRUN (blue asterisk) on The New Tree of Eukaryotes. Red ring, or half-red ring, indicates the lack of ATG genes in some clades. The colored groupings are the current “supergroups.” Multifurcations indicate unresolved branching orders among lineages while broken lines represent minor uncertainties about the monophyly of certain groups (Burki et al., 2020). We searched the NCBI Protein Database and the Conserved Domains Database to identify NBR1 and ILRUN homologs (Lu et al., 2020). The phylogenomic distribution was also determined using the SMART database (Letunic et al., 2006). The names of the groupings where sequence data were not available are indicated in gray. **(C)** The Ophisthokonta contains both the metazoans and fungi. The gene duplication and divergence of the ancestor NBR1 gene in the early metazoan lineage, and loss of UBA and loss or degeneration of PB1 domains in fungi are indicated.

(Jumper et al., 2021; Varadi et al., 2022) clearly suggest the presence of a PB1 domain in Atg34 (Fig. 3 C). In Atg19 the prediction is very uncertain, but the presence of a PB1-like domain is likely. Structure determinations of the N-terminal regions of Atg19 and Atg34 will give us clear answers. However, taken together, we suggest that Atg19 and Atg34 are clearly NBR1 homologs with PB1/PB1-like, CC, FW, and LIR domains (Fig. 3 A).

#### An early metazoan gene duplication created the paralogs p62/SQSTM1 and metazoan NBR1

The split of ancestor NBR1 into the current paralogs p62/SQSTM1 and NBR1 in vertebrates was likely initiated by a gene duplication very early in metazoan evolution (Svenning et al., 2011; Fig. 2 C). Further evolution led to one shortened paralog lacking the CC and FW domains (p62) and one full-length with a modified and monomeric PB1 domain (metazoan NBR1). The gain of an AH domain may have occurred before vertebrates evolved. To understand the functional consequence of the duplication event, it is important to relate it to the role of the PB1 domain in selective autophagy. PB1 is a ubiquitin-like domain that engages in homomeric or heteromeric PB1–PB1 interactions. The interaction involves two individual and oppositely charged binding surfaces. A negatively charged binding surface in one PB1 domain binds to a positively charged binding surface in the other (Jakobi et al., 2020; Lamark et al., 2003; Wilson et al., 2003). Individual PB1 domains may contain one or both binding surfaces. PB1 domains with both binding surfaces can result in homomeric polymerization of the PB1-containing protein, as seen for mammalian p62. Cryo-EM analyses demonstrated that the PB1 domain of p62 forms flexible helical polymers in vitro (Ciuffa et al., 2015). The PB1 domain constitutes the scaffold in p62 filaments, while the LIR and UBA domains are exposed (Ciuffa et al., 2015). We found that the plant ortholog from *Arabidopsis* (AtNBR1) has a PB1 domain that can homopolymerize (Svenning et al., 2011). The presence of a PB1 domain alone is not enough to predict self-interaction. Studies are therefore needed to determine how widespread polymerization is among non-metazoan NBR1 orthologs. Metazoan NBR1 orthologs have lost the basic binding surface resulting in a monomeric PB1 domain. To compensate, metazoan NBR1 and some fungal orthologs harbor a self-interacting CC domain, a domain absent in plant orthologs or p62. Despite the split of the ancestor NBR1 into p62 and NBR1 in metazoans, mammalian NBR1 remains attached to p62 via the acidic PB1 surface that is not mutated (Lamark et al., 2003). The only known interaction partners of mammalian NBR1 that bind via PB1–PB1 interactions are p62 (Lamark et al., 2003) and the kinase MEKK3 (Hernandez et al., 2014), and NBR1 is always recruited to p62 bodies.

We propose that the early metazoan gene duplication facilitated the evolution and divergence in domain structures, which allowed p62 and NBR1 to both tackle separate functions and collaborate on certain functions. The split into two proteins enabled different expression levels in cells and various tissues and different regulations by posttranslational modifications. The gene duplication enabled a deletion of domains from p62 streamlining it as an effective SAR facilitating p62 body formation, which requires high quantities of p62. NBR1 is less central in forming the scaffold of the p62 body, allowing the development of other functions such as gain of the AH domain enabling membrane binding. In humans, NBR1 is much less abundant in most cell types than p62, varying from 10 to almost 100-fold difference in protein levels (Cho et al., 2022; Wang et al., 2015). According to The Human Protein Atlas, both proteins are expressed in most tissues with little tissue specificity, but with particularly high levels of p62 in skeletal muscle and of NBR1 in late spermatids of the testis (Uhlen et al., 2015).

#### Plant NBR1 is polymeric, forms filaments similar to p62, and acts in stress responses

*Arabidopsis* NBR1 (AtNBR1) and mammalian p62 share the abilities of PB1 self-polymerization and helical filament formation, as well as LIR-ATG8 binding and UBA-ubiquitin interactions (Jakobi et al., 2020; Svenning et al., 2011). AtNBR1 forms cellular bodies with a striking similarity to those formed by mammalian p62, and the formation of AtNBR1 bodies depends on PB1-mediated polymerization and UBA-mediated ubiquitin binding (Svenning et al., 2011). High-resolution cryo-EM studies of the purified PB1 domain of AtNBR1 revealed similar types of filamentous structures as seen for the human p62 PB1 domain (Jakobi et al., 2020). A tandem arginine motif that is absent in human NBR1, but present in p62 (R21/22) and AtNBR1 (R19/20), is important for stabilizing a filamentous structure and for the formation of p62/AtNBR1 bodies with ubiquitin (Jakobi et al., 2020; Lin et al., 2017). This strongly supports the conclusion that p62 bodies and AtNBR1 bodies are structurally very similar. Another common feature of p62 and AtNbr1 is that their degradation by autophagy depends on a polymeric PB1 domain (Svenning et al., 2011). In comparison, mammalian NBR1 has a monomeric PB1 domain, and its degradation by autophagy does not depend on its PB1 domain (Kirkin et al., 2009).

The roles of NBR1-mediated selective autophagy in plant stress responses have recently been excellently reviewed (Zhang and Chen, 2020; Fig. 1 A). AtNBR1 is involved in heat tolerance, modulation of plant heat memory, plant–pathogen interactions, and aggregophagy (autophagic degradation of protein aggregates) during abiotic stress tolerance (Young et al., 2019; Zhou et al.,



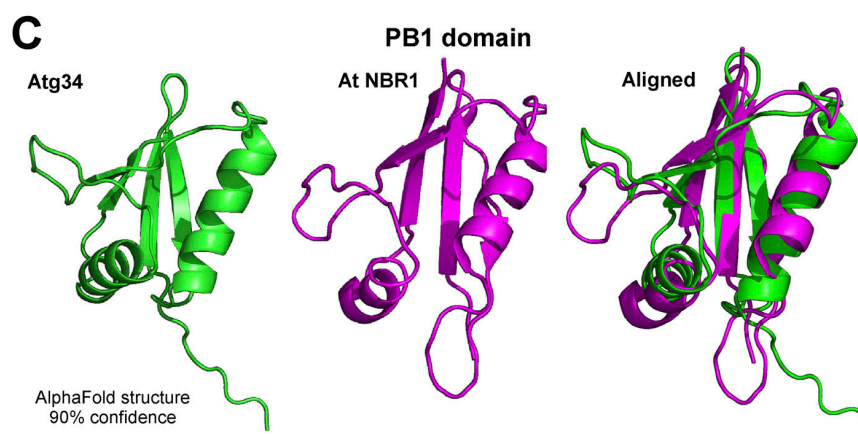
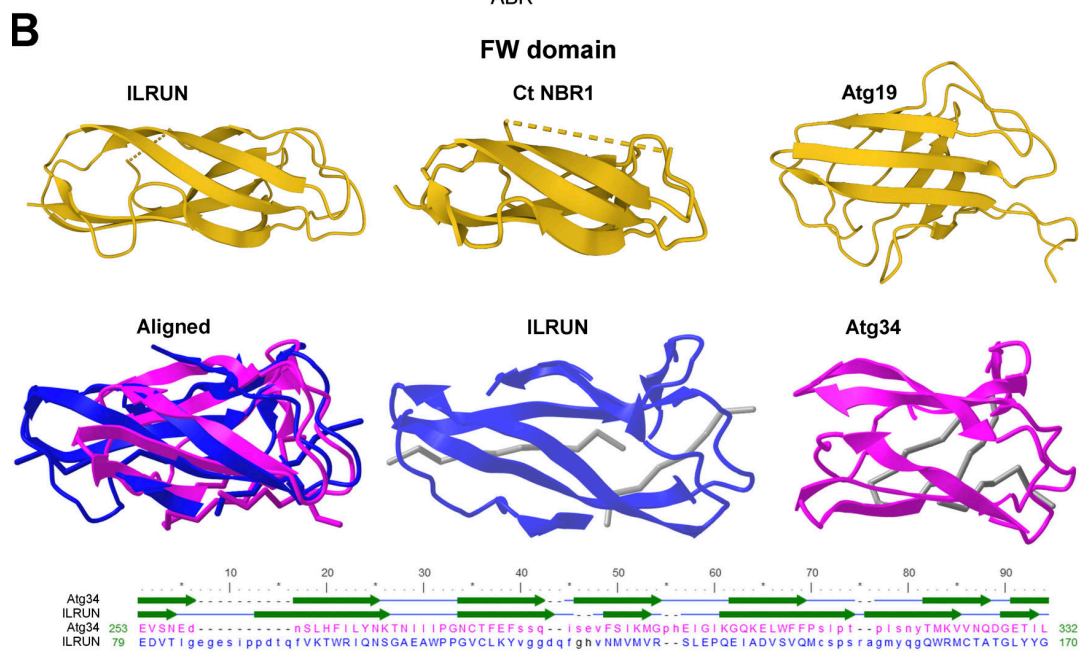
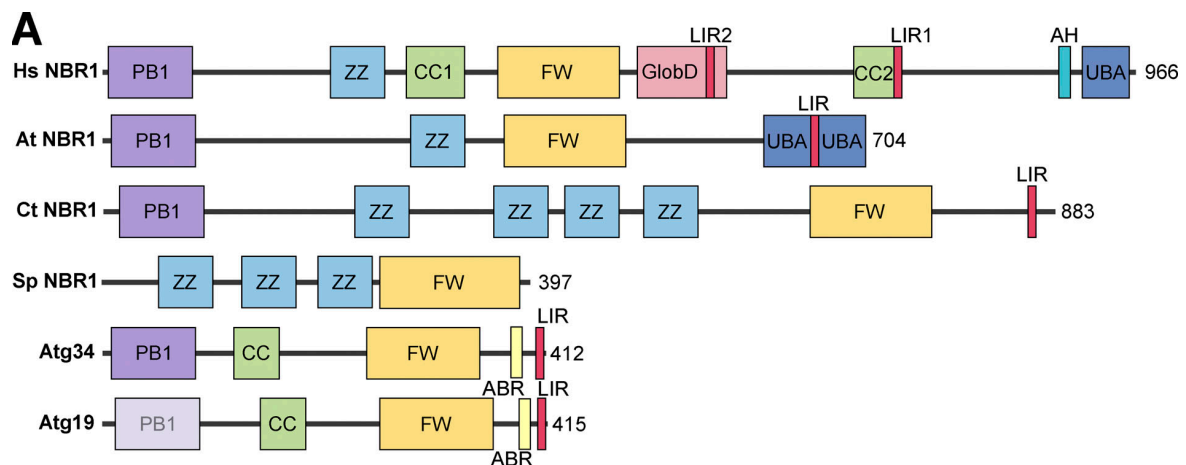


Figure 3. **The yeast Cvt receptor Atg19 and the paralog Atg34 are NBR1 homologs.** (A) Domain architecture of NBR1 homologs from humans, the plant *Arabidopsis thaliana*, the filamentous fungus *C. thermophilum*, fission yeast *S. pombe*, *S. cerevisiae* Atg19 and Atg34. (B) Comparison of FW domain structures between human ILRUN (PDB accession no. 6VHI), *C. thermophilum* (Ct NBR1; PDB accession no. 7VQO), and the ABD structures from yeast Atg19 (PDB accession no. 2KZB) and Atg34 (PDB accession no. 2KZK). Structural alignment of the ILRUN FW domain (blue) to the Atg34 ABD/FW domain (magenta) obtained

by a VAST search of the PDB database. A sequence alignment with positions of the structural elements ( $\beta$  strands) is shown below the structures. Despite only 7% sequence identity the alignment gives a root-mean-square deviation of 1.90 Å over a 60 amino acid sequence. **(C)** Atg34 contains a PB1 domain fold. The AlphaFold structure predicted with 90% confidence for the N-terminal domain of Atg34 (green) is a PB1 domain that can be structurally aligned to the solved structure (PDB accession no. 6TGN) of the PB1 domain of *Arabidopsis thaliana* (magenta). The structures were aligned using PyMol.

2013; Zhou et al., 2014). Upon high-temperature stress, plants require an equilibrium between poststress growth recovery and the establishment of heat stress memory (which relates to heat tolerance complexes being available during the early stages of a high-temperature event; Sedaghatmehr et al., 2019). The HSP90.1-ROF1 complex mediates the heat stress response through interaction with transcription factor HSFA2. A heat-responsive interaction between HSP90.1-ROF1 and HSFA2 in the cytoplasm leads to nuclear translocation and activation of heat-responsive genes. AtNBR1-mediated selective autophagy of HSP90.1 and ROF1 mitigates the HSFA2-dependent response to high temperature (Thirumalaikumar et al., 2021). Consequently, the heat stress response is attenuated. The degradation of heat-responsive elements like HSP90.1 and ROF1 promotes recovery after heat stress but weakens heat stress memory.

Following viral infection, autophagy is often initiated to curtail a viral particle increase by delivering viruses or their components to the lysosomes for degradation, a process known as xenophagy. AtNBR1-dependent selective autophagic degradation of both non-assembled and particle-associated P4 (one of the six cauliflower mosaic virus [CaMV] viral proteins important for viral particle assembly) is ubiquitin-independent and restricts CaMV infection in a process resembling mammalian xenophagy (Hafren et al., 2017). Since particle functions are imperative for successful CaMV infection in plants, AtNBR1-mediated xenophagy counteracts infection establishment. Beyond targeting of non-assembled and particle-associated proteins, RNA silencing is regarded as the main antiviral defense mechanism in plants, and viral suppressors of RNA silencing (VSRs) have co-evolved to escape this mechanism (Boualem et al., 2016). AtNBR1 has been shown to degrade the viral RNA silencing suppressor helper component proteinase (HCpro) of the Turnip mosaic virus (TuMV) by targeting ubiquitinated potyvirus-induced RNA granules (PGs) for autophagic destruction (Hafren et al., 2018; Fig. 1 A).

Unlike viruses, bacteria generally do not enter plant cells due to the plant cell wall and turgor pressure. Instead, bacteria express effector proteins that can be translocated into the plant cells and they manipulate the host cell to promote infection (Khan et al., 2018). NBR1-mediated autophagy has been shown to counteract the pathogenic effect of the bacterial effector protein HopM1, thereby suppressing bacterial proliferation (Ustun et al., 2018). Recently, it was demonstrated that NBR1 directly targets and promotes the selective degradation of the effector protein XopL of the plant bacterium *Xanthomonas campestris* pv. *Vesicatoria* (Leong et al., 2022). XopL suppresses autophagy through its E3 ligase activity, while also being targeted by NBR1-mediated selective autophagy. Furthermore, NBR1 restricts oomycete *Phytophthora infestans* infection (Dagdas et al., 2018). These studies demonstrate the complexity of host-pathogen

interactions and an important role of NBR1 in counteracting infection in plants.

### Aggrephagy—Roles of NBR1 in p62 bodies

Depletion of NBR1 inhibits the formation of p62 bodies (Kirkin et al., 2009). Human NBR1 binds to p62 by strong PB1–PB1 electrostatic interactions and competes with p62 polymerization, acting as a chain terminator. Hence, in vitro, the addition of NBR1 reduces filament length (Jakobi et al., 2020). The role of NBR1 may therefore be to regulate the length of p62 filaments in p62 bodies. By reducing filament length, NBR1 may promote the formation of p62 bodies since very long filaments are not easily packed into dynamic, phase-separated structures (Fig. 4 A). The addition of purified NBR1 increases in vitro phase separation of p62 upon mixing with ubiquitin (Zaffagnini et al., 2018). In mouse hepatocytes, the formation of p62 bodies is compromised by the loss of NBR1 and promoted by overexpression of NBR1 (Sanchez-Martin et al., 2020).

Using a combination of in vitro reconstitution assays and cell biological studies, NBR1 contributes to efficient cargo clustering in p62 bodies by bringing its high-affinity ubiquitin-binding UBA domain to the p62 filaments via PB1–PB1 interactions between NBR1 and p62 (Turco et al., 2021). NBR1 uses its FW domain to recruit TAX1BP1 to p62 filaments, and the core autophagy machinery component FIP200 of the ULK complex is recruited by both TAX1BP1 and by NBR1. The SKICH domain of TAX1BP1 (and NDP52) is known to bind to FIP200 (Ravenhill et al., 2019), while NBR1 binds to FIP200 via its CC2 domain (Turco et al., 2021; Fig. 4 B). Previously, it was shown that p62 bound to the C-terminal Claw domain of FIP200 (Turco et al., 2019). NBR1 also binds to the Claw domain, but much more strongly than p62, even somewhat stronger than TAX1BP1. However, TAX1BP1 is suggested to be the main recruiter of FIP200 to p62 bodies. The Claw domain in FIP200 is homologous to the C-terminal region of the yeast selective autophagy adaptor and Atg1 activator, Atg11 (Turco et al., 2019). The yeast NBR1 homolog, Atg19, recruits Atg11 by binding to this C-terminal region in Atg11 (Yorimitsu and Klionsky, 2005). Hence, the parallel here is clear between mammalian NBR1 and FIP200 and yeast Atg19 and Atg11. In contrast to p62 and NBR1, TAX1BP1 does not contribute directly to the formation of ubiquitin condensates in vitro (Turco et al., 2021) or in cells treated with puromycin that causes ubiquitinated protein aggregates to form in cells (Sarraf et al., 2020). However, TAX1BP1 is needed for the efficient autophagic degradation of these aggregates, and mice expressing a deletion mutant of TAX1BP1 that cannot bind ubiquitin show the accumulation of ubiquitin-conjugated proteins and Lipofuscin pathology (Sarraf et al., 2020). Upon ATG7-independent autophagy in K562 cells, NBR1 forms a heterotypic autophagy receptor complex with p62 and TAX1BP1 that requires TAX1BP1 to induce local autophagosome formation

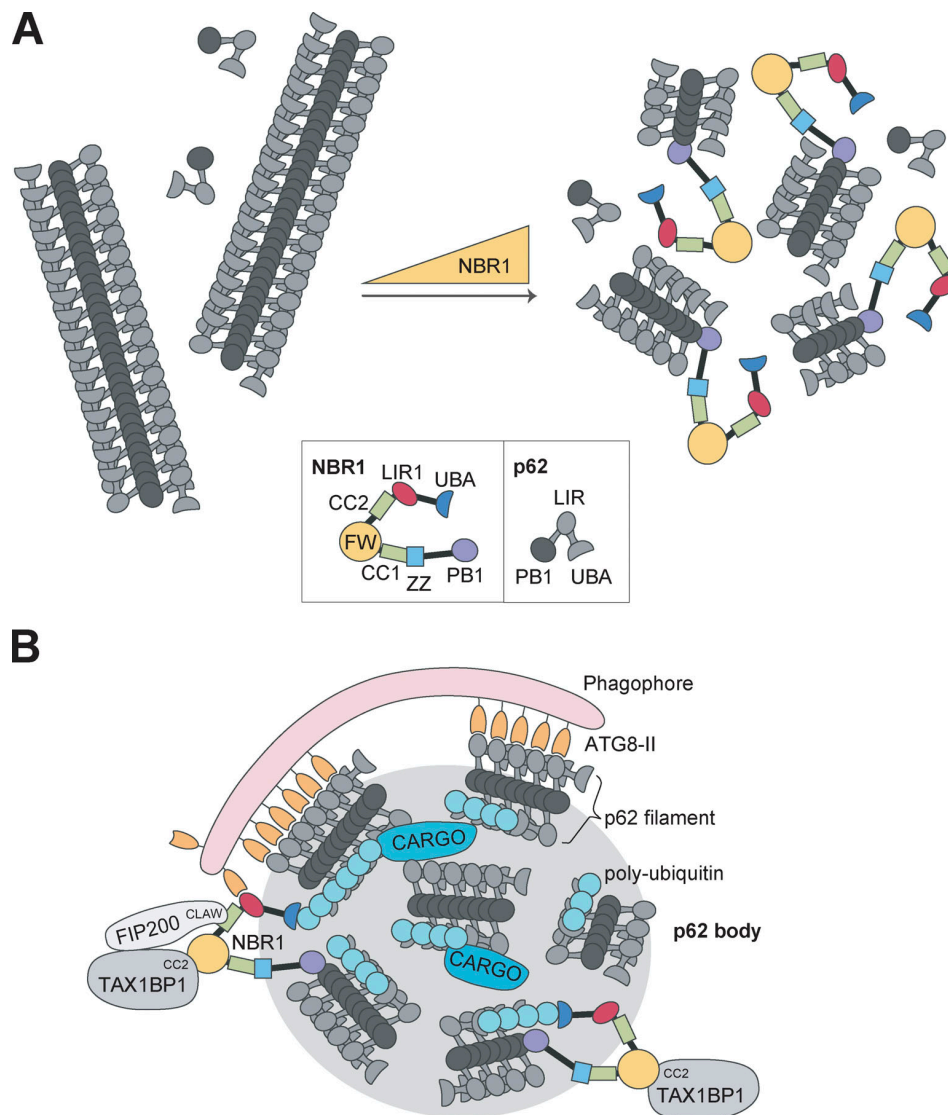


**Figure 4. NBR1 collaborates with p62 in the formation of p62 bodies and with TAX1BP1 in the recruitment of core autophagy components to p62 bodies.** (A) p62 forms long filaments in vitro as a result of PB1-mediated polymerization. Due to the monomeric nature of NBR1, it is hypothesized that NBR1 can act as a chain terminator of p62 filaments. With increasing amounts of NBR1 in vitro, the length of the p62 filaments is reduced. Shorter p62 filaments will likely form p62 bodies more easily. Therefore, a role for NBR1 in cells may be to promote p62 body formation by regulating p62 filament length. (B) The role for NBR1 in p62 body dynamics. NBR1 promotes p62 body formation by PB1-mediated regulation of p62 filament length and high-affinity ubiquitin binding. Furthermore, NBR1 facilitates autophagosome formation by recruiting TAX1BP1 and FIP200. FIP200 is recruited by direct binding between the FIP200 CLAW domain to the CC2 of NBR1. TAX1BP1 binds NBR1 FW domain via its CC2 domain and also recruits FIP200. NBR1 LIR1 also binds ATG8 proteins in the growing phagophore. In addition, NBR1 contains multiple domains that may be involved in cargo recruitment (UBA, ZZ, FW, AH).

(Ohnstad et al., 2020). TAX1BP1 binds to NBR1 via its CC2 domain. Taken together, these studies show that in human cells, a trio of SLRs work together for the efficient formation and degradation of p62 bodies. NBR1 affects p62 filament length by PB1 domain interactions, as well as recruitment of ubiquitinated cargo via the UBA domain, recruitment of TAX1BP1 via the FW domain, FIP200 via the CC2 domain, and ATG8s via the LIR1 domain (Fig. 4).

Phase separation of plant NBR1 has not been demonstrated experimentally. However, AtNBR1 ectopically expressed in HeLa cells or plant tissues form ubiquitin aggregates resembling those

formed by p62 (Svenning et al., 2011). We therefore believe that AtNBR1/p62 bodies represent a unique type of preautophagic structures or phagophore assembly sites (PAS) that are evolutionary conserved and formed in all eukaryotic cells expressing p62 or polymeric NBR1 orthologs.

A functionally distinct type of p62 bodies named dendritic aggresome-like induced structures (DALIS) are transiently formed by p62 in activated dendritic cells and involved in antigen processing (Lelouard et al., 2004; Lelouard et al., 2002). Ubiquitinated substrates recruited to DALIS, including defective ribosomal products (DRiPs), are either degraded by the



proteasome or by autophagy. NBR1 is not required for the formation of DALIS, but for their degradation by autophagy and antigen presentation via MHC class II, which may occur even in the absence of p62 (Arguello et al., 2016). In cells lacking NBR1, ubiquitinated substrates in DALIS are degraded by the proteasome, presumably depending on the solubilization of DALIS. Puromycin induction of p62 bodies in HeLa cells involving recruitment of ubiquitinated DRiPs into p62 bodies is highly dependent on NBR1 (Kirkin et al., 2009). While the degradation of p62 does not depend on NBR1, ubiquitinated proteins in p62 bodies are not degraded by autophagy in cells lacking NBR1 (Kirkin et al., 2009).

NBR1 is efficiently degraded by ATG7- and ATG8-dependent autophagy independent of p62 (Kirkin et al., 2009), but also ATG7-independent autophagy pathways exist for NBR1. The SLRs p62, NBR1, TAX1BP1, and NDP52 are degraded by endosomal microautophagy in response to acute starvation (Mejlvang et al., 2018). Degradation of NBR1 is in this case partially ATG7-independent. ATG7-independent degradation of NBR1 and TAX1BP1 requires direct interaction of NBR1 with TAX1BP1 (Ohnstad et al., 2020) and also depends on a SKICH-mediated binding of TAX1BP1 to FIP200 (Ravenhill et al., 2019; Thurston et al., 2016). Hence, the SLR-dependent recruitment of FIP200 allows ATG8-independent autophagy to occur to degrade NBR1 in the absence of functional conjugation machinery mediating lipidation of ATG8s (Ohnstad et al., 2020).

### Pexophagy

NBR1 acts as a receptor for pexophagy in mammalian cells (Deosaran et al., 2013; Fig. 1 A). Interestingly, the NBR1 homolog in the filamentous ascomycete *Sordaria macrospora* is required for pexophagy, and human NBR1 can rescue growth defects under stress conditions when the fungal protein is lost (Werner et al., 2019). In *Arabidopsis*, pexophagy occurs independently of AtNBR1 (Young et al., 2019). We found that the amphipathic alpha-helix (AH) located immediately N-terminal to the UBA domain as well as the UBA, LIR, and CC domains of mammalian NBR1 are required for pexophagy. Coincident binding of the AH and UBA domains directs NBR1 to ubiquitinated peroxisomes and targets them for selective autophagy. Electron microscopy studies revealed that aggregates of overexpressed NBR1 contain clusters of 50-nm vesicles together with peroxisomes, autophagosomes, and some larger vesicle structures (possibly late endosomes; Deosaran et al., 2013). Endogenous p62 is recruited to NBR1 vesicle aggregates via its direct binding to NBR1. Its presence has a positive effect on NBR1-mediated pexophagy. However, pexophagy occurs also in the absence of p62, and p62 overexpression does not induce pexophagy (Deosaran et al., 2013).

Activation of the hypoxia-inducible factor HIF-2 $\alpha$  augments NBR1-mediated pexophagy, and peroxisome numbers are reduced in VHL-deficient human clear cell renal cell carcinomas with elevated levels of HIF-2 $\alpha$  (Walter et al., 2014). Overexpression of the peroxisomal membrane protein PEX3 increases NBR1-mediated pexophagy, but it is not ubiquitination of PEX3 as such that leads to increased pexophagy (Yamashita et al., 2014). SQSTM1/p62 was required only for the clustering of

peroxisomes. The peroxisomal E3 ubiquitin ligase peroxin 2 (PEX2) is upregulated upon amino acid starvation and rapamycin treatment. PEX2 expression induces ubiquitination of PEX5 and PMP70 on peroxisomes and boosts NBR1-dependent pexophagy (Sargent et al., 2016).

### Xenophagy

Several soluble SLRs are involved in the autophagic clearance of invading pathogens, a process known as xenophagy (Goodall et al., 2022; Lamark and Johansen, 2021). Invading bacteria exposed in the cytosol become tagged with ubiquitin chains and sequestered into autophagosomes by ubiquitin-binding SLRs (Goodall et al., 2022). NBR1, NDP52, and p62 are recruited to intracytosolic *Mycobacterium tuberculosis* (Manzanillo et al., 2013) and *Shigella flexneri* (Mostowy et al., 2011; Fig. 1 A). In the case of *S. flexneri* infection, NBR1 is necessary to recruit p62 and NDP52; yet the mechanism and functional significance of this remains elusive (Mostowy et al., 2011). Upon infection with *M. tuberculosis*, both NBR1 and p62 are recruited in a parkin2-dependent manner (Manzanillo et al., 2013). NBR1, but not p62, can also be recruited by the HECT E3 ligase Smurf1 to *M. tuberculosis* (Franco et al., 2017). Mice depleted of either parkin2 or Smurf1 are more sensitive to *M. tuberculosis* infection, suggesting that both E3 ligases are important for the recruitment of SLRs and subsequent xenophagy (Franco et al., 2017; Manzanillo et al., 2013). Furthermore, the *M. tuberculosis* surface protein Rv1468c binds polyubiquitin chains and recruits SLRs, including NBR1, in a UBA-dependent manner (Chai et al., 2019). NBR1 is also recruited to group A Streptococcus (GAS)-containing vesicles in a Tollip-dependent manner. Tollip knockout prevents the recruitment of NBR1, NDP52, and TAX1BP1 to GAS-containing vesicles, yet p62 recruitment is unaffected (Lin et al., 2020).

Viruses utilize various strategies to manipulate host cell autophagy to their advantage (Liu et al., 2022). One such strategy involves NBR1-mediated autophagic degradation of the antiviral adaptor protein MAVS (Zeng et al., 2021). The basic polymerase 1 (PB1, not to be confused with the PB1 domain) of the H7N9 strain of influenza A virus promotes K27-polyubiquitination of MAVS and specifically recruits NBR1 to mediate enhanced MAVS degradation by autophagy, which further facilitates viral replication. Interestingly, the autophagic degradation of MAVS is dependent on ATG7, but does not require components of the ULK-complex. Some viruses, like Coxsackievirus, also counter the antiviral activity of both p62 and NBR1 by encoding proteases that cleave p62 and NBR1, releasing C-terminal fragments exerting dominant negative effects on endogenous p62 and NBR1 (Shi et al., 2014).

### NBR1 and human disease

#### Proteinopathies

The giant protein titin acts as a scaffold for the assembly of the sarcomere and signaling complexes in muscle cells. Titin contains a serine/threonine kinase domain (TK) involved in mechanosensing (Puchner et al., 2008). NBR1 interacts with TK and recruits p62 and the E3 ligase MURF2 in active muscle, thereby regulating mechanical signaling and muscle gene transcription

(Lange et al., 2005). Analysis of two unrelated families with hereditary myopathy with early respiratory failure identified a mutation in the NBR1-interaction site within TK that disrupts NBR1 binding. NBR1 was more diffusely localized, p62 accumulated in many patient muscle samples, and MURF2 showed more nuclear localization, suggesting disruption of the NBR1-p62-MURF2 complex.

NBR1 function in aggregophagy may link it to diseases characterized by the accumulation of misfolded proteins. One such disease is sporadic inclusion body myositis (sIBM), a progressive degenerative myopathy that is the most common skeletal myopathy in older people. Pathological features of this disease include the accumulation of rimmed vacuoles (hence the name “inclusion body”) and misfolded protein aggregates in muscle fiber cells, indicating defects in autophagy and lysosomal degradation. Biopsies and cultured cells from sIBM patients show an increase in NBR1 protein, and NBR1 accumulation alongside p62 and LC3 in the ubiquitin-positive aggregates that are characteristic of this disease (D’Agostino et al., 2011). NBR1 is phosphorylated by GSK3B at Thr586, which promotes NBR1-mediated degradation of ubiquitinated proteins and prevents the formation of misfolded aggregates (Nicot et al., 2014). Meanwhile, in sIBM patient biopsies, NBR1 phosphorylation is reduced. This, in turn, prevents the clearance of ubiquitinated substrates, instead leading to the accumulation of misfolded proteins. NBR1 is also accumulated in Lewy bodies in Parkinson’s disease and glial cytoplasmic inclusions in multiple system atrophy (Odagiri et al., 2012). We also reported early on that NBR1 colocalized with p62 and ubiquitin in Mallory bodies in the liver of a patient with alcoholic steatohepatitis (Kirkin et al., 2009). However, given the cooperation of NBR1 and p62 in p62 bodies, it is often hard to distinguish NBR1-specific pathological effects.

### **NBR1 and cancer**

Data from the Human Protein Atlas show that NBR1 mRNA is expressed in most cancers with low-cancer specificity (Uhlen et al., 2017). Recently, whole exome sequencing on germline DNA from a family presenting with different subtypes of renal cell carcinoma (RCC) identified a frameshift mutation in NBR1 (Adolphe et al., 2021). The mutation results in the expression of a truncated form of NBR1 that no longer includes LIR and UBA domains. While this does not affect the ability of NBR1 to interact with itself and with p62, overexpression of the truncated NBR1 delays the turnover of p62 and peroxisomes. The overexpression of truncated NBR1 increases the proliferation capacity of renal cancer cells compared with cells overexpressing WT NBR1. Exactly how NBR1 may affect RCC development is unclear and will require further studies. Some rare cases of RCC present with eosinophilic cytoplasmic inclusions, which are aggregates associated with membrane-bound, electron-dense organelles (Yu et al., 2018). These aggregates contain p62, NBR1, and other autophagy markers, and maybe the result of defects in autophagy. Strikingly, these aggregates are surrounded by clusters of peroxisomes only when NBR1 is present. While these inclusions are relatively rare in RCC, their presence is generally associated with larger tumors (Yu et al., 2018). However, the exact effects

of these inclusions and clustering of peroxisomes on tumor progression are not known.

In recent years, several comprehensive studies have revealed potentially unique roles for NBR1 in cancer development, independent of p62. In migrating cells, focal adhesions (FAs) are continuously assembled and disassembled to allow cell protrusion, adhesion, and contraction. NBR1 has a specific role as a selective autophagy receptor in the turnover of FAs at the leading edge of the cell during cell migration (Kenific et al., 2016; Fig. 1 A). Knockdown of NBR1, but not other SLRs, inhibited cell migration and increased FA lifetime. NBR1 localizes to FAs and recruits autophagosomes to FAs at the leading edge of the cell, targeting FAs for autophagosomal degradation and thereby promoting cell migration. This process may be hijacked by cancer cells to facilitate cancer metastasis. A more recent study investigated the role of autophagy in different stages of breast cancer development in a mouse model (Marsh et al., 2020). As expected, impairment of autophagy led to an accumulation of NBR1 and p62. Intriguingly, the accumulation of NBR1, but not p62, promoted the development of an aggressive subpopulation of tumor cells. Injection of tumor cells overexpressing NBR1 led to metastatic outgrowth, while overexpression of p62 did not. Knockdown of NBR1 in the autophagy-deficient cells reversed the metastatic phenotype otherwise observed upon autophagy inhibition alone. Even in autophagy-competent cells, the ectopic overexpression of NBR1 was sufficient to promote tumor metastasis. These results suggest that aberrant accumulation of NBR1 can promote metastatic outgrowth during breast cancer progression.

NBR1 plays a role in the immune evasion of pancreatic cancer cells. Cytotoxic T cells can detect and eliminate cancerous cells that present tumor antigens via MHC class I molecules on their surface. Consequently, many cancers evade the immune system through mutations or loss of MHC class I molecules. In pancreatic ductal adenocarcinomas (PDACs), MHC class I surface expression is often downregulated, but rarely due to mutations. In PDAC cells, MHC class I molecules are being degraded by NBR1-mediated selective autophagy, effectively preventing them from reaching the cell surface (Yamamoto et al., 2020; Fig. 1 A). Inhibition of autophagy increases both the total and cell surface expression of MHC class I in PDAC cells and further leads to increased antigen presentation, T-cell infiltration, and tumor cell killing. Of the SLRs tested, NBR1 was found to co-precipitate with MHC class I proteins, while p62, NDP52, TAX1BP1, and OPTN did not co-precipitate. Knockdown of NBR1 increases the total and surface levels of MHC class I molecules. Altogether, this supports a role for NBR1 in targeting MHC class I molecules for autophagic degradation, facilitating immune evasion of PDAC cells. More studies are required to probe for possible direct or indirect roles of NBR1 and other SLRs on the turnover of MHC class I in different normal and cancer cells.

### **Possible autophagy-independent roles of NBR1**

NBR1 has been implicated in processes with no obvious link to autophagy, including the downregulation of receptor tyrosine kinases and inhibition of ERK1/2 (Mardakheh et al., 2010; Mardakheh et al., 2009). Several PBI domain-containing

proteins are implicated in the differentiation of activated T cells, including NBR1 and p62 (Martin et al., 2006; Yang et al., 2010). NBR1 is required for proper differentiation of T helper 2 cells. Whether this relates to the function of NBR1 as an autophagy receptor or potentially autophagy-independent functions is not known. NBR1 also acts as a regulator of JNK signaling and adipose tissue inflammation by engaging in a PBI–PBI interaction with MEKK3 (Hernandez et al., 2014). Furthermore, p62 and NBR1 regulate PPAR $\gamma$ –RXR $\alpha$  heterodimerization to control thermogenesis in brown adipocytes. NBR1 represses the activity of PPAR $\gamma$  when p62 is inactivated. (Huang et al., 2021). NBR1 has been shown to deliver IL-12 to late endosomes in intestinal myeloid cells (Merkley et al., 2022).

NBR1 is reported to interact with activated p38 and limit its activity (Kim et al., 2019; Whitehouse et al., 2010). In mice, the expression of a truncated version of NBR1 that is unable to bind p38 and mitigate its activity results in an age-dependent increase in bone mass (Whitehouse et al., 2010). Furthermore, loss of NBR1 in both transformed and non-transformed cell lines causes cellular senescence because of p38-induced ER stress (Kim et al., 2019). Whether or not this negative regulation of p38 requires autophagy is not clear.

#### Concluding remarks and future questions/perspectives

NBR1 is the archetypal autophagy receptor, likely present as early as in the latest eukaryotic common ancestor. Gene duplication in the early metazoan lineage and subsequent molecular evolution gave rise to mammalian NBR1 and the much more studied paralogue p62. Studies of NBR1 homologs in plants, fungi, and mammals are beginning to shed light on some of the unique roles of NBR1, gradually bringing it out of the shadow of p62. Structural and functional comparisons clearly suggest that yeast Atg19 and Atg34 are NBR1 homologs. NBR1 plays a central role in pexophagy in mammals, while its role in xenophagy is far better understood in plants than in mammals. Exciting new information has come from studies on the collaboration between p62, TAX1BP1, and NBR1 in the recruitment of core autophagy components to p62 bodies to facilitate autophagosome formation. Here, NBR1 plays a much more central role than anticipated. Important p62-independent roles of NBR1 in cancer metastasis and immune evasion in cancer have been revealed. NBR1 also has autophagy-independent roles in regulating signaling pathways and immune cell differentiation.

NBR1 is understudied and future research must address this. In future studies, a deeper understanding of the evolution and interplay between NBR1 and p62 may reveal further functions of NBR1, not only as a SAR but also in regulating the dynamics of p62 bodies. Very likely, new autophagic substrates unique to NBR1 will be discovered. It will be important to penetrate more mechanisms of pexophagy and xenophagy involving NBR1. Studies of fungal NBR1 homologs ask the question if there are analogous roles of mammalian NBR1 in pathways similar to the Cvt and NVT pathways. Further elucidation of pathophysiological roles of NBR1 in human disease is required to evaluate NBR1 as a potential target for therapeutic strategies in cancer and proteinopathies.

#### Acknowledgments

The authors thank all researchers who contributed data and discoveries mentioned here. We apologize to colleagues whose work was not cited due to space limitations.

Research in the lab of T. Johansen is supported by grant 190214 from Norwegian Cancer Society and grant 249884 from The Research Council of Norway to T. Johansen.

The authors declare no competing financial interests.

Submitted: 17 August 2022

Revised: 3 October 2022

Accepted: 3 October 2022

#### References

- Adolphe, F., S. Ferlicot, V. Verkarre, K. Posseme, S. Couve, P. Garnier, N. Droin, M. Deloger, B. Job, S. Giraud, et al. 2021. Germline mutation in the NBR1 gene involved in autophagy detected in a family with renal tumors. *Cancer Genet.* 258–259:51–56. <https://doi.org/10.1016/j.cancergen.2021.07.003>
- Arguello, R.J., M. Reverendo, E. Gatti, and P. Pierre. 2016. Regulation of protein synthesis and autophagy in activated dendritic cells: Implications for antigen processing and presentation. *Immunol. Rev.* 272: 28–38. <https://doi.org/10.1111/imr.12427>
- Boualem, A., C. Dogimont, and A. Bendahmane. 2016. The battle for survival between viruses and their host plants. *Curr. Opin. Virol.* 17:32–38. <https://doi.org/10.1016/j.coviro.2015.12.001>
- Burki, F., A.J. Roger, M.W. Brown, and A.G.B. Simpson. 2020. The new tree of eukaryotes. *Trends Ecol. Evol.* 35:43–55. <https://doi.org/10.1016/j.tree.2019.08.008>
- Cha-Molstad, H., J.E. Yu, Z. Feng, S.H. Lee, J.G. Kim, P. Yang, B. Han, K.W. Sung, Y.D. Yoo, J. Hwang, et al. 2017. p62/SQSTM1/Sequestosome-1 is an N-recognin of the N-end rule pathway which modulates autophagosome biogenesis. *Nat. Commun.* 8:102. <https://doi.org/10.1038/s41467-017-00085-7>
- Chai, Q., X. Wang, L. Qiang, Y. Zhang, P. Ge, Z. Lu, Y. Zhong, B. Li, J. Wang, L. Zhang, et al. 2019. A Mycobacterium tuberculosis surface protein recruits ubiquitin to trigger host xenophagy. *Nat. Commun.* 10:1973. <https://doi.org/10.1038/s41467-019-09955-8>
- Chang, C., L.E. Jensen, and J.H. Hurley. 2021. Autophagosome biogenesis comes out of the black box. *Nat. Cell Biol.* 23:450–456. <https://doi.org/10.1038/s41556-021-00669-y>
- Cho, N.H., K.C. Cheveralls, A.D. Brunner, K. Kim, A.C. Michaelis, P. Raghavan, H. Kobayashi, L. Savy, J.Y. Li, H. Canaj, et al. 2022. OpenCell: Endogenous tagging for the cartography of human cellular organization. *Science.* 375:eabi6983. <https://doi.org/10.1126/science.abi6983>
- Ciuffa, R., T. Lamark, A.K. Tarafder, A. Guesdon, S. Rybina, W.J. Hagen, T. Johansen, and C. Sachse. 2015. The selective autophagy receptor p62 forms a flexible filamentous helical scaffold. *Cell Rep.* 11:748–758. <https://doi.org/10.1016/j.celrep.2015.03.062>
- D'Agostino, C., A. Nogalska, M. Cacciottolo, W.K. Engel, and V. Askanas. 2011. Abnormalities of NBR1, a novel autophagy-associated protein, in muscle fibers of sporadic inclusion-body myositis. *Acta Neuropathol.* 122: 627–636. <https://doi.org/10.1007/s00401-011-0874-3>
- Dagdas, Y.F., P. Pandey, Y. Tumbas, N. Sanguankiatichai, K. Belhaj, C. Duggan, A.Y. Leary, M.E. Segretin, M.P. Contreras, Z. Savage, et al. 2018. Host autophagy machinery is diverted to the pathogen interface to mediate focal defense responses against the Irish potato famine pathogen. *Elife.* 7:e37476. <https://doi.org/10.7554/eLife.37476>
- Deosaran, E., K.B. Larsen, R. Hua, G. Sargent, Y. Wang, S. Kim, T. Lamark, M. Jauregui, K. Law, J. Lippincott-Schwartz, et al. 2013. NBR1 acts as an autophagy receptor for peroxisomes. *J. Cell Sci.* 126:939–952. <https://doi.org/10.1242/jcs.114819>
- Deretic, V. 2012. Autophagy as an innate immunity paradigm: Expanding the scope and repertoire of pattern recognition receptors. *Curr. Opin. Immunol.* 24:21–31. <https://doi.org/10.1016/j.coi.2011.10.006>
- Franco, L.H., V.R. Nair, C.R. Scharn, R.J. Xavier, J.R. Torrealba, M.U. Shiloh, and B. Levine. 2017. The ubiquitin ligase Smurf1 functions in selective autophagy of Mycobacterium tuberculosis and anti-tuberculous host



- defense. *Cell Host Microbe*. 22:421–423. <https://doi.org/10.1016/j.chom.2017.08.005>
- Goodall, E.A., F. Kraus, and J.W. Harper. 2022. Mechanisms underlying ubiquitin-driven selective mitochondrial and bacterial autophagy. *Mol. Cell*. 82:1501–1513. <https://doi.org/10.1016/j.molcel.2022.03.012>
- Hafren, A., J.L. Macia, A.J. Love, J.J. Milner, M. Drucker, and D. Hofius. 2017. Selective autophagy limits cauliflower mosaic virus infection by NBR1-mediated targeting of viral capsid protein and particles. *Proc. Natl. Acad. Sci. USA*. 114:E2026–E2035. <https://doi.org/10.1073/pnas.1610687114>
- Hafren, A., S. Ustun, A. Hochmuth, S. Svenning, T. Johansen, and D. Hofius. 2018. Turnip mosaic virus counteracts selective autophagy of the viral silencing suppressor HCpro. *Plant Physiol*. 176:649–662. <https://doi.org/10.1104/pp.17.01198>
- Hama, Y., S. Zhang, and N. Mizushima. 2021. ZZ domains keep cytosol to vacuole delivery whiZing along. *EMBO J*. 40:e108777. <https://doi.org/10.15252/emj.2021108777>
- Hernandez, E.D., S.J. Lee, J.Y. Kim, A. Duran, J.F. Linares, T. Yajima, T.D. Muller, M.H. Tschop, S.R. Smith, M.T. Diaz-Meco, and J. Moscat. 2014. A macrophage NBR1-MEKK3 complex triggers JNK-mediated adipose tissue inflammation in obesity. *Cell Metabol*. 20:499–511. <https://doi.org/10.1016/j.cmet.2014.06.008>
- Huang, J., J.F. Linares, A. Duran, W. Xia, A.R. Saltiel, T.D. Muller, M.T. Diaz-Meco, and J. Moscat. 2021. NBR1 is a critical step in the repression of thermogenesis of p62-deficient adipocytes through PPAR $\gamma$ . *Nat. Commun*. 12:2876. <https://doi.org/10.1038/s41467-021-23085-0>
- Isakson, P., A.H. Lystad, K. Breen, G. Koster, H. Stenmark, and A. Simonsen. 2013. TRAF6 mediates ubiquitination of KIF23/MKLP1 and is required for midbody ring degradation by selective autophagy. *Autophagy*. 9:1955–1964. <https://doi.org/10.4161/aut.26085>
- Jakobi, A.J., S.T. Huber, S.A. Mortensen, S.W. Schultz, A. Palara, T. Kuhm, B.K. Shrestha, T. Lamark, W.J.H. Hagen, M. Wilmanns, et al. 2020. Structural basis of p62/SQSTM1 helical filaments and their role in cellular cargo uptake. *Nat. Commun*. 11:440. <https://doi.org/10.1038/s41467-020-14343-8>
- Ji, C., J. Zhou, R. Guo, Y. Lin, C.H. Kung, S. Hu, W.Y. Ng, X. Zhuang, and L. Jiang. 2020. AtNBR1 is a selective autophagic receptor for AtExo70E2 in Arabidopsis. *Plant Physiol*. 184:777–791. <https://doi.org/10.1104/pp.20.00470>
- Johansen, T., and T. Lamark. 2020. Selective autophagy: ATG8 family proteins, LIR motifs and cargo receptors. *J. Mol. Biol*. 432:80–103. <https://doi.org/10.1016/j.jmb.2019.07.016>
- Jumper, J., R. Evans, A. Pritzel, T. Green, M. Figurnov, O. Ronneberger, K. Tunyasuvunakool, R. Bates, A. Zidek, A. Potapenko, et al. 2021. Highly accurate protein structure prediction with AlphaFold. *Nature*. 596:583–589. <https://doi.org/10.1038/s41586-021-03819-2>
- Kenific, C.M., S.J. Stehens, J. Goldsmith, A.M. Leidal, N. Faure, J. Ye, T. Wittmann, and J. Debnath. 2016. NBR1 enables autophagy-dependent focal adhesion turnover. *J. Cell Biol*. 212:577–590. <https://doi.org/10.1083/jcb.201503075>
- Khan, M., D. Seto, R. Subramaniam, and D. Desveaux. 2018. Oh, the places they'll go! A survey of phytopathogen effectors and their host targets. *Plant J*. 93:651–663. <https://doi.org/10.1111/tpj.13780>
- Kim, H.S., Y. Kim, M.J. Lim, Y.G. Park, S.I. Park, and J. Sohn. 2019. The p38-activated ER stress-ATF6 $\alpha$  axis mediates cellular senescence. *FASEB J*. 33:2422–2434. <https://doi.org/10.1096/fj.201800836R>
- King, N., M.J. Westbrook, S.L. Young, A. Kuo, M. Abedin, J. Chapman, S. Fairclough, U. Hellsten, Y. Isogai, I. Letunic, et al. 2008. The genome of the choanoflagellate *Monosiga brevicollis* and the origin of metazoans. *Nature*. 451:783–788. <https://doi.org/10.1038/nature06617>
- Kirkin, V., T. Lamark, Y.S. Sou, G. Bjorkoy, J.L. Nunn, J.A. Bruun, E. Shvets, D.G. McEwan, T.H. Clausen, P. Wild, et al. 2009. A role for NBR1 in autophagosomal degradation of ubiquitinated substrates. *Mol. Cell*. 33:505–516. <https://doi.org/10.1016/j.molcel.2009.01.020>
- Kraft, C., M. Peter, and K. Hofmann. 2010. Selective autophagy: Ubiquitin-mediated recognition and beyond. *Nat. Cell Biol*. 12:836–841. <https://doi.org/10.1038/ncb0910-836>
- Kuo, T.C., C.T. Chen, D. Baron, T.T. Onder, S. Loewer, S. Almeida, C.M. Weismann, P. Xu, J.M. Houghton, F.B. Gao, et al. 2011. Midbody accumulation through evasion of autophagy contributes to cellular reprogramming and tumorigenicity. *Nat. Cell Biol*. 13:1214–1223. <https://doi.org/10.1038/ncb2332>
- Lamark, T., and T. Johansen. 2021. Mechanisms of selective autophagy. *Annu. Rev. Cell Dev. Biol*. 37:143–169. <https://doi.org/10.1146/annurev-cellbio-120219-035530>
- Lamark, T., M. Perander, H. Outzen, K. Kristiansen, A. Øvervatn, E. Michaelsen, G. Bjørkøy, and T. Johansen. 2003. Interaction codes within the family of mammalian Phox and Bem1p domain-containing proteins. *J. Biol. Chem*. 278:34568–34581. <https://doi.org/10.1074/jbc.M303221200>
- Lange, S., F. Xiang, A. Yakovenko, A. Vihola, P. Hackman, E. Rostkova, J. Kristensen, B. Brandmeier, G. Franzen, B. Hedberg, et al. 2005. The kinase domain of titin controls muscle gene expression and protein turnover. *Science*. 308:1599–1603. <https://doi.org/10.1126/science.1110463>
- Leber, R., E. Silles, I.V. Sandoval, and M.J. Mazon. 2001. Yol082p, a novel CVT protein involved in the selective targeting of aminopeptidase I to the yeast vacuole. *J. Biol. Chem*. 276:29210–29217. <https://doi.org/10.1074/jbc.M101438200>
- Lelouard, H., V. Ferrand, D. Marguet, J. Bania, V. Camosseto, A. David, E. Gatti, and P. Pierre. 2004. Dendritic cell aggresome-like induced structures are dedicated areas for ubiquitination and storage of newly synthesized defective proteins. *J. Cell Biol*. 164:667–675. <https://doi.org/10.1083/jcb.200312073>
- Lelouard, H., E. Gatti, F. Cappello, O. Gresser, V. Camosseto, and P. Pierre. 2002. Transient aggregation of ubiquitinated proteins during dendritic cell maturation. *Nature*. 417:177–182. <https://doi.org/10.1038/417177a>
- Leong, J.X., M. Raffener, D. Spinti, G. Langin, M. Franz-Wachtel, A.R. Guzman, J.G. Kim, P. Pandey, A.E. Minina, B. Macek, et al. 2022. A bacterial effector counteracts host autophagy by promoting degradation of an autophagy component. *EMBO J*. 41:e110352. <https://doi.org/10.15252/emj.202110352>
- Letunic, I., R.R. Copley, B. Pils, S. Pinkert, J. Schultz, and P. Bork. 2006. SMART 5: Domains in the context of genomes and networks. *Nucleic Acids Res*. 34:D257–D260. <https://doi.org/10.1093/nar/gkj079>
- Li, X., Q. Xia, M. Mao, H. Zhou, L. Zheng, Y. Wang, Z. Zeng, L. Yan, Y. Zhao, and J. Shi. 2021. Annexin-A1 SUMOylation regulates microglial polarization after cerebral ischemia by modulating IKK $\alpha$  stability via selective autophagy. *Sci. Adv*. 7:eabc5539. <https://doi.org/10.1126/sciadv.abc5539>
- Lin, C.Y., T. Nozawa, A. Minowa-Nozawa, H. Toh, M. Hikichi, J. Iibushi, and I. Nakagawa. 2020. Autophagy receptor Tollip facilitates bacterial autophagy by recruiting galectin-7 in response to group A *Streptococcus* infection. *Front. Cell. Infect. Microbiol*. 10:583137. <https://doi.org/10.3389/fcimb.2020.583137>
- Lin, Q., Q. Dai, H. Meng, A. Sun, J. Wei, K. Peng, C. Childress, M. Chen, G. Shao, and W. Yang. 2017. The HECT E3 ubiquitin ligase NEDD4 interacts with and ubiquitylates SQSTM1 for inclusion body autophagy. *J. Cell Sci*. 130:3839–3850. <https://doi.org/10.1242/jcs.207068>
- Liu, X.M., L.L. Sun, W. Hu, Y.H. Ding, M.Q. Dong, and L.L. Du. 2015. ESCRTs cooperate with a selective autophagy receptor to mediate vacuolar targeting of soluble cargos. *Mol. Cell*. 59:1035–1042. <https://doi.org/10.1016/j.molcel.2015.07.034>
- Liu, Y., T. Zhou, J. Hu, S. Jin, J. Wu, X. Guan, Y. Wu, and J. Cui. 2022. Targeting selective autophagy as a therapeutic strategy for viral infectious diseases. *Front. Microbiol*. 13:889835. <https://doi.org/10.3389/fmicb.2022.889835>
- Lu, S., J. Wang, F. Chitsaz, M.K. Derbyshire, R.C. Geer, N.R. Gonzales, M. Gwadz, D.I. Hurwitz, G.H. Marchler, J.S. Song, et al. 2020. CDD/SPARCLE: The conserved domain database in 2020. *Nucleic Acids Res*. 48:D265–D268. <https://doi.org/10.1093/nar/gkz991>
- Lystad, A.H., and A. Simonsen. 2019. Mechanisms and pathophysiological roles of the ATG8 conjugation machinery. *Cells*. 8:973. <https://doi.org/10.3390/cells8090973>
- Manzanillo, P.S., J.S. Ayres, R.O. Watson, A.C. Collins, G. Souza, C.S. Rae, D.S. Schneider, K. Nakamura, M.U. Shiloh, and J.S. Cox. 2013. The ubiquitin ligase parkin mediates resistance to intracellular pathogens. *Nature*. 501:512–516. <https://doi.org/10.1038/nature12566>
- Marchbank, K., S. Waters, R.G. Roberts, E. Solomon, and C.A. Whitehouse. 2012. MAPIB interaction with the FW domain of the autophagic receptor Nbr1 facilitates its association to the microtubule network. *Int. J. Cell Biol*. 2012:208014. <https://doi.org/10.1155/2012/208014>
- Mardakheh, F.K., G. Auciello, T.R. Dafforn, J.Z. Rappoport, and J.K. Heath. 2010. Nbr1 is a novel inhibitor of ligand-mediated receptor tyrosine kinase degradation. *Mol. Cell. Biol*. 30:5672–5685. <https://doi.org/10.1128/MCB.00878-10>
- Mardakheh, F.K., M. Yekezare, L.M. Machesky, and J.K. Heath. 2009. Spred2 interaction with the late endosomal protein NBR1 down-regulates fibroblast growth factor receptor signaling. *J. Cell Biol*. 187:265–277. <https://doi.org/10.1083/jcb.200905118>
- Marsh, T., C.M. Kenific, D. Suresh, H. Gonzalez, E.R. Shamir, W. Mei, A. Tankka, A.M. Leidal, S. Kalavacherla, K. Woo, et al. 2020. Autophagic degradation of NBR1 restricts metastatic outgrowth during mammary tumor progression. *Dev. Cell*. 52:591–604.e6. <https://doi.org/10.1016/j.devcel.2020.01.025>

- Martin, P., M.T. Diaz-Meco, and J. Moscat. 2006. The signaling adapter p62 is an important mediator of T helper 2 cell function and allergic airway inflammation. *EMBO J.* 25:3524–3533. <https://doi.org/10.1038/sj.emboj.7601250>
- Mejlvang, J., H. Olsvik, S. Svenning, J.A. Bruun, Y.P. Abudu, K.B. Larsen, A. Brech, T.E. Hansen, H. Brenne, T. Hansen, et al. 2018. Starvation induces rapid degradation of selective autophagy receptors by endosomal microautophagy. *J. Cell Biol.* 217:3640–3655. <https://doi.org/10.1083/jcb.201711002>
- Merkley, S.D., S.M. Goodfellow, Y. Guo, Z.E.R. Wilton, J.R. Byrum, K.C. Schwalm, D.L. Dinwiddie, R.R. Gullapalli, V. Deretic, A. Jimenez Hernandez, et al. 2022. Non-autophagy role of Atg5 and NBR1 in unconventional secretion of IL-12 prevents gut dysbiosis and inflammation. *J. Crohn's Colitis.* 16:259–274. <https://doi.org/10.1093/ecco-jcc/jjab144>
- Mizushima, N., T. Yoshimori, and Y. Ohsumi. 2011. The role of Atg proteins in autophagosome formation. *Annu. Rev. Cell Dev. Biol.* 27:107–132. <https://doi.org/10.1146/annurev-cellbio-092910-154005>
- Mostowy, S., V. Sancho-Shimizu, M.A. Hamon, R. Simeone, R. Brosch, T. Johansen, and P. Cossart. 2011. p62 and NDP52 proteins target intracytosolic Shigella and Listeria to different autophagy pathways. *J. Biol. Chem.* 286:26987–26995. <https://doi.org/10.1074/jbc.M111.223610>
- Nicot, A.S., F. Lo Verso, F. Ratti, F. Pilot-Storck, N. Streichenberger, M. Sandri, L. Schaeffer, and E. Goillot. 2014. Phosphorylation of NBR1 by GSK3 modulates protein aggregation. *Autophagy.* 10:1036–1053. <https://doi.org/10.4161/auto.28479>
- Nthiga, T.M., B. Kumar Shrestha, E. Sjøttem, J.A. Bruun, K. Bowitz Larsen, Z. Bhujabal, T. Lamark, and T. Johansen. 2020. CALCOCO1 acts with VAMP-associated proteins to mediate ER-phagy. *EMBO J.* 39:e103649. <https://doi.org/10.15252/embj.2019103649>
- Odagiri, S., K. Tanji, F. Mori, A. Kakita, H. Takahashi, and K. Wakabayashi. 2012. Autophagic adapter protein NBR1 is localized in Lewy bodies and glial cytoplasmic inclusions and is involved in aggregate formation in alpha-synucleinopathy. *Acta Neuropathol.* 124:173–186. <https://doi.org/10.1007/s00401-012-0975-7>
- Ohnstad, A.E., J.M. Delgado, B.J. North, I. Nasa, A.N. Kettenbach, S.W. Schultz, and C.J. Shoemaker. 2020. Receptor-mediated clustering of FIP200 bypasses the role of LC3 lipidation in autophagy. *EMBO J.* 39:e104948. <https://doi.org/10.15252/embj.2020104948>
- Puchner, E.M., A. Alexandrovich, A.L. Kho, U. Hensen, L.V. Schafer, B. Brandmeier, F. Grater, H. Grubmuller, H.E. Gaub, and M. Gautel. 2008. Mechanoenzymatics of titin kinase. *Proc. Natl. Acad. Sci. USA.* 105:13385–13390. <https://doi.org/10.1073/pnas.0805034105>
- Ravenhill, B.J., K.B. Boyle, N. von Muhlinen, C.J. Ellison, G.R. Masson, E.G. Otten, A. Foeglein, R. Williams, and F. Randow. 2019. The cargo receptor NDP52 initiates selective autophagy by recruiting the ULK complex to cytosol-invading bacteria. *Mol. Cell.* 74:320–329.e6. <https://doi.org/10.1016/j.molcel.2019.01.041>
- Ruiz-Trillo, I., Y. Inagaki, L.A. Davis, S. Sperstad, B. Landfald, and A.J. Roger. 2004. Capsaspora owczarzakii is an independent opisthokont lineage. *Curr. Biol.* 14:R946–R947. <https://doi.org/10.1016/j.cub.2004.10.037>
- Sanchez-Martin, P., Y.S. Sou, S. Kageyama, M. Koike, S. Waguri, and M. Komatsu. 2020. NBR1-mediated p62-liquid droplets enhance the Keap1-Nrf2 system. *EMBO Rep.* 21:e48902. <https://doi.org/10.15252/embr.201948902>
- Sargent, G., T. van Zutphen, T. Shatseva, L. Zhang, V. Di Giovanni, R. Bandsma, and P.K. Kim. 2016. PEX2 is the E3 ubiquitin ligase required for pexophagy during starvation. *J. Cell Biol.* 214:677–690. <https://doi.org/10.1083/jcb.201511034>
- Sarraf, S.A., H.V. Shah, G. Kanfer, A.M. Pickrell, L.A. Holtzclaw, M.E. Ward, and R.J. Youle. 2020. Loss of TAX1BP1-directed autophagy results in protein aggregate accumulation in the brain. *Mol. Cell.* 80:779–795.e10. <https://doi.org/10.1016/j.molcel.2020.10.041>
- Scott, S.V., J. Guan, M.U. Hutchins, J. Kim, and D.J. Klionsky. 2001. Cvt19 is a receptor for the cytoplasm-to-vacuole targeting pathway. *Mol. Cell.* 7:1131–1141. [https://doi.org/10.1016/s1097-2765\(01\)00263-5](https://doi.org/10.1016/s1097-2765(01)00263-5)
- Sedaghatmehr, M., V.P. Thirumalaikumar, I. Kamranfar, A. Marmagne, C. Masclaux-Daubresse, and S. Balazadeh. 2019. A regulatory role of autophagy for resetting the memory of heat stress in plants. *Plant Cell Environ.* 42:1054–1064. <https://doi.org/10.1111/pce.13426>
- Shi, J., G. Fung, P. Piesik, J. Zhang, and H. Luo. 2014. Dominant-negative function of the C-terminal fragments of NBR1 and SQSTM1 generated during enteroviral infection. *Cell Death Differ.* 21:1432–1441. <https://doi.org/10.1038/cdd.2014.58>
- Spang, A., T.A. Mahendrarajah, P. Offre, and C.W. Stairs. 2022. Evolving perspective on the origin and diversification of cellular life and the virosphere. *Genome Biol. Evol.* 14:evac034. <https://doi.org/10.1093/gbe/evac034>
- Sun, D., R. Wu, J. Zheng, P. Li, and L. Yu. 2018. Polyubiquitin chain-induced p62 phase separation drives autophagic cargo segregation. *Cell Res.* 28:405–415. <https://doi.org/10.1038/s41422-018-0017-7>
- Suzuki, K., C. Kondo, M. Morimoto, and Y. Ohsumi. 2010. Selective transport of alpha-mannosidase by autophagic pathways: Identification of a novel receptor, Atg34p. *J. Biol. Chem.* 285:30019–30025. <https://doi.org/10.1074/jbc.M110.143511>
- Svenning, S., T. Lamark, K. Krause, and T. Johansen. 2011. Plant NBR1 is a selective autophagy substrate and a functional hybrid of the mammalian autophagic adapters NBR1 and p62/SQSTM1. *Autophagy.* 7:993–1010. <https://doi.org/10.4161/auto.7.9.16389>
- Thirumalaikumar, V.P., M. Gorka, K. Schulz, C. Masclaux-Daubresse, A. Sampathkumar, A. Skirycz, R.D. Vierstra, and S. Balazadeh. 2021. Selective autophagy regulates heat stress memory in Arabidopsis by NBR1-mediated targeting of HSP90.1 and ROF1. *Autophagy.* 17:2184–2199. <https://doi.org/10.1080/15548627.2020.1820778>
- Thurston, T.L., K.B. Boyle, M. Allen, B.J. Ravenhill, M. Karpiyevich, S. Bloor, A. Kaul, J. Noad, A. Foeglein, S.A. Matthews, et al. 2016. Recruitment of TBK1 to cytosol-invading Salmonella induces WIP2-dependent antibacterial autophagy. *EMBO J.* 35:1779–1792. <https://doi.org/10.15252/embj.201694491>
- Turco, E., A. Savova, F. Gere, L. Ferrari, J. Romanov, M. Schuschnig, and S. Martens. 2021. Reconstitution defines the roles of p62, NBR1 and TAX1BP1 in ubiquitin condensate formation and autophagy initiation. *Nat. Commun.* 12:5212. <https://doi.org/10.1038/s41467-021-25572-w>
- Turco, E., M. Witt, C. Abert, T. Bock-Bierbaum, M.Y. Su, R. Trapannone, M. Sztacho, A. Danieli, X. Shi, G. Zaffagnini, et al. 2019. FIP200 Claw domain binding to p62 promotes autophagosome formation at ubiquitin condensates. *Mol. Cell.* 74:330–346.e11. <https://doi.org/10.1016/j.molcel.2019.01.035>
- Uhlen, M., L. Fagerberg, B.M. Hallstrom, C. Lindskog, P. Oksvold, A. Mardinnoglu, A. Sivertsson, C. Kampf, E. Sjostedt, A. Asplund, et al. 2015. Proteomics. Tissue-based map of the human proteome. *Science.* 347:1260419. <https://doi.org/10.1126/science.1260419>
- Uhlen, M., C. Zhang, S. Lee, E. Sjostedt, L. Fagerberg, G. Bidkhorri, R. Benfeitas, M. Arif, Z. Liu, F. Edfors, et al. 2017. A pathology atlas of the human cancer transcriptome. *Science.* 357:eaan2507. <https://doi.org/10.1126/science.aan2507>
- Ustun, S., A. Hafren, Q. Liu, R.S. Marshall, E.A. Minina, P.V. Bozhkov, R.D. Vierstra, and D. Hofius. 2018. Bacteria exploit autophagy for proteasome degradation and enhanced virulence in plants. *Plant Cell.* 30:668–685. <https://doi.org/10.1105/tpc.17.00815>
- Ustun, S., and D. Hofius. 2018. Anti- and pro-microbial roles of autophagy in plant-bacteria interactions. *Autophagy.* 14:1465–1466. <https://doi.org/10.1080/15548627.2018.1475817>
- Varadi, M., S. Anyango, M. Deshpande, S. Nair, C. Natassia, G. Yordanova, D. Yuan, O. Stroe, G. Wood, A. Laydon, et al. 2022. AlphaFold protein structure database: Massively expanding the structural coverage of protein-sequence space with high-accuracy models. *Nucleic Acids Res.* 50:D439–D444. <https://doi.org/10.1093/nar/gkab1061>
- Walter, K.M., M.J. Schonenberger, M. Trotschmuller, M. Horn, H.P. Elsasser, A.B. Moser, M.S. Lucas, T. Schwarz, P.A. Gerber, P.L. Faust, et al. 2014. Hif-2 $\alpha$  promotes degradation of mammalian peroxisomes by selective autophagy. *Cell Metabol.* 20:882–897. <https://doi.org/10.1016/j.cmet.2014.09.017>
- Wang, M., C.J. Herrmann, M. Simonovic, D. Szklarczyk, and C. von Mering. 2015. Version 4.0 of PaxDb: Protein abundance data, integrated across model organisms, tissues, and cell-lines. *Proteomics.* 15:3163–3168. <https://doi.org/10.1002/pmic.201400441>
- Wang, Y.Y., J. Zhang, X.M. Liu, Y. Li, J. Sui, M.Q. Dong, K. Ye, and L.L. Du. 2021. Molecular and structural mechanisms of ZZ domain-mediated cargo selection by Nbr1. *EMBO J.* 40:e107497. <https://doi.org/10.15252/embj.2020107497>
- Watanabe, Y., N.N. Noda, H. Kumeta, K. Suzuki, Y. Ohsumi, and F. Inagaki. 2010. Selective transport of alpha-mannosidase by autophagic pathways: Structural basis for cargo recognition by Atg19 and Atg34. *J. Biol. Chem.* 285:30026–30033. <https://doi.org/10.1074/jbc.M110.143545>
- Waters, S., K. Marchbank, E. Solomon, C. Whitehouse, and M. Gautel. 2009. Interactions with LC3 and polyubiquitin chains link nbr1 to autophagic protein turnover. *FEBS Lett.* 583:1846–1852. <https://doi.org/10.1016/j.febslet.2009.04.049>
- Werner, A., B. Herzog, O. Voigt, O. Valerius, G.H. Braus, and S. Poggeler. 2019. NBR1 is involved in selective pexophagy in filamentous ascomycetes and can be functionally replaced by a tagged version of its human



- homolog. *Autophagy*. 15:78–97. <https://doi.org/10.1080/15548627.2018.1507440>
- Whitehouse, C.A., S. Waters, K. Marchbank, A. Horner, N.W.A. McGowan, J.V. Jovanovic, G.M. Xavier, T.G. Kashima, M.T. Cobourne, G.O. Richards, et al. 2010. Neighbor of Brca1 gene (Nbr1) functions as a negative regulator of postnatal osteoblastic bone formation and p38 MAPK activity. *Proc. Natl. Acad. Sci. USA*. 107:12913–12918. <https://doi.org/10.1073/pnas.0913058107>
- Wilson, M.I., D.J. Gill, O. Perisic, M.T. Quinn, and R.L. Williams. 2003. PBI domain-mediated heterodimerization in NADPH oxidase and signaling complexes of atypical protein kinase C with Par6 and p62. *Mol. Cell*. 12:39–50. [https://doi.org/10.1016/s1097-2765\(03\)00246-6](https://doi.org/10.1016/s1097-2765(03)00246-6)
- Yamamoto, K., A. Venida, J. Yano, D.E. Biancur, M. Kakiuchi, S. Gupta, A.S.W. Sohn, S. Mukhopadhyay, E.Y. Lin, S.J. Parker, et al. 2020. Autophagy promotes immune evasion of pancreatic cancer by degrading MHC-I. *Nature*. 581:100–105. <https://doi.org/10.1038/s41586-020-2229-5>
- Yamasaki, A., and N.N. Noda. 2017. Structural biology of the Cvt pathway. *J. Mol. Biol.* 429:531–542. <https://doi.org/10.1016/j.jmb.2017.01.003>
- Yamashita, S.i., K. Abe, Y. Tatemichi, and Y. Fujiki. 2014. The membrane peroxin PEX3 induces peroxisome-ubiquitination-linked pexophagy. *Autophagy*. 10:1549–1564. <https://doi.org/10.4161/auto.29329>
- Yang, J.Q., H. Liu, M.T. Diaz-Meco, and J. Moscat. 2010. NBR1 is a new PBI signalling adapter in Th2 differentiation and allergic airway inflammation in vivo. *EMBO J*. 29:3421–3433. <https://doi.org/10.1038/emboj.2010.214>
- Yang, Z., S. Yang, Y.H. Cui, J. Wei, P. Shah, G. Park, X. Cui, C. He, and Y.Y. He. 2021. METTL14 facilitates global genome repair and suppresses skin tumorigenesis. *Proc. Natl. Acad. Sci. USA*. 118:e2025948118. <https://doi.org/10.1073/pnas.2025948118>
- Yorimitsu, T., and D.J. Klionsky. 2005. Atg11 links cargo to the vesicle-forming machinery in the cytoplasm to vacuole targeting pathway. *Mol. Biol. Cell*. 16:1593–1605. <https://doi.org/10.1091/mbc.e04-11-1035>
- Young, P.G., M.J. Passalacqua, K. Chappell, R.J. Llinas, and B. Bartel. 2019. A facile forward-genetic screen for Arabidopsis autophagy mutants reveals twenty-one loss-of-function mutations disrupting six ATG genes. *Autophagy*. 15:941–959. <https://doi.org/10.1080/15548627.2019.1569915>
- Yu, Z., J. Ma, X. Li, Y. Liu, M. Li, L. Wang, M. Zhao, H. He, Y. Zhang, Q. Rao, et al. 2018. Autophagy defects and related genetic variations in renal cell carcinoma with eosinophilic cytoplasmic inclusions. *Sci. Rep.* 8:9972. <https://doi.org/10.1038/s41598-018-28369-y>
- Zaffagnini, G., A. Savova, A. Danieli, J. Romanov, S. Tremel, M. Ebner, T. Peterbauer, M. Sztacho, R. Trapannone, A.K. Tarafder, et al. 2018. p62 filaments capture and present ubiquitinated cargos for autophagy. *EMBO J*. 37:e98308. <https://doi.org/10.15252/emj.201798308>
- Zeng, Y., S. Xu, Y. Wei, X. Zhang, Q. Wang, Y. Jia, W. Wang, L. Han, Z. Chen, Z. Wang, et al. 2021. The PBI protein of influenza A virus inhibits the innate immune response by targeting MAVS for NBR1-mediated selective autophagic degradation. *PLoS Pathog*. 17:e1009300. <https://doi.org/10.1371/journal.ppat.1009300>
- Zhang, J., Y.Y. Wang, Z.Q. Pan, Y. Li, J. Sui, L.L. Du, and K. Ye. 2022a. Structural mechanism of protein recognition by the FW domain of autophagy receptor Nbr1. *Nat. Commun.* 13:3650. <https://doi.org/10.1038/s41467-022-31439-5>
- Zhang, S., Y. Hama, and N. Mizushima. 2021. The evolution of autophagy proteins - diversification in eukaryotes and potential ancestors in prokaryotes. *J. Cell Sci*. 134:jcs233742. <https://doi.org/10.1242/jcs.233742>
- Zhang, S., E. Yazaki, H. Sakamoto, H. Yamamoto, and N. Mizushima. 2022b. Evolutionary diversification of the autophagy-related ubiquitin-like conjugation systems. *Autophagy*:1–16. <https://doi.org/10.1080/15548627.2022.2059168>
- Zhang, Y., and Z. Chen. 2020. Broad and complex roles of NBR1-mediated selective autophagy in plant stress responses. *Cells*. 9:2562. <https://doi.org/10.3390/cells9122562>
- Zhou, J., J. Wang, Y. Cheng, Y.J. Chi, B. Fan, J.Q. Yu, and Z. Chen. 2013. NBR1-mediated selective autophagy targets insoluble ubiquitinated protein aggregates in plant stress responses. *PLoS Genet*. 9:e1003196. <https://doi.org/10.1371/journal.pgen.1003196>
- Zhou, J., J. Wang, J.Q. Yu, and Z. Chen. 2014. Role and regulation of autophagy in heat stress responses of tomato plants. *Front. Plant Sci*. 5:174. <https://doi.org/10.3389/fpls.2014.00174>



